UNIVERSITÀ
DI PAVIA

DOTTORATO IN SCIENZE CHIMICHE E FARMACEUTICHE XXXIV CICLO

Coordinatore Chiar.mo Prof. Giorgio Colombo

Veterinary pharmaceutical development of freeze-dried secretome from mesenchymal stromal cells: GMP production and clinical trials for equine and canine tissue regeneration

Tutore:
Chiar.ma Prof.ssa Maria Luisa Torre
Co-tutore:
Dr. Stefano Grolli

Tesi di dottorato di
Michela Mocchi

Anno Accademico 2020/2021

Non fermatevi là dove siete arrivati.

(Pitagora)

GENERAL INDEX

PREFACE:

Veterinary pharmaceutical development of freeze-dried secretome for equine and canine models

The regenerative therapeutic efficacy of mesenchymal stromal cells is mainly due to the release of paracrine factors, known as secretome. It is composed of free soluble factors (including cytokines, chemokines and growth factors) and of insoluble nano/microstructured extracellular vesicles (EVs). The use of secretome is become very attractive: as a cell-free product, brings numerous advantages avoiding all the practical difficulties related to both clinical application of stem cells, unpredictable long-term behaviour associated with direct cell transplantation and regarding regulation/costs for the whole treatment. Moreover, secretome compared to their parent cells is less immunogenic, no tumorigenic and its vascular administration does not cause vascular clotting thus, resulting safer. There are also some advantages regarding the technological features as the possibility of sterilization, it is easy to handle and easy to storage and characterized; finally, it is also a ready-to-use product for immediate procedures. Although it is considered a promising approach its clinical translation from bench to bedside is still in its infancy, indeed for human and especially in veterinary field, there are very few clinical on the use of secretome. Until now, a standardized isolation process was lacking, generating uncertainty about secretome biological effects, which seem to be strongly influenced by the preparation method. Based on these premises, a

validated GMP-compliant procedure for the large-scale production of human secretome has been recently proposed and applied for veterinary use. An important application branch of secretome derived MSCs is the musculoskeletal system (MMS); a heterogeneous group of pathologies (post-traumatic, autoimmune or degenerative) that can affect the osteoarticular apparatus, associated with painful symptoms both acute or chronic.

This Ph.D. project concerns the technological-pharmaceutical development of freeze-dried secretome (named Lyosecretome) taken from mesenchymal stromal cells of canine and equine species. Safety and efficacy have been evaluated in vitro, and clinical trials were performed by injecting secretome in the lesion site of the animal patients. Clinical trials were conducted on spontaneous degenerative pathologies owing that induced pathology models are not completely predictive due to the inter-species differences. Finally, the European Union recently approved an animal-testing law inspired by the 3R principle (aiming at reducing, replace and refine the use of animals, 2010/63/EU) making the traditional preclinical experimentation on induced pathologies even more difficult.

The present study was conducted according to the protocol presented by Stefano Cinotti and approved by the Italian Ministry of Health (Prot. n. 0000778 del 15/01/2020 7.1.2.0.0.0/17/2019-AGD 809). The regulatory authority declares “Refers to (omissis) verified the requirements of the D.M. November 12, 2011 good practices of clinical trials of medicines, veterinary on animals, after hearing the opinion of the Istituto Superiore di Sanità, expressed a favorable opinion for the conduction of the aforementioned trial ".

The thesis is structured into four chapters: the first part is an introduction to understand the state of art of the MSCs e their secretome regarding musculoskeletal disorders in veterinary practice

(Chapter 1). The second chapter (Chapter 2) describe the optimization of the Lyosecretome formulation and manufacturing process robustness, the aim was to give a partial answer to the uncertainties concerning the secretome formulation. In detail, we found a way to obtain a more standardized product and investigate sources of variability that can affect the process. Chaper 3 described the preparation and characterization of a freeze-dried secretome (Lyosecretome) from equine adipose tissue-derived mesenchymal stromal cells, the work provides a proof-of-concept for the manufacturing of clinical-grade equine freeze-dried secretome, and prototypes for safety and efficacy clinical trials in the treatment of equine musculoskeletal diseases. As for equine, Chapter 4 brings a characterization of the canine Lyosecretome and then, three-case report were reported on dogs affected by bilateral knee or elbow osteoarthritis. The objective of this study was to demonstrate the safety of secretome treatment as a new potential alternative to the cell therapy.

Each chapter is assembled by published data or submitted results for publication, also supported by their specific references. Finally, conclusions at the end complete the present thesis.

The aim of the thesis was:

- to obtain a validated, reproducible, well-defined and cost-affordable GMP clinical grade secretome based products from equine and canine MSCs.
- to prove the safety and efficacy of the products in vitro and in vivo on animals spontaneously affected by osteoarticular and musculoskeletal diseases.
- replacing animal models of induced pathology with a novel approach, combining in vitro safety and potency studies and in vivo efficacy assessment on spontaneous animal pathologies.

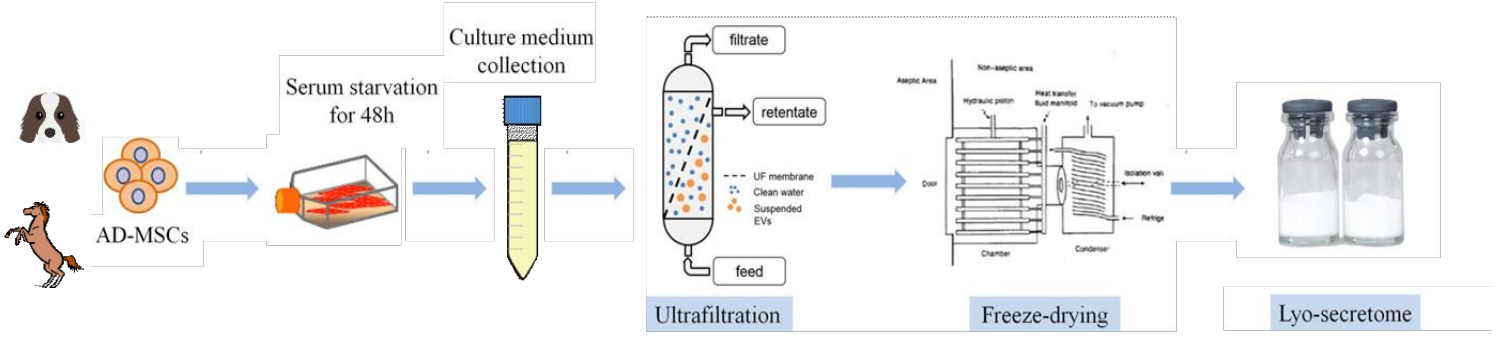
AD-MSCs
Serum starvation for 48h
Culture medium collection
filtrate
retentate
UF membrane
Clean water
Suspended EVs
feed
Ultrafiltration
Freeze-drying
Lyo-secretome

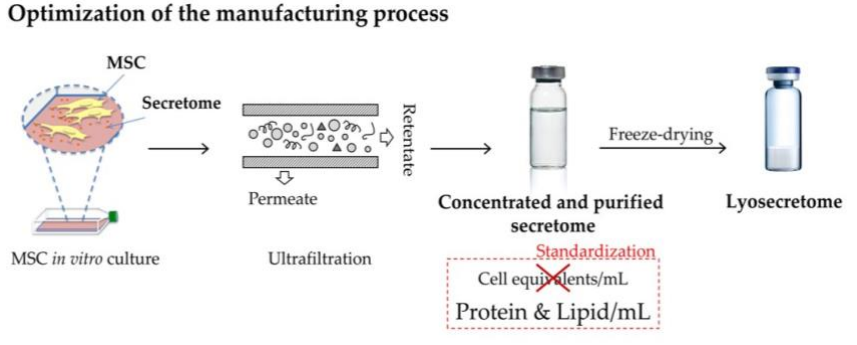
Optimization of the manufacturing process
MSC
Secretome
MSC in vitro culture
Retentate
Permeate
Ultrafiltration
Concentrated and purified secretome
Freeze-drying
Lyosecretome
Standardization
Cell equivalents/mL
Protein & Lipid/mL

CHAPTER 1:
INTRODUCTION

The potential using of MSCs for treating joint injury and osteoarthritis have not yet been extensively explored in veterinary field and at the present no consensus among the researchers have been achieved. To apply an MSCs therapy it is important to consider several aspects, such as identify the elective cells sources, the isolation process, the culturing conditions, route of administration and the disease targets.

The following review (**Paper 1)** presents the state of art of MSCs and their use in the veterinary medicine focusing on clinical reports of dogs and horses in musculoskeletal diseases, moreover a perspective regarding the use of the secretome in the veterinary field is provided.

Osteoarthritis (OA) is the most common form of arthritis related to the progressive degeneration of articular cartilage and subchondral bone, leading to serious debilitating conditions. Intervertebral Disk Degeneration (IDD) is a complex multifactorial process considered as the primary cause of low back pain. Tendon ligament injury (TLI) affects the largest part of the population, and it ranges from acute traumatic ruptures to chronic overuse and degenerative tendinopathies. All these pathologies are incurable, and all the available treatment strategies are mainly focused on pain relief only. Therefore, a lot of effort is dedicated to the development of strategies able to regenerate or at least repair and preserve the functioning of the intervertebral disk structure. Among these, intradiscal injection of

allogeneic or autologous MSCs has become highly topical in experimental and clinical investigations. Only lately, secretome has been evaluated to replace the cell-therapy with some encouraging results regarding the safety and efficacy, unfortunately, the mechanisms of action responsible for the beneficial effects of the paracrine molecules is not yet clear and further investigation are needed.

Paper 1. Mocchi M, Dotti S, Del Bue M, Villa R, Bari E, Perteghella S, Torre ML, Grolli S (2020). Veterinary Regenerative Medicine for Musculoskeletal Disorders: Can Mesenchymal Stem/Stromal Cells and Their Secretome Be the New Frontier? Cells 9, 1453; doi: 10.3390/cells9061453.

Abstract: Regenerative medicine aims to restore the normal function of diseased or damaged cells, tissues, and organs using a set of different approaches, including cell-based therapies. In the veterinary field, regenerative medicine is strongly related to the use of mesenchymal stromal cells (MSCs), which belong to the body repair system and are defined as multipotent progenitor cells, able to self-replicate and to differentiate into different cell types. This review aims to take stock of what is known about the MSCs and their use in the veterinary medicine focusing on clinical reports on dogs and horses in musculoskeletal diseases, a research field extensively reported in the literature data. Finally, a perspective regarding the use of the secretome and/or extracellular vesicles (EVs) in the veterinary field to replace parental MSCs is provided. The pharmaceuticalization of EVs is wished due to the realization of a Good Manufacturing Practice (GMP) product suitable for clinical trials.

Keywords: mesenchymal stem cells; regenerative medicine; veterinary; secretome; extracellular vesicles; microvesicles; exosomes

1. Introduction

In recent years, the focus of medical science has shifted from repair to regeneration. Regenerative medicine aims to recover the normal function of diseased or damaged cells, tissues, and organs using a set of different approaches, including cell-based therapies, able to stimulate and coordinate the processes headed to biological

restoration. Regenerative medicine stands out as a top research interest area in medical fields, including both human and veterinary medicine. Regenerative medicine is strongly related to the use of mesenchymal stromal cells (MSCs), whose safety and efficacy are now considered well established for humans [1,2]. In veterinary medicine, the reality is much diversified. Above all, there is enormous variability in terms of anatomy and physiology among the animal species in which regenerative medicine can be applied (mainly horses and dogs), with consequences on stem cells biology, mechanisms of action, and several aspects on their application, such as minor/major inflammation responses after MSCs administration in vivo. Moreover, sometimes, even between breeds, there is a large variability related to the predisposition to a certain type of pathologies than others (for example, an impact factor could be the animal lifestyle, their weight and size, or their genetic background). In this scenario, finding a common thread to describe the state of the art of veterinary regenerative medicine is not easy because the landscape of clinical studies is quite limited (http://www.clinicaltrials. gov, last access 25 March 2020); nevertheless, new knowledge is rapidly accumulating as a result of both induced animal disease models used in human pre-clinical studies, and a more rigorous approach in the designing of clinical trials based on naturally occurring diseases. This review aims to take stock of what is known about the MSCs and their use in the veterinary field. Aware that translating clinical results from one species to another is not so easy and often not realistically possible, it has been decided to focus and limit the research field on what has been more extensively reported in the literature data. Nowadays, the therapeutic application of MSCs seems to have the most promising results in musculoskeletal diseases, based on several works published in the last few years. Dogs and horses are the most actively studied species, as it results from the evaluation of the literature, thus they will be considered more in detail. Finally, a perspective regarding the use

of the secretome and/or extracellular vesicles (EVs) in the veterinary field, instead of parental MSCs, is provided.

2. 2. Mesenchymal Stromal Cells and Veterinary Regenerative Medicine: Main Features, Sources, Isolation, and Cryopreservation Procedures

MSCs are defined as multipotent progenitor cells able to self-replicate and differentiate into different cell types, thus repairing/regenerating the damaged tissues [3]. In addition to stemness-associated features, the clinical utility of MSCs is also due to other characteristics, which include (i) the secretion of trophic factors that promote repair of the damaged tissue [4]; (ii) immunosuppressive activity, through secretion of several cytokines that inhibit the activity of natural killer cells, helper T cells, and cytotoxic T cells while activating the generation of regulatory T cells; and (iii) homing abilities, which allow cells to migrate across the endothelium to the sites of injury and inflammation [5]. Due to all these biological properties, MSCs have been widely used in the veterinary field as an Advanced Therapy Medicinal Product (ATMP), demonstrating significant potential in clinical application [6]. Many factors pave the way for their use, including (i) a feasible and relatively easy isolation process; (ii) the lack of immunogenic properties, which permit the usage of allogeneic transplantation in pre-clinical and clinical trials [5]; and (iii) the absence of ethical controversy. However, the costs related to their application, mainly in musculoskeletal and joint diseases, limit their use mainly to the equine and canine species (and, at a lower extent, feline species). In veterinary medicine, everything regarding tissue sampling, MSC culture, expansion, and cryopreservation is essentially similar to what is commonly applied in human medicine [7–9]. A summary panel of the main procedure is shown in Figure 1. Even in this case, many factors can influence MSC therapeutic effectiveness, including tissue source, isolation procedures, culturing

conditions (pH, temperature, incubation time, medium supplementary, serum starvation) and cryopreservation. All these must be standardised in order to reduce the variability among the different cell batches.

2.1. MSC Isolation Tissue

Experimental evidence indicates that MSCs can be isolated from almost every tissue of the body (comprising bone marrow, adipose tissue, peripheral blood, and extra-embryonic tissues) [10]. The source of MSCs is of extreme importance, as it has been recently reported that MSCs derived from different anatomical sites possess different in vivo differentiation potentials [11] as well as subtle differences in biological features. Nevertheless, clear indications concerning which source is best indicated for a specific disease are not always available, and, for musculoskeletal therapy, it remains controversial which source of MSCs could represent the most valuable and reliable in terms of cell yield and biological features [12].

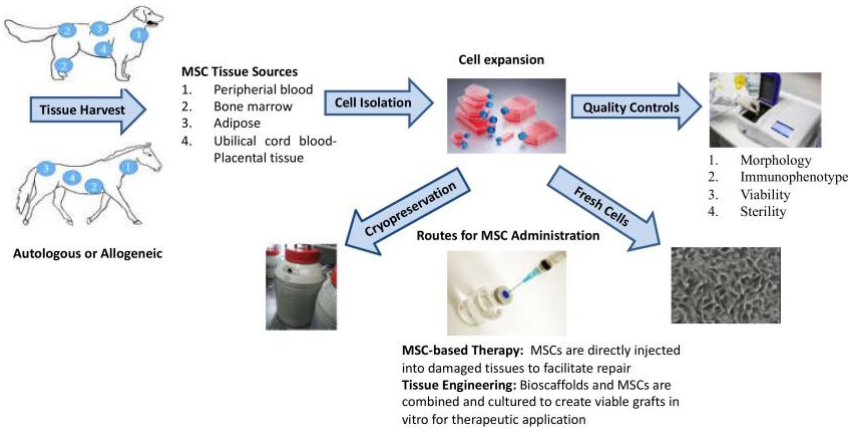

Figure 1. Schematic of equine and canine adult mesenchymal stromal cell (MSC) processing.(Adapted from Duan, W. et al. [8]).

As in human medicine, bone marrow (BM) has been historically the first and most investigated source of MSCs in horse and dog

[13,14]. Yet, a strong disadvantage of BM-MSC is the invasive collection method associated with the risk of complications, such as infection, haemorrhage, and, in the horse, pneumothorax, or pneumopericardium [15,16]. One of the most extensively investigated sources of MSCs is the adipose tissue (AD) [15,17–19]. Its success as an MSCs tissue source is due to the easier access, that allows safe and rapid recovery of tissue samples, via lipectomy or lipoaspiration (used for examples in horses and dog) [15,20]. Along with the use AD-MSCs, recently active investigation has been focused on the adipose-tissue-derived stromal vascular fraction (SVF) which is believed to bring some practical advantages over the use of in-vitro expanded AD-MSCs [21]. SVF results easier to isolate and allows to obtain a ready to use the product after minimal contact with xeno-reagents, without the need for any cell separation or expansion, leading to less strict regulatory criteria. One limitation of its application, in substitution of AD-MSCs, is due to the presence of different cell types which can potentially cause immunological rejection so that SVF indeed applicable for autologous treatments only. Nevertheless, in vivo studies have been performed using allogeneic SVF demonstrating its safety and efficacy [22]. In some species, i.e., dog and cat, abdominal visceral fat has been proposed as a source of MSCs. In this case, fat tissue can be collected with a relatively simple surgery from the patient or during elective surgery. As an example, ovariohysterectomies, a common surgical procedure in dogs and cats, has been proposed as a useful approach for the collection of visceral fat [18,23]. Peripheral blood seems to be a valid alternative source compared to bone marrow and adipose tissue for some authors. However, findings regarding the availability of MSCs in peripheral blood are controversial. Positive results have been reported in rabbits, mice and guinea pigs [24], but they stand in contrast to poor

success described in humans, dogs, and horses [6,16,25,26]. In detail, one of these studies has demonstrated that fibroblast-like cells isolated from dog, guinea pig, and rat peripheral blood possess a certain capacity to differentiate into several mesenchymal lineages. Equine peripheral-blood-derived fibroblast-like cells, instead, can differentiate into different mesenchymal lineages but have less multipotency than BM-MSCs [26]. Although results need to be studied more extensively, other promising outcomes were obtained from the investigation of the equine synovial membrane and synovial fluid as a potential MSCs source in which cell collection is feasible with a minimally invasive procedure [27]. Finally, knowing that MSCs yield decreases with the increasing age of the donor [28,29], umbilical cord blood (UBC) and matrix, amniotic fluid [30,31], or placental tissue are an auspicious source of MSCs. Equine UCB samples appeared to be a rich source of readily available and highly proliferative MSCs that could be applied for therapeutic use [29]. The disadvantages of these sources are due to their collection procedure, performed in a no-sterile condition environment, at the parturition [32].

2.2 MSC Isolation Procedures

As reported above, MSCs can be isolated either from 'liquid' sources, such as peripheral blood, or from 'solid' sources, such as adipose tissue. In the first case, the isolation process will employ a gradient centrifugation protocol, whereas, for the second one, an enzymatic treatment will be needed. Afterward, cells are seeded in plates for their adhesion, while the non-adhered ones will be wiped out when replacing culture medium with fresh one [7,33]. Depending on the type of cells and technical factors, usually within a week or 10 days, colonies of adherent cells will appear and gradually cover as a layer the culture plate bottom, until they reach the confluence. Cell

layers will be then detached by trypsinization and reseeded to permit a continuous proliferation every time confluence is reached; this step is called 'cell sub-cultivation', and each one is referred to as passage number. MSCs should not be expanded more than four passages for clinical applications to maintain their stemness; indeed, further passages lead to senescence, meaning lower proliferation and morphological as well as biological changes. For instance, previous studies have shown how the onset of senescence is related to a telomere length reduction; senescence of equine BM-MSCs occurs faster than adipose and umbilical cord-derived MSCs [34]. These results indicate the adipose tissue and, to a lesser extent, for difficulties in the collection, the umbilical cord, as preferable choices for tissue regeneration.

2.3 MSC Culturing Conditions

The medium used for MSC culture is mainly represented by the Basal Medium Eagle (BME), Minimum Essential Media (MEM), and Dulbecco's Modified Eagle's Medium (DMEM); they are different in the content of amino acids and mineral salts, and the concentration of glucose.

Supplementation of the medium is performed to mimic in vivo conditions in order to sustain cell growth. Foetal bovine serum (FBS) or platelet lysate [35,36] are used in the cell culture medium as a source of growth factors [37], which supports attachment and further expansion of MSCs. The use of antibiotics is important in order to prevent bacterial contaminations, and the most commonly used are penicillin and streptomycin.

The pH value of the medium ranges between 7.2 and 7.4, and in order to keep this value constant, cell plates are usually incubated in 5% CO2 atmosphere, and the medium culture contains NaHCO3 as a buffer.

2.4. Cryopreservation

Cryopreservation is a conservation method which allows storing biological material at very low temperatures (−196 ◦C using liquid nitrogen or −80 ◦C using carbon dioxide). Cryopreservation process turns to be useful for the storage of cells for extended periods; indeed, freezing in liquid nitrogen keeps cells alive in a complete quiescence phase for years. By default, it should be considered that cryopreservation alters or compromises the structure and function of cells; in the worst cases, the ice crystals formed during the freezing process can cause cell damage. For this reason, due to the complexity of the whole process (freezing and thawing), a choice of excipients and process parameters, to protect the cell integrity from stresses, is challenging. These excipients are generally named as cryo-protectants and are mainly divided into two categories—membrane-permeable and impermeable. Cryo-protectants with high permeability are, for example, dimethyl sulfoxide (DMSO), ethylene glycol, methanol, propylene glycol, and dimethylacetamide. They tend to be the most cytotoxic. Cryo-protectants less permeable are methylcellulose (MC), polyvinylpyrrolidone (PVP), hydroxyethyl starch (HES), polyethylene glycol, and dextran. In association, FBS is used as a source of protein with synergic cryoprotectant effect [38]. A mixture of DMSO and FBS is considered as the standard cryo-protectant in veterinary medicine, even if the oncogenic and xenogeneic properties of DMSO and FBS, respectively, may alter cells and impact in vitro and in vivo behaviour after implantation [8].

Regarding cell transportation, many studies have shown which are the shipping criteria that should be considered—for instance, supplementing media, transport temperature, and other variables, such as the type of container for the shipping. The latter did not show meaningful evidence; in detail, the use of plastic rather than glass containers did not show differences in terms of cell viability after 24 h at room temperature (20–22 ◦C) at several MSC concentrations [39]. Shipping temperature is up to cell storage conditions: frozen cells

should be transported in dry ice around −80 ◦C, inside cryovials often wrapped with precooled material and placed in a leak-proof container to prevent direct contact of samples; otherwise, they can be transported in liquid nitrogen to maintain −196 ◦C temperature. In the literature, it is reported that shipping frozen equine BM-MSCs is the most appropriate method to maintain about 80% of cell viability [40] up to six months [41]. Fresh cells, instead, have been valued differently in several studies: transport was evaluated at different temperature (4 ◦C, 37 ◦C, and room temperature 20–22 ◦C) in PBS or DMEM, either alone [42] or supplemented with FBS or with horse serum [9]. As a result, the majority agreed that MSC transport should be performed at 4 ◦C, which seems to be the most practical one. According to this, shipping fresh equine MSCs in isotonic saline solution at 4 ◦C within 24 h is considered ideal for immediate administration, although, in these conditions, MSC viability decreases up to 70% [39,40,43]. Only one study considered room temperature as superior in the case of short-duration transport [43].

The consciousness of differences between the employment of fresh and frozen MSCs is now ongoing. As mentioned before, each step of cryopreservation can affect MSC viability. Concerning this, two reports have demonstrated that while frozen canine AD-MSCs and BM-MSCs had a lower proliferation capacity, lower telomerase activity, and a loss of cells expansion, fresh cells maintained their capacities exploring the same parameters. Similarly, feline cryopreserved AD-MSCs showed lower CD9 and CD105 expression compared to fresh cells [44]. On the other hand, several other studies led to different results. In detail, Martinello et al. proved that, after cryopreservation, equine peripheral blood MSCs conserved their morphology, telomerase activity, proliferation rate, and CD expression pattern [45]. Overall, the use of fresh and cryopreserved MSCs is controversial, and particular care on the cell viability and passage level must be taken before their administration.

2.5 Quality Controls

Another important aspect that should be considered when isolating MSCs is their characterization, performing quality, and quantity controls on the starting material and the final product. In such a way, it can ensure the quality, reproducibility, functionality, potency, efficacy, and safety of the clinical product. Required quality controls regard the morphology, immunophenotype, differentiative potential, viability, and sterility testing [46].

2.6 Routes for MSC Administration

Although MSCs delivery routes are different, typically, clinical treatment requires the administration of cells using needles. Cells activity and survival could be affected not only by needles type and diameter but, notably, also by following the aspiration and re-injection of MSCs suspension, probably due to the negative pressure during aspiration [47]. Since the passage of MSCs through a needle may affect cell viability, the appropriate catheter aspects should be taken into considerations. Usually, for joint pathologies, for instance, osteoarthritis, MSCs suspension is directly injected intra-articularly. In tendon core lesions, intra-lesional direct administration of MSCs is the preferred route, while administration within the tendon sheath or by regional perfusion with the use of intravenous catheter is used in the case of multi-focal lesions or when the damaged site is difficult to access [48]. Intra-arterial delivery could be effective, but this route is discouraged because of the risk of thrombosis [49]. In the case of focal cartilage lesions, MSCs could be encapsulated into a scaffold and be placed directly into the damage region under arthroscopic guidance [48].

2.7. Autologous vs Allogeneic MSCs

There are mainly two approaches for stem cell therapy in regenerative medicine—autologous or allogeneic cell transplantation.

An autologous transplant uses the patient's stem cells, while allogeneic transplant uses stem cells from a donor. Allogeneic versus autologous MSCs is a hot topic in veterinary regenerative medicine, debating whether there is a difference in terms of safety and efficacy. The use of allogeneic MSCs is subjected to specific national regulations, which are important to consider for trials and clinical applications. However, the use of allogeneic MSCs would represent an important advantage offering availability of banked cells, previously characterized for their safety and biological features, as a proven differentiation capacity. This approach would reduce the typical variability of autologous cellular products, allowing greater homogeneity in treatments and, presumably, results. Moreover, by this approach, it is possible to have a ready-to-use product for appropriate timing of therapeutic applications, without the need to wait for the autologous cell culture expansion.

Using the patient's cells to treat an injury or disease is believed to be safer, but on the other hand, one of the major challenges of this approach is due to timing. Indeed, the timing to expand the right amount of cells for implantation is highly dependent on the harvested tissue, as well as on their reproduction capacity, and thus by age, gender and disease type [50].

Some trials have been conducted on different animal models to compare allogeneic and autologous MSCs. In one of them, self and non-self placenta-derived MSCs were injected into contralateral joints of 16 healthy horses. A comparison was made in terms of lameness evaluation and synovial fluid analysis from 0 h up to 72 h post-injection. The injection of allogeneic MSCs did not provoke a systemic response, while local response such as swelling was minimal, and inflammatory response was not significantly different between the two treatments. Thus, this pre-clinical work is an important step in the development of equine allogeneic stem cell therapies [51]. Furthermore, Shah et al. reported the outcome of the treatment

conducted on 203 dogs suffering from osteoarthritis and other joint defects with allogeneic stem cells derived from adipose tissue. Dogs of various breeds and different ages were enrolled in the study. Most of the patients received an intra-articular therapy, while 68 patients were treated intravenously. The large majority of younger animals (90% of < nine-year-old dog) and a large percentage of older patients treated with the allogeneic adult stem cells improved symptoms and demonstrated better quality of life. Only a single patient had a worsening of the symptoms. The large number of dogs enrolled in the study, and the administration routes of the cells, point out the safety of the allogeneic treatment, although the follow-up was limited to 10 weeks [52]. The result of this report strengthens similar findings, where allogeneic MSCs have been able to aid the body's regeneration abilities without causing an immune response or other adverse effects [52,53]. Another proof of allogeneic MSCs safety has been reported by Brandão et al., who analysed autologous and allogeneic AD-MSCs in order to evaluate the inflammatory response in healthy equine tendon [54]. The outcome in the two groups has been compared to a control group where only PBS was administered. After injection, all the groups presented mild pain sensitivity on the second day, which can be explained as a consequence of the healthy tissue response to an injury application. There were no significant differences among the groups in the physical, morphological, thermography, and ultrasonography analyses. Moreover, even the lameness analysis presented similar behaviour between the two cell-treated groups. Interestingly, the authors analysed tissue and cellular response to MSCs administration, concluding that both allogeneic and autologous AD-MSCs did not induce a significant inflammatory response, although a higher number of T lymphocytes have been observed in the group treated with allogeneic cells. Based on their result, the authors suggest that allogeneic MSCs did not have adverse effects in comparison to the autologous cells, thus reinforcing the hypotheses that allogeneic

banked cells could be a safe and effective approach to regenerative therapies. According to this, a similar conclusion came from a different study conducted on allogeneic BM-MSCs transplantation in equine tendons. The analysis showed no significant differences compared to the autologous cells [53]. In this latter study, small lesions were created in the equine superficial digital flexor tendon, followed by injection with autologous, allogeneic, or bone marrow supernatant alone, respectively. Post-mortem examinations revealed there was no cell-mediated immune response to the host for both autologous and allogeneic MSC treatment.

These results seem to be promising and lead to the conclusion that allogeneic rather than autologous MSCs could be used for regenerative medicine purposes in veterinary medicine. Hence, it would be important to implement studies related to the immunomodulation of MSCs in order to understand cell response better and reinforce, accordingly, therapeutic applications. In particular, immunoreactivity tests performed both in vitro and in vivo using allogeneic MSCs are important to guarantee safe and effective therapy. Moreover, further in-depth studies still need to be performed to understand the real behaviour of the stem cells at the site of application and their crosstalk with resident cells [55].

Finally, most of the clinical applications to investigate MSCs behaviour are conducted on experimentally damaged tissue models. Some authors, indeed, suggest that to evaluate MSCs action mechanisms and attitude better, it would be necessary to apply cells in healthy tissues [53]. The injection of allogeneic MSCs in the considered area would allow the assessment of the possible local inflammatory reaction. Thus, this could reveal the interaction of any other aspects, proving that alterations are caused by cell transplantation [56]. Working on healthy tissues is also important to predict the side effects of allogeneic MSC transplantation in animals. All the considered

studies regarding autologous vs allogeneic MSCs are summarised in Table 1.

Table 1. Summary of autologous vs allogeneic MSCs.

Study	Animal	Study Design	Time	Outcome	Dosage
Carrade et al. [51]	Horses	Autologous vs Allogeneic placenta-derived MSCs	0–72 h post-injection	Allogeneic MSCs did not provoke a systemic response, and the minimal inflammatory reaction was found to be similar to the autologous effect	7.5×10^6 in 2 mL sterile injectable 0.9% NaCl
Shah et al. [52]	Dogs	Allogeneic adipose tissue (AD)-MSCs	10 weeks	Better quality of life also demonstrating the safety of the allogeneic treatment	Data not recorded
Guest et al. [53]	Horses	Autologous and Allogeneic progenitor cells (MPCs) purified from bone marrow and bone marrow	10 or 34 days	Post-mortem examinations showed no visible cell-mediated immune response to allogeneic MPCs in any of the treated horses	1×10^6 cells suspended in 0.5 mL of autologous bone marrow supernatant

		supernatant alone			
Brandão et al. [54]	Horses	Autologous and allogeneic AD-MSCs and only PBS as a control group	6 days	All groups presented mild pain sensitivity, there were no significant differences among the groups in the physical, morphological, thermography, and ultrasonography analyses. Also, the lameness analysis presented similar behaviour between the two cell-treated groups. Both allogeneic and autologous AD-MSCs did not induce a significant inflammatory response, although a	1×10^7 cells for each application resuspended in PBS.

higher number of T lymphocytes have been found in the allogeneic treatment.

3. MSCs in the Veterinary Field: Disease Targets

Musculoskeletal disorders (MSDs) represent common pathologies in veterinary clinical practice. MSDs affect the osteoarticular apparatus, including muscles, bones, and joints. They are associated with painful symptoms that can be both acute and chronic. These disorders often result from overuse injuries, muscle fatigue, inflammation of the tendon structure, or intervertebral disk degeneration of the vertebral column. Examples of MSDs include osteoarthritis (OA), tendon ligament injury (TLI), and intervertebral disk degeneration (IVDD) [57].

Up to now, treatment options for MSDs include systemic or intra-articular administration of anti-inflammatory drugs, hyaluronic acid (HA), cells-based products including platelet-rich plasma (PRP), and autologous/ allogeneic cells implantation [57,58]. Since MSDs have a high prevalence, regenerative therapies, including the use of MSCs, have been brought to the attention of veterinary practitioners as an alternative to the more traditional treatments [54,59,60]. Below, the employment of MSCs to treat each specific MSD is reported.

3.1. Osteoarthritis

OA is the most common form of arthritis related to the progressive degeneration of articular cartilage and subchondral bone, leading to severely debilitating conditions. It is a chronic and

irreversible condition involving the cycle of inflammation and tissue degradation [61].

In recent years, MSCs have been proposed as a therapy for the treatment of OA in both dogs and horses. The currently available evidence of the MSCs effectiveness and safety profile is confirmed in the clinical trials reported in Table 2. In all cases, whether it is a dog or a horse, veterinarian practitioners directly administered MSCs into the joint by intra-articular injection [40,62].

Regarding dogs' treatments, the most common approach is to use adipose tissue as cells source, favored by the possibility of minimal-invasive collection. In detail, as reported in a review, different clinical trials on the use of AD-MSCs have been investigated comparing the AD-MSCs alone or in combination either with intra-articular autologous PRP or HA as a chondroprotective agent [63]. Considering the common outcomes of the studies reported in Table 2, the most important element is the safety and efficacy of the therapy, expressed in term of the absence of any side effects (including local and systemic inflammation), reduction of lameness, improvement of joint functionality, and pain reduction. As a general trend, better endpoints were noticed in dogs treated with AD-MSCs associated with plasma rich in growth factor (PRGF-Endoret) [64] than AD-MSC alone [65]. It has been indeed demonstrated that in vitro PRP releases growth factors, including Transforming growth factor beta (TGF-β), platelet-derived growth factor (PDGF), epidermal (EGF), and insulin-like growth factor (IGF) that affect cartilage regeneration [66]. Another study demonstrated the superiority of AD-MSCs alone over PRP at the six-month follow-up, although outcomes were not described beyond this period [67]. OA in dogs has also been treated by injection of AD-MSC suspended in saline solution, comparing the outcome to dogs treated using saline solution only, as a control group. This experiment was reproduced afterwards by the same group of research administering

a higher amount of cells and with a longer follow-up. In fact, since the pain grade of the affected joint was severe, the success rate after the injection was not significantly high in the first study; however, clear evidence of the efficacy of MSCs therapy was observed in the second work [68,69].

To examine the impact of MSCs in the treatment of equine model of OA, several clinical studies have been performed. A recent review compares intra-articular injection of MSCs in both naturally occurring and induced equine OA; results have been variable, which may be caused by the changing environment, follow-up, MSC dosage and source, as well as inter-observer differences in subjective outcome parameters [70]. Considering bone marrow as MSCs source, autologous cells have been dispersed in HA, and their effect has been compared to the HA alone used as a control [71]. Horses had defects arthroscopically created on both stifle joints and received an intra-articular injection; after 12 months, horses were euthanized. Results showed no significant improvement, but evaluation post-mortem performing histologic and immunohistochemical analyses confirmed a significant increase in joint repair. Naturally occurring OA treated with BM-MSCs dissolved in HA have also been investigated, post-surgery (arthroscopy), supporting the amelioration of horse condition after cells injection even after 24 months [72]. When treating naturally occurring OA, there is more variation because duration and severity of the disease vary, and it is difficult to judge whether or not the treatment with MSCs results efficacious and in what extent [73]. Such conditions often lead to a lack of objective conclusions due to, for example, of variation in joints treated and lack of control groups [41]. Comparison between cell treatments and elective drugs has been explored; in detail, the injection of autologous AD-MSC versus steroid drugs (betamethasone) was evaluated up to 180 days [74]. At the end of the period, no inflammatory response was observed in

any groups, and improvements were noticeable in AD-MSC treated horses but not in the one cured with betamethasone and group control. Recently, Broeckx et al. [75] proposed a somehow alternative approach to the therapy of equine degenerative joint disease. Their randomised, double-blinded, and placebo-controlled clinical trial enrolled 75 horses affected by fetlock joint osteoarthritis. The treated group of fifty horses received a single intraarticular injection of blood-derived, allogeneic chondrogenic-induced MSCs. Cells were resuspended in allogeneic plasma. The authors report better scores for treated animals regarding lameness, flexion test, joint effusion both at short (3–18 weeks) and long-term (one year) follow up. The novelty of this study lies in the use of blood-derived MSCs, to replace the most widely used adipose-tissue or bone marrow-derived cells and their combination to allogeneic plasma to improve cell viability, replication, and chondrogenic differentiation. All the MSCs were prepared from a single donor and pre-differentiated at P9; no adverse effects are reported following the application of allogeneic MSCs and plasma.

Table 2. Summary of osteoarthritis (OA) disease treated with MSCs.

Disease	Animal	Treatment	Route and Dosage	Outcome	Ref
AO- hip	Dog (n = 8)	Autologous AD-MSCs in combination with plasma rich in growth factor (PRGF-Endoret)	Intra-articular injection of over 30 × 10^6 AD-MSC	Reduced of lameness and absence of side effects for all the period (six months).	[64]
AO- hip	Dog (n = 15)	Autologous AD-MSCs alone	Intra-articular injection of over 30 × 10^6 AD-MSC	Reduced of lameness only in the first month (less than three months).	[65]
AO- hip	Dog (n = 39)	Comparison between AD-MSCs versus PRGF	Intra-articular injection of 30 × 10^6 AD-MSC	Dog's pain was reduced, physical function was improved, and no side effects were found. AD-MSC showed better results in the period considered (six months).	[67]

AO- hip (coxofemoral joints)	Dog (n = 4)	Autologous AD-MSCs in phosphate-buffered saline (PBS)	Dogs received intra-articular injection of either suspension of 4.2–5 × 10^6 (depending on cell yield) AD-MSCs in 0.6 mL PBS or only 0.6 mL of PBS as a control group	Significant improvement in lameness compared to the control group in the considered period (three months).	[68]
AO-humeroradial (elbow) joints	Dog (n = 14)	Autologous AD-MSCs in phosphate-buffered saline (PBS)	Dogs received an intra-articular injection of 3–5 × 10^6 (depending on cell yield) AD-MSC in 0.6 mL PBS	Significant improvement in lameness, range of motion, and pain on manipulation over time (six months).	[69]

OA-stifle injury (femoral condyles)	Horses (n=10)	Autologous bone marrow (BM)-MSCs in hyaluronan (HA)	Intra-articular injection of either 20×10^6 BMSCs with 22 mg of HA or 22 mg of HA alone	In the period of 12 months: no evidence of clinically significant improvement but arthroscopic evaluation confirmed a significant increase in tissue repair. Immunohistochemical analysis demonstrated more aggrecan levels in the repaired tissue treated with BM-MSC.	[71]
OA	Horses (n=16)	Comparison between autologous AD-MSC versus steroid drugs (Betamethasone)	Intra-articular injection of 3 groups: (1): 1 mL of AD-MSC in normal saline, at a concentration of 5×10^6 cells/mL (2): 1 mL of betamethasone (3): control untreated	No change in lameness at 30 days but reduced at 60 days. At the period of 180 days, improvement remained in AD-MSC group but not in the steroid group. In the control group, the level of lameness did not change.	[74]

OA-degenerated stifle, fetlock, pastern, and coffin joints	Horses (n = 165) In detail: stifle (n = 30), fetlock (n = 58), pastern (n = 34) and coffin (n = 43) joints	Allogenic peripheral blood MSCs with or without chondrogenic induction in combination with PRP	Intra-articular injection. Dosage not stated	Considering 180 weeks period: no adverse effects were noticed, except for three patients. Already after six weeks, 45% (native MSCs) and 60% (chondrogenic-induced MSCs) of the treated patients returned to normality, and the beneficial effects further increased after 18 weeks (78% for native MSCs and 86% for chondrogenic induced MSCs).	[41]
OA-stifle injury (femorotibial lesions (meniscal, cartilage or ligamentous)	Horses (n = 33)	Autologous BM-MSCs post-surgery (arthroscopy)	Intra-articular injection of 15–20 × 10^6 BM-MSC in autologous serum/5% DMSO + HA compared to surgery alone	Considering 24 months of follow up: Improvements in ability were realised with BMSC treatment compared to surgery alone.	[72]
OA-degenerative fetlock joint disease	Horses (n = 75)	Allogeneic chondrogenic induced MSCs added to allogeneic	Intra-articular injection of 2 × 10^6 allogeneic	After long-term follow-up (one year), horses were returned to	[75]

	plasma (EAP)	chondrogenic induced MSCs with EAP	their previous level of work

3.2. Tendon Ligament Injury

Tendon ligament injury (TLI) affects a large part of the equine population ranging from acute traumatic ruptures to chronic overuse and degenerative tendinopathies [76]. The outcomes of conventional therapies are quite often unsatisfactory due to the poor regeneration capacities of tendon tissue in equine species [77,78]. In fact, apart from a primary inflammatory reaction following the injury, spontaneous healing is characterised by fibroplasia and can be referred to as a repair rather than a regeneration process [79]. The repairing system leads to the formation of cellular scar tissue with low extracellular matrix organization, in which stiffness is increased, but elasticity is decreased compared to the original tendon tissue [55,79–81]. Indeed, the primary outcomes investigated to evaluate tendon regeneration are the stiffness, modulus of elasticity, histological score, DNA content, vascularity, and compositional parameters, which could be considered indicators of regeneration, when compared to levels observed in the normal tendon.

In recent years, research has focused on regenerative therapies and tissue engineering approaches, with the aim to recover the original function of the damaged tendon. Typically, as the tendon core lesion is clearly visible by ultrasonography, the application of MSCs is simply performed by injection of the cell suspension directly into the damaged tissue [82]. Specifically, some studies have been conducted to evaluate the role of MSCs on equine tendon healing, injecting cells derived from different sources (mainly adipose tissue and bone marrow), autologous or allogeneic, alone

or associated with other treatments (PRP, HA) [80,83]. Although most of the reports are not blinded or do not provide sufficient information about controls, the literature describes encouraging outcomes, giving evidence of the benefit and safety of MSC application for tendon regeneration [84] MSCs treatment has been described either in healthy animals, in which experimental lesions were induced surgically or by collagenase gel in the superficial digital flexor tendon [80,85]; or in naturally occurring TLI [84,86,87]. Romero et al. evaluated tissue healing in an experimental tendonitis model after administration of autologous bone marrow and adipose tissue-derived MSCs and platelet-rich plasma (PRP). BM-MSCs and PRP produced similar results, although PRP-treatment resulted in higher expression of COL3A1 and ACAN genes, suggesting lower tendon regeneration. Although all the treatments showed beneficial effects compared to the control group, the authors concluded that BM-MSCs might provide better healing properties [88]. Brandao et al. [45] studied the local inflammatory response of tendon injected with autologous or allogeneic AD-MSCs, concluding that no adverse or inflammatory reaction was observed in horses treated with allogeneic cells. Actually, allogeneic cells have been extensively used also for the treatment of naturally occurring tendon lesions supporting the safety of allogeneic cells administration in the horse [85–87,89]. In most clinical studies, outcomes are evaluated comparing results to conventional therapies in term of re-injury rate following the return to activity. Although this approach does not give an accurate indication about the quality of tissue recovery, it provides practical information about the possibility of the animal to return to their previous normal activities. Interestingly, cell treatment resulted in a significantly lower re-injury rate in comparison to conventional therapies. Generally, re-injury rate following traditional treatment such as hyaluronan, beta aminopropionitrile fumarate or polysulfated

glycosaminoglycans, ranges between 23–80% [77,90], while the re-injury rate following MSCs medication is reported to be lower. In this regard, Pacini et al. observed that nine out of 11 racehorses could return to competition without any re-injury event, within a follow-up period of two years [91]. Similar results have been observed in a different clinical report, where after MSCs treatment, the majority of the patients returned to their previous activities, avoiding re-injury [84]. Smith et al. conducted a clinical study on 82 racehorses and 24 other sports horses; after rehabilitation follow-up, only 13–36% of the horses were re-injured, depending on their disciplines [92]. Smith et al. [81] compared the mechanical and morphological characteristics of the tendon extracellular matrix in horses affected by spontaneous tendonitis. BM-MSC treated tendons demonstrated improvements in several parameters compared to not treated tendons, providing evidence on the role of cell therapy on tendon healing in naturally occurring tendonitis. Regarding tendinopathy in canine clinical reports, the scenario is way less documented and investigated than horses; nevertheless, the beneficial effects of MSCs seen in few studies, are quite significant. Although tendonitis has not a high prevalence in dogs, supraspinatus tendinopathy (ST) represents a quite common cause of forelimb lameness. Aetiology is probably related to overuse from chronic repetitive activity. Canapp et al. applied adipose-tissue-derived MSCs in combination with PRP to the treatment of 55 dogs with ST [93]. Based on ultrasonography and objective gait analysis results, the authors suggest that MSCs administration is a promising therapy for ST. More recently, the same group extended the study to the use bone marrow aspirate concentrate (BMAC) combined with PRP, observing positive sonographic results with improvement of tendon size (significant reduction of the affected tendon), fiber pattern and echogenicity, even if only 13.8% dogs treated recovered entirely to a normal fiber pattern at 90 days post-

treatment [94]. This could be related to the short follow-up in comparison to the longer time needed for tendon healing.

Finally, a study made a comparison between BMAC and AD-MSC added to PRP for the therapy of cranial cruciate ligament tear in dogs [94]. In this research, the dogs recruited were different in terms of breeds, age, weight, and sex; the outcomes were based on diagnostic stifle arthroscopy, radiographs, orthopaedic examinations, gait evaluation, and functional questionnaire. Results proved cells efficacy, but there are limitations due to a lack of standardization of PRP preparations the uncertain number of administered cells. This could have affected the outcomes of the two treatments (AD-MSC and BM-MSC). While all these results are encouraging, the long-term success of MSC treatment remains to be proven.

Although semitendinosus myopathy is not tendonitis, this fibrotic musculoskeletal disorder of working dogs affects a muscle whose long tendon is part of the Achilles tendon. Gibson et al. recently conducted a study using a single administration of AD-MSCs to treat semitendinosus myopathy in 11 police dogs, comparing follow-up at six months and one year. At six months follow-up, all patients had returned to work, while at long term follow-up, the dogs were still active in their previous activity, showing an improvement in gait [95]. The authors do not report a recurrence of the disease, and most of the dogs worked until retirement, suggesting a long-term efficacy of the therapy. Table 3 reports all the considered studies regarding TLI treated with MSCs.

Table 3. Summary of tendon ligament injury (TLI) disease treated with MSCs.

Disease	Animal	Treatment	Route and Dosage	Outcome	Ref.
TLI-superficial digital flexor tendon (SDFT)	Horses (n = 8)	AD-MSC suspended in platelet concentrate (PC)	Intralesional administration of 10×10^6 AD-MSC in in 1 mL of PC. 1 mL of PBS was used as a control group	After 16 weeks improvements were reported for AD-MSC group. In detail: decrease of the lesion progression and inflammatory reaction, better organization of collagen fibres, an increase of blood flow. No difference in terms of gene expression was found.	[80]

TLI- SDFT	Horses (n = 141 racehorses)	BM-MSC resuspended in their bone marrow supernatant	Intralesional BM-MSC injection was performed resuspending cells in their bone marrow supernatant at the concentration of 5 × 10^6 cells/mL	Two years follow up: no side effects; the need for reinjury was lower than other published works	[84]
TLI	Horses (n = 6)	Allogeneic AD-MSC	Injection of 100 × 10^6 allogeneic AD-MSCs via atlanto-occipital (AO) and lumbosacral (LS) injection	AD-MSCs administration was safe. No alterations in blood and neurological examinations at any time (30 days) either with AO or LS injections. OA had better distribution.	[86]
TLI	Horses (n = 10)	Allogeneic AD-MSC compared with BM-MSC	Intravenous injections of three doses of 25 × 10^6 allogeneic	After the first injection, horses were followed up for 35 days.	[85]

			AD-MSC and BM-MSC respectively	Evaluation was made on the inflammatory and immune response showing that repeated BM-MSC injection increased blood CD8+ T-cell numbers.	
TLI-SDFT (forelimbs)	Horses (n = 12)	Comparison between autologous AD-MSC, BM-MSC, and platelet-rich plasma (PRP)	Injury injections of 20×10^6 BM-MSCs or AD-MSCs suspended in 7 mL of lactated Ringer's solution (LRS), and 7 mL of PRP. 7mL of LRS was used as control	After 45 weeks, all treatments had beneficial effects, but in detail, data suggest BM-MSCs might be the better approach for tendon healing.	[88]

TLI-suspensory ligament (SL) or superficial digital flexor tendon (SDFT) lesion	Horses (SL n=68) (SDFT n=36)	Tenogenically induced allogeneic Peripheral blood (PB)MSCs combined with PRP	Intralesional injection of 1ml of PB-derived MSCs (containing 2—3 × 10^6) with 1 mL of PRP	In two years, no adverse effects have been observed. At 12 weeks, results were convincing in lesions improvement where about 80% of both SL and SDFT groups went back to their previous performance.	[87]
TLI-SDFT	Horses (n = 11)	Autologous BM-MSC	Injections of at least 1 × 10^6 of BM-MSCs were re-suspended in 1.5 mL of autologous serum	Patients were back to their sports activities, without having suffered a re-injury.	[91]

TLI-SDFT	Horses (n = 12)	Autologous BM-MSC suspended in 2 mL of BM supernatant	Implantation of 10×10^6 BM-MSCs were suspended in 2 mL of citrated BM supernatant. 2 mL of PBS were used as a control group	In six months, there were significant benefits in terms of safety and healing tendon process (reduced stiffness, histological showed better organization and reduction in re-injury rate).	[81]
TLI-supraspinatus tendinopathy	Dogs (n = 41)	BM-MSCs in combination with PRP	Ultrasound-guided intratendineous injection of BM-MSCs with PRP (1:1 ratio)	On 90 days post-treatment: in most cases, the fibre pattern and echogenicity have improved, while only a minority resolved fibre pattern and echogenicity abnormalities.	[96]

TLI- partial cranial cruciate ligament tear	Dogs (n = 36) 19 cases received BM-MSC while 17 cases received AD-MSC	Autologous BM-MSCs vs AD-MSCs were combined with platelet-rich plasma (PRP) in 1:1 ratio when injected.	2–4mL of BM-MSCs + PRP or 1–2mL of AD-MSCs + PRP was injected intra-articularly into the stifle (volume depended on the dog's size)	Neither treatment was superior to the other in terms of outcome (90 days).	[94]

3.3. Intervertebral Disk Degeneration

Intervertebral disk degeneration (IVDD) is a complex multifactorial process considered as the primary cause of lower back pain in humans. Since intervertebral disk degeneration is incurable, all available treatment strategies are mainly focused on pain relief only [97]. Therefore, efforts are dedicated to the development of strategies able to regenerate, or at least repair, and preserve the functioning of the intervertebral disk structure. Among these, intradiscal injection of MSCs has become highly topical in experimental and clinical investigations.

Dogs with IVDD are the only patients where medical and surgical approaches similar to humans are used [63]. For this reason, canine IVDD is considered a valuable and reliable disease model for the investigations of novel and effective healing treatment for human IVDD. In a recent study by Steffen et al. [98], six dogs suffering from naturally occurring degenerative disc disease received autologous bone-marrow-derived MSCs. Although results showed no adverse effects, the authors were not able to demonstrate

by MRI any apparent regenerative effect of the treatment. This work was pioneering in naturally occurring IVDD, thus negative result may be caused by biological and biomechanical differences between injury-induced and naturally occurring IVD degeneration. To improve the therapeutic approach, the authors, in a following study [99], introduced collagen microcarriers as a scaffold for MSCs. Twenty dogs affected by spontaneous lumbosacral IVD degeneration confirmed by MRI and clinical signs (lumbosacral back pain) were included in the study. Autologous MSCs were isolated from bone marrow and, before the injection, MSCs were mixed with collagen microcarriers, as a delivery system, with or without TGF-β1 crosslinking. After decompressing surgery, dogs were divided into three groups, which received three different intradiscal injections of 1) intradiscal injection of MSC-microcarriers, 2) MSC-TGF-β1-microcarriers, of 3) microcarriers only. Clinical performance and Pfirrmann grading, assessed through magnetic resonance imaging, were evaluated at 10 months after the injection. In vivo injection was successful in all dogs, and clinical functioning returned to normality. However, post-operative Pfirrmann grade remained unchanged in all dogs, and the undesired side-effect formation of Schmorl's nodes occurred in 45% of the dogs. This side effect was reduced by halving the injection volume. Therefore, clinical improvement was observed in all groups, despite the formation of Schmorl's nodes, but microcarriers and MSCs failed to regenerate the structure of degenerated IVD [99]. A successful work was conducted using fetal allogeneic BM-MSCs on seven dogs in which, by the end of the period of 90 days, all dogs had an improvement in functional movements and were able to take steps; moreover, none of them presented adverse symptoms at any time [100]. Two years later, a randomized control case report was conducted on 34 dogs suffering from IVDD disorder with no deep pain; in this study, surgery was evaluated alone and in combination

with transplantation of allogenic AD-MSC into the spinal cord. Neurological progress was noticed, and the success rate for the AD-MSCs group was significantly higher (77.8%) than surgery alone, thus demonstrating the potential therapeutic efficacy of MSCs [101].

Even though the use of MSCs in veterinary regenerative medicine for IVDD treatment seems to be promising, as mentioned above, there are also clinical results that suggest that MSCs are not always capable of repairing the damaged tissue, at least using the therapeutic protocols proposed so far [102]. Table 4 reports all the considered studies regarding IVDD treated with MSCs.

Table 4. Summary of intervertebral disk degeneration (IVDD) disorders treated with MSCs.

Disease	Animal	Treatment	Route and Dosage	Outcome	Ref
IVDD	Dog (n = 6)	Autologous BM-MSCs	Intradiscal injection of 2×10^6 BM-MSCs suspended in 1 mL 10% autologous plasma in PBS. Only PSB solution was used for group control	Twelve months after treatment: even if the injection was well tolerated with no side effects, no successful treatment was found in any dogs.	[98]
IVDD lumbosacral	Dog (n = 20)	Autologous BM-MSCs	Intradiscal injection of 3×10^6 was applied in three		

			different groups (1) intradiscal injection of MSC-microcarriers (n = 11), (2) MSC-TGF-β1 microcarriers (n = 6), and (3) microcarriers only during a decompressing spinal surgery (n = 3)	Ten months after treatment: injection was successful in all dogs; thus, they returned to normality. Schmorl's nodes were found as side effects.	[99]
IVDD-chronic spinal cord injury	Dog (n = 39)	Allogeneic fetal BM-MSCs	Intramedullary injection of 1×10^6 allogeneic BM-MSCs	Ninety days evaluation showed no side effects, increased movement of the hind limbs, and increased locomotory function.	[100]

IVDDThoracolumbar intervertebral disc diseas	Dog (n = 34)	Allogeneic AD-MSCs + surgery	Intraoperative intraspinal allogeneic AD-MSCs of 1×10^7 cells	Six months after treatment: Improvement in the neurological exam and better endpoint with AD-MSCs application rather than surgery only.	[101]

4. Animal Spontaneous Pathologies as Potential Preclinical Models for Human Therapy

Experimental animal models are still widely used to study biological properties and therapeutic potential of MSCs in regenerative medicine. From this point of view, a key point is the choice of the animal species to develop a useful and scientifically relevant model. Resorting to laboratory animal species (mice, rats, rabbits) to establish the safety and efficacy of novel therapeutic strategies leads to the use of induced experimental models very far from the clinical reality of human medicine, making their use uninformative and leading to the sacrifice of a high number of animal lives. This aspect is in contrast with the European Parliament directive (Directive 2010/63/EU) which limits the use of animal models and suggests to the scientific community the use of alternative methods, as a result of the 3Rs principle promoted by

Russell and Burch in 1959 [103].

Using spontaneous animal pathologies may be a strategy. Specifically, referring to naturally occurring, spontaneous diseases of domestic animals (primarily dog, cat and horse) allow using model diseases much more similar to human ones from pathogenesis, evolution and biological mechanisms of healing. Thus, companion animal clinical models represent an important contribution to human studies [104]; indeed, similarities concerning symptoms, etiopathology, biomarkers [105] and even genetic [63] can be found with the human counterpart. Also, dogs and cats share with humans the living environment and underlying pathologies (e.g., obesity, diabetes) which often influence the pathological onset, evolution, and healing processes. Finally, their relatively long-life expectancies make companion animals a model for long-term studies. Using spontaneous pathologies of these animals for the development of innovative regenerative therapies is, therefore, of extreme interest forhuman and veterinary medicine, thus avoiding experimental animal models.

Musculoskeletal disorders are an important example of this concept. Cell therapies based on the application of MSCs aim to regenerate damaged tissues exploiting tissue's intrinsic potential for repair. The complexity of the healing processes induced by MSCs makes it necessary to use natural pathologies (and not experimentally induced disease models) to understand the real therapeutic potential of the cells. In dogs and horses, musculoskeletal disorders have a high prevalence and are considered quite similar to those developed in humans. Innovative cell therapies for osteoarthritis, tendonitis, and intervertebral disk diseases are actively investigated in veterinary medicine, providing useful therapeutic protocols for human medicine [106]. A further advantage of the use of spontaneous diseases to assess the efficacy of MSCs treatment is not only that experimental animals are

preserved but affected companion animals enrolled in the studies can receive up-to-date therapeutic opportunity and long-term follow-up.

5. Secretome and Extracellular Vesicles as a Potential Therapy for Different Disease Areas

During the last decade, it has been demonstrated that MSCs therapeutic effectiveness is mainly due to the release of paracrine factors, named secretome, composed of free soluble factors (including cytokines, chemokines, and growth factors) and non-soluble nano/microstructured extracellular vesicles (EVs) [107,108]. Several studies support the hypothesis that the EVs fraction alone may be sufficient to heal the injured tissue or prevent tissue damage in several contexts [49]. EVs isolated from MSCs exhibit the same functions as stem cells, for example, their anti-inflammatory and pro-regenerative activity [2,109,110]; but they also can elide some issues related to the usage of the whole stem cell. In detail, they have lower immunogenicity, smaller size, and so they could represent a safer alternative compared to the cell injection [111–113]. Despite these advantages, more studies need to be conducted to elucidate kinetics, mechanisms of action, bioavailability (including factors like dosage and frequency), and route of administration. EVs delivery could be provided by using suitable materials and methods such as the encapsulation within hydrogel or scaffold, improving EVs immobilization plus frequency and dosage of administration.

However, this approach, especially in the veterinary sphere, is still in its early stages. Only recently, the therapeutic use of the MSCs-secretome, instead of the parental cells, has been proposed for veterinary applications, also overcoming the practical difficulties related to stem cell application. In detail, based on the hypothesis that cells may promote tendon repair via paracrine factors, an interesting study has been recently published regarding the

secretome profile in eight dogs [114]. In detail, exosomes and soluble factor derived from BM-MSCs and AD-MSCs of the same canine donor have been described and compared for the first time, paying attention also to their immunomodulatory capacity. Both cells types share analogy as morphology, but they also have their biological features such as gene expression and proliferation and differentiation. Outcomes showed a higher proliferation rate for AD-MSCs, whereas the production of exosomes and soluble factors, comprising several cytokines, was more active in BM-MSCs. These results were also confirmed by the proteomic analysis. The limitation of this work was the small number and size of the animal model; nevertheless, it is the first step toward secretome characterisation and application [115]. In this contest, El-Tookhy et al. investigated the exosome and microvesicles role in wounds healing process of experimentally induced critical size defects in six dogs. Wound reduction size was observed in 14 days comparing skin area treated with exosomes and the one treated with PBS as a control group. As expected, photographs and histopathological evaluation showed better and faster endpoints of the healing process in dogs treated with exosomes, in particular about the formation of extracellular matrix, angiogenesis, and re-epithelization. The findings underline the efficacy and safety of cell-free therapy in wound repair, paving the way for future new therapy approach that overcome the limitations associated with the use of cells implantation [116].

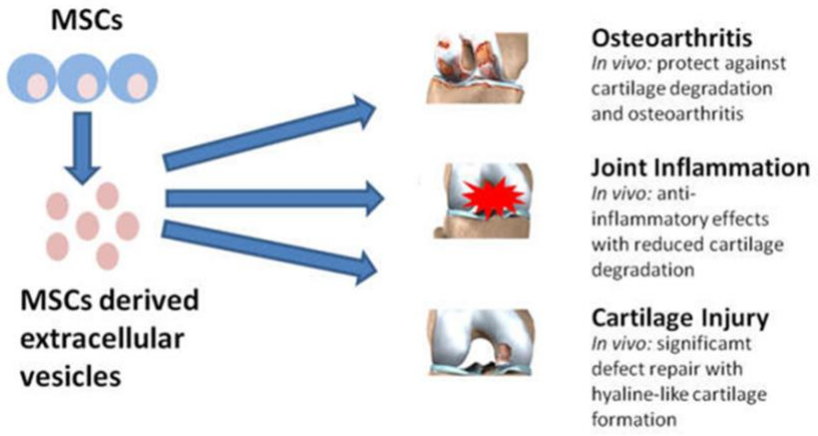

Figure 2. Regarding the human field, stem-cell-derived extracellular vesicles (EVs) can exert a multitude of beneficial effects in the treatment of osteoarthritis, joint inflammation, and cartilage or osteochondral injury. (Modified from Phinney, D.G. [120]).

A key aspect which is missing for EVs and/or secretome pharmaceuticalization is a standardised, reproducible and GMP-compliant production process, in order to obtain validate products suitable for future clinical trials. Isolation method and characterization process are reported in human literature, but unfortunately, in the veterinary field, more evidence is required to confirm the feasibility of this innovative cell-free treatment [2].

6. Conclusions

MSCs belong to body repair system and are defined as multipotent progenitor cells able to self-replicate and to differentiate into different cell types, demonstrating significant potential in clinical use. In the veterinary field, many studies have been conducted for the development of the most effective procedures for MSC-based treatment, taking into consideration cell tissue sources, isolation

process, culturing conditions, cryopreservation, cell dosage, administration route, and frequency. As a matter of fact, in the last decade, MSCs have emerged as a promising therapeutic tool for the treatment of musculoskeletal pathologies in veterinary medicine. Interestingly, the results accumulated so far have provided evidence that veterinary patients affected by naturally occurring diseases should provide more reliable outcomes of cell therapy than laboratory animals, thus allowing translating potential therapies to the human field. More recently, a cell-free therapy based on MSC-secretome has been proposed. Even though there are very few clinical reports to refer to in veterinary medicine, recent acquisitions suggest that MSC-derived products may have major advantages compared to the related cells, e.g., they are considered safer and less immunogenic. Although several studies propose secretome as a novel therapeutic biological product, a better understanding of the nature, bioavailability, and the mechanisms of action responsible for the beneficial effects of the paracrine molecules is needed. Based on these sceneries, a secretome GMP-compliant production process is needed for veterinary clinical use and further studies on in vivo animal models; indeed, a veterinary medicinal product based on stable secretome formulation represents a valid strategy for MSDs therapy.

References

1. De Girolamo, L.; Lucarelli, E.; Alessandri, G.; Avanzini, M.A.; Bernardo, M.E.; Biagi, E.; Brini, A.T.; D'Amico, G.; Fagioli, F.; Ferrero, I.; et al. Mesenchymal Stem/Stromal Cells: A New "Cells as Drugs" Paradigm. Efficacy and Critical Aspects in Cell Therapy. Curr. Pharm. Des. 2013, 19, 2459–2473. [CrossRef]
2. Bari, E.; Perteghella, S.; Di Silvestre, D.; Sorlini, M.; Catenacci, L.; Sorrenti, M.; Marrubini, G.; Rossi, R.; Tripodo, G.; Mauri, P.; et al. Pilot Production of Mesenchymal Stem/Stromal Freeze-Dried Secretome for Cell-Free Regenerative Nanomedicine: A Validated GMP-Compliant Process. Cells 2018, 7, 190. [CrossRef]

3. Robey, P. “Mesenchymal stem cells”: Fact or fiction, and implications in their therapeutic use. F1000Research 2017, 6. [CrossRef]

4. Katsuda, T.; Kosaka, N.; Takeshita, F.; Ochiya, T. The therapeutic potential of mesenchymal stem cell-derived extracellular vesicles. Proteomics 2013, 13, 1637–1653. [CrossRef]

5. Kidd, S.; Spaeth, E.; Dembinski, J.L.; Dietrich, M.; Watson, K.; Klopp, A.; Battula, V.L.; Weil, M.; Andreeff, M.; Marini, F.C. Direct Evidence of Mesenchymal Stem Cell Tropism for Tumor and Wounding Microenvironments Using In Vivo Bioluminescent Imaging. Stem Cells 2009, 27, 2614–2623. [CrossRef]

6. Da Silva Meirelles, L.; Chagastelles, P.C.; Nardi, N.B. Mesenchymal stem cells reside in virtually all post-natal organs and tissues. J. Cell Sci. 2006, 119, 2204–2213. [CrossRef] [PubMed]

7. Tessier, L.; Bienzle, D.; Williams, L.B.; Koch, T.G. Phenotypic and Immunomodulatory Properties of Equine Cord Blood-Derived Mesenchymal Stromal Cells. PLOS ONE 2015, 10, e0122954. [CrossRef] [PubMed]

8. Duan, W.; Lopez, M.J.; Hicok, K. Adult multipotent stromal cell cryopreservation: Pluses and pitfalls. Vet. Surg. 2018, 47, 19–29. [CrossRef] [PubMed]

9. Barrachina, L.; Romero, A.; Zaragoza, P.; Rodellar, C.; Vazquez, F.J. Practical considerations for clinical use of mesenchymal stem cells: From the laboratory to the horse. Vet. J. 2018, 238, 49–57. [CrossRef] [PubMed]

10. Orbay, H.; Tobita, M.; Mizuno, H. Mesenchymal Stem Cells Isolated from Adipose and Other Tissues: Basic Biological Properties and Clinical Applications. Stem Cells Int. 2012. [CrossRef] [PubMed]

11. Sacchetti, B.; Funari, A.; Remoli, C.; Giannicola, G.; Kogler, G.; Liedtke, S.; Cossu, G.; Serafini, M.; Sampaolesi, M.; Tagliafico, E.; et al. No Identical “Mesenchymal Stem Cells” at Different Times and Sites: Human Committed Progenitors of Distinct Origin and Differentiation Potential Are Incorporated as Adventitial Cells in Microvessels. Stem Cell Rep. 2016, 6, 897–913. [CrossRef] [PubMed]

12. Iacono, E.; Merlo, B.; Romagnoli, N.; Rossi, B.; Ricci, F.; Spadari, A. Equine Bone Marrow and Adipose Tissue Mesenchymal Stem Cells:

Cytofluorimetric Characterization, In Vitro Differentiation, and Clinical Application. J. Equine Vet. Sci. 2015, 35, 130–140. [CrossRef]

13. Bearden, R.N.; Huggins, S.S.; Cummings, K.J.; Smith, R.; Gregory, C.A.; Saunders, W.B. In-vitro characterization of canine multipotent stromal cells isolated from synovium, bone marrow, and adipose tissue: A donor-matched comparative study. Stem Cell Res. Ther. 2017, 8. [CrossRef] [PubMed]
14. Toupadakis, C.A.; Wong, A.; Genetos, D.C.; Cheung, W.K.; Borjesson, D.L.; Ferraro, G.L.; Galuppo, L.D.; Leach, J.K.; Owens, S.D.; Yellowley, C.E. Comparison of the osteogenic potential of equine mesenchymal stem cells from bone marrow, adipose tissue, umbilical cord blood, and umbilical cord tissue. Am. J. Vet. Res. 2010, 71, 1237–1245. [CrossRef]
15. Vidal, M.A.; Kilroy, G.E.; Lopez, M.J.; Johnson, J.R.; Moore, R.M.; Gimble, J.M. Characterization of equine adipose tissue-derived stromal cells: Adipogenic and osteogenic capacity and comparison with bone marrow-derived mesenchymal stromal cells. Vet. Surg. 2007, 36, 613–622. [CrossRef]
16. Giovannini, S.; Brehm, W.; Mainil-Varlet, P.; Nesic, D. Multilineage differentiation potential of equine blood-derived fibroblast-like cells. Differentiation 2008, 76, 118–129. [CrossRef]
17. Del Bue, M.; Ricco, S.; Ramoni, R.; Conti, V.; Gnudi, G.; Grolli, S. Equine adipose-tissue derived mesenchymal stem cells and platelet concentrates: Their association in vitro and in vivo. Vet. Res. Commun. 2008, 32, S51–S55. [CrossRef]
18. Martinello, T.; Bronzini, I.; Maccatrozzo, L.; Mollo, A.; Sampaolesi, M.; Mascarello, F.; Decaminada, M.; Patruno, M. Canine adipose-derived-mesenchymal stem cells do not lose stem features after a long-term cryopreservation. Res. Vet. Sci. 2011, 91, 18–24. [CrossRef]
19. Jezierska-Wozniak, K.; Nosarzewska, D.; Tutas, A.; Mikolajczyk, A.; Oklinski, M.; Jurkowski, M.K. Use of adipose tissue as a source of mesenchymal stem cells. Postepy Hig. Med. Dosw. 2010, 64, 326–332.
20. Nava, S.; Sordi, V.; Pascucci, L.; Tremolada, C.; Ciusani, E.; Zeira, O.; Cadei, M.; Soldati, G.; Pessina, A.; Parati, E.; et al. Long-Lasting Anti-Inflammatory Activity of Human Microfragmented Adipose Tissue. Stem Cells Int. 2019, 2019, 5901479. [CrossRef]

21. You, D.; Jang, M.J.; Kim, B.H.; Song, G.; Lee, C.; Suh, N.; Jeong, I.G.; Ahn, T.Y.; Kim, C.-S. Comparative Study of Autologous Stromal Vascular Fraction and Adipose-Derived Stem Cells for Erectile Function Recovery in a Rat Model of Cavernous Nerve Injury. Stem Cells Transl. Med. 2015, 4, 351–358. [CrossRef] [PubMed]

22. Kemilew, J.; Sobczyska-Rak, A.; Zyliska, B.; Szponder, T.; Nowicka, B.; Urban, B. The Use of Allogenic Stromal Vascular Fraction (SVF) Cells in Degenerative Joint Disease of the Spine in Dogs. In Vivo 2019, 33, 1109–1117. [CrossRef] [PubMed]

23. Minteer, D.; Marra, K.G.; Rubin, J.P. Adipose-Derived Mesenchymal Stem Cells: Biology and Potential Applications. Mesenchymal Stem Cells Basics Clin. Appl. I 2013, 129, 59–71. [CrossRef]

24. Kuznetsov, S.A.; Mankani, M.H.; Gronthos, S.; Satomura, K.; Bianco, P.; Robey, P.G. Circulating skeletal stem cells. J. Cell Biol. 2001, 153, 1133–1139. [CrossRef] [PubMed]

25. Roufosse, C.A.; Direkze, N.C.; Otto, W.R.; Wright, N.A. Circulating mesenchymal stem cells. Int. J. Biochem. Cell Biol. 2004, 36, 585–597. [CrossRef]

26. Koerner, J.; Nesic, D.; Romero, J.D.; Brehm, W.; Mainil-Varlet, P.; Grogan, S.P. Equine peripheral blood-derived progenitors in comparison to bone marrow-derived mesenchymal stem cells. Stem Cells 2006, 24, 1613–1619. [CrossRef]

27. Santos, V.H.; Pfeifer, J.P.H.; de Souza, J.B.; Milani, B.H.G.; de Oliveira, R.A.; Assis, M.G.; Deffune, E.; Moroz, A.; Alves, A.L.G. Culture of mesenchymal stem cells derived from equine synovial membrane in alginate hydrogel microcapsules. BMC Vet. Res. 2018, 14. [CrossRef]

28. Kern, S.; Eichler, H.; Stoeve, J.; Klueter, H.; Bieback, K. Comparative analysis of mesenchymal stem cells from bone marrow, umbilical cord blood, or adipose tissue. Stem Cells 2006, 24, 1294–1301. [CrossRef]

29. Schuh, E.M.; Friedman, M.S.; Carrade, D.D.; Li, J.; Heeke, D.; Oyserman, S.M.; Galuppo, L.D.; Lara, D.J.; Walker, N.J.; Ferraro, G.L.; et al. Identification of variables that optimize isolation and culture of multipotent mesenchymal stem cells from equine umbilical-cord blood. Am. J. Vet. Res. 2009, 70, 1526–1535. [CrossRef]

30. Iacono, E.; Lanci, A.; Merlo, B.; Ricci, F.; Pirrone, A.; Antonelli, C.; Mariella, J.; Castagnetti, C. Effects of amniotic fluid mesenchymal stem cells in carboxymethyl cellulose gel on healing of spontaneous pressure sores: Clinical outcome in seven hospitalized neonatal foals. Turk. J. Biol. 2016, 40, 484–492. [CrossRef]

31. Iacono, E.; Brunori, L.; Pirrone, A.; Pagliaro, P.P.; Ricci, F.; Tazzari, P.L.; Merlo, B. Isolation, characterization and differentiation of mesenchymal stem cells from amniotic fluid, umbilical cord blood and Wharton's jelly in the horse. Reproduction 2012, 143, 455–468. [CrossRef] [PubMed]

32. Passeri, S.; Nocchi, F.; Lamanna, R.; Lapi, S.; Miragliotta, V.; Giannessi, E.; Abramo, F.; Stornelli, M.R.; Matarazzo, M.; Plenteda, D.; et al. Isolation and expansion of equine umbilical cord-derived matrix cells (EUCMCs). Cell Biol. Int. 2009, 33, 100–105. [CrossRef] [PubMed]

33. Ranera, B.; Lyahyai, J.; Romero, A.; Jose Vazquez, F.; Rosa Remacha, A.; Luisa Bernal, M.; Zaragoza, P.; Rodellar, C.; Martin-Burriel, I. Immunophenotype and gene expression profiles of cell surface markers of mesenchymal stem cells derived from equine bone marrow and adipose tissue. Vet. Immunol. Immunopathol. 2011, 144, 147–154. [CrossRef] [PubMed]

34. Vidal, M.A.; Walker, N.J.; Napoli, E.; Borjesson, D.L. Evaluation of Senescence in Mesenchymal Stem Cells Isolated from Equine Bone Marrow, Adipose Tissue, and Umbilical Cord Tissue. Stem Cells Dev. 2012, 21, 273–283. [CrossRef] [PubMed]

35. Naskou, M.C.; Sumner, S.M.; Chocallo, A.; Kemelmakher, H.; Thoresen, M.; Copland, I.; Galipeau, J.; Peroni, J.F. Platelet lysate as a novel serum-free media supplement for the culture of equine bone marrow-derived mesenchymal stem cells. Stem Cell Res. Ther. 2018, 9. [CrossRef]

36. Russell, K.A.; Koch, T.G. Equine platelet lysate as an alternative to fetal bovine serum in equine mesenchymal stromal cell culture—Too much of a good thing? Equine Vet. J. 2016, 48, 261–264. [CrossRef]

37. Bari, E.; Perteghella, S.; Farago, S.; Torre, M.L. Association of silk sericin and platelet lysate: Premises for the formulation of wound healing active medications. Int. J. Biol. Macromol. 2018, 119, 37–47. [CrossRef]

38. Verdanova, M.; Pytlik, R.; Kalbacova, M.H. Evaluation of Sericin as a Fetal Bovine Serum-Replacing Cryoprotectant During Freezing of Human Mesenchymal Stromal Cells and Human Osteoblast-Like Cells. Biopreserv. Biobank. 2014, 12, 99–105. [CrossRef]

39. Espina, M.; Juelke, H.; Brehm, W.; Ribitsch, I.; Winter, K.; Delling, U. Evaluation of transport conditions for autologous bone marrow-derived mesenchymal stromal cells for therapeutic application in horses. PeerJ 2016, 4. [CrossRef]

40. Garvican, E.R.; Cree, S.; Bull, L.; Smith, R.K.W.; Dudhia, J. Viability of equine mesenchymal stem cells during transport and implantation (vol 5, 94, 2014). Stem Cell Res. Ther. 2016, 7. [CrossRef]

41. Broeckx, S.; Suls, M.; Beerts, C.; Vandenberghe, A.; Seys, B.; Wuertz-Kozak, K.; Duchateau, L.; Spaas, J.H. Allogenic Mesenchymal Stem Cells as a Treatment for Equine Degenerative Joint Disease: A Pilot Study. Curr. Stem Cell Res. Ther. 2014, 9, 497–503. [CrossRef] [PubMed]

42. Mercati, F.; Pascucci, L.; Curina, G.; Scocco, P.; Tardella, F.M.; Dall'Aglio, C.; Marini, C.; Ceccarelli, P. Evaluation of storage conditions on equine adipose tissue-derived multipotent mesenchymal stromal cells. Vet. J. 2014, 200, 339–342. [CrossRef]

43. Bronzini, I.; Patruno, M.; Iacopetti, I.; Martinello, T. Influence of temperature, time and different media on mesenchymal stromal cells shipped for clinical application. Vet. J. 2012, 194, 121–123. [CrossRef] [PubMed]

44. Zhang, N.; Dietrich, M.A.; Lopez, M.J. Therapeutic Doses of Multipotent Stromal Cells from Minimal Adipose Tissue. Stem Cell Rev. Rep. 2014, 10, 600–611. [CrossRef]

45. Martinello, T.; Bronzini, I.; Maccatrozzo, L.; Iacopetti, I.; Sampaolesi, M.; Mascarello, F.; Patruno, M. Cryopreservation Does Not Affect the Stem Characteristics of Multipotent Cells Isolated from Equine Peripheral Blood. Tissue Eng. Part C Methods 2010, 16, 771–781. [CrossRef] [PubMed]

46. Torre, M.L.; Lucarelli, E.; Guidi, S.; Ferrari, M.; Alessandri, G.; De Girolamo, L.; Pessina, A.; Ferrero, I.; Gism. Ex Vivo Expanded Mesenchymal Stromal Cell Minimal Quality Requirements for Clinical Application. Stem Cells Dev. 2015, 24, 677–685. [CrossRef] [PubMed]

47. Williams, L.B.; Russell, K.A.; Koenig, J.B.; Koch, T.G. Aspiration, but not injection, decreases cultured equine mesenchymal stromal cell viability. BMC Vet. Res. 2016, 12. [CrossRef]

48. Schnabel, L.V.; Fortier, L.A.; McIlwraith, C.W.; Nobert, K.M. Therapeutic use of stem cells in horses: Which type, how, and when? Vet. J. 2013, 197, 570–577. [CrossRef]

49. Sole, A.; Spriet, M.; Galuppo, L.D.; Padgett, K.A.; Borjesson, D.L.; Wisner, E.R.; Brosnan, R.J.; Vidal, M.A. Scintigraphic evaluation of intra-arterial and intravenous regional limb perfusion of allogeneic bone marrow-derived mesenchymal stem cells in the normal equine distal limb using 99mTc-HMPAO. Equine Vet. J. 2012, 44, 594–599. [CrossRef]

50. Siegel, G.; Kluba, T.; Hermanutz-Klein, U.; Bieback, K.; Northoff, H.; Schaefer, R. Phenotype, donor age and gender affect function of human bone marrow-derived mesenchymal stromal cells. BMC Med. 2013, 11. [CrossRef]

51. Carrade, D.D.; Owens, S.D.; Galuppo, L.D.; Vidal, M.A.; Ferraro, G.L.; Librach, F.; Buerchler, S.; Friedman, M.S.; Walker, N.J.; Borjesson, D.L. Clinicopathologic findings following intra-articular injection of autologous and allogeneic placentally derived equine mesenchymal stem cells in horses. Cytotherapy 2011, 13, 419–430. [CrossRef] [PubMed]

52. Shah, K.; Drury, T.; Roic, I.; Hansen, P.; Malin, M.; Boyd, R.; Sumer, H.; Ferguson, R. Outcome of Allogeneic Adult Stem Cell Therapy in Dogs Suffering from Osteoarthritis and Other Joint Defects. Stem Cells Int. 2018, 2018, 7309201. [CrossRef] [PubMed]

53. Guest, D.J.; Smith, M.R.W.; Allen, W.R. Monitoring the fate of autologous and allogeneic mesenchymal progenitor cells injected into the superficial digital flexor tendon of horses: Preliminary study. Equine Vet. J. 2008, 40, 178–181. [CrossRef] [PubMed]

54. Brandao, J.S.; Alvarenga, M.L.; Hubbe Pfeifer, J.P.; dos Santos, V.H.; Fonseca-Alves, C.E.; Rodrigues, M.; Laufer-Amorim, R.; Lucas Castillo, J.A.; Garcia Alves, A.L. Allogeneic mesenchymal stem cell transplantation in healthy equine superficial digital flexor tendon: A study of the local inflammatory response. Res. Vet. Sci. 2018, 118, 423–430. [CrossRef] [PubMed]

55. Brehm, W.; Burk, J.; Delling, U.; Gittel, C.; Ribitsch, I. Stem cell-based tissue engineering in veterinary orthopaedics. Cell Tissue Res. 2012, 347, 677–688. [CrossRef]

56. Gala, K.; Burdzinska, A.; Idziak, M.; Wilczek, E.; Paczek, L. Transplantation of mesenchymal stem cells into the skeletal muscle induces cytokine generation. Cytokine 2013, 64, 243–250. [CrossRef]

57. Zayed, M.; Adair, S.; Ursini, T.; Schumacher, J.; Misk, N.; Dhar, M. Concepts and challenges in the use of mesenchymal stem cells as a treatment for cartilage damage in the horse. Res. Vet. Sci. 2018, 118, 317–323. [CrossRef]

58. Litzke, L.F.; Wagner, E.; Baumgaertner, W.; Hetzel, U.; Josimovic-Alasevic, O.; Libera, J. Repair of extensive articular cartilage defects in horses by autologous chondrocyte transplantation. Ann. Biomed. Eng. 2004, 32, 57–69. [CrossRef]

59. Sasaki, A.; Mizuno, M.; Ozeki, N.; Katano, H.; Otabe, K.; Tsuji, K.; Koga, H.; Mochizuki, M.; Sekiya, I. Canine mesenchymal stem cells from synovium have a higher chondrogenic potential than those from infrapatellar fat pad, adipose tissue, and bone marrow. PLoS ONE 2018, 13, e0202922. [CrossRef]

60. Lim, J.K.; Hui, J.; Li, L.; Thambyah, A.; Goh, J.; Lee, E.H. Enhancement of tendon graft osteointegration using mesenchymal stem cells in a rabbit model of anterior cruciate ligament reconstruction. Arthrosc. J. Arthrosc. Relat. Surg. 2004, 20, 899–910. [CrossRef]

61. Zeira, O.; Scaccia, S.; Pettinari, L.; Ghezzi, E.; Asiag, N.; Martinelli, L.; Zahirpour, D.; Dumas, M.P.; Konar, M.; Lupi, D.M.; et al. Intra-Articular Administration of Autologous Micro-Fragmented Adipose Tissue in Dogs with Spontaneous Osteoarthritis: Safety, Feasibility, and Clinical Outcomes. Stem Cells Transl. Med. 2018, 7, 819–828. [CrossRef] [PubMed]

62. Guercio, A.; Di Marco, P.; Casella, S.; Cannella, V.; Russotto, L.; Purpari, G.; Di Bella, S.; Piccione, G. Production of canine mesenchymal stem cells from adipose tissue and their application in dogs with chronic osteoarthritis of the humeroradial joints. Cell Biol. Int. 2012, 36, 189–194. [CrossRef] [PubMed]

63. Hoffman, A.M.; Dow, S.W. Concise Review: Stem Cell Trials Using Companion Animal Disease Models. Stem Cells 2016, 34, 1709–1729. [CrossRef] [PubMed]

64. Vilar, J.M.; Morales, M.; Santana, A.; Spinella, G.; Rubio, M.; Cuervo, B.; Cugat, R.; Carrillo, J.M. Controlled, blinded force platform analysis of the effect of intraarticular injection of autologous adipose-derived mesenchymal stem cells associated to PRGF-Endoret in osteoarthritic dogs. BMC Vet. Res. 2013, 9. [CrossRef]

65. Vilar, J.M.; Batista, M.; Morales, M.; Santana, A.; Cuervo, B.; Rubio, M.; Cugat, R.; Sopena, J.; Carrillo, J.M. Assessment of the effect of intraarticular injection of autologous adipose-derived mesenchymal stem cells in osteoarthritic dogs using a double blinded force platform analysis. BMC Vet. Res. 2014, 10. [CrossRef]

66. Amable, P.R.; Vieira Carias, R.B.; Telles Teixeira, M.V.; Pacheco, I.d.C.; Farias Correa do Amaral, R.J.; Granjeiro, J.M.; Borojevic, R. Platelet-rich plasma preparation for regenerative medicine: Optimization and quantification of cytokines and growth factors. Stem Cell Res. Ther. 2013, 4. [CrossRef]

67. Cuervo, B.; Rubio, M.; Sopena, J.; Manuel Dominguez, J.; Vilar, J.; Morales, M.; Cugat, R.; Maria Carrillo, J. Hip Osteoarthritis in Dogs: A Randomized Study Using Mesenchymal Stem Cells from Adipose Tissue and Plasma Rich in Growth Factors. Int. J. Mol. Sci. 2014, 15, 13437–13460. [CrossRef]

68. Black, L.L.; Gaynor, J.; Gahring, D.; Adams, C.; Aron, D.; Harman, S.; Gingerich, D.A.; Harman, R. Effect of adipose-derived mesenchymal stem and regenerative cells on lameness in dogs with chronic osteoarthritis of the coxofemoral joints: A randomized, double-blinded, multicenter, controlled trial. Vet. Ther. 2007, 8, 272–284.

69. Black, L.; Gaynor, J.; Adams, C.; Dhupa, S.; Sams, A.; Taylor, R.; Harman, S.; Gingerich, D.; Harman, R. Effect of Intraarticular Injection of Autologous Adipose-Derived Mesenchymal Stem and Regenerative Cells on Clinical Signs of Chronic Osteoarthritis of the Elbow Joint in Dogs. Vet. Ther. 2008, 9, 192–200.

70. Bogers, S.H. Cell-Based Therapies for Joint Disease in Veterinary Medicine: What We Have Learned and What We Need to Know. Front. Vet. Sci. 2018, 5. [CrossRef]

71. McIlwraith, C.W.; Frisbie, D.D.; Rodkey, W.G.; Kisiday, J.D.; Werpy, N.M.; Kawcak, C.E.; Steadman, J.R. Evaluation of Intra-Articular Mesenchymal Stem Cells to Augment Healing of Microfractured

Chondral Defects. Arthrosc. J. Arthrosc. Relat. Surg. 2011, 27, 1552–1561. [CrossRef] [PubMed]

72. Ferris, D.J.; Frisbie, D.D.; Kisiday, J.D.; McIlwraith, C.W.; Hague, B.A.; Major, M.D.; Schneider, R.K.; Zubrod, C.J.; Kawcak, C.E.; Goodrich, L.R. Clinical Outcome After Intra-Articular Administration of Bone Marrow Derived Mesenchymal Stem Cells in 33 Horses With Stifle Injury. Vet. Surg. 2014, 43, 255–265. [CrossRef] [PubMed]

73. Wang, Y.; Chen, X.; Cao, W.; Shi, Y. Plasticity of mesenchymal stem cells in immunomodulation: Pathological and therapeutic implications. Nat. Immunol. 2014, 15, 1009–1016. [CrossRef] [PubMed]

74. Nicpon, J.; Marycz, K.; Grzesiak, J. Therapeutic effect of adipose-derived mesenchymal stem cell injection in horses suffering from bone spavin. Pol. J. Vet. Sci. 2013, 16, 753–754. [CrossRef]

75. Broeckx, S.Y.; Seys, B.; Suls, M.; Vandenberghe, A.; Marien, T.; Adriaensen, E.; Declercq, J.; Van Hecke, L.; Braun, G.; Hellmann, K.; et al. Equine Allogeneic Chondrogenic Induced Mesenchymal Stem Cells Are an Effective Treatment for Degenerative Joint Disease in Horses. Stem Cells Dev. 2019, 28, 410–422. [CrossRef]

76. Smith, R.; McIlwraith, W.; Schweitzer, R.; Kadler, K.; Cook, J.; Caterson, B.; Dakin, S.; Heinegard, D.; Screen, H.; Stover, S.; et al. Advances in the understanding of tendinopathies: A report on the Second Havemeyer Workshop on equine tendon disease. Equine Vet. J. 2014, 46, 4–9. [CrossRef]

77. Dowling, B.A.; Dart, A.J.; Hodgson, D.R.; Smith, R.K.W. Superficial digital flexor tendonitis in the horse. Equine Vet. J. 2000, 32, 369–378. [CrossRef]

78. Chong, A.K.S.; Chang, J.; Go, J.C.H. Mesenchymal stem cells and tendon healing. Front. Biosci. 2009, 14, 4598–4605. [CrossRef]

79. Richardson, L.E.; Dudhia, J.; Clegg, P.D.; Smith, R. Stem cells in veterinary medicine—Attempts at regenerating equine tendon after injury. Trends Biotechnol. 2007, 25, 409–416. [CrossRef]

80. Carvalho, A.d.M.; Badial, P.R.; Cisneros Alvarez, L.E.; Miluzzi Yamada, A.L.; Borges, A.S.; Deffune, E.; Hussni, C.A.; Garcia Alves, A.L. Equine tendonitis therapy using mesenchymal stem cells and

platelet concentrates: A randomized controlled trial. Stem Cell Res. Ther. 2013, 4. [CrossRef]

81. Smith, R.K.W.; Werling, N.J.; Dakin, S.G.; Alam, R.; Goodship, A.E.; Dudhia, J. Beneficial Effects of Autologous Bone Marrow-Derived Mesenchymal Stem Cells in Naturally Occurring Tendinopathy. PLoS ONE 2013, 8, e0075697. [CrossRef]

82. Smith, R.K.W.; Korda, M.; Blunn, G.W.; Goodship, A.E. Isolation and implantation of autologous equine mesenchymal stem cells from bone marrow into the superficial digital flexor tendon as a potential novel treatment. Equine Vet. J. 2003, 35, 99–102. [CrossRef] [PubMed]

83. Alves, A.G.L.; Stewart, A.A.; Dudhia, J.; Kasashima, Y.; Goodship, A.E.; Smith, R.K.W. Cell-based Therapies for Tendon and Ligament Injuries. Vet. Clin. North Am. Equine Pract. 2011, 27, 315–333. [CrossRef]

84. Godwin, E.E.; Young, N.J.; Dudhia, J.; Beamish, I.C.; Smith, R.K.W. Implantation of bone marrow-derived mesenchymal stem cells demonstrates improved outcome in horses with overstrain injury of the superficial digital flexor tendon. Equine Vet. J. 2012, 44, 25–32. [CrossRef]

85. Kol, A.; Wood, J.A.; Holt, D.D.C.; Gillette, J.A.; Bohannon-Worsley, L.K.; Puchalski, S.M.; Walker, N.J.; Clark, K.C.; Watson, J.L.; Borjesson, D.L. Multiple intravenous injections of allogeneic equine mesenchymal stem cells do not induce a systemic inflammatory response but do alter lymphocyte subsets in healthy horses. Stem Cell Res. Ther. 2015, 6. [CrossRef] [PubMed]

86. Barberini, D.J.; Aleman, M.; Aristizabal, F.; Spriet, M.; Clark, K.C.; Walker, N.J.; Galuppo, L.D.; Amorim, R.M.; Woolard, K.D.; Borjesson, D.L. Safety and tracking of intrathecal allogeneic mesenchymal stem cell transplantation in healthy and diseased horses. Stem Cell Res. Ther. 2018, 9. [CrossRef]

87. Beerts, C.; Suls, M.; Broeckx, S.Y.; Seys, B.; Vandenberghe, A.; Declercq, J.; Duchateau, L.; Vidal, M.A.; Spaas, J.H. Tenogenically induced allogeneic Peripheral Blood Mesenchymal stem cells in allogeneic Platelet-Rich Plasma: 2-Year Follow-up after Tendon or ligament Treatment in horses. Front. Vet. Sci. 2017, 4. [CrossRef]

88. Romero, A.; Barrachina, L.; Ranera, B.; Remacha, A.R.; Moreno, B.; de Blas, I.; Sanz, A.; Vazquez, F.J.; Vitoria, A.; Junquera, C.; et al.

Comparison of autologous bone marrow and adipose tissue derived mesenchymal stem cells, and platelet rich plasma, for treating surgically induced lesions of the equine superficial digital flexor tendon. Vet. J. 2017, 224, 76–84. [CrossRef]

89. Ricco, S.; Renzi, S.; Del Bue, M.; Conti, V.; Merli, E.; Ramoni, R.; Lucarelli, E.; Gnudi, G.; Ferrari, M.; Grolli, S. Allogeneic Adipose Tissue-Derived Mesenchymal Stem Cells in Combination with Platelet Rich Plasma are Safe and Effective in the Therapy of Superficial Digital Flexor Tendonitis in the horse. Int. J. Immunopathol. Pharmacol. 2013, 26, 61–68. [CrossRef]
90. Dyson, S.J. Medical management of superficial digital flexor tendonitis: A comparative study in 219 horses (1992–2000). Equine Vet. J. 2004, 36, 415–419. [CrossRef]
91. Pacini, S.; Spinabella, S.; Trombi, L.; Fazzi, R.; Galimberti, S.; Dini, F.; Carlucci, F.; Petrini, M. Suspension of bone marrow-derived undifferentiated mesenchymal stromal cells for repair of superficial digital flexor tendon in race horses. Tissue Eng. 2007, 13, 2949–2955. [CrossRef] [PubMed]
92. Smith, R.K.W. Mesenchymal stem cell therapy for equine tendinopathy. Disabil. Rehabil. 2008, 30, 1752–1758. [CrossRef] [PubMed]
93. Canapp, S.O.; Canapp, D.A.; Ibrahim, V.; Carr, B.J.; Cox, C.; Barrett, J.G. The Use of Adipose-Derived Progenitor Cells and Platelet-Rich Plasma Combination for the Treatment of Supraspinatus Tendinopathy in 55 Dogs: A Retrospective Study. Front. Vet. Sci. 2016, 3. [CrossRef] [PubMed]
94. Canapp, S.O.; Leasure, C.S.; Cox, C.; Ibrahim, V.; Carr, B.J. Partial Cranial Cruciate Ligament Tears Treated with Stem Cell and Platelet-Rich Plasma Combination Therapy in 36 Dogs: A Retrospective Study. Front. Vet. Sci. 2016, 3. [CrossRef] [PubMed]
95. Gibson, M.A.; Brown, S.G.; Brown, N.O. Semitendinosus myopathy and treatment with adipose-derived stem cells in working German shepherd police dogs. Can. Vet. J. Rev. Vet. Can. 2017, 58, 241–246.
96. McDougall, R.A.; Canapp, S.O.; Canapp, D.A. Ultrasonographic Findings in 41 Dogs Treated with Bone Marrow Aspirate Concentrate and Platelet-Rich Plasma for a Supraspinatus Tendinopathy: A Retrospective Study. Front. Vet. Sci. 2018, 5. [CrossRef]

97. Bari, E.; Perteghella, S.; Marrubini, G.; Sorrenti, M.; Catenacci, L.; Tripodo, G.; Mastrogiacomo, M.; Mandracchia, D.; Trapani, A.; Farago, S.; et al. In vitro efficacy of silk sericin microparticles and platelet lysate for intervertebral disk regeneration. Int. J. Biol. Macromol. 2018, 118, 792–799. [CrossRef]

98. Steffen, F.; Smolders, L.A.; Roentgen, A.M.; Bertolo, A.; Stoyanov, J. Bone Marrow-Derived Mesenchymal Stem Cells as Autologous Therapy in Dogs with Naturally Occurring Intervertebral Disc Disease: Feasibility, Safety, and Preliminary Results. Tissue Eng. Part C Methods 2017, 23, 643–651. [CrossRef]

99. Steffen, F.; Bertolo, A.; Affentranger, R.; Ferguson, S.J.; Stoyanov, J. Treatment of Naturally Degenerated Canine Lumbosacral Intervertebral Discs with Autologous Mesenchymal Stromal Cells and Collagen Microcarriers: A Prospective Clinical Study. Cell Transplant. 2019, 28, 201–211. [CrossRef]

100. Sarmento, C.A.P.; Rodrigues, M.N.; Bocabello, R.Z.; Mess, A.M.; Miglino, M.A. Pilot study: Bone marrow stem cells as a treatment for dogs with chronic spinal cord injury. Regen. Med. Res. 2014, 2, 9. [CrossRef]

101. Kim, Y.; Lee, S.H.; Kim, W.H.; Kweon, O.-K. Transplantation of adipose derived mesenchymal stem cells for acute thoracolumbar disc disease with no deep pain perception in dogs. J. Vet. Sci. 2016, 17, 123–126. [CrossRef] [PubMed]

102. Besalti, O.; Can, P.; Akpinar, E.; Aktas, Z.; Elcin, A.E.; Elcin, Y.M. Intraspinal Transplantation of Autologous Neurogenically-Induced Bone Marrow-Derived Mesenchymal Stem Cells in the Treatment of Paraplegic Dogs without Deep Pain Perception Secondary to Intervertebral Disk Disease. Turk. Neurosurg. 2015, 25, 625–632. [CrossRef] [PubMed]

103. Russell, W.M.S.; Burch, R.L. The Principles of Humane Experimental Technique; Methuen: Wheathampstead, UK, 1959.

104. Reiner, A.T.; Witwer, K.W.; van Balkom, B.W.M.; de Beer, J.; Brodie, C.; Corteling, R.L.; Gabrielsson, S.; Gimona, M.; Ibrahim, A.G.; de Kleijn, D.; et al. Concise Review: Developing Best-Practice Models for the Therapeutic Use of Extracellular Vesicles. Stem Cells Transl. Med. 2017, 6, 1730–1739. [CrossRef] [PubMed]

105. Laible, G.; Wei, J.; Wagner, S. Improving livestock for agriculture—Technological progress from random transgenesis to precision genome editing heralds a new era. Biotechnol. J. 2015, 10, 109–120. [CrossRef]

106. Van Weeren, P.R.; Tryfonidou, M.A. Musculoskeletal health from the "One Medicine" perspective—What can we learn from large and small animal models (with emphasis on articular cartilage)? BMC Musculoskelet. Disord. 2015, 16, S6. [CrossRef]

107. Crivelli, B.; Chlapanidas, T.; Perteghella, S.; Lucarelli, E.; Pascucci, L.; Brini, A.T.; Ferrero, I.; Marazzi, M.; Pessina, A.; Torre, M.L.; et al. Mesenchymal stem/stromal cell extracellular vesicles: From active principle to next generation drug delivery system. J. Control. Release 2017, 262, 104–117. [CrossRef]

108. Bari, E.; Ferrarotti, I.; Torre, M.L.; Corsico, A.G.; Perteghella, S. Mesenchymal stem/stromal cell secretome for lung regeneration: The long way through "pharmaceuticalization" for the best formulation. J. Control. Release 2019, 309, 11–24. [CrossRef]

109. Bari, E.; Perteghella, S.; Catenacci, L.; Sorlini, M.; Croce, S.; Mantelli, M.; Avanzini, M.A.; Sorrenti, M.; Torre, M.L. Freeze-dried and GMP-compliant pharmaceuticals containing exosomes for acellular mesenchymal stromal cell immunomodulant therapy. Nanomedicine 2019, 14, 753–765. [CrossRef]

110. Del Fattore, A.; Luciano, R.; Pascucci, L.; Goffredo, B.M.; Giorda, E.; Scapaticci, M.; Fierabracci, A.; Muraca, M. Immunoregulatory Effects of Mesenchymal Stem Cell-Derived Extracellular Vesicles on T Lymphocytes. Cell Transplant. 2015, 24, 2615–2627. [CrossRef]

111. Capomaccio, S.; Cappelli, K.; Bazzucchi, C.; Coletti, M.; Gialletti, R.; Moriconi, F.; Passamonti, F.; Pepe, M.; Petrini, S.; Mecocci, S.; et al. Equine Adipose-Derived Mesenchymal Stromal Cells Release Extracellular Vesicles Enclosing Different Subsets of Small RNAs. Stem Cells Int. 2019, 2019, 4957806. [CrossRef]

112. Malda, J.; Boere, J.; van de Lest, C.H.A.; van Weeren, P.R.; Wauben, A.H.M. Extracellular vesicles—New tool for joint repair and regeneration. Nat. Rev. Rheumatol. 2016, 12, 243–249. [CrossRef] [PubMed]

113. Pascucci, L.; Cocce, V.; Bonomi, A.; Ami, D.; Ceccarelli, P.; Ciusani, E.; Vigano, L.; Locatelli, A.; Sisto, F.; Doglia, S.M.; et al. Paclitaxel is

incorporated by mesenchymal stromal cells and released in exosomes that inhibit in vitro tumor growth: A new approach for drug delivery. J. Control. Release 2014, 192, 262–270. [CrossRef] [PubMed]

114. Phinney, D.G.; Pittenger, M.F. Concise Review: MSC-Derived Exosomes for Cell-Free Therapy. Stem Cells 2017, 35, 851–858. [CrossRef] [PubMed]

115. Villatoro, A.J.; Alcoholado, C.; Martin-Astorga, M.C.; Fernandez, V.; Cifuentes, M.; Becerra, J. Comparative analysis and characterization of soluble factors and exosomes from cultured adipose tissue and bone marrow mesenchymal stem cells in canine species. Vet. Immunol. Immunopathol. 2019, 208, 6–15. [CrossRef]

116. El-Tookhy, O.S.; Shamaa, A.A.; Shehab, G.G.; Abdallah, A.N.; Azzam, O.M. Histological Evaluation of Experimentally Induced Critical Size Defect Skin Wounds Using Exosomal Solution of Mesenchymal Stem Cells Derived Microvesicles. Int. J. Stem Cells 2017, 10, 144–153. [CrossRef]

117. Lange-Consiglio, A.; Rossi, D.; Tassan, S.; Perego, R.; Cremonesi, F.; Parolini, O. Conditioned Medium from Horse Amniotic Membrane-Derived Multipotent Progenitor Cells: Immunomodulatory Activity In Vitro and First Clinical Application in Tendon and Ligament Injuries In Vivo. Stem Cells Dev. 2013, 22, 3015–3024. [CrossRef]

118. Lange-Consiglio, A.; Romele, P.; Magatti, M.; Silini, A.; Idda, A.; Martino, N.A.; Cremonesi, F.; Parolini, O. Priming with inflammatory cytokines is not a prerequisite to increase immune-suppressive effects and responsiveness of equine amniotic mesenchymal stromal cells. Stem Cell Res. Ther. 2020, 11. [CrossRef]

119. Bari, E.; Ferrarotti, I.; Di Silvestre, D.; Grisoli, P.; Barzon, V.; Balderacchi, A.; Torre, M.L.; Rossi, R.; Mauri, P.; Corsico, A.G.; et al. Adipose Mesenchymal Extracellular Vesicles as Alpha-1-Antitrypsin Physiological Delivery Systems for Lung Regeneration. Cells 2019, 8, 965. [CrossRef]

120. Li, J.J.; Hosseini-Beheshti, E.; Grau, G.E.; Zreiqat, H.; Little, C.B. Stem Cell-Derived Extracellular Vesicles for Treating Joint Injury and Osteoarthritis. Nanomaterials 2019, 9, 261. [CrossRef]

121. Ranganath, S.H.; Levy, O.; Inamdar, M.S.; Karp, J.M. Harnessing the Mesenchymal Stem Cell Secretome for the Treatment of Cardiovascular Disease. Cell Stem Cell 2012, 10, 244–258. [CrossRef]

122. Han, C.; Sun, X.; Liu, L.; Jiang, H.; Shen, Y.; Xu, X.; Li, J.; Zhang, G.; Huang, J.; Lin, Z.; et al. Exosomes and Their Therapeutic Potentials of Stem Cells. Stem Cells Int. 2016, 2016, 7653489. [CrossRef] [PubMed]

123. Pawitan, J.A. Prospect of Stem Cell Conditioned Medium in Regenerative Medicine. Biomed Res. Int. 2014, 2014, 965849. [CrossRef] [PubMed]

CHAPTER 2:

MSC-SECRETOME OPTIMIZATION PROCESS

Producing MSC-secretome in a perspective of clinical practice requires scalable and standardized medicinal product; to do so, a method that combines ultrafiltration and freeze-drying was implied to transform secretome into Lyosecretome.

Since the starting point to produce the secretome is a living organism (the cell), it determines a certain degree of the intrinsic variability of the final product, as happens for all the biological drugs. Any slight change in the production process can modify the qualitative-quantitative composition of the finished product and, therefore, its biological activity. Thus, through the concept of a quality by design, the idea was to set the quality of the pharmaceutical product from the beginning, standardizing, and arranging quality controls along with all the process phases, to demonstrate that the final characteristics conform to those determined for the batch release. Therefore, there is the need to have complementary characterization techniques to analyze different chemical-physical, immunochemical, and biological parameters of the finished product. Each of these techniques has its advantages and limitations. Certainly, it remains to be understood which of them can be validated at pharmaceutical grade and which, above all, have an acceptable cost to be implemented on the quality controls that are carried out routinely. Therefore, the goal is through multiple characterization methods to identify the so-called

molecular fingerprint or the qualitative-quantitative composition of the sample. In **Paper 2,** we have proposed various aspects for our product, including the total protein and lipid content and the EV particle size and concentration. However, this is not enough, and it is necessary to demonstrate that the finished product, after having undergone all the processes of isolation, purification and formulation, maintains a certain biological activity.

Paper 2. Mocchi M, Bari E, Marrubini G, Foglio Bonda A, Perteghella S, Tartara F, Cofano F, Di Perna G, Giovannelli L, Mandracchia D, Sorlini M, Garbossa D, Torre M.L, Segale L, (2021). Freeze-Dried Mesenchymal Stem Cell-Secretome Pharmaceuticalization: Optimization of Formulation and Manufacturing Process Robustness. Pharmaceuticals 13, 1129; doi: 10.3390/pharmaceutics13081129.

Abstract: Producing mesenchymal stem cell (MSC)-secretome for dose escalation studies and clinical practice requires scalable and good manufacturing practice (GMP)-compliant production procedures and formulation into a standardized medicinal product. Starting from a method that combines ultrafiltration and freeze-drying to transform MSC-secretome into a pharmaceutical product, the lyosecretome, this work aims to: (i) optimize the lyosecretome formulation; (ii) investigate sources of variability that can affect the robustness of the manufacturing process; (iii) modify the ultrafiltration step to obtain a more standardized final product. Design of experiments and principal component analysis of the data were used to study the influence of batch production, lyophilization, mannitol (M)/sucrose (S) binary mixture, selected as cryoprotectant excipients, and the total amount of excipients on the extracellular vesicles (EV) particle size, the protein and lipid content and the in vitro anti-elastase. The different excipients ratios did not affect residual moisture or EV particle size; simultaneously, proteins and lipids were better preserved in the freeze-dried product using the maximum total concentration of excipients (1.5% w/v) with a M:S ratio of about 60% w/w. The anti-elastase activity was instead better preserved using 0.5% w/w of M as excipient. The secretome batch showed to be the primary source of variability; therefore, the manufacturing process has been modified and then validated: the final product is now concentrated to reach a specific protein (and lipid) concentration instead of cell equivalent

concentration. The new standardization approach led to a final product with more reproducible quali-quantitative composition and higher biological activity.

Keywords: mesenchymal stem cells; secretome; freeze-drying; formulation.

1. Introduction

In the 1990s, the multipotency of mesenchymal stem cells (MSCs) was identified as a promise for developing new and more effective cell therapies intended to revolutionize the clinical practice in regenerative medicine and improve the patient quality of life [1,2]. Since then, more than 800 worldwide clinical trials have proven MSC therapeutic effectiveness and safety, spanning from cardiovascular to neurological, from tegumentary to respiratory (source: http://clinicaltrials.gov, term search: Mesenchymal Stem Cells, last search 18 May 2021). Twenty years later from their discovery, Caplan suggested renaming MSCs as "Medicinal Signaling Cells" since multipotency seemed to be no longer the key aspect of their therapeutic effects [3]. In fact, after transplantation, the number of MSCs that effectively engraft and differentiate into the damaged tissue is very low, suggesting a paracrine mechanism of action [4-6]. The substances secreted by MSCs that modulate the resident cell responses are collectively named secretome, composed of free-soluble factors (including cytokines, chemokines and growth factors) and insoluble nano/microstructured extracellular vesicles (EVs) [7,8]. MSC-secretome can reproduce the therapeutic effects of stem cells themselves and cell-free therapies should provide numerous advantages compared with whole-cell MSC infusions in terms of safety and technological advantages [9]. Unfortunately, it remains a significant challenge translating this therapy into the clinic: with the focus on therapeutic applications, conventional manufacturing

processes (such as ultracentrifugation or chromatography) limit secretome applications and the ability to evaluate safety and efficacy at high doses on a large animal or clinical trials [10,11]. Producing MSC-secretome for dose escalation studies and clinical practice requires a scalable production procedure, including raw materials or consumables, compatible with current good manufacturing practice (cGMP) procedures [12]. Finally, to have a meaningful role in medicine, the secretome needs to be turned into a format easy to manage by the clinical community. In other words, MSC-secretome needs, as for all the Active Pharmaceutical Ingredients, to be formulated into a standardized medicinal product [7]. In this regard, recently, Bari and co-workers proposed a method to transform MSC-secretome into a pharmaceutical product for its large-scale production [13]. For this purpose, ultrafiltration and freeze-drying were combined: MSC-secretome was purified from culture supernatants by ultrafiltration in a GMP-compliant cell factory, concentrated at 0.5×10^6 cell equivalents per mL, added with cryoprotectant and lyophilized. A freeze-dried and "ready-off-the-shelf" powder – the lyosecretome – containing extracellular vesicles and proteins was obtained. Although the described process is successful in scalability and GMP compliance, it fails to obtain a product standardized in protein and lipid content and thus in vitro biological activity. Such batch-to-batch variability has also been reported in terms of biological activity for secretomes derived from both human [14] or equine MSCs [15]. Indeed, like any other biological drug, the starting point for the production of the secretome is a living organism, the cell and the process mentioned above standardizes the final product in terms of cell equivalents: a precise quantity of the final product is obtained by a specific number of cells. Therefore, the amount of proteins and lipids of the final product depends on how many of them have been produced by that number of cells. With this in mind, it is questionable whether some process

variables can be modified to optimize the manufacturing process. Moreover, to protect biological material, especially EVs, mannitol was chosen as a stabilizer from freeze-drying stresses. The tendency of mannitol to maintain its crystalline form is well appreciated for giving the best cake appearance and a high collapse temperature, associated with having a shorter freeze-drying time [16]. However, other stabilizers may be used to avoid affecting secretome components in quality and quantity, such as other sugars/polyols, proteins and amino acids or surfactants [17]. Especially, sucrose is appreciated for its vitrification capability: forming an amorphous phase with high viscosity may help to protect the lipid layer of the EVs and to reduce the merge of vesicles [18].

Given these premises, this work aims to: i) optimize the lyosecretome formulation; ii) investigate sources of variability that can affect the robustness of the manufacturing process described by Bari and colleagues [13]; iii) modify the concentration step to ob-tain a more standardized final product. At first, a multi-level 5 × 2 factorial design was used to optimize lyosecretome formulation, using mannitol and sucrose as excipients. Then, a quadratic D-optimal design was computed to evaluate the effect of secretome batch (S), lyophilization (L), concentration of excipients (C) and the manni-tol/sucrose ratio in the excipient mixture (M, to indicate the proportion of mannitol in the binary mixture mannitol/sucrose) on the pharmaceutical dosage form characteristics (residual humidity and cake appearance) and on the product performances (protein and lipid yields, the EV particle size, and in vitro anti-elastase activity). Finally, the manufacturing process has been modified to reduce batch-to-batch variability: the final product is now concentrated to reach a specific protein (and lipid) concentration instead of cell equivalent concentration. The ability of the new standardization meth-od in obtaining a final product with more reproducible quali-quantitative composition and biological activity has been

investigated, and the modified manufacturing process has been validated.

2. Materials and Methods

2.1 Materials

Reagents used for the cell culture were purchased from Euroclone (Milan, Italy) and platelet lysate (PLy) from Sclavo Diagnostics (Siena, Italy). Acetone, bovine serum albumin (BSA), collagenase, mannitol, Nile red, phosphatidylcholine and sucrose were obtained from Sigma–Aldrich (Milan, Italy). Epigallocatechin gallate (EGCG), N-succinyl-Ala-Ala-Ala-p-nitroanilide and pancreatic porcine elastase were bought from Merck Life Science S.r.l., Milan, Italy.

2.2 Design of Experiments

A multi-level 5 × 2 design was used to understand how formulation attributes can influence product performances (Table 1). In details, a mannitol/sucrose binary mixture was selected as an excipient. Variable 1 (coded V1) represented the percentage of mannitol in the mixture and had 5 levels corresponding to the 25, 45, 65, 85 and 100% w/v (coded as -1.0, -0.5, 0.0, 0.6, 1.0). Variable 2 (V2) represented the amount of the mixture expressed as % w/v in the pre-freeze-dryer solutions. For V2, two levels (-1 and +1) were selected, corresponding to 0.5 and 1.5% w/v.

Table 1. Details of the factorial design used.

Formulation	V1	V2	V1 = Mannitol %	% *w*/*v*
1	-1.0	-1.0	25	0.5
2	-0.5	-1.0	45	0.5
3	0.0	-1.0	65	0.5
4	0.6	-1.0	85	0.5
5	1.0	-1.0	100	0.5
6	-1.0	+1.0	25	1.5
7	-0.5	+1.0	45	1.5
8	0.0	+1.0	65	1.5
9	0.6	+1.0	85	1.5
10	1.0	+1.0	100	1.5

2.3 Sample Preparation

2.3.1. Isolation and Expansion of Human Adipose-Derived MSCs (AD-MSCs)

AD-MSCs were harvested from adipose tissues collected from patients undergoing abdominoplasty, as previously reported [19,20], after informed consent (ASST Grande Ospedale Metropolitano Niguarda, Milan, Ref. 12 November 2009). MSCs were seeded into flasks (10,000 cells/cm^2) at 37 °C and 5% CO_2 and cultured in complete culture medium (DMEM/F12 minimal medium plus 5% *v*/*v* PLy, plus 1% *v*/*v* penicillin/streptomycin and 1% *v*/*v* amphotericin B) until passage 3. Then, secretome release was induced by culturing MSCs in DMEM/F12 without platelet lysate for 48 h. MSCs were characterized to assess their identity according to the International Society for Cellular Therapy [21].

2.3.2. MSC-secretome Ultafiltration

Conditioned media was centrifuged at 3500 × *g* for 10 min to eliminate cell fragments and apoptotic bodies. Afterwards, supernatants were collected, and the MSC-secretome purification process was performed by tangential flow filtration using the KrosFlo®

Research 2i system (Spectrum Laboratories, Milan, Italy) using a 5 kDa Molecular Weight Cut Off (MWCO) filtration module (Spectrum Laboratories, Milan, Italy). Before proceeding with the ultrafiltration, all the instrument units were sterilized to operate in aseptic conditions under a laminar flow hood in a B cleanroom suite. The automated process allowed, at first, to concentrate and then to diafilter the samples. According to the manufacturer's guidelines, during each step, the shear rate of the feed stream was kept between 2000 s^{-1} and 6000 s^{-1}, while the trans-membrane pressure index did not exceed 5 psi. In the first part of the manuscript, the concentration process ended when a concentration of 0.5×10^6 cell equivalents per mL was achieved (CE). In the second part, the concentration process ended when a concentration of 115 μg/mL of proteins was reached (PL). Sterilized and ultrapure water was used as a dialysis buffer.

2.3.3. Freeze-drying

Under Bio-Hood (Steril-VBH EuroClone S.p.a., Milan, Italy), vials (Colaver Srl, Vimodrone, Italy) were filled with 1 mL of solution using a manual pipette. Stoppers were pre-labelled to differentiate formulations, and vials containing the different formulations were randomly placed on the bottomless shelves. Four temperature probes were installed in defined vials. The freeze dryer (Epsilon 2-6D LSCplus, Martin Christ GmbH, Osterode am Harz, Germany) was loaded, protecting the drying chamber from dust with a laminar air flow cabinet equipped with a fan filtration unit (Success Way Clean Technology Co. Ltd, Suzhou, Jiangsu, China) and the freeze-dryer polyacrylate panel was covered with an isolation panel built by own. A conservative freeze-drying process was adopted (parameters are reported in Table 2) and the well-known "freezing step program" was applied to reduce samples variability. At the end of the process, vacuum stoppering was carried out, the freeze-dryer was unloaded,

and vials were crimped and labelled. Vials were stored at – 20 °C until use (maximum six months).

Table 2. Parameters of the lyophilization process.

Phase	Section	Time (h:min)	Shelf's temperature (°C)	Pressure (mbar)
Loading	1	-	25	1000
Freezing	2-ramp	0:20	5	
	3-hold	0:40	5	
	4-ramp	0:10	-5	
	5-hold	1:00	-5	
	6-ramp	0:45	-45	
	7-hold	4:30	-45	
Primary drying	8	0:20	-45	0.08
	9	0:30	-40	
	10	79:09	-40	
Secondary drying	11	2:30	22	
	12	8:00	22	

2.4. Sample Characterization

2.4.1. Residual Moisture

The test was carried out with Coulometric Titrator HI904 (Hanna Instruments, Villafranca Padovana, Italy). An external extraction method with an anolyte solution was adopted. In detail, approximately 2.5 mL of anolyte (Hydranal™ Culomat AD, Honeywell, Charlotte, NC, USA) were injected into the septum bottle by a syringe. The weight of the anolyte injected was determined by back weighing. The vial was sonicated for 30 min at 40 °C, and then an aliquot of the dispersion/solution was drawn again into the same syringe, weighed and injected into the titration cell. Again, the weight was determined by back weighing. Titration was performed twice for each vial. The vial back pressure inlet was controlled with a syringe containing molecular sieves to reduce ambient moisture influence. All

the samples were allowed to equilibrate at ambient temperature before analyses.

2.4.2. Cake Aspect

Four vials for each formulation were randomly removed from – 20 °C and equilibrated at room temperature for 24 h before performing the cake aspect evaluation. A cake aspect questionnaire was submitted to five of the authors having experience in freeze-drying (M.M., E.B., A.F.B, L.G., L.S). The subject shall give a score to 6 selected typical defects observed in the freeze-dried cake. The following defects were evaluated: i) collapse, ii) cake shrinkage, iii) cracked cake, iv) skin formation, v) minor splashing and vi) non-uniform cake appearance. The subjects evaluated the appearance of the cakes giving a score from 0 to 5, where five corresponded to a higher level of noticeable defect. A visual legend (adapted from Patel et al. [22] and showing images of the defects) was provided to the subjects to reduce individual variability. For each defect, the score was calculated summing the five single evaluators' outcome and removing the corresponding minimum and maximum expressed values.

2.4.3. Total Protein Content

A micro BCA-Protein Assay Kit (Thermo Fischer Scientific, Milan, Italy) was used following the manufacturer's instructions to evaluate the total protein content of the samples before and after lyophilization. Freeze-dried samples were first resuspended in deionized water. The absorbance–concentration calibration curve was produced using bovine serum albumin (BSA) as standard. Working reagent solution was added to each sample and the calibration curve (ratio 1:1), then incubated at 37 °C for 2 h before reading. The absorbance was measured at 562 nm using a microplate reader (Synergy HT, Milan, Italy). The concentration of unknown protein content was calculated from a plot of concentration vs. absorbance obtained for the standard

protein solutions, using a third-order polynomial equation, with R^2 = 0.99. Each sample was measured in triplicate.

2.4.4. Phospholipid Quantification by Nile Red Assay

A Nile Red stock solution was prepared starting from Nile Red powder dissolved in acetone (3.14 M). The stock solution was stored at 4 °C in the dark, avoiding light exposure. The stock solution was diluted 100× using filtered PBS (pH = 7.14), and 10 µL of it were incubated with 90 µL of samples. After 5 min, Synergy HT measured the relative fluorescence at fixed wavelengths (530/25 excitation and 645/40 emission). The fluorescence–concentration calibration curve was developed using phosphatidylcholine (PC) as standard, with R^2 = 0.99. Each sample was tested in triplicate.

2.4.5 EV Particle Size Determination

The freeze-dried samples were dispersed in 1 mL of deionized water and analyzed by Nanoparticle Tracking Analysis (NTA, NanoSight NS 300 equipment, Malvern Panalytical Ltd., Malvern, UK)). Measurements were carried out at room temperature with a detection angle of 90° and the NTA software elaborated the data. All analyses were in triplicate.

2.4.6 Anti-elastase Activity

The anti-elastase activity of all samples has been evaluated by an in vitro method, as previously reported [15]. Briefly, the substrate N-succinyl-Ala-Ala-Ala-p-nitroanilide was dissolved in TRIS buffer at 0.41 mmol/L, and the pancreatic porcine elastase was solubilized in phosphate buffer pH 6.8 at 0.5 IU/mL. All the samples were incubated with the enzyme for 20 min. Then, the substrate was added and the kinetic reaction was monitored by spectrophotometric analysis

(Synergy HT) at the absorbance of 410 nm for 60 min (one measurement each minute). EGCG was used as a positive control (at 7.2 mg/mL), while the reaction mixture in the absence of sample was used as a negative control. Analyses were performed in triplicate.

2.5 D-optimal Design

All calculations were performed using Microsoft Excel and R version 3.1.0 (2014-04-10) Copyright (C) 2014 The R Foundation for Statistical Computing. R-based chemometric software routines were used for the design of experiments calculations. The R-based software has been developed by the Group of Chemometrics of the Italian Chemical Society [23]. The protein and lipid yield results and anti-elastase in vitro activity (Y_P, Y_L and Y_{NTA}, respectively) were fitted by a D-optimal design computed to study the information collected and summarized in the Supplementary materials section (Tables S1 and S2). In detail, the study was conducted by evaluating the effect of four factors on the responses: the secretome batch (S), the lyophilization (L), the concentration of excipients (C) and the concentration ratio of mannitol and sucrose (M, to indicate the proportion of mannitol in the binary mixture mannitol:sucrose). Table 3 summarizes the factors and levels at which they were studied.

Table 3. Factors and levels studied.

Factors	Levels	Encoding
Secretome batch (S)	1	$S_1 = 1$, $S_2 = 0$
	2	$S_1 = 0$, $S_2 = 1$
	3	$S_1 = S_2 = 0$
Lyophilization (L)	Pre	1
	Post	+1
Total concentration of excipients (% *w*/*v*)	0.5	-1
	1.5	+1
Mannitol/sucrose concentration ratio (% *w*/*w*)	25/75	-1
	100/0	+1

For proteins and lipids, two non-canonical quadratic models were postulated that included two qualitative factors (S and L, studied at three and two levels, respectively) and two continuous factors, C and M. The factor C was studied at two levels. In contrast, the M factor was examined at five different concentration levels with respect to sucrose (25/75, 45/55, 65/35, 85/15, 100/0). The postulated model for both responses is the following:

$$Y_K = b_0 + b_1 \times S_1 + b_2 \times S_2 + b_2 \times L + b_3 \times C + b_4 \times M + b_{44} \times M^2 \quad (1)$$

with K = P, L. The coding of the qualitative factor at three levels is $S_1 = 1$ and $S_2 = 0$ referring to the batch 1, $S_1 = 0$, $S_2 = 1$ to batch 2, and S1 = S2 = 0 to batch 3.

For EV particle size, the postulated model is the following:

$$Y_{NTA} = b_0 + b_1 \times S + b_2 \times C + b_3 \times M + b_{33} \times M^2 \quad (2)$$

In this case, the qualitative factor lyophilization (L) was fixed because only lyophilized formulations were studied.

For in vitro anti-elastase activity, all the data reported in each row of Table S1 are strongly correlated with each other since they originate

from enzymatic kinetics [24], and can thus be represented with a very good fit by exponential curves of the general form:

$$y = k \times e^{-at} \quad (3)$$

in which *k* and *a* are constant, and *t* is the reading time of the anti-elastase activity. Considering this, the choice adopted to study the data was to use principal component analysis (PCA) to examine the internal correlation structure of the dataset and verify in what relationship the different curves of the anti-elastase readings were. The data were then autoscaled, and the study of the relationships between the variables S, C and M, and the reading times of the anti-elastase activity was conducted using the PCA directly on the data without further preprocessing.

2.6 Optimization and Validation of the Manufacturing Process

Following the information collected by analyzing protein and lipid yields and in vitro anti-elastase activity, which revealed substantial batch-to-batch variability, the process has been optimized. Briefly, all the procedures described in section 2.3 have been repeated, but the concentration step was stopped when a protein concentration of 115 μg/mL was reached (the value was conventionally selected). In addition, characterization in terms of protein and lipid content and anti-elastase activity has been performed on the new batches prepared according to the procedures reported in sections 2.4.3, 2.4.4 and 2.4.6. The control charts for protein and lipid content have been designed, and the anti-elastase activity data have been analyzed by the PCA analysis as described in section 2.5.

3. Results and Discussion

Many challenges still need to be faced in the transition of MSC-secretome therapies into the clinic. These include practical problems, such as the need for an adequate number of cells (which may be solved using bioreactors [25]), the necessity of scalable, reproducible, and

GMP-compliant manufacturing protocols, and the MSC-secretome formulation into a standardized pharmaceutical dosage form (possibly in a steady dry state). In this regard, starting from a method that combines ultrafiltration and freeze-drying to transform MSC-secretome into a pharmaceutical product – the lyosecretome, this work used a multi-level 5 × 2 design to develop a freeze-dried formulation of MSC-secretome by using mannitol/sucrose binary mixture.

At first, the residual humidity and the cake aspect have been evaluated. Residual moisture did not exceed 4%, indicating an effective drying of the products and that the different excipients ratio does not affect this parameter. Three main defects were noted in cake appearance evaluation: collapse, cake shrinkage and cracked cake (Figure S1). Figure 1 represents the defect scores plotted as a function of the different formulations. For the formulations containing a low amount of mannitol (i.e., the high amount of sucrose), the only defect observed was the collapse of the cake. The collapse score decreased by increasing the amount of mannitol, and an increase of cracks in the cake was observed. Even the defect "Cake Shrinkage" increased by increasing the mannitol amount. These findings can be explained by the ability of mannitol to crystallize and by the behavior of sucrose, which produces amorphous structures. The increase of the amount of mannitol in the formulation allows to reduce the cakes collapse, leading the evaluators to notice other defects that are not masked or do not occur when the collapse is present. These defects (i.e., skin formation, minor splashing, and non-uniform cake appearance) were not reported because they were rarely noticed.

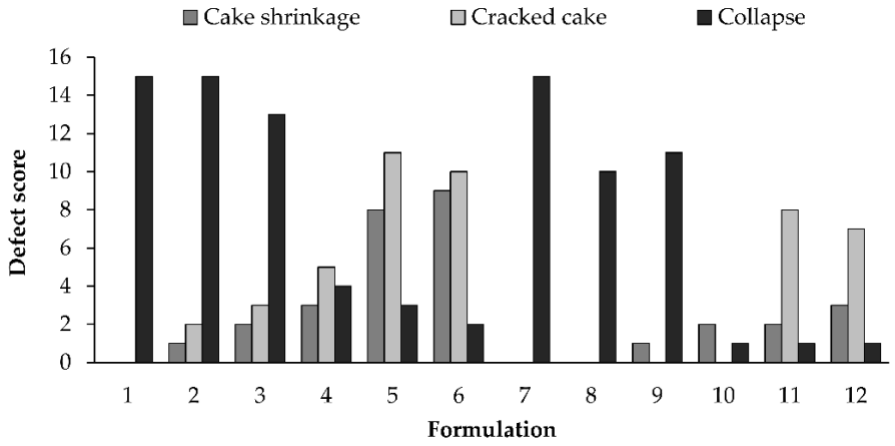

Figure 1. Defect scores for the evaluated formulations.

Then, the protein and lipid yield, the EV particle size and the in vitro anti-elastase activity of the prepared samples were studied by evaluating the effect of the secretome batch (S), the lyophilization (L), the concentration of excipients (C) and the concentration ratio of mannitol and sucrose, as detailed below.

3.1. Model for the "protein content" response, Y_P.

The data acquired on the protein yield (Table S2) are not conclusive. As shown in Figure S1, the experimental variance of the results is too high, and the replicated data show to be aggregated "in series". The predictive ability of the model, therefore, is not good. In some cases, the estimate predicted by the model is very far from the observed value (Table S3 and Figure S3). However, only considering the trend indicated by the data through the calculated model, two effects are observed: i) the first, more important, is due to the secretome preparation batch, and ii) the second derives from freeze-drying. For the first effect we noted that batch 1 has an amount of protein higher than batch 2 and 3; while for the second effect, it was noticed that freeze-drying process reduces the amount of protein (the protein amount is greater before freeze-drying process). This aspect can be

explained considering that the stresses generated during the freeze-drying process can alter the reducing power of proteins (thus, the BCA kit detect a low amount of proteins because less Cu^{2+} is reduced to Cu^{+}). The factors C, the concentration of excipients, and M, the proportion of mannitol in the preparation, on the other hand, do not influence the Y_P response. Likely, each mixture of excipients selected can preserve the protein content in the range of concentrations considered. However, it was not possible to increase the total amount of the excipients because the product would be exceedingly diluted to have biological activity. Moreover, at high concentrations of excipients, safety is compromised after administration due to hyperosmolarity. The model equation is:

$$Y_P = 24.83 + 165.78 \cdot S1^{(***)} - 12.24\ S_2 - 28.18\ L^{(***)} - 2.59\ C - 0.81\ M - 2.00\ C\ M + 0.48\ M^2 \quad (4)$$

Figure 2 shows the magnitude and sign of the coefficients. Their statistical significance is meaningless since the model is not validated (see Table S3 and Figures S2 and S3).

In batch 1, before freeze-drying, the maximum protein content is achieved when the maximum amount of mannitol is used, regardless of the total amount of excipients (Figure 3). This is probably because mannitol is more active than sucrose in the protection of proteins. Therefore, when the mannitol proportion increases, this effect is expected to be greater. If, on the other hand, C (which is given by mannitol + sucrose) increases, the effect of the less effective (sucrose) predominates and therefore interacts with the effect provided by mannitol.

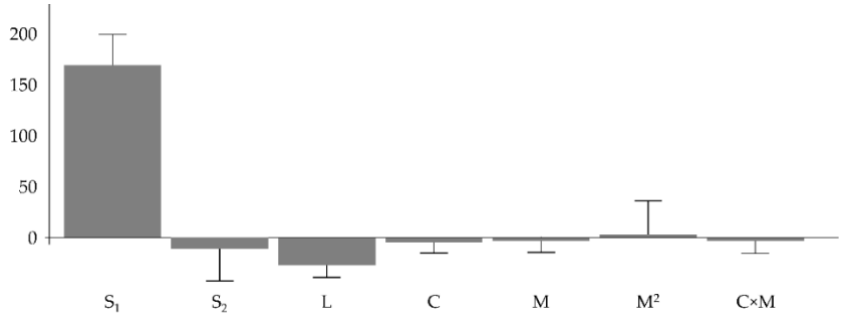

Figure 2. Coefficients for the model Y_P.

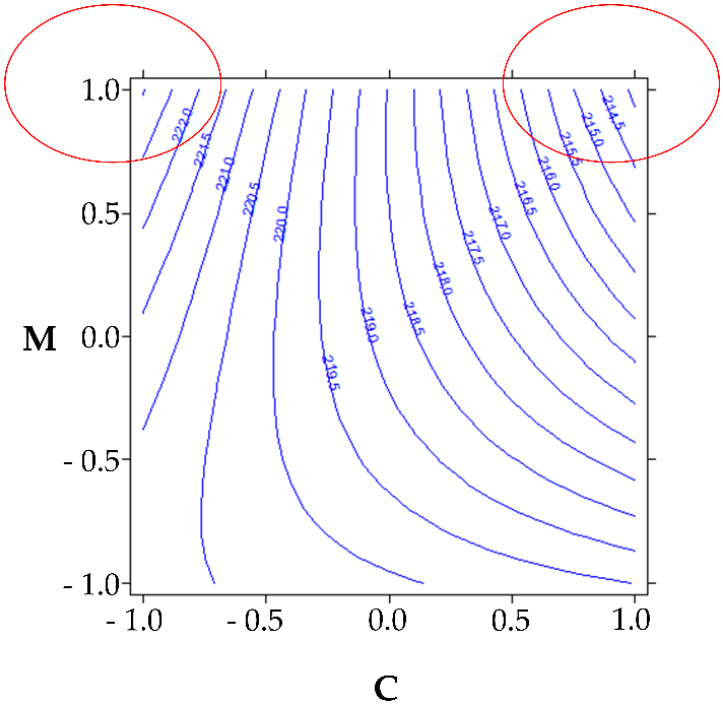

Figure 3. Isoresponse curves plot for batch 1 before freeze-drying.

3.2. Model for the "lipid content" response, Y_L

The observations illustrated for the model relating to the "protein content" response (Y_P), were replicated almost identical in the "lipid content" response, Y_L. The critical difference between the two models is that here the model for the Y_L response is validated and can be considered valid for describing the trend of the results (see Table S4).

So, in the case of the lipid content, the two effects described above, i.e., the effects of batch production and lyophilization, are evidenced. As shown in Figure 4 and by the model Equation (5), the first and the most relevant effect on the response is the secretome batch. Batch 1 shows the greater lipid content, whereas batch 2 has the lowest lipid content. Lyophilization decreases the lipid content. This aspect can be explained considering that the stresses generated during the freeze-drying process can damage the lipidic layer (thus, the Nile fluorescence is lowered). Factors C, the excipients' concentration and M, mannitol proportion in the preparation are also in this case almost irrelevant to the response.
The model equation is:

$$Y_L = 1.84 + 11.59 \cdot S_1^{(***)} - 0.91 \cdot S_2^{(*)} - 0.58 \cdot L^{(**)} + 0.15 \cdot C + 0.06 \cdot M + 0.28 \cdot C \cdot M - 0.34 \cdot M^2 \quad (5)$$

Figure 4 shows the coefficients magnitude and sign together with the confidence interval of their mean value. The coefficients of the factors C and M are not statistically significant and are numerically negligible compared to the coefficient of the batch effect (S_1).

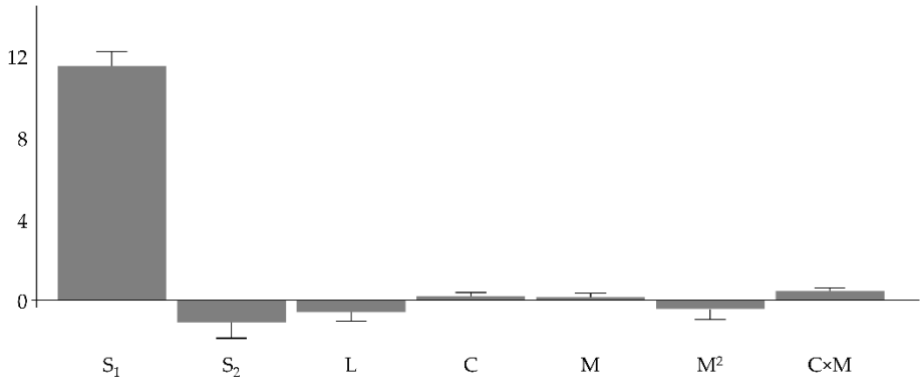

Figure 4. Coefficients for the model Y_L.

Overall, the data document an important batch effect for both the "protein content", Y_P, and "lipid content", Y_L responses. The

conditions that provide the preparations with both responses largest numerically are batch 1 and no lyophilization. The total concentration of excipients (C) and the ratio between the two sugars do not influence the two responses. The data examination also indicates that if the batch effect could be eliminated, the two responses would be maximum in the condition of before lyophilization, with the maximum total concentration of excipients (1.5% *w*/*v*) and with an M:S ratio of about 60% *w*/*w*. Accordingly, it was hypothesized that the maximum total concentration of excipients and an M:S ratio of about 60% *w*/*w* better preserve proteins and lipids during the lyophilization process.

3.3. Model for the "EV particle size" response, Y_{NTA}

The data presented in Table S5 about the mode, the first decile (d_{10}) and the ninth decile (d_{90}) of freeze-dried EVs are not described by the postulated model reported above (see Equation (2)). In particular, the value of the coefficient of determination adjusted for the degrees of freedom (R^2_{adj}) is equal to -0.059 for the mode, -0.055 for d_{10} and 0.230 for d_{90}. This result is to be interpreted assuming that none of the factors considered (S, C and M) affects the EV particle sizes in the prepared freeze-dried secretomes.

3.4. Model for the "In vitro Anti-elastase Activity" Response, Y_A

Using the PCA, the relationships between S, C and M and the anti-elastase activity values were investigated. The graph of Figure 5 shows that the data are described in the plane of the first two principal components (PC1, and PC2) with an explained variance equal to 99.3%. This indicates that almost all the variance of the results collected is explained in this plane. Furthermore, the colour codes show a secretome batch effect in the anti-elastase activity to discriminate batch 3 (green points) from batches 1 and 2 (red and black points, respectively). However, the discrimination is evident only along the PC2 and corresponds to an explained variance of 7.5%.

Along the PC1, the discrimination between the batches is not evident. However, by observing the loadings values in the bar graph of Figure 6, it can be better understood what is explained by the PC1. Indeed, PC1 reads the variation in anti-elastase activity from about 10 min to 61 min with positive loadings values. Therefore, on PC1 it is represented how the anti-elastase activity grows over the time for each sample studied as a function of the three variables examined (S, C and M). As it was already clear from the data, the anti-elastase activity increases exponentially from the beginning of the experiment and reaches a maximum but apparently asymptotic value at the end of the experiment. PC1 then shows the samples with the higher anti-elastase activity, especially from about the tenth minute of reading until the end of the experiment. Thus, higher values of anti-elastase activity correspond to higher values of PC1 in this time interval. The loadings on PC2 show how the anti-elastase activity reading varies in the first minutes of the experiment: positive loadings are computed from about 1 min onwards up to about 20 min and negative from 25 min at the end of the experiment. These observations help to understand the role of variables C and M, illustrated in subsequent Figures 7 and 8, respectively.

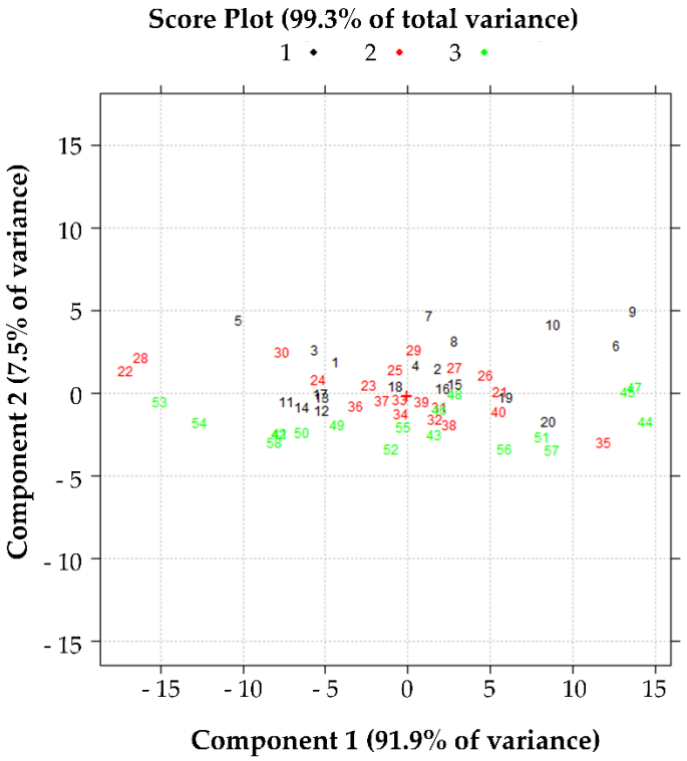

Figure 5. Effect of variable S, the batch production, on the anti-elastase activity. Score plot in the plane of the first two principal components of the data reported in Table S1.

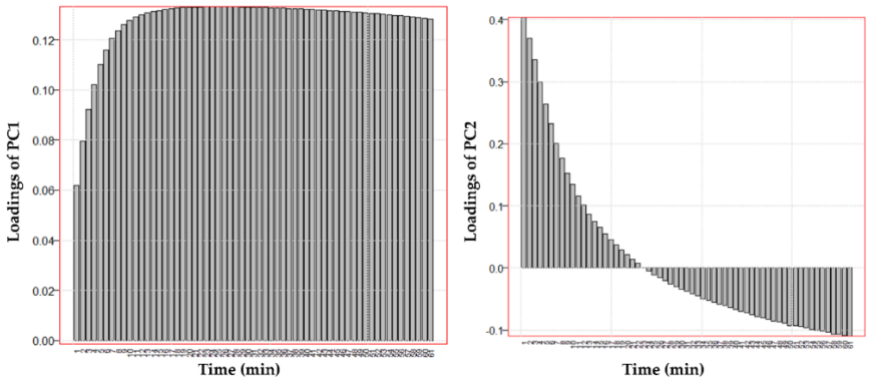

Figure 6. Loadings of the two principal components of the data reported in Table S1 as a function of time.

The data illustrated in Figure 7 show that the samples numbered in black have anti-elastase activity greater at the beginning of the experiment (from 1 to about 20 min). In comparison, those numbered in red have a greater variation in anti-elastase activity at the end of the experiment (from 25 min onwards). In general, the samples with greater anti-elastase activity at shorter read times are the ones of the rows n. 6, 9, 10 (batch 1), 44, 45 and 47 in black (batch 3) with C at level 0.5% *w*/*v*. The samples with greater anti-elastase activity at longer read times, and with C at the level of 1.5% *w*/*v* are those of rows n. 20 (batch 1), 35 (batch 2), 51 and 57 (batch 3) (refer to Table S1).

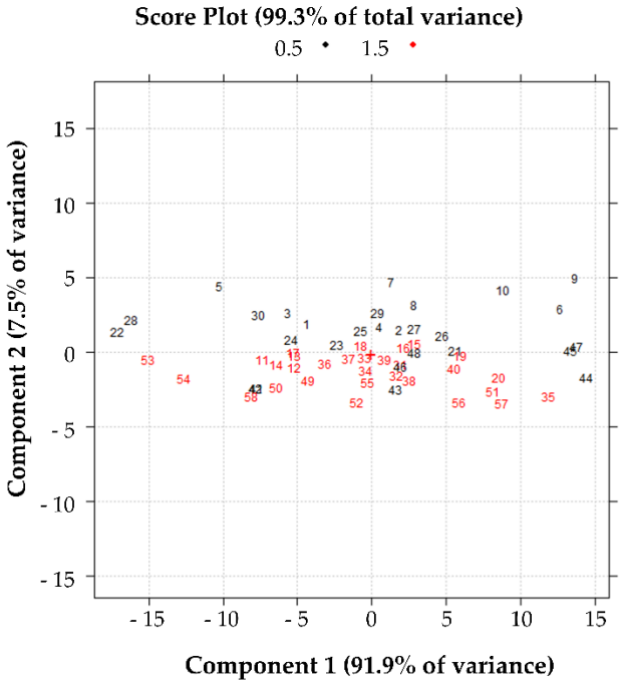

Figure 7. Effect of variable C on the anti-elastase activity. Score plot in the plane of the first two principal components of the data reported in Table S1.

The picture of the results represented in Figure 8, on the other hand, is less clear, but shows the correspondence of the values of the anti-elastase activity as a function of M.

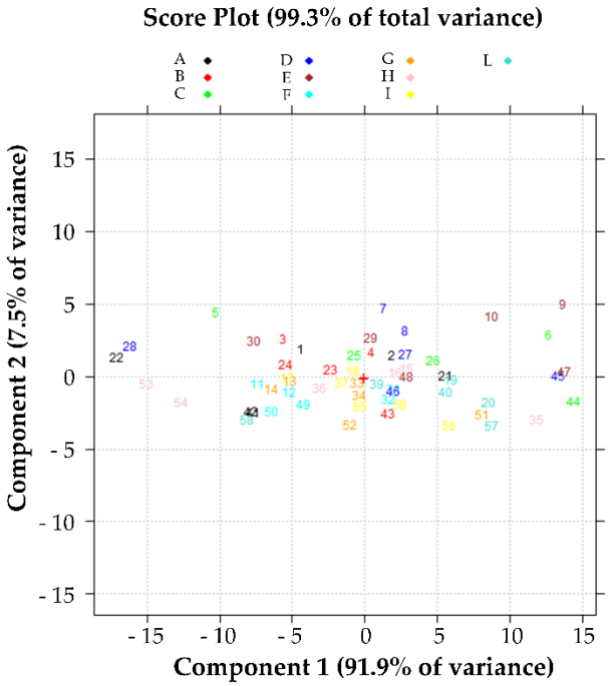

Figure 8. Effect of the variable M on the anti-elastase activity. Score plot in the plane of the first two principal components of the data reported in Table S1.

In conclusion, the anti-elastase activity depends on i) the secretome batch: the anti-elastase activity of batch 3 is different from that of batches 1 and 2 (Figure 5). ii) by the factor C; samples have anti-elastase activity dependent on factor C level and time. When C is at level 0.5% *w*/*v*, the highest anti-elastase activity is observed in the first minutes of the experiment (from 1 to 15 min approximately). From 15 min onwards, samples with C at the level of 1.5% *w*/*v* have higher anti-elastase activity. iii) The effect of M as such, is unclear and attributable to the two effects already described. It is essential to note that factors

C and M were evaluated, as reported in Sections 3.1 and 3.2, quantitatively and not qualitatively. Likely, different C and M values better preserve different MSC-secretome components, which influence the anti-elastase activity. Overall, based on such results, we concluded that the optimal formulation is the one already reported with 0.5% w/v mannitol, which showed to be active also in vivo [25].

3.5. Optimization and Validation of the Manufacturing Process

The data analysis reported in Section 3.1, Section 3.2, Section 3.3, Section 3.4 revealed that the batch strongly influences the product performances (protein and lipid yields and in vitro anti-elastase activity). Therefore, the ultrafiltration process used to isolate MSC-secretome from cell culture supernatants, which involves the standardization of the final product in terms of cell equivalents (CE), should be improved. In this regard, the process has been modified so that the final product is standardized to a specific protein concentration (115 µg/mL, PL) instead of CE. It has to be noted that, as a consequence, also the lipid content was standardized (the mean ± S.D. lipid content is 1.62 ± 0.71), probably because proteins and lipids have the same ratio in MSC-secretome. Therefore, the data of proteins and lipids (Table S6) were studied to verify the effect of PL or CE standardization. Figure 9 shows the box plots of the data as they are.

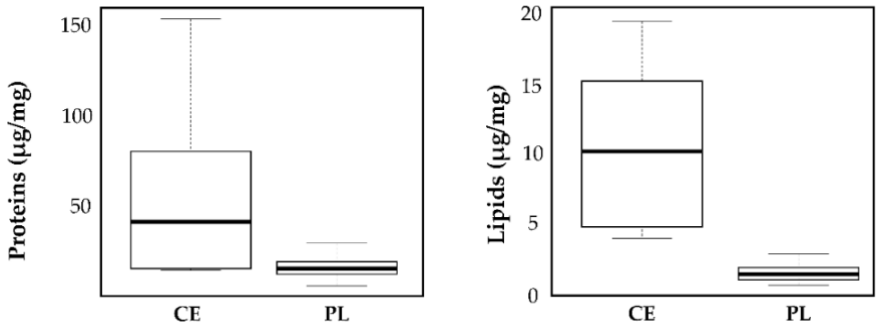

Figure 9. Results relative to the assays of proteins and lipids. CE = standardization for cell equivalents; PL = protein/lipid standardization.

The two groups of data, about both protein and lipid dosages, are heteroskedastic, and therefore do not satisfy one of the basic hypotheses that allow the use of ANOVA for data comparison. However, the comparison with hypothesis tests (which should necessarily be non-parametric) is entirely useless since, as expected, it is clear that the data are much more precise if the standardization is carried out with the PL method. In both cases, the median (the bold line) of the data measurements standardized with the PL method is lower than that obtained with CE standardization. The control charts of the same data are shown in Figures 10 and 11 below.

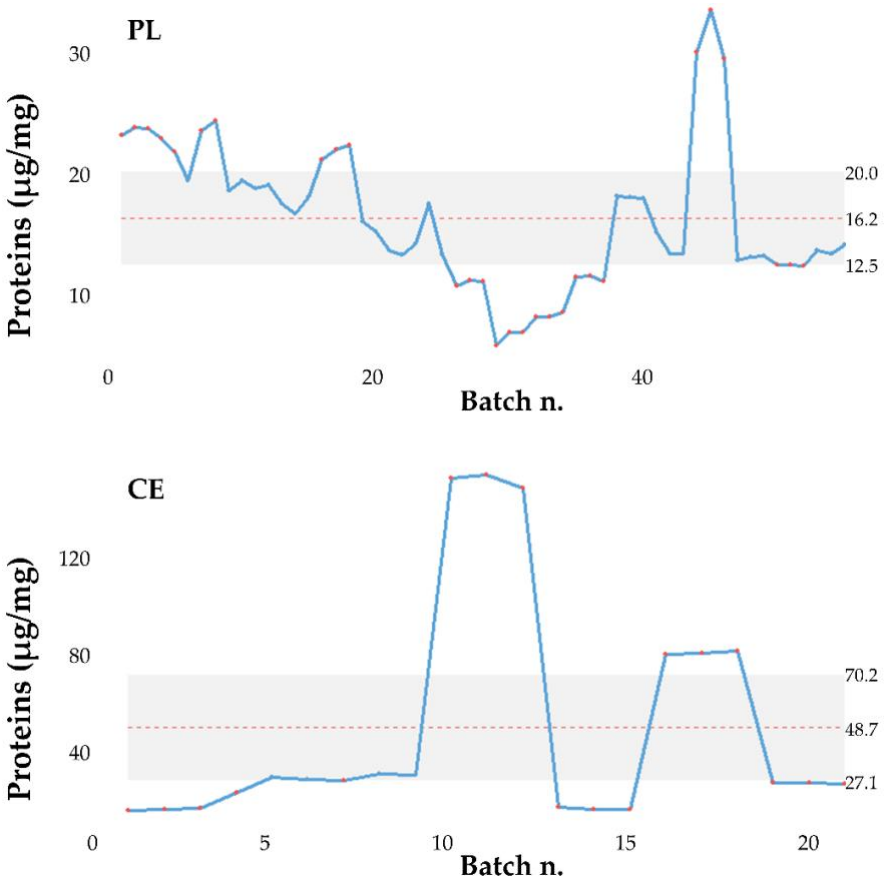

Figure 10. Control charts of the protein content in the batches studied. CE = standardization for cell equivalents; PL = protein/lipid standardization.

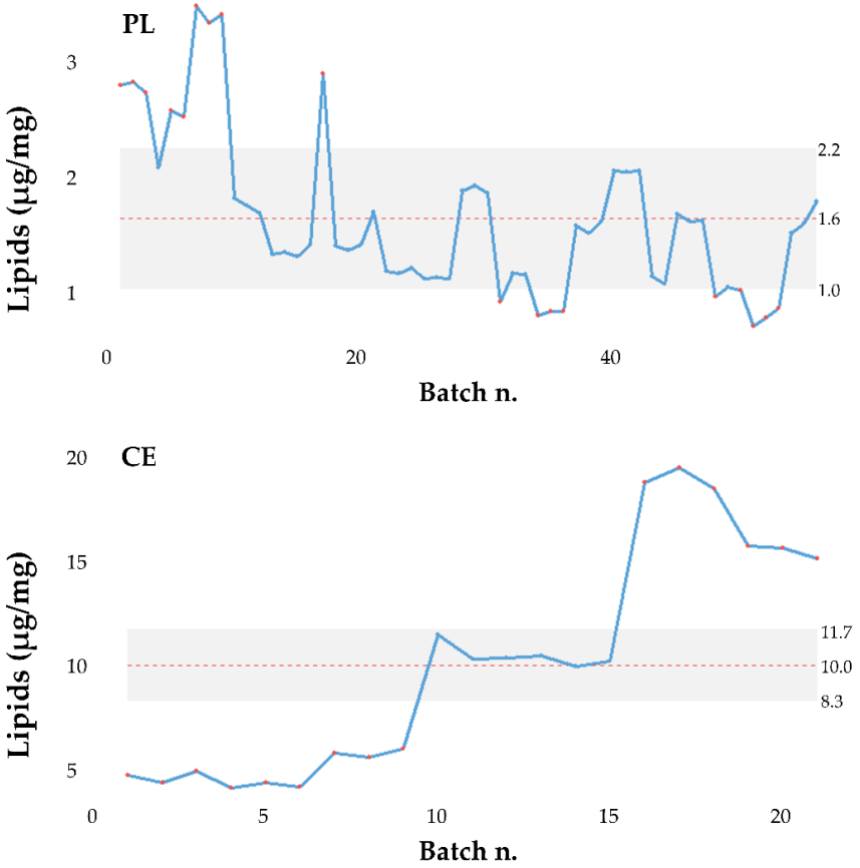

Figure 11. Control charts of the lipid content in the batches studied. CE = standardization for cell equivalents; PL = protein/lipid standardization.

Finally, the data of anti-elastase activity (Table S7) were studied by PCA. The score plot shown in Figure 12 shows that the data are well described in the plane of the first two PCs, with an explained variance of 99.4%. There is evident discrimination of the samples along with PC1, while the PC2 now explains only about 1% of the total variance of the data. There is evident discrimination of the samples along with PC1, while the PC2 now explains only about 1% of the total variance of the data.

Standardization with the PL method (red dots) produces batches with anti-elastase activity higher than that highlighted by the batches standardized with the CE method (black dots). In this case, PC1 describes the variation of the anti-elastase activity for almost all of the reading experiment. In contrast, the PC2 describes the variation of the residual anti-elastase activity in the first 2 min of the test (Figure 13). Therefore, almost all of the information provided by the anti-elastase activity readings is summarized in PC1 (Figure 13).

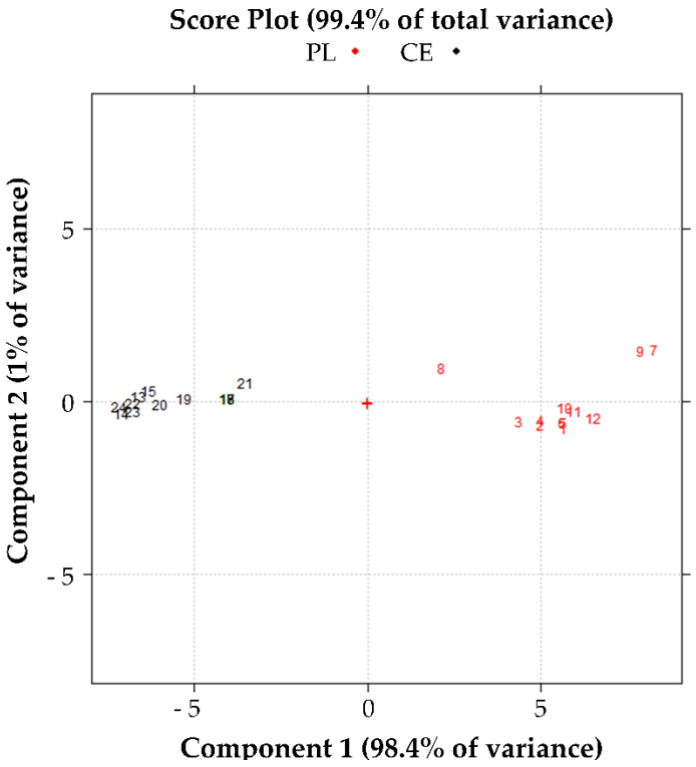

Figure 12. Effect of the batch on the anti-elastase activity. Score plot in the plane of the first two principal components of the data reported in Table S7.

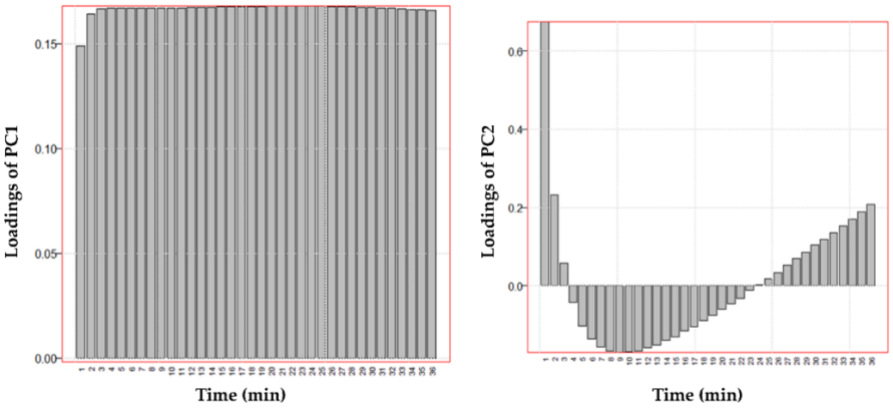

Figure 13. Loadings of the first two principal components of the data reported in Table S7 as a function of time.

5. Conclusions

Producing MSC-secretome for dose escalation studies and clinical practice requires scalable and GMP-compliant production procedures and formulation into a standardized medicinal product. Starting from a method that combines ultrafiltration and freeze-drying to transform MSC-secretome into a pharmaceutical product – the lyosecretome, in this work, a multi-level 5×2 design was used to study the influence of mannitol(M)/sucrose(S) binary mixture, selected as an excipient. A quadratic D-optimal design was computed to evaluate the effect of secretome batch (S), lyophilization (L), the concentration of excipients (C) and the mannitol/sucrose ratio in the excipient mixture (M) on the pharmaceutical dosage form characteristics (residual humidity and cake appearance) and on the product performances (protein and lipid yields, the EV particle size, and in vitro anti-elastase activity). The different excipients ratio did not affect residual moisture or EV particle size; simultaneously, proteins and lipids were better preserved in the freeze-dried product using the maximum total concentration of excipients (1.5% w/v) with an M:S ratio of around 60% w/w. On the other hand, the anti-elastase activity was better preserved using 0.5% *w/w* of mannitol as an excipient. The secretome batch resulted in being

the primary source of variability; therefore, the manufacturing process has been modified and then validated: the final product is now concentrated to reach a specific protein (and lipid) concentration instead of cell equivalents. This change in the quality assessment of our product resulted in a robust process and a tentative set of quality attributes that lead to a successful scale-up of the process.

Overall, this manuscript suggests a strategy to optimize the preparation and formulation of MSC-secretome, which can be applied, with suitable modifications, even to other biological drugs. Indeed, as the product is the process, any slight change in the production process can modify the qualitative-quantitative composition of the finished product and, therefore, its biological activity. Thus, through the concept of quality by design, the quality of the pharmaceutical product has to be built from the beginning, by complementary characterization techniques (validated at pharmaceutical grade and with an acceptable cost to be implemented on the quality controls that are carried out routinely) and by evaluating the expected therapeutic effect using standardized potency assays that possibly reflect the hypothesized MoA. In this regard, we chose the anti-elastase activity as we previously demonstrated that it is linked to the presence of elastase inhibitors, like alpha 1 antitrypsin [14].

Supplementary Materials

The following are available online at https://www.mdpi.com/article/10.3390/pharmaceutics13081129/s1, Figure S1. Cake aspect of freeze-dried Lyosecretome (numbers identify the formulation as detailed in Table 1). Figure S2. The plot of residuals for the model YP. Figure S3. Fitting for the model YP. Table S1. Summary of the in vitro elastase activity data; Table S2. Summary of the protein and lipid content. Table S3. The predictive ability for the model YP. NA = Not applicable. Table S4. The predictive ability for the model YL. NA = Not applicable. Table S5. Experimental plan (data in

black), experimental matrix (in blue) and responses (in the green field) were studied for the analysis of the data of the diameter of the lyophilized particles. Table S6. Summary of the protein and lipid content for batches standardized in proteins/lipids (PL) or cell equivalents (CE). Table S7. Summary of the anti-elastase data for batches standardized in proteins/lipids (PL) or cell equivalents (CE).

References

1. Fujita, Y.; Kadota, T.; Araya, J.; Ochiya, T.; Kuwano, K. Clinical Application of Mesenchymal Stem Cell-Derived Extracellular Vesicle-Based Therapeutics for Inflammatory Lung Diseases. Journal of Clinical Medicine 2018, 7, doi:10.3390/jcm7100355.
2. Caplan, A.I. What's in a Name? TISSUE ENGINEERING: Part A 2010, 16, 2415-2417.
3. Caplan, A.I. Mesenchymal Stem Cells: Time to Change the Name! Stem Cells Translational Medicine 2017, 6, 1445-1451, doi:10.1002/sctm.17-0051.
4. Gnecchi, M.; He, H.M.; Liang, O.D.; Melo, L.G.; Morello, F.; Mu, H.; Noiseux, N.; Zhang, L.N.; Pratt, R.E.; Ingwall, J.S.; et al. Paracrine action accounts for marked protection of ischemic heart by Akt-modified mesenchymal stem cells. Nature Medicine 2005, 11, 367-368, doi:10.1038/nm0405-367.
5. Hocking, A.M.; Gibran, N.S. Mesenchymal stem cells: Paracrine signaling and differentiation during cutaneous wound repair. Experimental Cell Research 2010, 316, 2213-2219, doi:10.1016/j.yexcr.2010.05.009.
6. Spees, J.L.; Lee, R.H.; Gregory, C.A. Mechanisms of mesenchymal stem/stromal cell function. Stem Cell Research & Therapy 2016, 7, doi:10.1186/s13287-016-0363-7.
7. Bari, E.; Ferrarotti, I.; Torre, M.L.; Corsico, A.G.; Perteghella, S. Mesenchymal stem/stromal cell secretome for lung regeneration: The long way through "pharmaceuticalization" for the best formulation. Journal of Controlled Release 2019, 309, 11-24, doi:10.1016/j.jconrel.2019.07.022.
8. Eleuteri, S.; Fierabracci, A. Insights into the Secretome of Mesenchymal Stem Cells and Its Potential Applications. International Journal of Molecular Sciences 2019, 20, doi:10.3390/ijms20184597.

9. Nagelkerke, A.; Ojansivu, M.; van der Koog, L.; Whittaker, T.E.; Cunnane, E.M.; Silva, A.M.; Dekker, N.; Stevens, M.M. Extracellular vesicles for tissue repair and regeneration: evidence, challenges and opportunities. Advanced drug delivery reviews 2021, doi:10.1016/j.addr.2021.04.013.

10. Gimona, M.; Pachler, K.; Laner-Plamberger, S.; Schallmoser, K.; Rohde, E. Manufacturing of Human Extracellular Vesicle-Based Therapeutics for Clinical Use. International Journal of Molecular Sciences 2017, 18, doi:10.3390/ijms18061190.

11. Reiner, A.T.; Witwer, K.W.; van Balkom, B.W.M.; de Beer, J.; Brodie, C.; Corteling, R.L.; Gabrielsson, S.; Gimona, M.; Ibrahim, A.G.; de Kleijn, D.; et al. Concise Review: Developing Best-Practice Models for the Therapeutic Use of Extracellular Vesicles. Stem Cells Translational Medicine 2017, 6, 1730-1739, doi:10.1002/sctm.17-0055.

12. Manandhar, S.; Kothandan, V.K.; Hwang, S.R.; 오지윤; 유성현; 황진수. A pharmaceutical investigation into exosomes. Journal of Pharmaceutical Investigation 2018, 48, 617-626, doi:10.1007/s40005-018-0391-7.

13. Bari, E.; Perteghella, S.; Di Silvestre, D.; Sorlini, M.; Catenacci, L.; Sorrenti, M.; Marrubini, G.; Rossi, R.; Tripodo, G.; Mauri, P.; et al. Pilot Production of Mesenchymal Stem/Stromal Freeze-Dried Secretome for Cell-Free Regenerative Nanomedicine: A Validated GMP-Compliant Process. Cells 2018, 7, doi:https://doi.org/10.3390/cells7110190.

14. Bari, E.; Ferrarotti, I.; Di Silvestre, D.; Grisoli, P.; Barzon, V.; Balderacchi, A.; Torre, M.L.; Rossi, R.; Mauri, P.; Corsico, A.G.; et al. Adipose Mesenchymal Extracellular Vesicles as Alpha-1-Antitrypsin Physiological Delivery Systems for Lung Regeneration. Cells 2019, 8, doi:10.3390/cells8090965.

15. Mocchi, M.; Grolli, S.; Dotti, S.; Di Silvestre, D.; Villa, R.; Berni, P.; Conti, V.; Passignani, G.; Brambilla, F.; Bue, M.D.; et al. Equine Mesenchymal Stem/Stromal Cells Freeze-Dried Secretome (Lyosecretome) for the Treatment of Musculoskeletal Diseases: Production Process Validation and Batch Release Test for Clinical Use. Pharmaceuticals 2021, 14, 553.

16. Kumar, K.N.; Mallik, S.; Sarkar, K. Role of freeze-drying in the presence of mannitol on the echogenicity of echogenic liposomes. Journal of the Acoustical Society of America 2017, 142, 3670-3676, doi:10.1121/1.5017607.

17. Ohtake, S.; Kita, Y.; Arakawa, T. Interactions of formulation excipients with proteins in solution and in the dried state. Advanced Drug Delivery Reviews 2011, 63, 1053-1073, doi:10.1016/j.addr.2011.06.011.

18. Franze, S.; Selmin, F.; Samaritani, E.; Minghetti, P.; Cilurzo, F. Lyophilization of Liposomal Formulations: Still Necessary, Still Challenging. Pharmaceutics 2018, 10, doi:10.3390/pharmaceutics10030139.

19. Faustini, M.; Bucco, M.; Chlapanidas, T.; Lucconi, G.; Marazzi, M.; Tosca, M.C.; Gaetani, P.; Klinger, M.; Villani, S.; Ferretti, V.V.; et al. Nonexpanded Mesenchymal Stem Cells for Regenerative Medicine: Yield in Stromal Vascular Fraction from Adipose Tissues. Tissue Engineering Part C-Methods 2010, 16, 1515-1521, doi:10.1089/ten.tec.2010.0214.

20. Gaetani, P.; Torre, M.L.; Klinger, M.; Faustini, M.; Crovato, F.; Bucco, M.; Marazzi, M.; Chlapanidas, T.; Levi, D.; Tancioni, F.; et al. Adipose-derived stem cell therapy for intervertebral disc regeneration: An in vitro reconstructed tissue in alginate capsules. Tissue Engineering Part A 2008, 14, 1415-1423, doi:10.1089/ten.tea.2007.0330.

21. Dominici, M.; Le Blanc, K.; Mueller, I.; Slaper-Cortenbach, I.; Marini, F.C.; Krause, D.S.; Deans, R.J.; Keating, A.; Prockop, D.J.; Horwitz, E.M. Minimal criteria for defining multipotent mesenchymal stromal cells. The International Society for Cellular Therapy position statement. Cytotherapy 2006, 8, 315-317, doi:10.1080/14653240600855905.

22. Patel, S.M.; Nail, S.L.; Pikal, M.J.; Geidobler, R.; Winter, G.; Hawe, A.; Davagnino, J.; Gupta, S.R. Lyophilized Drug Product Cake Appearance: What Is Acceptable? Journal of Pharmaceutical Sciences 2017, 106, 1706-1721, doi:10.1016/j.xphs.2017.03.014.

23. http://gruppochemiometria.it/index.php/software. Available online: (accessed on 17/05/2021).

24. Coccè, V.; La Monica, S.; Bonelli, M.; Alessandri, G.; Alfieri, R.; Lagrasta, C.A.; Madeddu, D.; Frati, C.; Flammini, L.; Lisini, D.; et al. Inhibition of Human Malignant Pleural Mesothelioma Growth by Mesenchymal Stromal Cells. Cells 2021, 10, 1427.

25. Bari, E.; Di Silvestre, D.; Mastracci, L.; Grillo, F.; Grisoli, P.; Marrubini, G.; Nardini, M.; Mastrogiacomo, M.; Sorlini, M.; Rossi, R.; et al. GMP-compliant sponge-like dressing containing MSC lyo-secretome: proteomic network of healing in a murine wound model. European journal of pharmaceutics and biopharmaceutics : official journal of Arbeitsgemeinschaft fur Pharmazeutische Verfahrenstechnik e.V 2020, doi:10.1016/j.ejpb.2020.08.003.

CHAPTER 3:

EQUINE MSC-SECRETOME

Mesenchymal stem cells are the most prominent cell type explored for their therapeutic potential in treating joint injury and osteoarthritis, most commonly those isolated from the bone marrow, adipose tissue, and synovium. Following on from these observations, it is now generally accepted that MSCs primarily exert their therapeutic effects through the secretion of trophic factors to reduce inflammation and enhance repair. The available evidences point out a strong potential of the MSC-secretome in promoting joint repair and providing protection from degeneration following joint injury. Equines represent a valid model to be investigated in this challenge, indeed it is driven by the high demand of horse owners for innovative regenerative therapies, primarily geared toward the treatment of musculoskeletal injuries, and it is also a well-characterized models for specific human diseases, most notably orthopedic injuries such as OA**,** of which have the potential to be managed by treatment with MSC-secretome.

Equine adipose-derived mesenchymal stromal cells exhibit attractive proregenerative properties, in this context, **Paper 3** described the preparation and characterization of a freeze-dried secretome (Lyosecretome) from adipose tissue-derived mesenchymal stromal cells for the therapy of equine musculoskeletal disorder. The work provides a proof-of-concept for the manufacturing of clinical-grade equine freeze-dried secretome, and prototypes for safety and efficacy clinical trials in the treatment of equine musculoskeletal diseases.

Paper 3. Mocchi M, Grolli S, Dotti, S, Di Silvestre D, Villa R, Berni P, Conti V, Passignani G, Brambilla F, Del Bue M, Catenacci L, Sorrenti M, Segale L, Bari E, Mauri P, Torre M.L, and Perteghella S (2021) Equine Mesenchymal Stem/Stromal Cells Freeze-Dried Secretome (Lyosecretome) for the Treatment of Musculoskeletal Diseases: Production Process Validation and Batch Release Test for Clinical Use. Pharmaceuticals 14, 553; doi: 10.3390/ph14060553.

Abstract. In the last decades, it has been demonstrated that the regenerative therapeutic efficacy of mesenchymal stromal cells is primarily due to the secretion of soluble factors and extracellular vesicles, collectively known as secretome. In this context, our work described the preparation and characterization of a freeze-dried secretome (Lyosecretome) from adipose tissue-derived mesenchymal stromal cells for the therapy of equine musculoskeletal disorder. An intraarticular injectable pharmaceutical powder has been formulated, and the technological process has been validated in an authorized facility for veterinary clinical-use medicinal production. Critical parameters for quality control and batch release have been identified regarding (i) physicochemical properties; (ii) extracellular vesicle morphology, size distribution, and surface biomarker; (iii) protein and lipid content; (iv) requirements for injectable pharmaceutical dosage forms such as sterility, bacterial endotoxin, and Mycoplasma; and (v) in vitro potency tests, as anti-elastase activity and proliferative activity on musculoskeletal cell lines (tenocytes and chondrocytes) and mesenchymal stromal cells. Finally, proteins putatively responsible for the biological effects have been identified by Lyosecretome proteomic investigation: IL10RA, MXRA5, RARRES2, and ANXA1 modulate the inflammatory process RARRES2, NOD1, SERPINE1, and SERPINB9 with antibacterial activity. The work provides a proof-of-concept for

the manufacturing of clinical-grade equine freeze-dried secretome, and prototypes are now available for safety and efficacy clinical trials in the treatment of equine musculoskeletal diseases.

Keywords: mesenchymal stem cells; secretome; regenerative medicine; musculoskeletal disorders; equine

1. Introduction

Musculoskeletal disorders (MSDs) have an extensive and growing impact representing a major health problem worldwide. Despite years of research, the understanding of these diseases and the control on their progression has not yet been achieved; indeed, different therapeutic approaches are being investigated to prevent the disorders or to promote recovery and/or regeneration of the musculoskeletal system, including muscles, bones, and joints [1,2]. MSDs often result from traumatic injuries due, for example, to vigorous physical activity leading to excessive muscle fatigue, damage of joint structures (articular cartilage, subchondral bone, synovial membrane), and inflammation or lesion of the tendon/ligament structure. Structural and genetic factors are also associated with musculoskeletal diseases onset and progression [3]. MSDs represent a high percentage of orthopedic clinical pathologies in veterinary practice and, mainly, in equine practice. Due to the low healing capacity of tissues involved in joint and tendon disorders, there is a tendency to develop chronic diseases with a significant clinical relevance [4]. Beyond the traditional treatments (local or systemic nonsteroidal anti-inflammatory drugs, intralesional steroids, correct shoeing, chondroprotectants such as hyaluronic acid), innovative regenerative therapies, including the use of Mesenchymal Stem/Stromal Cells (MSCs), have emerged over the past ten years as promising agents to promote local repair. Especially in the veterinary field, many clinical applications of cell-based therapies have been described, starting from the early 2000s with the first application of MSCs on the equine model [5,6]. Despite the

considerable amount of data suggesting the safety and efficacy of MSCs in experimental animal models and preclinical studies, cell-based therapies are not yet routinely applied in the clinic [7–10]. Over the years, the therapeutic application of MSCs has known a paradigm shift: Nowadays, their engraftment, proliferation, and differentiation properties are not considered key features of their therapeutic abilities. Instead, the main actors of MSCs benefit are now considered several bioactive molecules (including proteins, cytokines, chemokines, growth factors, but also nucleic acid) released by cells and involved in cell-to-cell communication and crosstalk [11]. Known as secretome, this complex set of secreted factors and vesicles seems to represent a valid alternative as a cell-free therapy, offering several advantages in comparison to cell-based therapy, such as lower immunogenicity, ease of storage and handling, and lower cost ensuring usefulness and feasibility in the clinic [12,13]. However, addressing a suitable medicinal product is challenging, and further investigations are needed to shed light on secretome composition, properties, and in vivo behavior. Indeed, while evaluating secretome safety and efficacy for clinical use, many aspects, ranging from production processes to molecular characterization, must be defined.

In this study, an injectable freeze-dried pharmaceutical powder containing equine secretome has been formulated (Lyosecretome); the technological process has been validated in an authorized facility for veterinary clinical-grade medicinal production. Critical parameters for quality control and batch release have been identified regarding (i) physicochemical powder properties; (ii) extracellular vesicle morphology, size distribution, and surface biomarkers; (iii) protein and lipid content; (iv) requirements for injectable pharmaceutical dosage forms (sterility, bacterial endotoxin, and Mycoplasma); and (v) in vitro potency tests, and efficacy on proliferative induction of selected cell lines. Finally, putative proteins responsible for the biological effects have been identified by a Lyosecretome proteomic

investigation based on nano Liquid Chromatography coupled with high-resolution mass spectrometry.

2. Materials and methods

The Lyosecretome production was made at an accredited facility to produce and control veterinary drugs for clinical use (Istituto Zooprofilattico Sperimentale Lombardia and Emilia-Romagna (IZSLER, Brescia, Italy). The production protocol has been approved by the Italian Ministry of Health (Prot. n. 0000778 del 15/01/2020 7.1.2.0.0.0/17/2019—AGD 809). Culture media, trypsin, and antibiotics used for cell cultures were purchased from Euroclone (Milan, Italy). A commercial platelet lysate kit (PL) was obtained from Carlo Erba Reagents (Milan, Italy). Fetal Bovine Serum (FBS) was purchased by Gibco-Thermofisher (Milan, Italy). Chemicals such as mannitol, bovine serum albumin, Nile Red, acetone, collagenase, and phosphatidylcholine were obtained from Merck Life Science S.r.l. (Milan, Italy) unless mentioned.

2.1. Lyosecretome Production

2.1.1. Mesenchymal Stem/Stromal Cell Isolation

Allogeneic AD-MSCs from equine species were obtained from the biobank at Istituto Zooprofilattico Sperimentale Lombardia and Emilia-Romagna (IZSLER) (Brescia, Italy). The clinical data related to the cells stored in the biobank as gender, age, the weight of the donor, and cell passage number, were recorded by the IZSLER. In detail, the secretome was produced by three donors. The donors were 10 years old, male, and the breed is unknown. The samples were tested for Equine Herpesvirus, Equine Arterivirus, Flavivirus, and Lentivirus (antibodies screening). All the samples were collected from animals killed at the slaughterhouse following the related Italian Law. Adipose tissue digestion was performed at 37 °C, 5% CO_2 using type II collagenase 0.075% (w/v) solubilized in Phosphate Buffer Saline (PBS)

with Ca^{2+} and Mg^{2+} supplemented with penicillin (50 U/mL), streptomycin (20 μg/mL), and amphotericin B (2.5 μg/mL). After 1 h, Dulbecco's modified Eagle's Medium (DMEM) with 10% (v/v) of equine platelet lysate was added to the cell suspension in a 1:1 ratio. The digested tissue was filtered with 70 μm filters and centrifuged at 600× g for 5 min. The recovered stromal vascular fraction was grown in a monolayer (100,000 cells/cm^2) in DMEM, enriched with 10% (v/v) platelet lysate, penicillin, streptomycin, and amphotericin B. On reaching sub-confluence, the MSCs were detached from the flask with 0.05% (w/v) trypsin-EDTA, counted, seeded in flasks (10,000 cells/cm^2) at 37 °C and 5% CO_2, and amplified. Upon reaching sub-confluence, the cells were ready for the induction of secretome production. All cells used were at passage 1 and tested for trilineage differentiation and microbiological controls.

2.1.2. Mesenchymal Stem/Stromal Cell-Derived Secretome Production

Adipose Secretome production was induced by platelet lysate starvation of MSCs. In detail, the culture medium was removed, and the cells were repeatedly washed (at least three times) with PBS without Ca^{2+} and Mg^{2+} to eliminate any residual platelet lysate [14]. MSCs were then cultured in a DMEM medium without platelet lysate for 24 h, replacing the culture medium after the first 9 h. Both conditioned media (collected at 9 and 24 h, respectively) were blended; MSCs were detached with trypsin-EDTA and counted in a Burker chamber.

2.1.3. Ultrafiltration

The collected conditioned media was firstly centrifuged at 3500× *g* for 10 min to eliminate cell fragments and apoptotic bodies. Subsequently, supernatants were collected, and the ultrafiltration process was performed applying a tangential flow filtration using KrosFlo® Research 2i system (Spectrum Laboratories, Milan, Italy), using Molecular Weight Cut Off (MWCO) of a 5 kDa filtration module (Spectrum Laboratories, Milan, Italy). For the ultrafiltration process, all the instrument components were sterilized to operate in aseptic conditions under a laminar flow hood. The ultrafiltration process consists of two phases, at first allowing to concentrate the sample, and then to diafilter with sterilized and ultrapure water; according to manufacturer's guidelines, during each step, the shear rate of the feed stream was kept between 2000 s^{-1} and 6000 s^{-1}, while the transmembrane pressure index was kept at maximum 5 psi. The concentration step led to a concentration of 0.5×10^6 cell equivalents per mL. The evaluation of the process scale-up was calculated as average liters per m^2 per h:

$$L/m^2/h = \text{permeate flux (mL/min)/cartridge superficial area } (m^2)\ 0.06$$

2.1.4. Secretome Freeze-Drying

As the elective cryoprotectant, mannitol was chosen for this study, and it was mixed with the purified secretome at the concentration of 0.5% (w/v). The resulting solution was at first frozen at −80 °C, and then a conservative freeze-drying process was adopted (Heto PowerDry PL3000) at 8×10^{-1} mbar and −50 °C for 72 h. The lyophilized secretome was kept at −20 °C up to the time of use (maximum 9 months). Before and after the freeze-drying process, Lyosecretome yield (mg) was established, and cell equivalents per mg were

calculated by dividing the total cell number used for production and the gained milligrams of Lyosecretome.

2.2. Lyosecretome Characterization

2.2.1. Residual Humidity and Osmolarity

After the samples rebalance at room temperature, residual humidity was determined by the Coulometric Titrator HI904 (Hanna Instruments). The titration was conducted two times on each vial (n = 3 vials). After reconstitution of 10 mg of lyophilized product in 2 mL saline (0.9% *w*/*v* NaCl in water) at 37 °C, the osmolarity was measured using a micro osmometer (Precision System Inc., Natick, MA, USA). The pH of the reconstituted product was measured by pH meter (Mettler-Toledo, Columbus, OH, USA).

2.2.2. Fourier Transform Infrared Spectroscopy (FT-IR)

FT-IR spectra of Lyosecretome were obtained using a Spectrum One Perkin-Elmer spectrophotometer (Perkin Elmer, Wellesley, MA, USA) equipped with a MIRacle™ ATR device (Pike Technologies, Madison, WI, USA). The IR spectra in transmittance mode were collected in the spectral region of 650–4000 cm^{-1} due to the accumulation of 64 scans with a resolution of 4 cm^{-1}.

2.2.3. Thermal Characterization

Differential scanning calorimetry (DSC) analysis measured temperature and enthalpy values with a Mettler STAR^e system (Mettler Toledo, Columbus, OH, USA) equipped with a DSC81^e Module and an Intracooler device (Jukabo FT 900) for subambient temperature analysis. Firstly, the instrument was previously calibrated with Indium as a standard reference. Outcome curves were achieved recording on about 3 mg of samples in 40 μL sealed aluminum pans with pierced lids (method: −30–350 °C temperature range; heating rate

10 K min^{-1}; nitrogen air atmosphere flux 50 mL min^{-1}). Experiments were performed in triplicate.

Thermogravimetric analysis (TGA) was measured with a Mettler STAR^e system equipped with a TGA/DSC1. Firstly, the instrument was calibrated with Indium as a standard reference. Outcome curves of the mass losses were obtained recording on 3–4 mg of samples in 70 μL alumina pans (method: 30–350 °C temperature range; heating rate 10 K min^{-1}; nitrogen air atmosphere flux 50 mL min^{-1}). Experiments were performed in triplicate.

2.2.4. Morphology Investigation by Scanning Electron Microscopy (SEM)

Lyosecretome morphology has been investigated by SEM with a Zeiss EVO MA 10 (Carl Zeiss, Oberkochen, Germany). For the analysis, the samples were coated with a gold-sputter under argon.

2.2.5. Particle Size Distribution

The particle size distribution of Lyosecretome was evaluated by performing Nanoparticle Tracking Analysis (NTA) using NanoSight NS 300 (Malvern Instruments, Malvern, UK). In detail, the freeze-dried powder was resuspended in 1 mL of deionized water (1 mg/mL) and analyzed with a dilution factor of 1:10. All measurements were repeated for 6 cycles of 60 s each, using NanoSight protocols.

2.2.6. Microvesicles Surface Biomarkers by ExoView Analysis

ExoView (Alfatest, I) is an innovative test to determine the size and number of exosomes in a sample by biomarker detection. The Tetraspanin Human Standard Kit with a thin layer of CD63, CD81, and CD9 was chosen, and solutions for sample dilution were supplied by the Nano View Bioscience company. The analysis method could be divided into two macro steps: Interferometric imaging that gives information about the exosome's number and exosome's size; and

fluorescence analysis that offers the intensity of a positive marker protein. Samples were prepared in triplicate and diluted according to the protocol suggested by the supplier for the tetraspanin kit (NanoView Biosciences; EV-TETRA) and incubated for 16 h on ExoView tetraspanin chips. The chips were coated with a fluorescent antibodies mixture of anti CD81, CD63, or CD9, placed on an orbital shaker at 500 rpm for 1 h, and then washed four times. Chips were transferred into a Petri plate with MilliQ water for the final washing step and, after drying with an adsorbent paper, placed onto ExoView instrument's chip holder and analyzed. The results are the average of three determinations.

2.2.7. Total Protein Quantification

At the end of the lyophilization process, Lyosecretome protein quantification was determined by using the BCA-Protein Assay Kit (Thermo Fischer Scientific, Milan, Italy) following the manufacturer's specifications. The absorbance–concentration calibration curve was generated using bovine serum albumin (BSA) standards. Working reagent solution was added to each sample and standard (ratio 1:1) and then incubated at 37 °C for 2 h before measuring the absorbance at 562 nm with a microplate reader (Synergy HT, Milan, Italy). The Lyosecretome protein amount was estimated as a plot function comparing concentration vs. absorbance obtained for the standard protein solutions, using a third-order polynomial equation, with R^2 = 0.99. Results are reported as μg of protein per mg of Lyosecretome. Each sample was tested in triplicate.

2.2.8. Total Lipid Quantification

To prepare the Nile Red stock solution, the Nile Red powder was solubilized in acetone (3.14 M), avoiding light exposure, and kept at 4 °C. The stock solution was diluted 100× in PBS (pH = 7.4) before use, and 10 μL of it were incubated with 90 μL of samples. After 5 min, the

relative fluorescence was calculated by Sinergy HT (530/25 excitation and 645/40 emission). The Lyosecretome lipid amount was estimated as a plot function comparing concentration vs. absorbance obtained for standard phosphatidylcholine solutions, using a third-degree polynomial equation, with $R^2 = 0.99$. Results are reported as μg of lipid per mg of Lyosecretome. Each sample was tested in triplicate.

2.2.9. Sterility Test and Microbiological Control

Each batch was investigated for sterility, endotoxins, Mycoplasma, and microbiological contaminations, as described in the current version of European Pharmacopoeia. Briefly, sterility and microbial examinations were performed as indicated in EuPh 2.6.27 and 2.6.1 chapters, respectively. Furthermore, a bacterial endotoxins evaluation was carried out by the Limulus Amebocyte Lysate test (EuPh 2.6.14), a chromogenic kinetic method, and measured as an Endotoxin Unit (EU). The test was performed following the manufacturer's instructions. Finally, mycoplasma contamination was investigated by performing specific tests (NAT test, EuPh 2.6.7.).

2.3. In Vitro Potency Test

2.3.1. Elastase Inhibitory Assay

The in vitro inhibitory effect of equine Lyosecretome on the elastase enzyme was evaluated using the method previously described in the literature, with some modifications [15]. Pancreatic porcine elastase (Merck Life Science S.r.l.) was solubilized in phosphate buffer pH 6.8 (0.5 IU mL^{-1}). The substrate N-succinyl-Ala-Ala-Ala-p-nitroanilide (Merck Life Science S.r.l.) was dissolved in TRIS buffer until a final concentration of 0.41 mmol L^{-1} was reached. All the tested concentrations (2, 5, 10, 20 mg mL^{-1}) were incubated with the enzyme for 20 min, and, consequently, the substrate was added right before reading the microplates to begin the reaction. The kinetic reaction was monitored by spectrophotometric analysis (Synergy HT) at the

absorbance of 410 nm for 35 min (measurements were made every minute). The reaction mixture in the absence of sample was used as a negative control, while the epigallocatechin gallate (EGCG) (Merck Life Science S.r.l.) was used as a positive control. The absorbance value of each sample was subtracted from the absorbance of the blank mixture (sample without the enzyme and substrate). Analyses were performed in triplicate. The inhibition rate was reported as a percentage of anti-elastase activity and calculated as follows:

$$\text{Activity (\%)} = [(A_{CTR} - A_{samp})/A_{CTR}] \times 100$$

where A_{CTR} is the negative control absorbance and A_{samp} is the Lyosecretome sample absorbance.

2.3.2. Proliferative Test

The proliferative effects of Lyosecretome were evaluated on four different equine cell lines: Chondrocytes, tenocytes, synovial fluid, and adipose tissue-derived MSCs. Tissue samples were collected at the local abattoir following the related Italian Law from three healthy 5- to 10-year-old male horses of unknown breed, ensuring the absence of viral and bacterial pathologies. AD-MSCs were isolated and expanded as described above (see paragraph 2.1.2).

Synovial Fluid Cells Collection and Expansion

The synovial fluid was collected from the metacarpophalangeal (fetlock) joint. Following trimming and disinfection, 4–5 mL of fluid were collected with a sterile syringe, transferred in a 50 mL falcon-type tube, and diluted 1:10 with sterile phosphate-buffered saline (PBS). After accurate mixing, the tube was centrifuged at 500× *g* for 20 min. The cell pellet was resuspended in 2 mL of DMEM supplemented with penicillin (50 U/mL), streptomycin (25 µg/mL), and amphotericin B (2 µg/mL) and transferred in two 25 cm^2 culture flasks. After 48 h, the medium was changed. The attached cells were expanded until they

reached about 80% confluence when they were trypsinized and expanded at a 1:3 ratio. Cells were used for further experiments at passage P3-P4.

Tenocytes Isolation and Expansion

Tissue samples of superficial digital flexor tendon (SDFT) were collected in sterility and dissected in 2–3 mm^3 pieces with a scalpel blade, removing tendon sheath. The tissue was digested overnight in 1 mg/mL collagenase II (5 mL/g of tissue) at 37 °C. After digestion, the cell suspension was strained (40 μm nylon mesh) and then centrifuged at 900× *g* for 15 min. The cell pellet was resuspended in 2 mL of DMEM supplemented with 1% (*v*/*v*) penicillin (100 U/mL), streptomycin (100 μg/mL), and amphotericin B (2 μg/mL). Cell viability was assessed by Trypan blue staining. Cells were then transferred in 25 cm^2 culture flasks (10,000 cm^2) and expanded in DMEM at 37 °C, 5% CO_2. Upon reaching P3–P4, cells were used for further experiments.

Chondrocytes Isolation and Expansion

Cartilage issue samples were collected from the metacarpophalangeal joint. The joint was exposed in sterility, and about 1 g of cartilage was collected with a scalpel blade in small pieces. Tissue samples were digested overnight in 5 mL of collagenase type II (0.1%, *v*/*v* in DMEM) at 37 °C [2]. After digestion, the cell suspension was strained (40 μm nylon mesh) and centrifuged at 180× *g* for 15 min. The cell pellet was resuspended in DMEM supplemented with 1% (*v*/*v*) penicillin (100 U/mL), streptomycin (100 μg/mL), and amphotericin B (2 μg/mL) and then seeded with the same medium in 25 cm^2 culture flasks (10,000 cells/cm^2). Cells were used for in vitro metabolic activity assay at passage P3–P4.

Proliferative Test by MTT

The MTT assay was performed to assess cell metabolic activity in the four different cell lines reported above (AD-MSCs, SF-MSC, tenocytes, and chondrocytes) as potential targets for the use of Lyosecretome in osteoarticular diseases. In detail, 10,000 cells/well were plated in 96-well plates in DMEM supplemented with 10% Fetal Bovine Serum (FBS); three replicates were prepared for each treatment. After 24 h, the medium was replaced with serum-free DMEM containing Lyosecretome at the concentrations of 400,000, 200,000, and 100,000 cells/well. Cells were cultured for a further 48 h, and then the MTT test was performed as previously reported [16]. Briefly, the cells' optical density (OD) after MTT treatment was measured at 570 nm and 670 nm (reference wavelength). The cell metabolic activity percentage was calculated as 100 × (ODsample/ODcontrol). Cells cultured with DMEM containing 10% FBS were considered a positive control (ODcontrol), while the cells cultured without serum (serum-free medium) were considered a negative control. The MTT assay was repeated with four different cell preparations for each cell line.

2.4. Proteomic Investigation

2.4.1. LC-MS/MS Analysis

Two milliliters of sample were concentrated to 100 μL in a vacuum concentrator at 60 °C, and the protein concentration was assessed using the SPN™ Protein Assay kit (G-Biosciences, St. Louis, MO, USA); 50 μg of proteins were added with 0.2% of Rapigest and held at 100 °C for 20 min. The sample was digested overnight at 37 °C by adding sequencing-grade modified trypsin (Promega, Madison, WI, USA) at an enzyme/substrate ratio of 1:50 (*w*/*w*). An additional aliquot of trypsin (enzyme/substrate ratio of 1:100 *w*/*w*) was added in the morning (4 h, 37 °C). The addition of 0.5% trifluoroacetic acid stopped the enzymatic reaction. Digested proteins were desalted using PepClean C-18 spin columns (Pierce Biotechnology, Inc., Rockford, IL,

USA), concentrated, and finally suspended in 20 μL of 0.1% (*v*/*v*) formic acid.

The sample was analyzed using two LC-MS/MS platforms for a total of seven technical replicates. The first LC-MS/MS system (n = 3) was equipped with an Eksigent nanoLC-Ultra 2D System (Eksigent, part of AB SCIEX, Dublin, CA, USA) coupled with a hybrid ion trap-Orbitrap mass spectrometer (LTQ Orbitrap XLTM ETD; Thermo Fisher Scientific, Inc., Milan, Italy). The loading pump runs in isocratic mode with 0.1% formic acid in water for 10 min at a flow rate of 3 μL/min; the gradient pump runs a 125-min gradient of 5 to 95% of eluent B (5–40% B in 110 min, 40–95% B in 15 min; eluent A, 0.1% formic acid in water; eluent B, 0.1% formic acid in acetonitrile) at a flow rate of 300 nL/min through the column (75 μm × 15 cm ChromXP C18-CL 3 μm, 120 Å). Eluting peptides were electrosprayed directly into a hybrid ion trap-Orbitrap mass spectrometer (LTQ Orbitrap XLTM ETD; Thermo Fisher Scientific, Inc., Milan, Italy), equipped with a nanospray ion source. The spray capillary voltage was set at 1.7 kV, and the ion transfer capillary temperature was maintained at 220 °C. Full mass spectra were recorded in the positive ion mode over a 400–1600 m/z range, with a resolving power of 60,000 (full width at half-maximum). This step was followed by five low-resolution MS/MS events that were sequentially generated in a data-dependent manner on the top five ions selected from the full MS spectrum, using dynamic exclusion for the MS/MS analysis. In particular, the MS/MS scans were acquired by setting normalized collision energy of 35% on the precursor ion and, when a peptide ion was analyzed twice, applying an exclusion duration of 0.5 min.

The second LC-MS/MS system (n = 4) was equipped with a two-dimensional micro-high-performance liquid chromatography system (Surveyor HPLC; Thermo Fisher Scientific, Inc., San Jose, CA, USA) coupled online to an LTQ mass spectrometer (Thermo Fisher Scientific, San Jose, CA, USA). Ten microliters of peptide mixtures were

concentrated and desalted online by C18 traps loaded on a 10-port valve before final separation on the capillary reversed-phase column (Biobasic-C18, 0.180 i.d. ×100 mm, 5 μm particle size, Thermo Fisher Scientific, San Jose, CA, USA). The flow rate was 100 μL/min, which was split to achieve a final flux of 2 μL/min. Peptides were separated with the following eluents: (A) 0.1% formic acid in water; (B) 0.1% formic acid in acetonitrile; the gradient profile was 5–40% B in 110 min, 40–95% B in 15 min; the flow rate on C-18 column was 1 μL/min. The peptides eluted from the C18 column were directly analyzed with an LTQ mass spectrometer (Thermo Fisher Scientific, San Jose, CA, USA) equipped with a nano-ESI source. Full MS spectra were acquired in positive mode over a 400−2000 *m*/*z* range, followed by five MS/MS events sequentially generated in a data-dependent manner on the first five most intense ions selected from the full MS spectrum (collision energy 35%) and using dynamic exclusion for MS/MS analysis.

2.4.2. Proteomic Data Processing

The experimental MS/MS spectra produced by LTQ and LTQ Orbitrap XLTM ETD mass spectrometers were matched against the in silico tryptic peptide sequences of the Equus caballus protein database retrieved from UNIPROT in March 2021 (44484 protein sequences). Data processing was performed by Discoverer 2.5 software, based on the SEQUEST HT algorithm [17]. Peptide and protein assignment was made according to specific guidelines [18]. The following criteria were used for peptide identification: Parent mass tolerance of 50 ppm and 200 ppm was set for LTQ Orbitrap XLTM ETD and LTQ, respectively; while for both peptides, fragment mass tolerance was set to 0.8 Da, respectively. Missed cleavage sites per peptide were set to 3. The percolator node was used with a target-decoy strategy to give a final false discovery rate (FDR) ≤ 0.01 (strict) based on q-values, considering a maximum ΔCN of 0.05. Only peptides with a minimum peptide length of 5 amino acids, confidence at "Medium" level, and rank 1

were considered. Protein grouping and strict parsimony principles were applied. To evaluate the correlation among replicate analyses, Spearman's rank correlation was computed by JMP15.2 SAS software. To provide a rank list of the most abundant proteins in the analyzed samples, the average Spectral count (SpC) of each protein was normalized on MW as previously reported [19]. Functional Annotation Tool of DAVID database [20] was used to characterize the most enriched molecular function (MF), biological process (BP), and cellular component categories; specifically, background = Equus caballus, count > 5 and $p < 0.01$ were set.

An *Equus caballus* protein–protein interaction (PPI) network was built by homology with *Homo sapiens*, as previously reported [21]. Proteins identified in at least 2 out of 7 replicate analysis were combined with the *Homo sapiens* PPI network retrieved from the STRING database [22]. Only experimentally and database defined PPIs with a score > 0.15 and 0.35, respectively, were considered. The resulting subnetwork was visualized and analyzed by Cytoscape and its plugins [23]. It was processed at the functional level using STRING Cytoscape APP [22]. Network topological analysis was performed by Centiscape2.2 Cytoscape plugin as previously reported [24]; betweenness, centroid, and bridging centralities were evaluated. A set of nodes with values above the average calculated on the whole network were defined as hubs [25]. The statistical significance of topological results was tested by considering randomized network models; they were reconstructed and analyzed by an in-house R script based on VertexSort (to build random models), igraph (to compute centralities), and ggplot2 (to plot results) libraries.

2.5. Statistical analysis

Raw data were processed through STATGRAPHICS XVII (Statpoint Techonologies, Inc., Warrenton, VA, USA). A general linear analysis of variance model (ANOVA) was generated to evaluate the

data. The function was then followed by an LSD test to estimate the differences between means. Each batch was processed, considering protein and lipid content as the response variable and the batch number as the fixed factor. To evaluate cell proliferation, the cell metabolic activity was set as the response variable and the Lyosecretome concentration as a fixed factor. Statistical significance was set at $p < 0.05$.

3. Results

3.1. Lyosecretome Production

Three different equine AD-MSCs lines from the biobank meet all the requirements for clinical use as all the steps were made according to ISO 9001:2018 clinical grade. Secretome production was induced by 24 h serum starvation; after this time, the supernatants were collected, and cells were detached to estimate their total amount and viability (Table 1).

Table 1. Lyosecretome batch production from three different equine AD-MSCs lines.

Batch n.	Total Cell Number × 10^6	Cell Viability (%)
1	224	99
2	170	98
3	65	99

The supernatants were first centrifuged to eliminate cell debris, followed by an ultrafiltration process to concentrate and filter. The concentration step allows to reduce the volume, reaching a fixed value of cell equivalents per mL (0.5×10^6 cell/mL); instead, the filtration phase with 5 kDa molecular weight cut-off allows one to retain both EVs and soluble proteins contained in the supernatants. At the end of the concentration step, the obtained volume was diafiltered at least five times with ultrapure deionized water to erase any tracks of undesired

compounds. The starting volume for all the produced batches was about 800 mL, the time process lasted approximately 3 h using a filtration module with a superficial area of 370 cm^2, and the calculated ultrafiltration efficiency was 17.8 ± 2.3 $L/m^2/h$ (mean value ± standard deviation, n = 3). Once the purified solution was obtained, mannitol was added as the selected cryoprotectant. Samples were stored at −80 °C before the freeze-drying process. In this timeframe, to ensure the quality of the product, microbiological tests were performed during all the production phases to prove that the sterility conditions were maintained during the formulation along with the final product. Microbiological tests were conducted by an accredited and certified facility (IZSLER, Brescia, Italy), which routinely controls cell and cell-derived products for veterinary clinical use. These tests affirmed: (i) The absence of any mycoplasma and (ii) bacterial endotoxin level in an acceptable range (Table 2).

Table 2. Lyosecretome microbiological test: Sterility, bacterial endotoxin, and Mycoplasma**.**

Batch n.	Sterility	Bacterial Endotoxin	Mycoplasma
1	compliant	3.4 Eu/mL	no presence
2	compliant	3.3 Eu/mL	no presence
3	compliant	3.4 Eu/mL	no presence

3.2. Lyosecretome Characterization

After the lyophilization process, a technological characterization was performed on Lyosecretome powder.

To check the suitability of each formulation for a future in vivo administration, further analyses were performed on the final product. For each formulation, cake's appearance was evaluated by randomly selecting four vials and performing a visual inspection. Following the aqueous solvent's evaporation during lyophilization, a solid and porous cake was formed, free of defects. The lyophilized secretome dissolved rapidly by a gentle agitation adding water, generating a clear

suspension free of visible particles. The osmolarity was always within the acceptable range for injectable formulations (250–350 mOsm/Kg) and always between 320 and 350 mOsm/Kg. The pH value was always in the range of 7.2 to 7.6.

FTIR spectra were performed on Lyosecretome batches. Comparing the three batches reported in Figure 1, the spectral region goes from 650 to 4000 cm^{-1}; the batches, as expected, have similar bands at around at 1082 cm^{-1} and 1019 cm^{-1} and 930 cm^{-1}; those picks are predominant, and unfortunately, in this region, there is an overlap with the characteristic mannitol vibrations bands; thus, it is difficult to distinguish the Lyosecretome presence (Figure 1). Lyosecretome bands were also detected in the spectral region between 1423 cm^{-1} and 1458 cm^{-1}, pointing out the presence of CH_2 groups and 1374 cm^{-1} and 1375 cm^{-1} related to CH_3 groups, thus confirming the presence of lipids and protein.

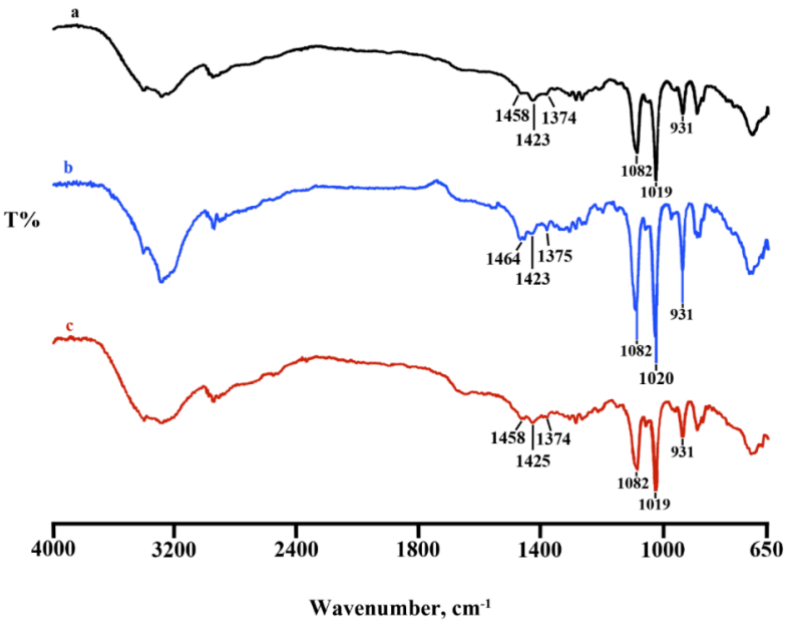

Figure 1. Comparison between FTIR spectra of Lyosecretome batch 1 (spectrum a), 2 (spectrum b), and 3 (spectrum c), respectively.

The three batches were analyzed by DSC, and the thermal profile was reported below as a comparison (Figure 2). The endothermic peak at 164.3 ± 0.8 °C ($\Delta H = 278 \pm 3$ Jg^{-1}) was due to the melting of crystalline mannitol (β form), followed by sample decomposition.

The anhydrous nature of the lyophilized samples was confirmed by TGA analysis (Figure 3), where no mass losses were recorded in the temperature range 50–100 °C, related to residual water. An almost complete mass loss was recorded for all the samples starting from about 244 °C due to sample decomposition, confirming the same thermal stability for the three batches.

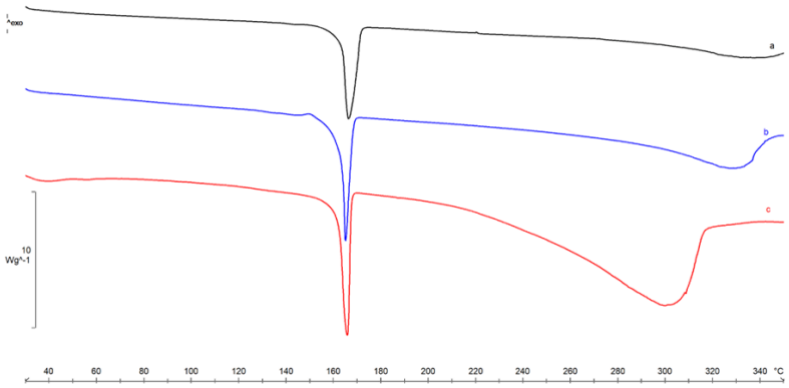

Figure 2. DSC profiles of Lyosecretome batches 1, 2, and 3 (curves a, b, and c).

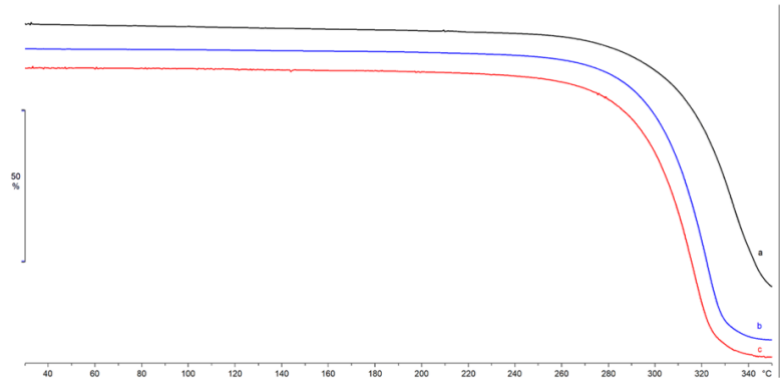

Figure 3. TGA profiles of Lyosecretome batches 1, 2, and 3 (curves a, b, and c).

Morphological investigation through SEM images showed that vesicles integrity and spherical shape were maintained for all three batches, demonstrating that ultrafiltration and lyophilization processes did not influence particle structure (data not presented).

Particle size characterization has been performed on Lyosecretome using NTA technology to (i) count nanoparticles observed in a specific volume, (ii) measure the diameter, and (iii) obtain the particle concentration. The analysis detected a heterogeneous population including nano/micro-structured vesicles; in detail, for all three batches, 10% of the population diameter (d_{10}) ranged 77–95 nm, 50% of the population diameter (d_{50}) ranged 115–156 nm, and 90% of the population diameter (d_{90}) was less than 260 nm. Regarding particle concentration, it ranged between 1.77×10^8 and 3.47×10^8 particle/mL based on the considered batches (Table 3 and Figure 4).

Table 3. Particle size distribution and concentration of batch 1 and 2 (mean values ± standard deviation, $n = 3$).

Batch n.	Mean (nm)	Mode (nm)	d_{10} (nm)	d_{50} (nm)	d_{90} (nm)	Concentration (particle/mL)
1	142.7 ± 4.9	81.0 ± 2.8	77.5 ± 2.1	117.5 ± 3.2	231.2 ± 9.5	$2.46 \times 10^8 \pm 1.48 \times 10^7$
2	198.5 ± 6.4	114.8 ± 11.8	94.8 ± 1.6	156.7 ± 8.6	253.5 ± 18.5	$3.47 \times 10^8 \pm 2.66 \times 10^7$
3	187.1 ± 3.9	94.9 ± 3.0	91.5 ± 2.2	151.2 ± 2.8	261.3 ± 7.4	$1.77 \times 10^8 \pm 7.77 \times 10^6$

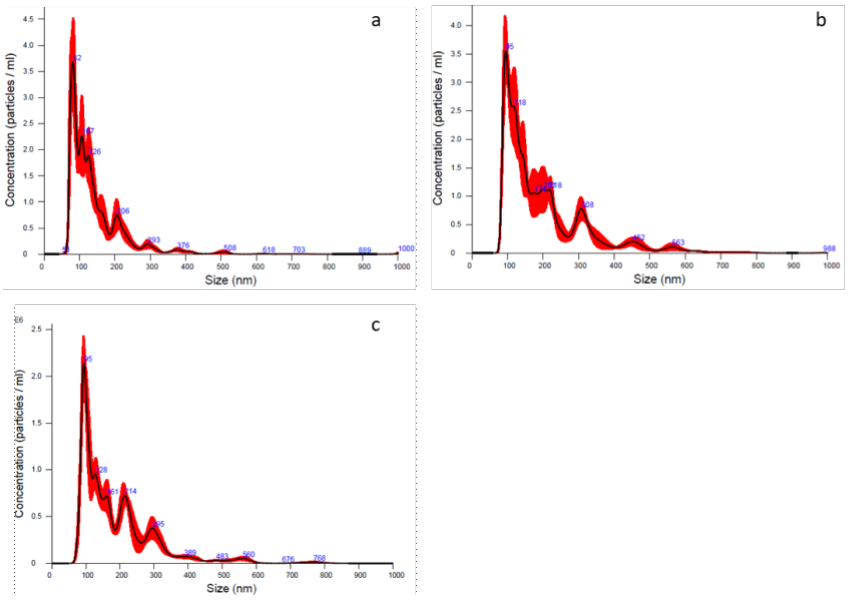

Figure 4. NTA analyses showing averaged particles concentration and size distribution of batch 1 (a), 2 (b), and 3 (c), respectively. The average of each batch was made by processing 6 cycles of 60 s each. The red part indicates the ± standard error of the mean values (n = 3). Particles concentration is expressed as mean value ± standard deviation (n = 3).

The number and size of exosomes were determined by ExoView with biomarker detection. This method is based on a direct-biomarker association that captures particles into a chip. ExoView also allows discriminating with fluorescence if a protein is expressed on the surface or into the exosome. The analysis method could be divided into two macro steps: Interferometric imaging that gives information regarding the exosome's number and size, and fluorescence analysis that gives the intensity of a positive-marker protein. The data accuracy depends on correct binding between proteins expressed by exosomes and extracellular vesicles and their specific antibodies marker. As a result, a first consideration was a correlation between the horse's protein and human protein: Data confirm that human capture

antibodies had a fixed animal ligand. Moreover, the average colocalization counts are shown in Figure 5 (triplicate analysis). The correlations between proteins expressed on exosome's surfaces and fluorescent antibody markers can be vertically read in the chart. The last plot column indicates the negative control performed by Murine IgG. In the first plot, column data show that in a horse's secretome, there is a high number of exosome's surface proteins responsive to the anti-CD-9 fluorescent human antibody, and the second most-expressed ligand is a protein that could be correlated to anti-CD-81 fluorescent human antibody. Finally, the lower capture marker is the anti-CD-63 fluorescent human antibody. There is also double or triple positive binding between the surface protein and human antibodies, as the seven exosomes are simultaneously expressed on the external membrane proteins positive to anti-CD-81 and anti-CD-63 fluorescent human antibodies.

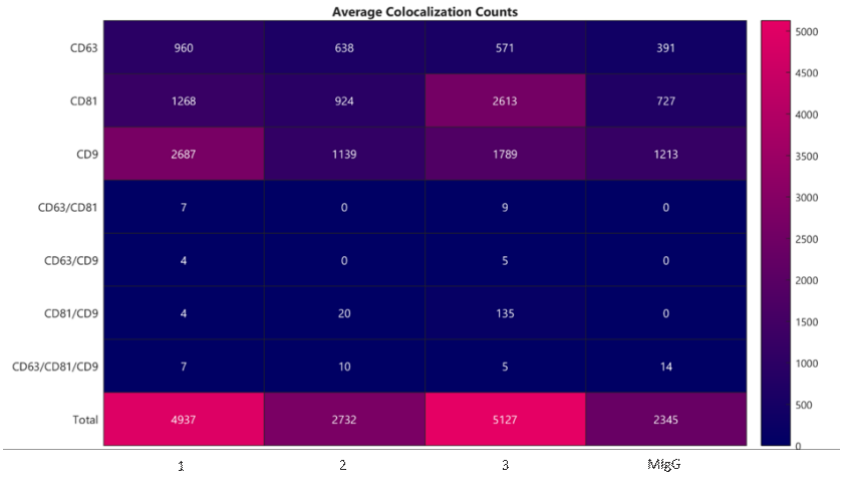

Figure 5. Average colocalization counts evaluating the correlations between proteins expressed on exosome's surfaces and fluorescent antibodies markers CD63, CD81, and CD9. According to the average results of the three determinations (without considering the negative control murine IgG), it is possible to underline that there were 723 exosomes positive only for the anti-CD-63 human

antibody, approximately 1601 exosomes positive only for the anti-CD-81 human antibody, 1871 exosomes positive only for the anti-CD-9 human antibody, 5 exosomes have a double positive match for anti-CD-81 and anti-CD-63 human antibodies, approximately 5 exosomes have a double positive match for anti-CD-63 and anti-CD-9 human antibodies, 53 exosomes are simultaneously positive for anti-CD-9 and anti-CD-81 human antibodies, and 7 exosomes present a triple positive match for human antibodies.

Lyosecretome was characterized in terms of total lipid and protein content, and results are reported in Table 4 expressed as μg of protein or lipid per mg of Lyosecretome.

Table 4. Lyosecretome total protein and lipid content; mean values ± standard deviation, n= 3. Different letters indicate a significant difference between groups ($p < 0.0001$).

Batch n.	μg Proteins/mg Lyosecretome	μg lipids/mg Lyosecretome
1	10.0 ± 0.07 a	0.7 ± 0.05 a
2	13.0 ± 0.20 b	1.0 ± 0.04 b
3	10.6 ± 0.02 c	0.6 ± 0.07 c

Focusing on the yield of each batch, for batch 2, we obtained a higher amount of both protein and lipid content, and comparing the three batches overall, a significant difference was found ($p < 0.05$). Moreover, it is evident that there was a correlation between protein and lipid content. It is well known that cell lines can highly affect secretome production and composition due to the variability within the same species. This aspect could explain the results in terms of different yield, although a certain reproducibility is maintained.

It should be noticed that the methods applied to analyze protein and lipid content meet the pharmaceutical conditions and were previously validated [26]. For BCA-protein quantification, the mean coefficient of calibration curve determination was in a range of 0 up to 100 μg/mL of BSA in water; the curve equation has an intercept not

statically significant, and the plot of the residuals had a common distribution of the error. These latter considerations mean that no systematic error influenced the calibration (data not shown). Considering the lipid quantification that was performed by a Nile Red assay, the mean coefficient of the calibration curve determination was within a range of 0–20 μg/mL of PC in water; the distribution of the plot residuals had a normal trend of the error; thus, no systematic error influenced the calibration (data not shown).

3.3. In Vitro Potency Test

The anti-elastase activity was tested on equine Lyosecretome at different concentrations (2, 5, 10, and 20 mg/mL), showing a dose-dependent trend (Figure 6). The activity assay consists of a kinetics enzymatic reaction considered from time 0 up to 40 min. The activity exhibited almost 50% at the higher concentration, considering Epigallocatechin gallate as a positive control due to its positive inhibition of the elastase enzyme.

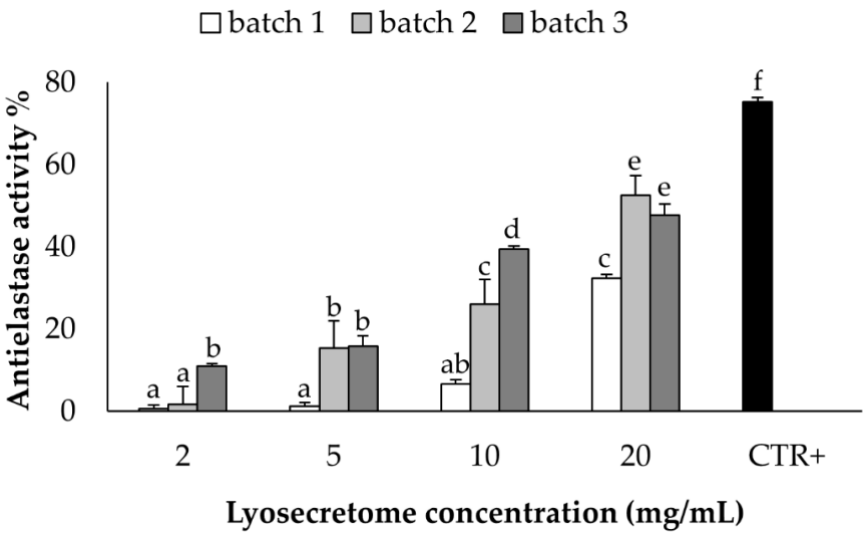

Figure 6. Anti-elastase activity was tested for the three batches at different Lyosecretome concentrations: 2, 5, 10, and 20 mg/mL, obtaining a dose-dependent trend. Mean values ± LSD (n = 3), ANOVA. Different

letters (a, b, c, d, e, and f) indicate significant differences between the means ($p < 0.05$), whereas the same letter indicates no significant difference ($p > 0.05$).

The metabolic activity of equine AD-MSCs, SF-MSCs, tenocytes, and chondrocytes was evaluated after treatment with Lyosecretome. In detail, Lyosecretome was tested at the concentrations of 400,000, 200,000, and 100,000 cell equivalents/well. For all cell types, the exposition to Lyosecretome stimulated cell proliferation compared to serum-free medium ($p < 0.0001$), and a dose-dependent trend of cell metabolic activity was observed. The effects of Lyosecretome treatment were statistically different in the four cell types ($p < 0.0001$). As shown in the figure below (Figure 7), the dose-dependency reached a plateau at 200,000 cell equivalent/well. The medium with 10% FBS added was considered a positive control, while the serum-free medium was used as a negative control.

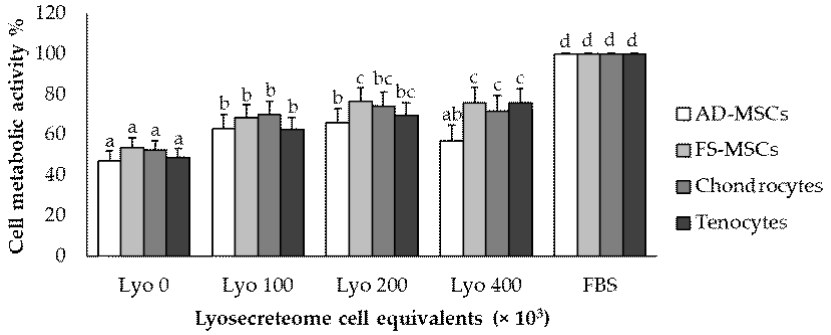

Figure 7. Cell metabolic activity on AD-MSCs, SF-MSCs, tenocytes, and chondrocytes tested at different Lyosecretome concentrations demonstrating a dose-dependency up to 200,000 cell equivalents/well. Mean values ± LSD ($n = 4$), ANOVA. Different letters (a, b, c, d) indicate significant differences between the means ($p < 0.05$), whereas the same letter indicates no significant difference ($p > 0.05$). FBS indicates the positive control, while Lyo 0 stands for the negative control.

3.4. Proteomic Investigation

The protein characterization of the secretome (Lyosecretome) isolated from equine mesenchymal stem cells allowed the identification of 647 distinct proteins (Table S1). This proteome was defined by seven technical replicate analyses performed with two different mass spectrometers. Regardless of the instrumentation used, all replicates showed good repeatability with R^2 values ranging from 0.92 to 0.99 (Figure 8A). About 25% of the proteins were identified by an average spectral count > 1 (Figure 8B). In addition, 95 proteins were identified in all analyzed samples, while 272 were found in at least 2 replicate analyses out of 7 (Table S1).

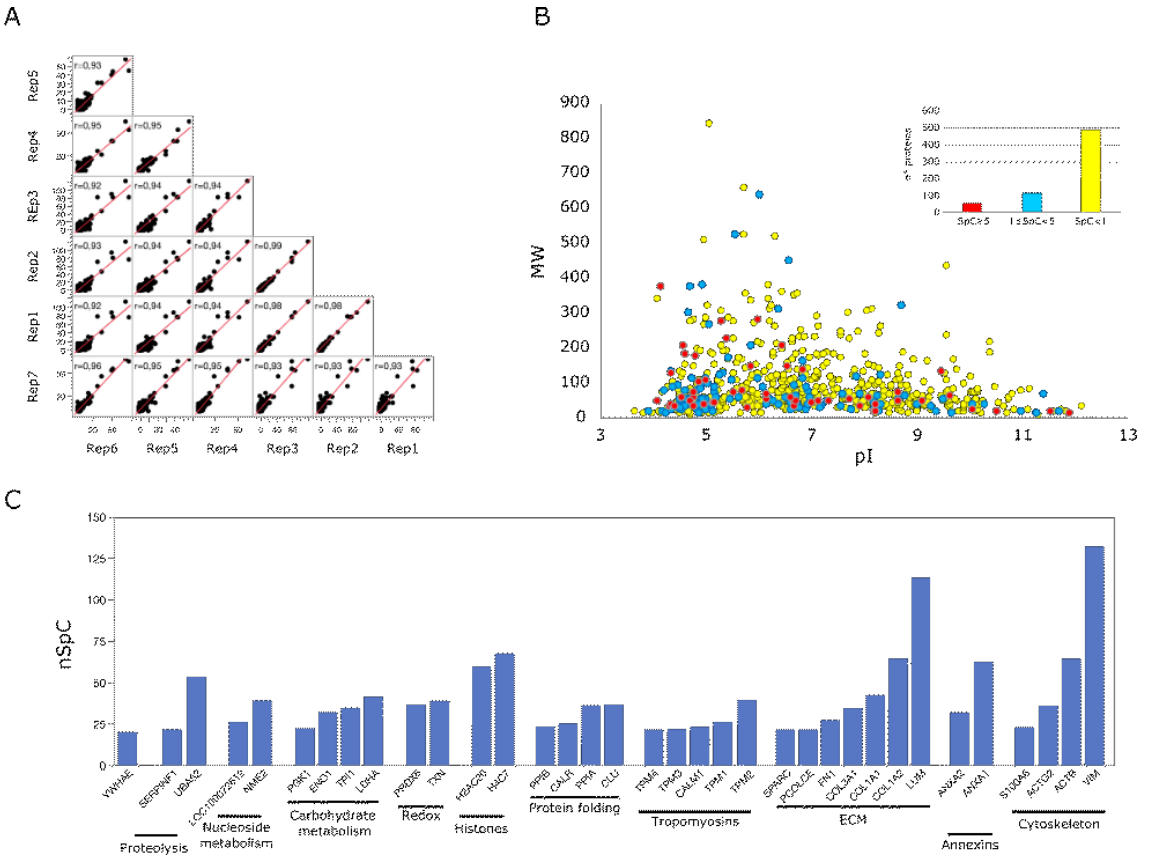
A
Rep5
Rep4
REp3
Rep2
Rep1
Rep7
Rep6
Rep5
Rep4
Rep3
Rep2
Rep1
B
MW
pI
nSpC
Proteolysis
Nucleoside metabolism
Carbohydrate metabolism
Redox
Histones
Protein folding
Tropomyosins
ECM
Annexins
Cytoskeleton

Figure 8. Proteomic analysis secreted from equine mesenchymal stem cells. (A) Spearman's correlation computed using Spectral counts of replicate LC-MS/MS analysis. (B) Virtual 2D-Map (pI vs. MW) of the total proteins identified (n = 647); color codes indicated the average spectral counts characterizing the identified proteins. (C) Rank list of the most abundant identified proteins (n = 35, nSpC > 20) clustered for functional categories.

The rank list of the most abundant identified proteins (Figure 8C) highlighted the presence of well-defined functional categories. Those most represented included ECM, Tropomyosins, Cytoskeleton, Carbohydrate metabolism, and Proteins folding. However, although less represented, other interesting proteins involved in Proteolysis regulation, Redox homeostasis, Histone proteins, and Annexins were found. All these categories agreed with those (Biological Process, Molecular Function, and Cellular Component) most enriched by considering the global characterizes protein profile (Figure S1); interestingly, a relevant enrichment of proteins involved in chaperone-mediated protein folding emerged from this analysis. A major level of detail concerning functional categories and proteins most relevant in the Lyosecretome from equine MSCs was reached by reconstructing and processing, at a functional and topological level, an *Equus caballus* protein–protein interaction (PPI) network; it was reconstructed exploiting the high sequence homology (>87%) between *Equus caballus* and *Homo sapiens* protein sequences (Figure S2).

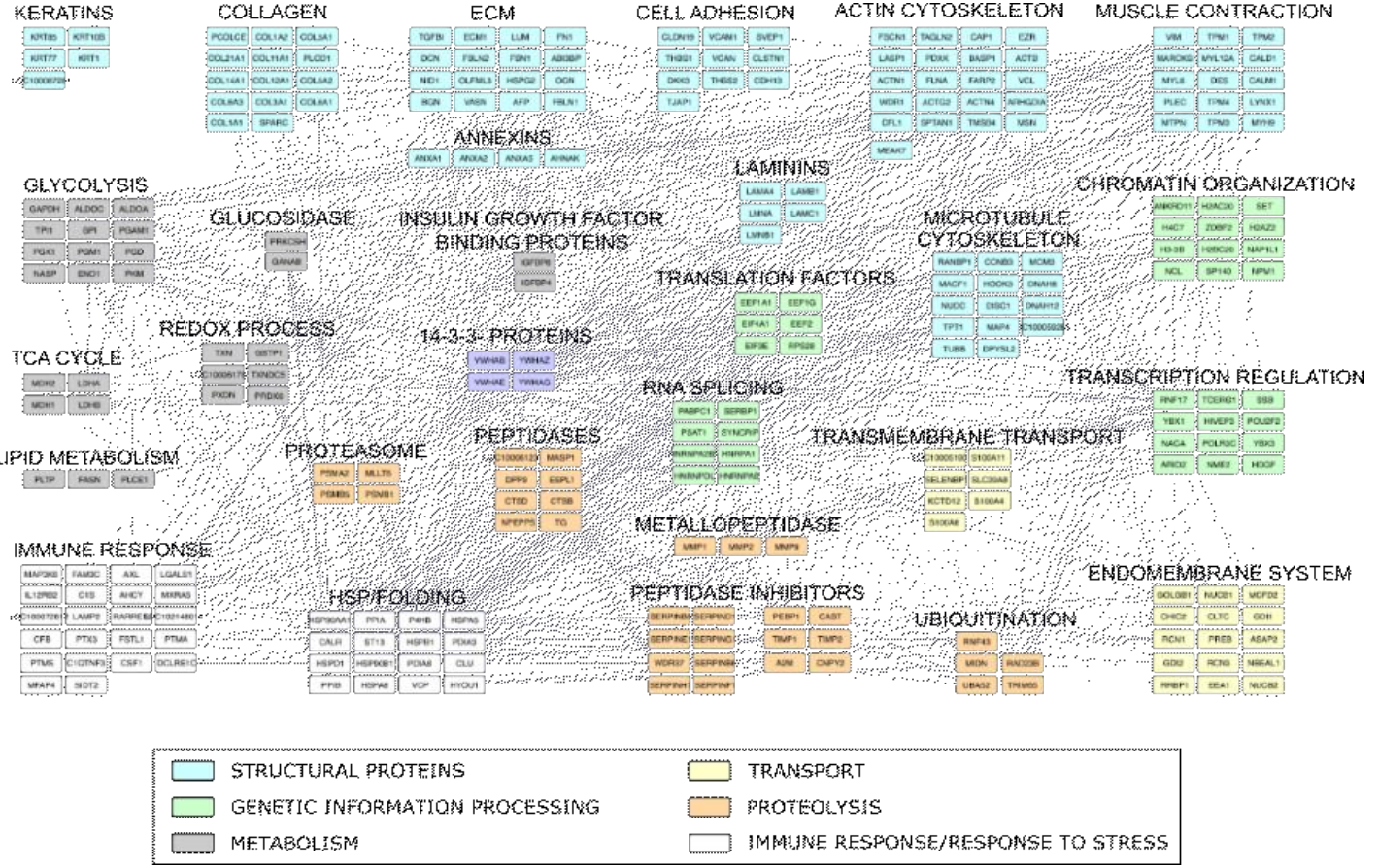
KERATINS
COLLAGEN
ECM
CELL ADHESION
ACTIN CYTOSKELETON
MUSCLE CONTRACTION
ANNEXINS
GLYCOLYSIS
GLUCOSIDASE
INSULIN GROWTH FACTOR BINDING PROTEINS
LAMININS
CHROMATIN ORGANIZATION
MICROTUBULE CYTOSKELETON
TRANSLATION FACTORS
REDOX PROCESS
14-3-3- PROTEINS
TCA CYCLE
RNA SPLICING
TRANSCRIPTION REGULATION
LIPID METABOLISM
PROTEASOME
PEPTIDASES
TRANSMEMBRANE TRANSPORT
METALLOPEPTIDASE
IMMUNE RESPONSE
HSP/FOLDING
PEPTIDASE INHIBITORS
ENDOMEMBRANE SYSTEM
UBIQUITINATION
STRUCTURAL PROTEINS
GENETIC INFORMATION PROCESSING
METABOLISM
TRANSPORT
PROTEOLYSIS
IMMUNE RESPONSE/RESPONSE TO STRESS

Figure 9. Equus caballus PPI network reconstructed by homology with Homo sapiens. The network was built by STRING Cytoscape APP starting from proteins secreted by mesenchymal stem/stromal cells and identified at least two out of seven replicate analyses.

The Equus caballus PPI network reconstructed starting from proteins secreted by mesenchymal stem cells counted 269 nodes and 2016 edges. They were clustered in 29 functional/topological modules (Figure 9) further classified in 6 macro-areas, including Structural proteins, Genetic Information Processing, Metabolism, Transport, Proteolysis, and Immune response/Response to stress. Following the Biological processes, Molecular Functions, and Protein families that emerged from network analysis, as well as the Lyosecretome therapeutic properties observed, we focused our attention on proteins involved in inflammatory processes and response to a bacterium (Table S2); specifically, six proteins (IL10RA, LTA4H, MXRA5, RARRES2, TEK, ANXA1) were annotated by "Anti-inflammatory activity", six proteins (C1QTNF3, ENPP3, GAPDH, KRT1, SERPINF1, SYNCRIP) by "Negative regulation of inflammation", while 35 were more generically "Involved in inflammatory response". In addition, seven proteins (RARRES2, NOD1, SERPINE1, H2BC20, SERPINB9, PENK, EPX) were annotated to be involved in "Response to bacterium". Of note, SERPINF1 and ANXA1 were also found among the most abundant proteins, suggesting a putative active role as a candidate in exerting anti-inflammatory properties (Figure 8C). With the purpose to shed light on other proteins with a potential regulatory role and functionally capable of holding together communicating proteins by signaling mechanisms, we selected a group of proteins that occupy specific network positions and that are defined as hubs (Figure 10); within this group, we found proteins "Involved in inflammatory reaction", such as IKBKE, ADCY1, MMP2, PARK7, THBS1, and IL6, which is also annotated to be involved in the defense response against the bacterium.

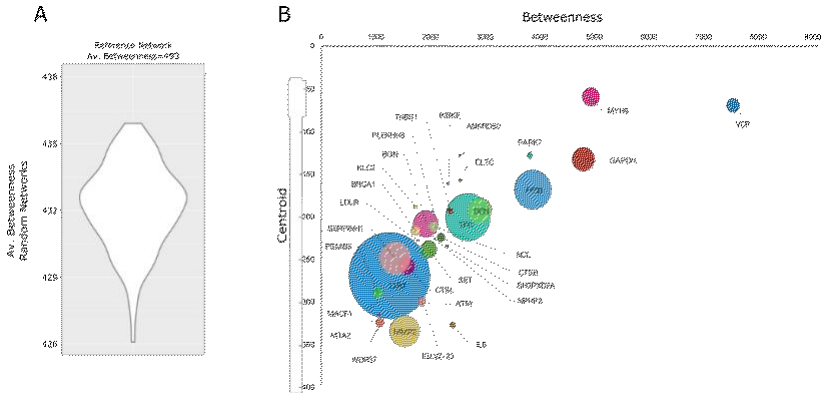

Figure 10. PPI network hubs in PPI network reconstructed from proteins secreted by *Equus caballus* mesenchymal stem/stromal. (A) Violin plot reporting the average Betweenness in Random networks. (B) PPI network hubs were selected considering Betweenness, Centroid, and Bridging (proportional to circle size) centralities; proteins were defined as hubs if all centrality values were above the average values calculated on the whole network.

4. Discussion

This study aimed to propose a procedure for a scalable production of equine Lyosecretome, define its characteristics, and pave the way for its use in in vivo pre-clinical studies in animals affected by musculoskeletal disorders. To this aim, secretome production was induced by serum starvation of expanded AD-MSCs, and then the freeze-dried secretome was characterized in terms of qualitative and quantitative parameters. Experimental evidence indicates that MSCs can be isolated from almost every tissue of the body [27], even if it is still unclear whether cells derived from different sources share the same biological and therapeutical features. However, compared to the Lyosecretome prepared from MSCs isolated from human adipose tissue, we found similar categories, including genetic information processing, immune response, and stress response. Adipose tissue and bone marrow are the preferred sources to isolate and expand MSCs for

equine clinical applications [13]. In our study, AD-MSCs were used for the preparation of Lyosecretome.

Ultrafiltration was chosen for the easy scalability to prepare large batches because it presents several advantages compared to other techniques commonly used to isolate MSC-secretome, including the affordable costs and the shorter time requested by the entire process [28]. Furthermore, this technique grants the choice between filtration modules with different molecular weight cut-offs (MWCO), allowing the preferred retention based on the desired yield in small vesicles (as, for example, extracellular vesicles) or the whole secretome. Other conventional methods commonly used for isolating EVs, such as ultracentrifugation, present several limitations regarding the possible damage of EVs membranes, due to the high g-force required by the centrifugation steps [29]. In the current study, we selected a relatively low MWCO able to retain the whole secretome to ensure a large-spectrum therapeutic potential to the preparation, even though several studies support the hypothesis that the EVs fraction alone might be sufficient to promote healing of the injured tissues [30]. A biotechnological product such as secretome can be thermolabile, and thus it cannot be dried applying thermal methods, responsible for possible modification and/or degradation of bioactive components (e.g., protein). For this reason, to reach a water-free product, the lyophilization process was considered. Lyophilization guarantees the maintenance of sterile conditions when changing from liquid to a powder state; moreover, the final product is easy to store and requires a short reconstitution time of the dried product; long-term stability is also provided [31]. Unfortunately, this technique has several limitations: Costs, limited capacity, long processing time (it lasts approximately 4 days), and difficulties in the "scale up" from laboratory to industrial production. Thus, its use is justified when the product's value is sufficiently high, such as producing biotechnological drugs, vaccines, vitamins, antibiotics, liposomes, and

oncological products. The freeze-drying method creates freezing and drying stresses that can alter the stability of the biological product; hence, before proceeding, the addiction of a cryoprotectant is needed. The cryoprotectant guarantees the protection of both protein and vesicles lipidic layer from the damages of ice crystals formed during the freezing step and inhibits vesicle size alteration by aggregation. In this regard, mannitol is the most suitable cryoprotectant due to its important stabilizing effects on freeze-dried pharmaceutical products [31]. Mannitol properties have been widely discussed and investigated [32,33]. Its role is to ensure long-term stability, easy reconstitution, and maintenance of biological features and activities. However, the use of mannitol still remains controversial and many other excipients, such as trehalose, can be adopted instead [34]. In the current work, mannitol was able to avoid vesicles/particles aggregation as revealed by NTA analysis; moreover, it prevented vesicle structure modification in terms of morphology as shown by SEM analysis. This latter aspect was also ensured by applying ultrafiltration process for the secretome isolation, rather than ultracentrifugation, which can possibly break-up vesicles membrane due to the high shear forces.

FTIR spectra revealed similar bands for each of the three batches, where the presence of lipids and protein content was confirmed. Overall, all samples' spectra were overlapping, thus ensuring the reproducibility of the batch production process. DSC has been employed to demonstrate the purity, polymorphic form, melting point, and thermal behavior of EV lipid bilayers, which can be affected in terms of stability under adverse conditions [35]. The lyophilization process was conducted successfully for all batches, as confirmed by TGA analysis, with a very low water residual and good thermal stability.

Regarding the analysis performed by the ExoView, the method is based on a direct-biomarker association that captures particles into a chip. The technique allows discriminating whether a protein is

expressed on the surface of the exosome or in the exosome by fluorescence analysis of the captured particles. Since a specific chip for analysis of equine secretome is not available, the microarray specific to human proteins was used. Although not validated for equine species, the chip is based on highly conserved proteins, and a cross-reaction is plausible. We observed differences between the analysis of the three batches. The number of exosomes presenting a double correlation anti-CD-81/CD-9 human antibody was higher than the other correlations; moreover, CD-9 binding is probably the most affine to horse secretome's surface protein due to a higher protein match.

The anti-elastase activity tested on equine Lyosecretome provides the rationale for using secretome in regenerative medicine [36]. High protease expression is a feature commonly found in several musculoskeletal disorders contributing to their onset and evolution. In this context, protease inhibitors work, contributing to restoring extracellular matrix homeostasis. Our results showed a dose-dependent trend for each batch. Significant variability was observed between the different preparation, probably caused by an intrinsic biological variability between the cell populations used for their preparation.

In vitro metabolic activity assays are the gold standard for studying cell viability and proliferation. In the present work, MTT assay was performed on four different cell types, i.e., AD-MSCs, SF-MSCs, tenocytes, and chondrocytes, considered potential targets for the use of Lyosecretome in musculoskeletal disorders. No cytotoxic effect was observed after Lyosecretome treatment in any of the four different cell lines, independently of the used concentration. Lyosecretome was able to maintain cell replication when compared to serum-free medium. A dose-dependent effect was observed for each cell line, and statistically significant differences were observed as a function of the cell type. Cell metabolic activity ranged from 30% to 75% compared to medium supplemented with FBS, with the higher

stimulus observed at a Lyosecretome concentration of 200 mg/mL. Interestingly, at this concentration, tenocytes, chondrocyte, and SF-MSCs were more responsive than AD-MSCs, reaching a plateau at 200 mg/mL.

The effect observed following Lyosecretome treatment, in particular elastase inhibition, could be attributable, at least partially, to its protein content. In fact, in addition to proteins involved in stress response, including the Heat Shock Proteins, we found protease/peptidase inhibitors among the protein classes better represented. In particular, the putative relevant role of some of them, such as SERPINs, was also suggested by their presence among the most abundant proteins (SERPIN1F) and proteins defined as hubs (SERPINH1). Moreover, about 10% of the identified proteins were annotated to be involved in the inflammatory response. In addition to SERPINE1, annotated to also be involved in "Response to bacterium", the presence of proteins with anti-inflammatory activity (IL10RA, LTA4H, MXRA5 [37], RARRES2 [38,39], TEK, ANXA1 [40]) emerged. Some of them, including MXRA5 (Chemerin), have been previously associated with osteoarthritis, and anti-inflammatory and anti-fibrotic properties have been proposed for this protein suggesting its potential role in chronic inflammation [41]. In this scenario, MACF1 has also been detected in Lyosecretome; this protein plays a core function in wound healing cell migration [42,43], primarily due to its ability to coordinate interaction between actin, microtubule, and cell junctions. Concerning the cytokine profile, several proteins with cytokine/chemokine activity have been observed in the Lyosecretome, i.e., IL-6, IL-7, CSF-1, IL10RA, IL12RB2, CXCL6, GDF7, and Wnt5B. IL-6 and IL-7 are two pro-inflammatory cytokines involved in MSCs immunomodulation [44,45]. The presence of IL-6 agrees with a recent paper by Bundgaard et al. that also demonstrated the presence of CXCL6 in equine bone marrow-derived MSCs [46]. Pro-inflammatory and chondrogenic treatments modulated the expression of both

proteins. IL6, acting as a pro-inflammatory mediator, contributes to host defense during infection and tissue injury, but anti-inflammatory properties have also been suggested depending on the presence of other cytokines [47]. CSF-1 plays a role in inflammatory processes and promotes bone regeneration and mobilization of vascular and osteogenic progenitor cells [48]. CSF-1 presence has also been demonstrated in equine bone-marrow-derived MSCs secretome [46]. GDF7 and WNT5B are two secreted signaling proteins whose role has been suggested in tenogenic (GDF7) and osteogenic and chondrogenic (WNT5B) differentiation pathways of MSCs [49,50]. IL10RA mediates the immunosuppressive signal of interleukin 10, an anti-inflammatory cytokine, already observed in bone marrow derived human MSCs secretome [51].

Highly expressed proteins belonging to the class I small leucine-rich proteoglycan (SLRP) family, including LUM (lumican), DCN (decorin), and BGN (biglycan), were found among proteins defined as hubs. SLRP family comprises a group of extracellular matrix components distributed in most tissue whose gene expression is modified in OA [52]. Lumican, one of the most abundant proteins found in the secretome, regulates collagen fibril organization, and its expression is reduced in OA cartilage [52]. Interestingly, lumican is a major component of the corneal stroma, and its therapeutic use has been proposed for ocular lesions [53]. Furthermore, lumican is considered a key effector in normal wound repair [54]. Decorin plays a role in fibril assembly in tension bearing tissues. It may contribute to stabilizing the cartilage matrix in OA [55]. Decorin upregulation has been proposed as an attempt to reduce aggrecan fragmentation in post-traumatic OA, and decorin-based therapeutics have been suggested to attenuate OA progression [56]. Concerning biglycan, this extracellular matrix component contributes to the regulation of chondrogenesis and ECM turnover in OA [57]. Interestingly, the Lyosecretome prepared from equine adipose tissue-derived MSCs shares with the equine bone-

marrow-derived MSCs secretome described by Bundgaard et al. [46] a number of proteins related to cartilage biology, i.e., LUM, DCN, COMP (cartilage oligomeric matrix protein), SCRG1 (stimulator of chondrogenesis-1), EPYC (Epiphycan), GAS6 (growth arrest specific 6).

Regarding Lyosecretome as a pharmaceutical product, the following acceptance criteria were defined: (i) Fulfilment of specific requirements by the cellular source: Viability over 98%, capable for trilineage differentiation and negative for bacterial/viral contamination. (ii) Protein and lipid content were between 10–13 and 0.6–1 μg per mg of powder, respectively, mean EV size in the range of 100–200 nm, EV concentration in the range of 1–4 × 10^8 particles when resuspended in dH_2O at 1 mg/mL, expression of CD-9, CD-63, and CD-81 markers, negative for bacterial/viral contamination, water content less than 2%, fulfilment of the criteria required for freeze-dried (cake aspect) and injectable formulations (osmolarity, pH, absence of visible particles after resuspension in physiological solution). The assessment on the final product has to be performed by characterization techniques that can be validated at pharmaceutical grade and have an acceptable cost to be routinely implemented [26,58,59]. (iii) Functional aspects should be included to demonstrate that the final product, after having undergone all the isolation, purification, and formulation processes, maintains biological activity. In detail, anti-elastase activity was higher than 20% at 20 mg/mL in dH_2O. Finally, due to the limited experience in preparing equine Lyosecretome (these are the first scaled-up batches prepared following ISO 9001:2018 for validation) the source of variability cannot be fully investigated yet. With a more consistent number of batches prepared, it will be possible to adopt specific measures to minimize the batch-to-batch variability.

5. Conclusions

This study provides the proof-of-principle of the feasibility of a clinical-grade injectable freeze-dried formulation containing the secretome from equine adipose tissue-derived mesenchymal stem/stromal cells. The technological production process has proven to be consistent, and a panel of tests for quality control and batch release has been defined. Lyosecretome exerts a direct activity on different musculoskeletal cell types such as tenocytes, chondrocytes, and tissue resident MSCs; also, proteomic composition suggests a possible role of Lyosecretome for regenerative medicine applications. In detail, our findings suggest the therapeutic role in musculoskeletal diseases and wound healing of many proteins found in the equine secretome, including SLRP family members. Certainly, a more in-depth evaluation of the role of these proteins could be performed, and it will be the object of future investigations. Although extensive in vitro characterization is needed, this work paves the way for the clinical use of Lyosecretome: The proof-of-concept for manufacturing clinical-grade equine Lyosecretome has been provided, and prototypes are now available to evaluate its safety and efficacy in the treatment of horse musculoskeletal diseases.

Supplementary Material

Supplementary material may be found in the online version of this article (https://www.mdpi.com/1424-8247/14/6/553).

References

1. Sevivas, N.; Teixeira, F.; Portugal, R.; Araújo, L.; Carriço, L.F.; Ferreira, N.V.; Da Silva, M.V.; Espregueira-Mendes, J.; Anjo, S.; Manadas, B.; et al. Mesenchymal Stem Cell Secretome: A Potential Tool for the Prevention of Muscle Degenerative Changes Associated with Chronic Rotator Cuff Tears. Am. J. Sports Med. 2016, 45, 179–188, doi:10.1177/0363546516657827.
2. Galuzzi, M.; Perteghella, S.; Antonioli, B.; Tosca, M.C.; Bari, E.; Tripodo, G.; Sorrenti, M.; Catenacci, L.; Mastracci, L.; Grillo, F.; et al. Human Engineered Cartilage and Decellularized Matrix as an Alternative to

Animal Osteoarthritis Model. Polymers 2018, 10, 738, doi:10.3390/polym10070738.

3. Martel-Pelletier, J.; Barr, A.J.; Cicuttini, F.M.; Conaghan, P.G.; Cooper, C.; Goldring, M.B.; Goldring, S.R.; Jones, G.; Teichtahl, A.J.; Pelletier, J.-P. Osteoarthritis. Nat. Rev. Dis. Prim. 2016, 2, 16072, doi:10.1038/nrdp.2016.72.

4. McIlwraith, C. W.; Kawcak,C.; Baxter G.M.; Goodrich L. R.; Valberg S.J. Joint injuries and disease and osteoarthritis. Principles of Musculoskeletal Disease; Gary M. Ed. Wiley; 2020, chapter 7, doi:10.1002/9781119276715.ch7

5. Markoski, M.M. Advances in the Use of Stem Cells in Veterinary Medicine: From Basic Research to Clinical Practice. Science 2016, 2016, 1–12, doi:10.1155/2016/4516920.

6. Smith, R.K.W.; Korda, M.; Blunn, G.W.; Goodship, A.E. Isolation and implantation of autologous equine mesenchymal stem cells from bone marrow into the superficial digital flexor tendon as a potential novel treatment. Equine Veter J. 2010, 35, 99–102, doi:10.2746/042516403775467388.

7. Lange-Consiglio, A.; Rossi, D.; Tassan, S.; Perego, R.; Cremonesi, F.; Parolini, O. Conditioned Medium from Horse Amniotic Membrane-Derived Multipotent Progenitor Cells: Immunomodulatory Activity In Vitro and First Clinical Application in Tendon and Ligament Injuries In Vivo. Stem Cells Dev. 2013, 22, 3015–3024, doi:10.1089/scd.2013.0214.

8. Brandão, J.S.; Alvarenga, M.L.; Pfeifer, J.P.H.; Santos, V.H.; Fonseca-Alves, C.E.; Rodrigues, M.; Laufer-Amorim, R.; Castillo, J.A.L.; Alves, A.L.G.; De Souza, J.B. Allogeneic mesenchymal stem cell transplantation in healthy equine superficial digital flexor tendon: A study of the local inflammatory response. Res. Veter Sci. 2018, 118, 423–430, doi:10.1016/j.rvsc.2018.03.012.

9. Ricco, S.; Renzi, S.; Del Bue, M.; Conti, V.; Merli, E.; Ramoni, R.; Lucarelli, E.; Gnudi, G.; Ferrari, M.; Grolli, S. Allogeneic Adipose Tissue-Derived Mesenchymal Stem Cells in Combination with Platelet Rich Plasma are Safe and Effective in the Therapy of Superficial Digital Flexor Tendonitis in the Horse. Int. J. Immunopathol. Pharmacol. 2013, 26, 61–68, doi:10.1177/03946320130260s108.

10. Abbasi-Malati, Z.; Roushandeh, A.M.; Kuwahara, Y.; Roudkenar, M.H. Mesenchymal Stem Cells on Horizon: A New Arsenal of Therapeutic

Agents. Stem Cell Rev. Rep. 2018, 14, 484–499, doi:10.1007/s12015-018-9817-x.

11. Konala, V.B.R.; Mamidi, M.K.; Bhonde, R.; Das, A.K.; Pochampally, R.; Pal, R. The current landscape of the mesenchymal stromal cell secretome: A new paradigm for cell-free regeneration. Cytotherapy 2016, 18, 13–24, doi:10.1016/j.jcyt.2015.10.008.
12. El Andaloussi, S.; Mäger, I.; Breakefield, X.O.; Wood, M.J.A. Extracellular vesicles: biology and emerging therapeutic opportunities. Nat. Rev. Drug Discov. 2013, 12, 347–357, doi:10.1038/nrd3978.
13. Mocchi, M.; Dotti, S.; Del Bue, M.; Villa, R.; Bari, E.; Perteghella, S.; Torre, M.L.; Grolli, S. Veterinary Regenerative Medicine for Musculoskeletal Disorders: Can Mesenchymal Stem/Stromal Cells and Their Secretome Be the New Frontier? Cells 2020, 9, 1453, doi:10.3390/cells9061453.
14. Mentkowski, K.; Snitzer, J.D.; Rusnak, S.; Lang, J.K. Therapeutic Potential of Engineered Extracellular Vesicles. AAPS J. 2018, 20, 50, doi:10.1208/s12248-018-0211-z.
15. Orlandi, G.; Faragò, S.; Menato, S.; Sorlini, M.; Butti, F.; Mocchi, M.; Donelli, I.; Catenacci, L.; Sorrenti, M.L.; Croce, S.; et al. Eco ‐ sustainable silk sericin from by ‐ product of textile industry can be employed for cosmetic, dermatology and drug delivery. J. Chem. Technol. Biotechnol. 2020, 95, 2549–2560, doi:10.1002/jctb.6441.
16. Orlandi, G.; Bari, E.; Catenacci, L.; Sorrenti, M.; Segale, L.; Faragò, S.; Sorlini, M.; Arciola, C.R.; Torre, M.L.; Perteghella, S. Polyphenols-Loaded Sericin Self-Assembling Nanoparticles: A Slow-Release for Regeneration by Tissue-Resident Mesenchymal Stem/Stromal Cells. Pharmaceutics 2020, 12, 381, doi:10.3390/pharmaceutics12040381.
17. Washburn, M.P. The H-Index of ‘An Approach to Correlate Tandem Mass Spectral Data of Peptides with Amino Acid Sequences in a Protein Database’. J. Am. Soc. Mass Spectrom. 2015, 26, 1799–1803, doi:10.1007/s13361-015-1181-3.
18. Deutsch, E.W.; Overall, C.M.; Van Eyk, J.E.; Baker, M.; Paik, Y.-K.; Weintraub, S.T.; Lane, L.; Martens, L.; Vandenbrouck, Y.; Kusebauch, U.; et al. Human Proteome Project Mass Spectrometry Data Interpretation Guidelines 2.1. J. Proteome Res. 2016, 15, 3961–3970, doi:10.1021/acs.jproteome.6b00392.

19. Motta, S.; Vecchietti, D.; Martorana, A.M.; Brunetti, P.; Bertoni, G.; Polissi, A.; Mauri, P.; Di Silvestre, D. The Landscape of Pseudomonas aeruginosa Membrane-Associated Proteins. Cells 2020, 9, 2421, doi:10.3390/cells9112421.

20. Huang, D.W.; Sherman, B.T.; Lempicki, R.A. Bioinformatics enrichment tools: paths toward the comprehensive functional analysis of large gene lists. Nucleic Acids Research 2009, 37, 1-13, doi:10.1093/nar/gkn923.

21. Di Silvestre, D.; Vigani, G.; Mauri, P.; Hammadi, S.; Morandini, P.; Murgia, I. Network Topological Analysis for the Identification of Novel Hubs in Plant Nutrition. Front. Plant Sci. 2021, 12, doi:10.3389/fpls.2021.629013.

22. Doncheva, N.T.; Morris, J.H.; Gorodkin, J.; Jensen, L.J. Cytoscape StringApp: Network Analysis and Visualization of Proteomics Data. J. Proteome Res. 2019, 18, 623–632, doi:10.1021/acs.jproteome.8b00702.

23. Su, G.; Morris, J.H.; Demchak, B.; Bader, G.D. Biological Network Exploration with Cytoscape 3. Curr. Protoc. Bioinform. 2014, 47, 8.13.1–8.13.24, doi:10.1002/0471250953.bi0813s47.

24. Scardoni, G.; Tosadori, G.; Faizan, M.; Spoto, F.; Fabbri, F.; Laudanna, C. Biological network analysis with CentiScaPe: centralities and experimental dataset integration. F1000Research 2014, 3, 139, doi:10.12688/f1000research.4477.1.

25. Sereni, L.; Castiello, M.C.; Di Silvestre, D.; Della Valle, P.; Brombin, C.; Ferrua, F.; Cicalese, M.P.; Pozzi, L.; Migliavacca, M.; Bernardo, M.E.; et al. Lentiviral gene therapy corrects platelet phenotype and function in patients with Wiskott-Aldrich syndrome. J. Allergy Clin. Immunol. 2019, 144, 825–838, doi:10.1016/j.jaci.2019.03.012.

26. Bari, E.; Perteghella, S.; Di Silvestre, D.; Sorlini, M.; Catenacci, L.; Sorrenti, M.; Marrubini, G.; Rossi, R.; Tripodo, G.; Mauri, P.; et al. Pilot Production of Mesenchymal Stem/Stromal Freeze-Dried Secretome for Cell-Free Regenerative Nanomedicine: A Validated GMP-Compliant Process. Cells 2018, 7, 190, doi:10.3390/cells7110190.

27. Orbay, H.; Tobita, M.; Mizuno, H. Mesenchymal Stem Cells Isolated from Adipose and Other Tissues: Basic Biological Properties and Clinical Applications. Stem Cells Int. 2012, 2012, 1–9, doi:10.1155/2012/461718.

28. Gaetani, P.; Torre, M.L.; Klinger, M.; Faustini, M.; Crovato, F.; Bucco, M.; Marazzi, M.; Chlapanidas, T.; Levi, D.; Tancioni, F.; et al. Adipose-

Derived Stem Cell Therapy for Intervertebral Disc Regeneration: AnIn VitroReconstructed Tissue in Alginate Capsules. Tissue Eng. Part A 2008, 14, 1415–1423, doi:10.1089/ten.tea.2007.0330.

29. Doyle, L.M.; Wang, M.Z. Overview of Extracellular Vesicles, Their Origin, Composition, Purpose, and Methods for Exosome Isolation and Analysis. Cells 2019, 8, 727, doi:10.3390/cells8070727.

30. Sole, A.; Spriet, M.; Galuppo, L.D.; Padgett, K.A.; Borjesson, D.L.; Wisner, E.R.; Brosnan, R.J.; Vidal, M.A. Scintigraphic evaluation of intra-arterial and intravenous regional limb perfusion of allogeneic bone marrow-derived mesenchymal stem cells in the normal equine distal limb using 99mTc-HMPAO. Equine Veter J. 2012, 44, 594–599, doi:10.1111/j.2042-3306.2011.00530.x.

31. Smith, R.K.W.; Werling, N.; Dakin, S.; Alam, R.; Goodship, A.E.; Dudhia, J. Beneficial Effects of Autologous Bone Marrow-Derived Mesenchymal Stem Cells in Naturally Occurring Tendinopathy. PLoS ONE 2013, 8, e75697, doi:10.1371/journal.pone.0075697.

32. Franzè, S.; Selmin, F.; Samaritani, E.; Minghetti, P.; Cilurzo, F. Lyophilization of liposomal formulations: Still necessary, still challenging. Pharmaceutics 2018, 10, 139, doi:10.3390/pharmaceutics10030139.

33. Kumar, K.N.; Mallik, S.; Sarkar, K. Role of freeze-drying in the presence of mannitol on the echogenicity of echogenic liposomes. J. Acoust. Soc. Am. 2017, 142, 3670–3676, doi:10.1121/1.5017607.

34. Olsson, C.; Jansson, H.; Swenson, J. The Role of Trehalose for the Stabilization of Proteins. J. Phys. Chem. B 2016, 120, 4723–4731, doi:10.1021/acs.jpcb.6b02517.

35. Demetzos, C. Differential Scanning Calorimetry (DSC): A Tool to Study the Thermal Behavior of Lipid Bilayers and Liposomal Stability. J. Liposome Res. 2008, 18, 159–173, doi:10.1080/08982100802310261.

36. Han, S.; Li, Y.Y.; Chan, B.P. Protease inhibitors enhance extracellular collagen fibril deposition in human mesenchymal stem cells. Stem Cell Res. Ther. 2015, 6, 197, doi:10.1186/s13287-015-0191-1.

37. Balakrishnan, L.; Nirujogi, R.S.; Ahmad, S.; Bhattacharjee, M.; Manda, S.S.; Renuse, S.; Kelkar, D.S.; Subbannayya, Y.; Raju, R.; Goel, R.; et al. Proteomic analysis of human osteoarthritis synovial fluid. Clin. Proteom. 2014, 11, 6, doi:10.1186/1559-0275-11-6.

38. Xie, C.; Chen, Q. Adipokines: New Therapeutic Target for Osteoarthritis? Curr. Rheumatol. Rep. 2019, 21, 71, doi:10.1007/s11926-019-0868-z.

39. Berenbaum, F.; Eymard, F.; Houard, X. Osteoarthritis, inflammation and obesity. Curr. Opin. Rheumatol. 2013, 25, 114–118, doi:10.1097/bor.0b013e32835a9414.

40. Pirozzi, C.; Francisco, V.; Di Guida, F.; Gómez, R.; Lago, F.; Pino, J.; Meli, R.; Gualillo, O. Butyrate Modulates Inflammation in Chondrocytes via GPR43 Receptor. Cell. Physiol. Biochem. 2018, 51, 228–243, doi:10.1159/000495203.

41. Poveda, J.; Sanz, A.B.; Fernandez-Fernandez, B.; Carrasco, S.; Ruiz-Ortega, M.; Cannata-Ortiz, P.; Ortiz, A.; Sanchez-Niño, M.D. MXRA5 is a TGF-β1-regulated human protein with anti-inflammatory and anti-fibrotic properties. J. Cell. Mol. Med. 2016, 21, 154–164, doi:10.1111/jcmm.12953.

42. Ning, W.; Yu, Y.; Xu, H.; Liu, X.; Wang, D.; Wang, J.; Wang, Y.; Meng, W. The CAMSAP3-ACF7 Complex Couples Noncentrosomal Microtubules with Actin Filaments to Coordinate Their Dynamics. Dev. Cell 2016, 39, 61–74, doi:10.1016/j.devcel.2016.09.003.

43. Zaoui, K.; Benseddik, K.; Daou, P.; Salaun, D.; Badache, A. ErbB2 receptor controls microtubule capture by recruiting ACF7 to the plasma membrane of migrating cells. Proc. Natl. Acad. Sci. USA 2010, 107, 18517–18522, doi:10.1073/pnas.1000975107.

44. Saldaña, L.; Bensiamar, F.; Vallés, G.; Mancebo, F.J.; García-Rey, E.; Vilaboa, N. Immunoregulatory potential of mesenchymal stem cells following activation by macrophage-derived soluble factors. Stem Cell Res. Ther. 2019, 10, 1–15, doi:10.1186/s13287-019-1156-6.

45. Mohme, M.; Maire, C.L.; Geumann, U.; Schliffke, S.; Dührsen, L.; Fita, K.D.; Akyüz, N.; Binder, M.; Westphal, M.; Guenther, C.; et al. Local Intracerebral Immunomodulation Using Interleukin-Expressing Mesenchymal Stem Cells in Glioblastoma. Clin. Cancer Res. 2020, 26, 2626–2639, doi:10.1158/1078-0432.ccr-19-0803.

46. Bundgaard, L.; Stensballe, A.; Elbæk, K.J.; Berg, L.C. Mass spectrometric analysis of the in vitro secretome from equine bone marrow-derived mesenchymal stromal cells to assess the effect of chondrogenic differentiation on response to interleukin-1β treatment. Stem Cell Res. Ther. 2020, 11, 1–10, doi:10.1186/s13287-020-01706-7.

47. Borsini, A.; Di Benedetto, M.G.; Giacobbe, J.; Pariante, C.M. Pro- and Anti-Inflammatory Properties of Interleukin in Vitro: Relevance for Major Depression and Human Hippocampal Neurogenesis. Int. J. Neuropsychopharmacol. 2020, 23, 738–750, doi:10.1093/ijnp/pyaa055.

48. Roseren, F.; Pithioux, M.; Robert, S.; Balasse, L.; Guillet, B.; Lamy, E.; Roffino, S. Systemic Administration of G-CSF Accelerates Bone Regeneration and Modulates Mobilization of Progenitor Cells in a Rat Model of Distraction Osteogenesis. Int. J. Mol. Sci. 2021, 22, 3505, doi:10.3390/ijms22073505.

49. Otabe, K.; Nakahara, H.; Hasegawa, A.; Matsukawa, T.; Ayabe, F.; Onizuka, N.; Inui, M.; Takada, S.; Ito, Y.; Sekiya, I.; et al. Transcription factor Mohawk controls tenogenic differentiation of bone marrow mesenchymal stem cells in vitro and in vivo. J. Orthop. Res. 2015, 33, 1–8, doi:10.1002/jor.22750.

50. Tornero-Esteban, P.; Peralta-Sastre, A.; Herranz, E.; Rodríguez-Rodríguez, L.; Mucientes, A.; Abásolo, L.; Marco, F.; Fernandez-Gutierrez, B.; Lamas, J.R. Altered Expression of Wnt Signaling Pathway Components in Osteogenesis of Mesenchymal Stem Cells in Osteoarthritis Patients. PLoS ONE 2015, 10, e0137170, doi:10.1371/journal.pone.0137170.

51. Bruno, S.; Grange, C.; Deregibus, M.C.; Calogero, R.; Saviozzi, S.; Collino, F.; Morando, L.; Busca, A.; Falda, M.; Bussolati, B.; et al. Mesenchymal Stem Cell-Derived Microvesicles Protect Against Acute Tubular Injury. J. Am. Soc. Nephrol. 2009, 20, 1053–1067, doi:10.1681/asn.2008070798.

52. Ni, G.-X.; Li, Z.; Zhou, Y.-Z. The role of small leucine-rich proteoglycans in osteoarthritis pathogenesis. Osteoarthr. Cartil. 2014, 22, 896–903, doi:10.1016/j.joca.2014.04.026.

53. Yazdanpanah, G.; Jiang, Y.; Rabiee, B.; Omidi, M.; Rosenblatt, M.I.; Shokuhfar, T.; Pan, Y.; Naba, A.; Djalilian, A.R. Fabrication, Rheological, and Compositional Characterization of Thermoresponsive Hydrogel from Cornea. Tissue Eng. Part C Methods 2021, 27, 307–321, doi:10.1089/ten.tec.2021.0011.

54. Karamanou, K.; Perrot, G.; Maquart, F.-X.; Brézillon, S. Lumican as a multivalent effector in wound healing. Adv. Drug Deliv. Rev. 2018, 129, 344–351, doi:10.1016/j.addr.2018.02.011.

55. Li, Q.; Han, B.; Wang, C.; Tong, W.; Wei, Y.; Tseng, W.; Han, L.; Liu, X.S.; Enomoto-Iwamoto, M.; Mauck, R.L.; et al. Mediation of Cartilage Matrix

Degeneration and Fibrillation by Decorin in Post-traumatic Osteoarthritis. Arthritis Rheumatol. 2020, 72, 1266–1277, doi:10.1002/art.41254.

56. Chery, D.R.; Han, B.; Zhou, Y.; Wang, C.; Adams, S.M.; Chandrasekaran, P.; Kwok, B.; Heo, S.-J.; Enomoto-Iwamoto, M.; Lu, X.L.; et al. Decorin regulates cartilage pericellular matrix micromechanobiology. Matrix Biol. 2021, 96, 1–17, doi:10.1016/j.matbio.2020.11.002.

57. Embree, M.C.; Kilts, T.M.; Ono, M.; Inkson, C.; Syed-Picard, F.; Karsdal, M.A.; Oldberg, Åke; Bi, Y.; Young, M.F. Biglycan and Fibromodulin Have Essential Roles in Regulating Chondrogenesis and Extracellular Matrix Turnover in Temporomandibular Joint Osteoarthritis. Am. J. Pathol. 2010, 176, 812–826, doi:10.2353/ajpath.2010.090450.

58. Bari, E.; Perteghella, S.; Catenacci, L.; Sorlini, M.; Croce, S.; Mantelli, M.; A Avanzini, M.; Sorrenti, M.; Torre, M.L. Freeze-dried and GMP-compliant pharmaceuticals containing exosomes for acellular mesenchymal stromal cell immunomodulant therapy. Nanomedicine 2019, 14, 753–765, doi:10.2217/nnm-2018-0240.

59. Bari, E.; Ferrarotti, I.; Torre, M.L.; Corsico, A.G.; Perteghella, S. Mesenchymal stem/stromal cell secretome for lung regeneration: The long way through "pharmaceuticalization" for the best formulation. J. Control. Release 2019, 309, 11–24, doi:10.1016/j.jconrel.2019.07.022.

CHAPTER 4:
CANINE MSC-SECRETOME

As for equine model, canine patients also represent an excellent model for human disease. Small companion animals, as most often dogs, share physical, emotional, and social needs by close daily relationships with humans. Indeed, human bonds to companion animals create a demand for new and optimal pet therapies, including cell-based treatment. Also, most important consideration is that pathologies in veterinary patients have an earlier development than in humans, this means that dogs who share similar environments with humans, naturally develop diseases that resemble pathologic conditions. Given these premises, MSCs based therapies have been widely investigated in dogs' diseases including osteoarthritis, spinal cord injury, bone regeneration, and intervertebral disk degeneration. Many strategies to optimize therapies with dog MSCs focus on enhancing the differentiation potential of these cells, primarily into chondrocytes and osteocytes. A main goal of establishing a stable chondrocyte phenotype from dog MSCs is to increase their deposition of articular cartilage proteins, so that these cells can become an effective treatment option for chronic OA. For example, it was found that exposing canine adipose-MSCs to hypoxic conditions resulted in increased proliferation.

As mentioned before, up to now in veterinary patients, the paracrine profile and clinical use of MSCs-secretome has been very poorly studied, in this regard **Paper 3** and **Paper 4** better state

secretome treatment. Regarding the following article (**Paper 4**), at first, a characterization of the biological product has been performed and then, three-case report were reported on dogs affected by bilateral knee or elbow osteoarthritis. The objective of this study was to demonstrate the safety of secretome treatment as a new potential alternative to the cell therapy.

Paper 4. Mocchi M, Bari E, Dotti S, Villa R, Berni P, Conti V, Del Bue M, Squassino G.P, Segale L, Ramoni R, Torre M.L, Perteghella S and Grolli S (2021). Canine Mesenchymal Cell Lyosecretome Production and Safety Evaluation after Allogenic Intraarticular Injection in Osteoarthritic Dogs. Animals 2021, 11, 3271; doi.org/10.3390/ani11113271.

Simple summary: Recently, mesenchymal stromal cells have been proposed as a valid approach for treating osteoarthritis diseases, mainly due to the secretion of soluble factors and extracellular vesicles known as secretome. In this paper, an injectable freeze-dried pharmaceutical powder containing canine mesenchymal stromal cells-secretome (Lyosecretome) has been formulated, and in vitro potency experiments were conducted. Furthermore, the Lyosecretome was applied in dogs affected by osteoarthritis to assess its safety. Results indicated that intra-articular injection of allogeneic Lyosecretome is safe and does not induce an adverse response, thus paving the way for future studies regarding the efficacy.

Abstract: In recent years, mesenchymal stromal cells (MSCs) have shown promise as a therapy in treating musculoskeletal diseases, and it is currently believed that their therapeutic effect is mainly related to the release of proteins and extracellular vesicles (EVs), known as secretome. In this work, three batches of canine MSC-secretome were prepared by standardized processes according to the current standard ISO9001 and formulated as a freeze-dried powder named Lyosecretome. The final products were characterized in protein and lipid content, EV size distribution and tested to ensure the microbiological safety required for intraarticular injection. Lyosecretome induced the proliferation of adipose tissue-derived canine MSCs, tenocytes and chondrocytes in a dose-dependent

manner and showed anti-elastase activity, reaching 85% of inhibitory activity at a 20 mg/mL concentration. Finally, to evaluate the safety of the preparation, three patients affected by bilateral knee or elbow osteoarthritis were treated with two intra-articular injections (t=0 and t=40) of the allogeneic Lyosecretome resuspended in hyaluronic acid in one joint and placebo (mannitol resuspended in hyaluronic acid) in the other joint. The follow-up included a questionnaire addressed to the owner and orthopaedic examinations to assess lameness grade, pain score, functional disability score and range of motion up to day 80 post-treatment. Overall, the collected data suggest that intra-articular injection of allogeneic Lyosecretome is safe and does not induce a clinically significant local or systemic adverse response.

Keywords: mesenchymal stem/stromal cells; MSC-secretome; canine regenerative medicine; osteoarthritis

1. Introduction

In recent years, mesenchymal stem/stromal cells (MSCs) have shown promise as a therapy in the treatment of musculoskeletal diseases (MSDs), including different pathological conditions such as disorders of muscle, joint, bone, nerves, and tendons [1]. The disease burden of MSDs in veterinary medicine is considerable and represents a significant threat to animal welfare worldwide, particularly in canine and equine species [2,3]. MSDs are related to various factors, such as intensive and repetitive works, sport-related trauma, ageing and genetic background [1]. Although the MSCs ability to undergo multi-lineage differentiation has long been considered a critical feature to justify their clinical application, currently it is proved that the therapeutic effect of MSCs is mainly related to the secretion of a wide variety of trophic factors, encompassed under the name of secretome [4,5], playing an important paracrine activity. MSCs secretome is composed of a complex mixture of soluble factors (mainly cytokines,

chemokines and growth factors) and extracellular vesicles, including exosomes and microvesicles. The numerous different features associated with the secretome suggest that it could be used as an MSCs substitute [6] to mediate their biological activity, including anti-inflammatory and tissue regenerative properties [7]. The use of MSC-secretome as an alternative to their parental cells brings several advantages in regenerative medicine: the use of a cell-free product would reduce the unwanted immune reaction, and the tumorigenic risk related to the MSCs proliferation and differentiation capability; it is also easier to handle, store and ensure a sterile product by filtration [8-10]. We recently proposed a GMP-compliant human secretome production process that allowed us to obtain a stable and effective product named Lyosecretome (freeze-dried secretome) from human adipose tissue-derived MSCs [11,12]; this process included an ultrafiltration step for the concentration and the purification of MSCs-derived secretome, and the following lyophilization, obtaining a powder dosage form ensuring an improved long-term stability of the secretome.

In the current work, we applied the same procedure to obtain canine Lyosecretome from adipose tissue-derived MSCs, as a candidate for in vivo testing on naturally occurring diseases, thanks to the promising regenerative potential of MSCs secretome. Canine Lyosecretome was first characterized through quality controls regarding physicochemical properties, vesicles morphology and size distribution, protein and lipid content; furthermore, the requirements for the preparation of injectable pharmaceutical dosage forms were evaluated. Next, in vitro potency tests were performed to assess proliferative effects on different cell lines. Finally, the proof of principle of the safety of the canine allogenic Lyosecretome was performed by intraarticular administration to osteoarthritic dogs. To the best of our knowledge, this study is the first canine study based on the use of MSCs secretome in naturally occurring musculoskeletal

diseases. The application of Lyosecretome to animals affected by spontaneous osteoarthritis, avoiding the use of experimentally induced disease models, could provide interesting information about the safety and feasibility of an allogenic cell-free regenerative medicine approach in companion animals that share with the owner's environment and lifestyle [13], thus providing valuable clues for osteoarthritis therapy in the human counterpart.

2. Materials and Methods

2.1 Materials

The Lyosecretome production was made at an accredited facility to produce and control veterinary products for clinical use (Istituto Zooprofilattico Sperimentale Lombardia and Emilia-Romagna, IZLER, Brescia, Italy). The production protocol has been approved by the Italian Ministry of Health (Prot. n. 0000778 del 15/01/2020 7.1.2.0.0.0/17/2019 - AGD 809). Adipose-derived MSCs were obtained by IZLER Biobank. All reagents for cell culture, e.g. DMEM, fetal bovine serum (FBS) and antibiotics, were purchased from Euroclone, Milan, Italy. Acetone, bovine serum albumin (BSA), mannitol and phosphatidylcholine (PC) were bought from Sigma Aldrich, Milan, Italy. Epigallocatechin gallate (EGCG), N-succinyl-Ala-Ala-Ala-p-nitroanilide and pancreatic porcine elastase were purchased from Merck Life Science, Milan, Italy. Otherwise specified, all the reagents used were of analytical grade.

2.2 Preparation and Characterization of Injectable Lyosecretome Formulations

Freeze-dried MSC-secretome (Lyosecretome) was prepared and characterized by adapting previously reported procedures compliant with the current standard ISO 9001 [14-17]. Adipose-derived MSCs (AD-MSCs) were seeded into flasks at 10,000 cells/cm^2 and expanded

in DMEM/F12 minimal medium plus 10% v/v FBS, plus 1% v/v penicillin/streptomycin and 1% v/v amphotericin B at 37 °C and 5% CO_2 until P3. The release of secretome was induced by culturing MSCs in DMEM/F12 without FBS (FBS starvation) for 48 h. MSCs used fulfilled the requirements needed for clinical use in terms of cell viability, cellular identity, genomic stability (as stated by the International Society for Cellular Therapy [18]), sterility and apyrogenicity (according to Eu. Ph. 9.0, 2.6.7). Cell culture supernatants were centrifuged at 3500× g for 10 min to remove cell debris and apoptotic bodies. Supernatants were recovered and then ultrafiltered by tangential flow filtration (KrosFlo® Research 2i system, Spectrum Laboratories, Milan, Italy) using a filtration module with a superficial area of 235 cm2 and a molecular Weight Cut Off (MWCO) of 5 kDa (Spectrum Laboratories, Milan, Italy). The samples were first concentrated at 0.5 × 10^6 cell equivalents per mL (calculated by dividing the total cell number and the concentrated mL of supernatant). Then, they were diafiltered using sterile ultrapure water as a buffer. The processed sample was then added of mannitol at a final concentration of 0.5% w/v, frozen at −80 °C and freeze-dried (Christ Epsilon 2–16D LSCplus) at −50 °C and 8 × 10^{-1} mbar for 72 h. The obtained Lyosecretome was stored at −20 °C until use (6 months). Each mg of Lyosecretome corresponds to 0.1 × 10^6 cell equivalents (calculated by dividing the total cell number and the obtained milligrams of Lyosecretome).

2.2.1. Lyosecretome Characterization

Total Proteins and Lipids

Total proteins were dosed by the BCA Protein Assay Kit (Thermo Fisher Scientific, Milan, Italy) according to the manufacturer instructions. Briefly, the working reagent solution was added to each sample (or standard) in a 1:1 ratio and incubated at 37 °C for 2 h. The absorbance was measured at 562 nm with a microplate reader (Synergy

HT, BioTek, United Kingdom). Standard protein solutions (BSA) were used to build a calibration curve ($R^2 = 0.99$). Total lipids were dosed by the Nile Red method, which was previously validated [14]. The Nile Red powder was solubilized in acetone at a concentration of 3.14 M and then diluted 100× in PBS. Nile Red solution was added to samples (1:9 ratio) and incubated for 5 min at room temperature. The fluorescence was measured by Synergy HT at 530/25 excitation and 645/40 emission. Standard lipid solutions (PC) were used to build a calibration curve ($R^2 = 0.99$). All analyses were done in triplicate.

EV Particle Size and Concentration

Nanoparticle Tracking Analysis (NTA, NanoSight NS 300 equipment, Malvern Instruments) was used to measure EVs' particle size and concentration into Lyosecretome. The freeze-dried powder was analyzed at the concentration of 1 mg/mL in deionized water at room temperature with a detection angle of 90°. Raw data were elaborated by the NTA software. All analyses were done in triplicate.

Physical-chemical Characterization

Fourier Transform Infrared Spectroscopy (FT-IR) spectra of the Lyosecretome were collected in the spectral region between 650 and 4000 cm^{-1} with a resolution of at least 4 cm^{-1}. A Spectrum One Perkin-Elmer spectrophotometer equipped with a MIRacle™ ATR device was used. All measurements were done in triplicate. Differential Scanning Calorimetry (DSC) analysis was performed with a Mettler $STAR^e$ system equipped with a DSC821e Module and an Intracooler device (Julabo FT 900) for sub-ambient temperature analysis. The instrument was previously calibrated with Indium as a standard reference; then, the curves were recorded on about 3 mg of sample in 40 μL sealed aluminium pans with pierced lid. The following parameters were considered: temperature range -30-250 °C; heating rate 10 K min^{-1}; nitrogen air atmosphere flux 50 ml min^{-1}). Each experiment was

performed in triplicate. Thermo Gravimetric Analysis (TGA) was performed with a Mettler STAR^{e} system equipped with a TGA/DSC1. The instrument was previously calibrated with Indium as a standard reference; then, the curves were recorded on about 4 mg of samples in 70 μL alumina pans. The following parameters were considered: temperature range 30-300 °C; heating rate 10 K min^{-1}; nitrogen air atmosphere flux 50 mL min^{-1}). Each experiment was performed in triplicate.

Sterility and Apyrogenicity

Sterility, endotoxins, mycoplasma and other microbiological contaminations were evaluated on a representative sample using the same tests applied to ensure the sterile conditions of the starting cells. In detail, for microbial control, the samples were examined through a microbiology test according to the provisions of the European Pharmacopoeia (EuPh 2.6.2). Apyrogenicity was ensured by quantitatively detecting bacterial endotoxins using the Limulus Amebocyte Lysate (LAL) test (EuPh 2.6.14) and measured as Endotoxin Unit (EU). Possible mycoplasma contamination was detected by carrying out specific tests (NAT test) following the provisions of European Pharmacopoeia (EuPh 2.6.7).

2.3. In Vitro Potency and Efficacy Tests

2.3.1. Specimen collection

Adipose tissue, tendon, and cartilage tissue samples were collected from animals at the local Veterinary Teaching Hospital. All animal owners were aware of the study and signed an informed consensus, and the protocols were approved by the Italian Ministry of Health (Prot. n. 0000778 del 15/01/2020 7.1.2.0.0.0/17/2019 - AGD 809). All the animals were subjected to a complete clinical examination, blood count (CBC), and serum biochemistry analysis. Tendons and

cartilage were collected from the knee joint of animals who died of natural causes and were subjected to necroscopy. Patients affected by infectious diseases were excluded.

2.3.2. MSCs isolation from Adipose Tissue, Tendon and Cartilage

Once collected, each type of tissue was washed in 70% ethanol and stored in phosphate-buffered saline (PBS) containing penicillin (50 U/mL), streptomycin (20 μg/mL), and amphotericin B (2.5 μg/mL) before being processed (maximum 2 h). Then, 1-1.5 g of tissue were fragmented in 0.3–0.5 cm^3 pieces in a Petri dish with scalpels and sterile pliers. The fragments were transferred to a 15 mL conical centrifuge tube containing a solution of 0.1% w/v collagenase type I, prepared in DMEM, supplemented with 100 U/mL penicillin, 100 μg/mL streptomycin, 2.5 μg/mL amphotericin B, at a ratio of 5 mL of medium per gram of minced tissue. The samples were enzymatically digested in a water bath at 37 ° C, in moderate agitation, for 1 h for adipose tissue and 2 h for tendon and cartilage fragments. The solution was then filtered with a nylon filter (mesh 100 μm) and centrifuged at 190× g for 15 min. The pellet obtained was resuspended in a couple of ml of maintenance medium (mDMEM), consisting of DMEM supplemented with 10% v/v FBS, penicillin 100 U/mL, streptomycin 100 μg/mL, amphotericin B 2.5 μg/mL, and then seeded in 25 cm^2 cultures flasks. The cells were maintained in an incubator at 37 °C in a 5 % CO atmosphere, renewing the medium every 72 h. Once 80% confluence was reached, the cells were detached with 0.05% Trypsin-EDTA in PBS and expanded to P3-P4 when used for the experiments described below.

2.3.3. Cell Metabolic Activity Evaluation

The cytocompatibility and proliferation ability of Lyosecretome were evaluated on three different cell lines: canine MSCs, canine tenocytes and canine chondrocytes. Cells were seeded in 96-well plates

at 10,000 cells/well for 24 h and treated with increasing doses of Lyosecretome (50,000, 100,000 and 200,000 cell equivalents/well) in a serum-free medium. Cells not treated with Lyosecretome or treated with 10% v/v FBS were considered negative and positive control. After 48 h, an MTT test was performed. The absorbance was measured by a microplate reader (Victor Nivo, Perkin Elmer, USA) at 570 nm and 670 nm (reference wavelength), and the cell metabolic activity percentage was calculated as:

$$\text{Cell metabolic activity (\%)} = 100 \times (\text{Abs}_{\text{sample}}/\text{Abs}_{\text{positive control}})$$

2.3.4. Anti-elastase Activity

The inhibitory effect of Lyosecretome on pancreatic porcine elastase was assessed in vitro. Briefly, the enzyme was solubilized in phosphate buffer pH 6.8 at 0.5 IU mL^{-1}. Simultaneously, the substrate (N-succinyl-Ala-Ala-Ala-p-nitroanilide) was dissolved at a final concentration of 0.41 mmol L^{-1} in TRIS buffer. Increasing concentrations of Lyosecretome (2, 5, 10, 20 mg mL^{-1}) were incubated at room temperature with the enzyme for 20 min; then, the substrate was added, and the kinetic reaction was monitored by spectrophotometric analysis (Synergy HT) at the absorbance of 410 nm for 35 min (one measurement/minute). EGCG at 7.2 mg/mL was used as a positive control, while the reaction mixture in the absence of Lyosecretome was used as a negative control. Analyses were performed in triplicate, and the percentage anti-elastase activity (%) was calculated as:

$$\text{Anti-elastase activity (\%)} = [(A_{CTR} - A_{samp}) / A_{CTR}] \times 100$$

where A_{CTR} is the absorbance of the negative control, and A_{samp} is the absorbance of the Lyosecretome sample.

2.4. In Vivo Treatment

In vivo safety of Lyosecretome was evaluated on dogs affected by naturally occurring osteoarthritis (OA).

2.4.1. Ethical Concerns

The clinical trial has been approved by the Italian Ministry of Health (Prot. n. 0000778 del 15/01/2020 7.1.2.0.0.0/17/2019- AGD 809). The clinical experimentation has also been approved by the ethical committee of Istituto Sperimentale della Lombardia ed Emilia Romagna (IZSLER, n. 1/2019, 21 March 2019).

2.4.2 Animal Recruiting and Inclusion/exclusion Criteria

The current study enrolled 5 client-owned dogs presenting bilateral elbow or knee osteoarthritis (Table 1). The animals were treated with two intra-articular injections of Lyosecretome at 40-days intervals. All animal owners involved in the study signed a written consent after being notified of the relevant project information. For the enrollment, the patients underwent a complete clinical examination, complete blood count and serum biochemistry analysis to exclude other pathologies, followed by an orthopaedic examination to confirm and grade the OA. Details on the different clinical cases are reported in the Supplementary materials (Section S.1, Figures S1, S2 and S3).

Table 1. Summary of cases included in this study regarding the breed, age, gender, weight and affected joint.

Animal	Breed	Age (years)	Gender	Weight	Joint
1	Labrador	8	F	35	Knee
2	Labrador	9	F	35	Elbow
3	Golden retriever	5	M	34	Elbow

4	Labrador	3	M	32	Elbow
5	Labrador	9	M	30	Elbow

This study evaluated the following orthopaedic parameters: lameness, pain, functional disability, range of motion, and OA grade (Tables 2, 3 and 4). A disease score was obtained by adding scores for each of these parameters, ranging from grade 1 to 5 (Table 5). Only Grade 5 dogs were enrolled in this study.

Table 2. Overview of the score systems used for the orthopaedic examination.

Parameter	Score	Definition
Lameness	1	Stands, walks and trots normally
	2	Stands normally, slightly painful gait when trotting
	3	Stands normally, slightly painful gait when walking
	4	Stands normally, evident painful gait when walking
	5	Stands abnormally, evident painful gait when walking
Pain	1	None
	2	Mild signs
	3	Moderate signs
	4	Severe signs
	5	The dog will not allow palpation
Functional disability	1	Normal
	2	Slightly stiff
	3	Stiff
	4	Very stiff, unwilling to walk
	5	Need assistance to walk
Range of motion	1	No limitation of movement or crepitus
	2	10 to 20% decrease in range of motion, no crepitus
	3	10 to 20% decrease in range of motion with crepitus

4	20 to 50% decrease in range of motion
5	More than 50% decrease in range of motion

2.4.3. Pre-treatment and Post-treatment Evaluations

A complete orthopaedic examination was performed with X-rays under sedation to assess the baseline severity of OA in each animal. Radiographic signs of OA were evaluated using the Kellgren-Lawrence scale for the knee joint [19] and the International Elbow Working Group (IEWG) guidelines for the elbow joint [20]. The OA was categorized as shown in Tables 3 and 4. The orthopaedic examination of the animals included the assessment of lameness grade, pain score, functional disability score and range of motion (ROM) on day 0 (t0) and 40 days after each intra-articular treatment (t40 and t80). In detail, to assess the lameness score, gait was observed at stand, walk and trot and recorded by video, and lameness was categorized from grade 1 to 5 (Table 2) [21]. Each joint was then manipulated for pain and functional disability, and the ROM was assessed with an orthopaedic goniometer, giving a score from 1 to 5 to each parameter (Table 2) [19,21].

Table 3. The Kellgren-Lawrence grading of osteoarthritis for the knee joint.

OA	Grading	Radiographic features
Absent	0	No abnormalities
Doubtful	1	Minute osteophytes
Minimal	2	Definite osteophytes
Moderate	3	Diminished joint space
Severe	4	Greatly diminished joint space + sclerosis of the subchondral bone

Table 4. International Elbow Working Group (IEWG) guidelines for elbow osteoarthritis.

OA	Grading	Radiographic features
Absent	0	Normal elbow joint, no evidence of incongruency, sclerosis, or arthrosis
Mild	1	Presence of osteophytes < 2 mm high, sclerosis of the base of the coronoid process—trabecular pattern still visible
Moderate	2	Presence of osteophytes of 2-5 mm high, obvious sclerosis (no trabecular pattern) of the base of the coronoid processes
Severe	3	Osteophytes of over 5 mm found anywhere in the joint

Table 5. Disease score obtained by adding the scores of all the parameters evaluated in this study.

Sum of scores	Disease score
0 - 2	1
3 - 6	2
7 - 10	3
11 - 14	4
15 - 20	5

The follow-up included an owner questionnaire (Table 6) containing the validated Helsinki chronic pain index (HCPI) for up to 80 days (t0, t2, t4…t20, t40 and t80). The questionnaire inquired about the dog's general condition (body temperature, appetite) and local reactions in the treated joints (heat, pain, and joint swelling). Owners were also asked to report any abnormal response of the patient or NSAID treatment needed. Chronic pain signs were assessed with the HCPI that contained questions regarding the dog's mood, lameness, and

willingness to move, play, and jump. The HCPI included 11 questions, whose answers were given by a score of 0 to 4, where 0 and 1 indicate normal behaviour and movement, while 2, 3, and 4 indicate pain with increasing severity [22-24].

Table 6. Questionnaire submitted to the owners. The questionnaire is based on Helsinki chronic pain index (HCPI), with additional information collected to evaluate local and systemic adverse reactions reported by the animal owners.

Question asked	0 points	1 point	2 points	3 points	4 points
D2. Pain upon right joint palpation	Absent	Mild	Moderate	Severe	Does not allow palpation
D3. Pain upon left joint palpation	Absent	Mild	Moderate	Severe	Does not allow palpation
D4. Swelling upon right joint palpation	Absent	Mild	Moderate	Severe	Does not allow palpation
D5. Swelling upon left joint palpation	Absent	Mild	Moderate	Severe	Does not allow palpation
D6.1 Heat in the right joint	No warmer than contralateral limb	Mildly warmer	Moderately warmer	Markedly warmer	-
D6.2 Heat in the left joint	No warmer than contralateral limb	Mildly warmer	Moderately warmer	Markedly warmer	-
D7. Rate your dog's mood	Very alert	Alert	Neither alert nor indifferent	Indifferent	Very indifferent

D8. Rate your dog's willingness to participate in play	Very willing	Willing	Reluctantly	Very reluctantly	Does not play at all
D9. Rate your dog's complaining and groaning	Never	Hardly ever	Sometimes	Often	Very often
D10. Rate your dog's willingness to walk	Very willing	Willing	Reluctantly	Very reluctantly	Does not walk at all
D11. Rate your dog's willingness to trot	Very willing	Willing	Reluctantly	Very reluctantly	Does not trot at all
D12. Rate your dog's willingness to gallop	Very willing	Willing	Reluctantly	Very reluctantly	Does not gallop at all
D13. Rate your dog's willingness to jump (e.g., into a car, onto a sofa)	Very willing	Willing	Reluctantly	Very reluctantly	Does not jump at all
D14. Rate your dog's ease in lying down	With great ease	Easily	Neither easily nor difficultly	With difficulty	With great difficulty
D15. Rate your dog's ease in rising from a lying position	With great ease	Easily	Neither easily nor difficultly	With difficulty	With great difficulty
D16. Rate your dog's ease of movement	With great ease	Easily	Neither easily nor difficultly	With difficulty	Very often/always difficulty

after long rest					
D17. Rate your dog's ease of movement after major activity or heavy exercise	With great ease	Easily	Neither easily nor difficultly	With difficulty	Very often/always difficulty
D18. Dog's appetite	Normal	Capricious	Decreased	Markedly decreased	Does not eat at all
D19. Dog's body temperature	Normal	Fever	-	-	-
D20. Use of analgesic/anti-inflammatory drugs	No	Yes	-	-	-
D21. Abnormal post-treatment reactions	None	Physical tiredness	Physical tiredness + joint pain/swelling	Increased lameness	Does not stand and walk at all

2.4.4. Intra-articular Injection of Lyosecretome

After examination, dogs were sedated, and the skin over the joint was prepared for a sterile invasive procedure. Two product stocks were prepared by suspending Lyosecretome or mannitol (placebo) in 1 ml hyaluronic acid (Athenavis 1%), containing 20 mg of sodium hyaluronate, 800-1300 KDa, in 2 mL, Ibn Savio, Italy). For each animal, the right joint was infiltrated with the same stock and the left joint with the other stock, both times. Both the veterinarian and the owner were unaware of which treatment the joint received. In detail, a 20 Gauge needle was introduced into the joint space, synovial fluid was

aspirated, and the product was injected through the same needle and a syringe of 2.5 ml. At the end of the infiltration, the joints were subjected to slight flexion-extension movements to promote the spread of the product. After the procedure, the patient was sent home, prescribing rest for the first two days, resuming normal activity from the third day. The use of any anti-inflammatory medication was prohibited during the entire course of the 180 days study except in exceptional circumstances. The orthopaedic evaluation and the owner questionnaire were performed to evaluate the response to treatment and compare it with the initial clinical condition.

2.5 Statistical Analysis

Raw data were processed through STATGRAPHICS XVII (Statpoint Techonologies, Inc., Warrenton, VA, USA). A general linear analysis of variance model (ANOVA) was generated to evaluate the data. The function was then followed by an LSD test to estimate the differences between means. In detail, each batch was processed considering protein and lipid content as the response variable and the batch number as the fixed factor. The cell metabolic activity was set as the response variable and the Lyosecretome concentration as a fixed factor to evaluate cell proliferation. The anti-elastase activity data were elaborated considering the batch, concentration and time as fixed factors, and the activity % as the response variable. Statistical significance was determined at $p < 0.05$.

3. Results and Discussion

Injectable Lyosecretome (freeze-dried secretome) formulations have been prepared by standardized processes under ISO9001 clinical grade. Overall, three batches were produced starting from three different cell lines, as summarized in Table 7.

Table 7. Lyosecretome batch report.

Batch n.	Cell Source	Total Cell Number × 10^6	Cell Viability (%)
1	AD-MSC	190	99
2	AD-MSC	96	98
3	AD-MSC	92	99

After ultrafiltration to concentrate and purify the cell culture supernatant, the product was added of the cryoprotectant and freeze-dried. A filtering module with a 5 kDa molecular weight cut-off was used to retain in the ultrafiltrate both extracellular vesicles (EVs) and proteins with weight above the cut-off. The use of this membrane size was justified by preliminary investigations, demonstrating a higher immunomodulatory potency in 5 kD ultrafiltrate (containing both EVs and soluble factors) instead of the 300 kD ultrafiltrate (containing only EVs) [15]. Furthermore, Bari et al. [14] demonstrated that the concentration of IL-6 was higher in samples prepared by ultrafiltration rather than ultracentrifugation. Since IL-6 is a key player in the immunomodulatory features of the MSCs secretome, the large amounts of IL-6 discarded in the ultracentrifugation procedure suggest ultrafiltration is an effective procedure to prepare EV fraction. Similarly, higher anti-elastase activity was demonstrated for the whole secretome and attributed to the large amount of Alpha-1-Antitrypsin, the main inhibitor of neutrophil elastase, in the soluble fraction of the secretome [17]. Accordingly, Mitchell and colleagues found that EVs and soluble molecules act synergistically to promote tissue

regeneration [25], supporting low cut-off ultrafiltration as a valuable process to prepare MSCs secretome.

The pharmaceutical quality of Lyosecretome was defined by setting up a complete characterization of total protein and lipid content, physical-chemical properties, and particle size. The amount of proteins and lipids for each batch produced is reported in Table 8. It is worth noting that no systematic error influenced the calibration for both assays as the intercept of the curve equation is not statically significant, and the plot of the residuals had an ordinary distribution of the error (data not shown). Overall, the yield of each batch is different, meaning that the cell line and, more in general, the variability within the same species can strongly influence the secretome composition in terms of protein and lipid quantity ($p<0.05$). Maximum protein production was obtained in batch n. 1; by contrast, lipid amount is higher in batch n. 2. This aspect underlines that there is no correlation between the two assays, probably depending on cell density at the starvation time that can influence secretome production.

Table 8. Total protein and lipid content in Lyosecretome batches; mean values ± standard deviation, n = 3. Different letters (a, b and c) indicate a significant difference between groups of the same column ($p < 0.0001$).

Batch n.	μg proteins/mg Lyosecretome	μg lipids/mg Lyosecretome
1	79.5 ± 0.6^{a}	18.9 ± 0.5^{a}
2	28.6 ± 1.5^{b}	5.7 ± 0.1^{b}
3	25.9 ± 0.1^{c}	15.5 ± 0.3^{c}

The physical-chemical characterization confirmed the simultaneous presence of both proteins and lipids in the Lyosecretome. In detail, FTIR spectra revealed low-intensity bands at around 1653 cm^{-1} and 1547 cm^{-1} (amide I C=O stretching vibrations and amide II N-H bending vibrations of the peptide groups, respectively), absorbance bands at about 1457 cm^{-1} and 1377 cm^{-1} (CH_2 and CH_3

groups) and 1260 and 880 cm^{-1} (due to the stretching vibrations typical of phospholipids, triglycerides and cholesterol esters, and to the vibrations bands of mannitol) [14,15]. By DSC and TGA analysis, it was instead confirmed that the lyophilization process occurred successfully (data not shown).

Lyosecretome particles size distribution and characterization were evaluated using NTA technology. In detail, the diameter ranges between 190-230 nm, matching the choice to consider both exosomes (40–120 nm) and microvesicles (250–1000 nm). Furthermore, a heterogeneous population is shown by means analyzing curve, whereas d10 is set between 106-122 nm, d50 is set between 157-180 nm, and d90 is set between 316-400 nm. Thanks to this technique, the particle concentration per mL was estimated, ranging between 1.86 $\times 10^8$ and 2.60 $\times 10^8$ particle/mL (Table 9 and Figure 1).

Table 9. Particle size distribution and concentration of batch 1 and 2 (mean values ± standard deviation, n = 3).

Batch n	Mean (nm)	Mode (nm)	d10 (nm)	d50 (nm)	d90 (nm)	Concentration Particle /mL
1	231.6 ± 8.4	143.6 ± 11.7	122.3 ± 4.1	180.6 ± 5.5	403.5 ± 20.3	$1.86x10^8$ ± $6.37x10^7$
2	189.1 ± 2.7	109.7 ± 3.7	106.2 ± 2.7	157.5 ± 2.8	316.6 ± 1.8	$2.60x10^8$ ± $1.35x10^7$
3	197.1 ± 6.0	148.0 ± 15.4	116.7 ± 1.3	171.6 ± 6.5	319.7 ± 16.6	$2.12x10^8$ ± $1.06x10^6$

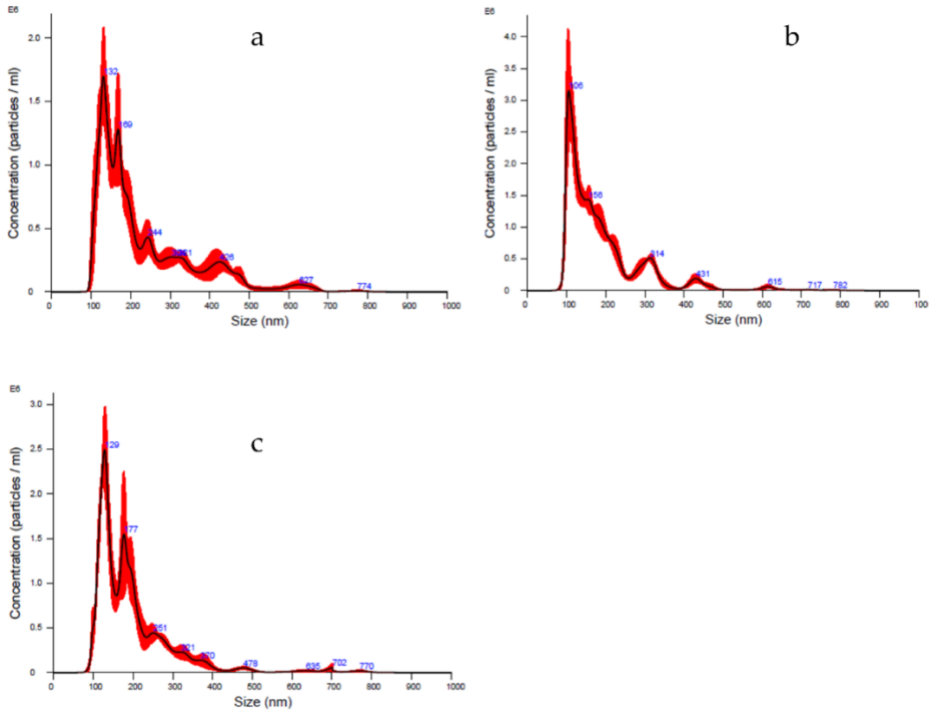

Figure 1. NTA averaged curves as particles concentration and size distribution of batch 1 (a), 2 (b), and 3 (c), respectively. The averaged curve was generated by processing six cycles of 60 s each per batch. Concentration is indicated as mean value ± standard deviation (n = 3). The red part shows the ± standard error of the mean values (n = 3).

Finally, since the Lyosecretome production was aimed at in vivo application, to guarantee the quality of the final product, microbiological tests were conducted before and after lyophilization, thus, on both secretome solution and lyophilized secretome (Lyosecretome) powder. Analyses were performed at a certified institute (IZSLER, Brescia, Italy), and the sterility conditions were ascertained in the same establishment. The results proved the absence of any mycoplasma and bacterial endotoxin level in each examined samples (data not shown).

Regarding the in vitro efficacy, Lyosecretome proliferation potency was assessed by MTT assay. Canine tenocytes, chondrocytes and adipose tissue-derived MSCs were chosen as target cells, the latter because the tissues resident MSCs can mediate tissue regeneration [26]. Lyosecretome stimulated cell metabolic activity in a dose-dependent trend for all cell types; in detail, the treatment with higher Lyosecretome concentrations reached almost 85% of cell metabolic activity compared to 10% FBS supplemented cultures. As shown in Figure 2, the dose-dependent effect was evaluated up to 200,000 cell equivalent/well. The effect of Lyosecretome treatment was statistically different for the three cell types ($p<0.0001$).

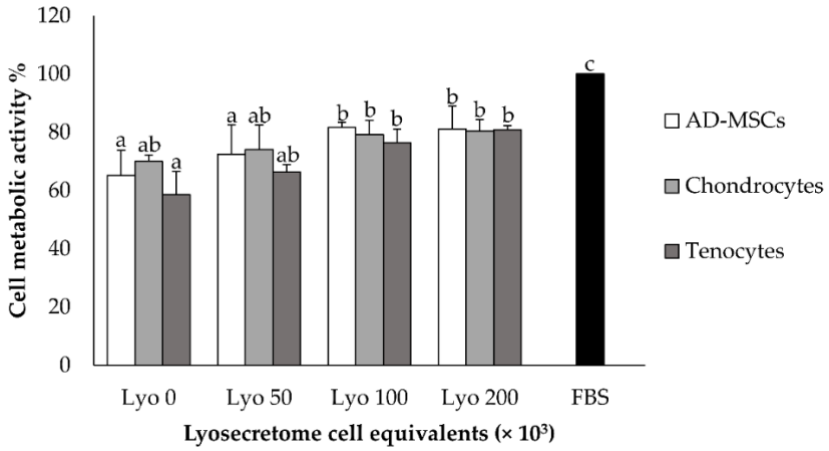

Figure 2. The dose-dependent trend of cell metabolic activity on AD-MSCs, chondrocytes and tenocytes tested at the Lyosecretome concentrations of 50, 100, 200 cell equivalents × 10^3/well. 10% v/v FBS was considered as positive control. Multifactor ANOVA, mean values ± LSD (n = 3). Different letters (a, b and c) indicate a significant difference between the means ($p<0.05$), while the same letters indicate no significant differences ($p>0.05$).

The anti-elastase activity of canine Lyosecretome demonstrated a dose-dependent trend for all the tested concentrations of 2, 5, 10 and 20 mg/ml (Figure 3). The assay consists of an enzymatic reaction which

was evaluated for up to 40 min. At the higher concentration of 20 mg/mL, the activity reached 85%, considering Epigallocatechin gallate as a positive control due to its inhibition of elastase activity.

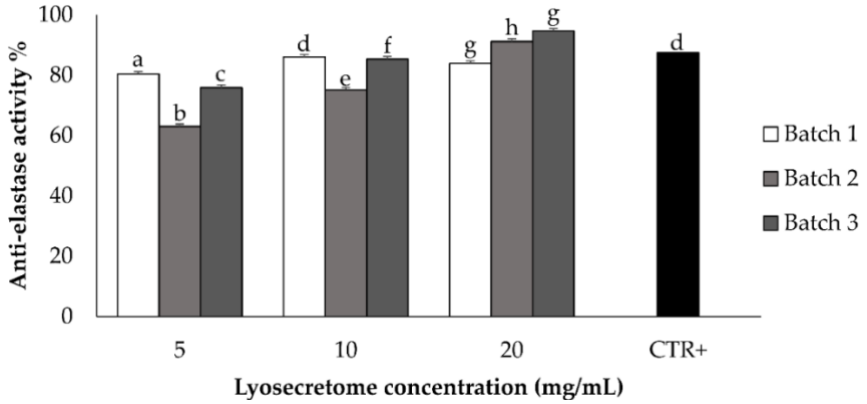

Figure 3. The anti-elastase activity was tested for the three batches at the concentrations of 2, 5, 10 and 20 mg/mL of Lyosecretome. A dose-dependent trend was obtained. CTR+ was epigallocatechin gallate at a concentration of 7.2 mg/mL in deionized water. Multifactor ANOVA, mean values ± LSD (n = 3). Different letters (a-h) indicate a significant difference between the means ($p<0.05$), while the same letters indicate no significant differences ($p>0.05$).

Despite this study has not performed a qualitative analysis of protein, RNA, and lipid contents of canine Lyosecretome, proteomic analyses of equine [2] and human [10] Lyosecretome revealed proteins involved in controlling the inflammatory pathways activated in osteoarthritic joints and proteins related to cartilage biology. This suggests using Lyosecretome as a substitute for cells in treating musculoskeletal system diseases [27]. Furthermore, microvesicles are considered safer both from the point of view of immuno-reactivity and for the lower potential risks compared to the administration of in vitro expanded cells [28]. Still, before testing Lyosecretome efficacy, the in vivo safety must be evaluated. In this regard, this study enrolled five dogs affected by bilateral OA to test Lyosecretome for clinical use. One

dog was excluded from the beginning for recent nonsteroidal anti-inflammatory drugs (NSAIDs) treatment (Animal 5, Table 1), and another dog was excluded before the second administration of the treatment for a recurrent skin infection that could negatively affect the intra-articular treatment (Animal 4, Table 1).

Lyosecretome and a placebo, consisting of mannitol (used in Lyosecretome formulation as a stabilizer), were resuspended in hyaluronic acid and injected in each animal's right and left joint, respectively. The choice to treat both affected joints with hyaluronic acid, whose lubricating properties support its widespread use in treating OA in dogs [29], was made to ensure patients enrolled in the study effective therapy in the control of clinical symptoms. The data collected with the questionnaire (Table 6) and reported in Table S1 have been analyzed to evaluate the onset of undesired effects following therapy (see Supplementary materials, Figure S4 and S5). No systemic adverse reactions were observed, even after the second administration. After each treatment, short-time side effects were observed for all the patients' as reluctance to trotting or galloping. However, these adverse effects resolved within 2 days without the need for additional treatment. Since the administration of Lyosecretome (in the right joint) and placebo (in the left joint) co-occurred, it was not possible to attribute the observed symptoms to one of the two treatments. Similar sides effects were also observed by Lee et al. [30]; they reported that following hyaluronic acid intraarticular injection, a dog showed a mild systemic inflammatory reaction, and two dogs showed non-weight-bearing lameness.

Only patient 3 was affected by swelling at the level of both the right and left joints (See Supplementary Figure S2) accompanied by complaining and groaning and not ease of movement for both lying down and moving after a long rest period. Thus, patient 3 likely showed an adverse reaction that was not directly attributable to the administration of Lyosecretome, as the same response was evidenced

even when administering the placebo. The reported effects are commonly noticed immediately after intra-articular injections when animals' lameness score is enhanced [31,32]. Finally, regarding the clinical data, the examination by the veterinary practitioners, performed at days 40 and 80 after the first treatment, were used to assess the possible onset of unexpected symptoms after therapy administration. No significant results were observed in terms of lameness and pain worsening.

In conclusion, given the limited number of enrolled patients, the present work does not provide any direct evidence of the efficacy or safety of the Lyosecretome in the treatment of canine OA. Nevertheless, it is the proof-of-concept for veterinary clinical-grade MSC-secretome production; moreover, the feasibility of two consecutive allogeneic Lyosecretome intraarticular administration in osteoarthritic dogs is proved, without evidence of adverse reactions. Therefore, this paper represents the premise for patient recruitment in a safety/efficacy clinical trial, with a proper number of cases.

Supplementary Materials The following are available online at https://www.mdpi.com/article/10.3390/ani11113271/s1, Table S1. Data collected from the questionnaire. File S1: History and clinical findings of the three dogs treated in the study. Figure S1. Cranio-caudal radiographic projection of the knee of Animal 1. Figure S2. Medio-lateral radiographic projections of the elbow of Animal 2. (A) Maximally flexed view of the right limb. (B) Maximally flexed view of the left limb. Figure S3. Medio-lateral radiographic projections of the elbow of Animal 3. (A) Maximally flexed view of the right limb. (B) Maximally flexed view of the left limb. Figure S4. Scores for questions 11 (A), 12 (B) and 21 (C) as a function of time. The treatment (Lyosecretome or placebo) was administered on day 0 and day 40 (circled). Multifactor ANOVA, mean values ± LSD (n = 3). * $p<0.05$ vs t = 0; # $p<0.05$ vs t = 2. Figure S5. Scores for questions 4 (A), 5 (B), 9 (C),

14 (D) and 16 (E) for each participant. Multifactor ANOVA, mean values ± LSD (n = 3). Different letters (a-h) indicate a significant difference between the means ($p<0.05$), while the same letters indicate no significant differences ($p>0.05$).

References:

1. Chung, M.-J.; Son, J.-Y.; Park, S.; Park, S.-S.; Hur, K.; Lee, S.-H.; Lee, E.-J.; Park, J.-K.; Hong, I.-H.; Kim, T.-H.; et al. Mesenchymal Stem Cell and MicroRNA Therapy of Musculoskeletal Diseases. International journal of stem cells 2020, doi:10.15283/ijsc20167.
2. Mocchi, M.; Grolli, S.; Dotti, S.; Di Silvestre, D.; Villa, R.; Berni, P.; Conti, V.; Passignani, G.; Brambilla, F.; Del Bue, M.; et al. Equine Mesenchymal Stem/Stromal Cells Freeze-Dried Secretome (Lyosecretome) for the Treatment of Musculoskeletal Diseases: Production Process Validation and Batch Release Test for Clinical Use. Pharmaceuticals 2021, 14, doi:10.3390/ph14060553.
3. Michela, M.; Stefano, G.; Silvia, D.; Dario, D.S.; Riccardo, V.; Priscilla, B.; Virna, C.; Giulia, P.; Francesca, B.; Maurizio, D.B.; et al. Equine Mesenchymal Stem/Stromal Cells Freeze-Dried Secretome (Lyosecretome) for the Treatment of Musculoskeletal Diseases: Production Process Validation and Batch Release Test for Clinical Use. Pharmaceuticals 2021, 14, 553, doi:10.3390/ph14060553.
4. Herrmann, M.; Diederichs, S.; Melnik, S.; Riegger, J.; Trivanović, D.; Li, S.; Jenei-Lanzl, Z.; Brenner, R.E.; Huber-Lang, M.; Zaucke, F.; et al. Extracellular Vesicles in Musculoskeletal Pathologies and Regeneration. Frontiers in Bioengineering and Biotechnology 2021, 8, doi:10.3389/fbioe.2020.624096.
5. Mocchi, M.; Dotti, S.; Del Bue, M.; Villa, R.; Bari, E.; Perteghella, S.; Torre, M.L.; Grolli, S. Veterinary Regenerative Medicine for Musculoskeletal Disorders: Can Mesenchymal Stem/Stromal

Cells and Their Secretome Be the New Frontier? Cells 2020, 9, doi:10.3390/cells9061453.

6. Crivelli, B.; Chlapanidas, T.; Perteghella, S.; Lucarelli, E.; Pascucci, L.; Brini, A.T.; Ferrero, I.; Marazzi, M.; Pessina, A.; Torre, M.L.; et al. Mesenchymal stem/stromal cell extracellular vesicles: From active principle to next generation drug delivery system. Journal of Controlled Release 2017, 262, 104-117, doi:10.1016/j.jconrel.2017.07.023.

7. Nakamura, M.; Nishida, H.; Yoshizaki, K.; Akiyoshi, H.; Hatoya, S.; Sugiura, K.; Inaba, T. Canine mesenchymal stromal cell-conditioned medium promotes survival and neurite outgrowth of neural stem cells. Journal of Veterinary Medical Science 2020, 82, 668-672, doi:10.1292/jvms.19-0141.

8. Godwin, E.E.; Young, N.J.; Dudhia, J.; Beamish, I.C.; Smith, R.K.W. Implantation of bone marrow-derived mesenchymal stem cells demonstrates improved outcome in horses with overstrain injury of the superficial digital flexor tendon. Equine Veterinary Journal 2012, 44, 25-32, doi:10.1111/j.2042-3306.2011.00363.x.

9. Carvalho, A.d.M.; Badial, P.R.; Cisneros Alvarez, L.E.; Miluzzi Yamada, A.L.; Borges, A.S.; Deffune, E.; Hussni, C.A.; Garcia Alves, A.L. Equine tendonitis therapy using mesenchymal stem cells and platelet concentrates: a randomized controlled trial. Stem Cell Research & Therapy 2013, 4, doi:10.1186/scrt236.

10. Romero, A.; Barrachina, L.; Ranera, B.; Remacha, A.R.; Moreno, B.; de Blas, I.; Sanz, A.; Vazquez, F.J.; Vitoria, A.; Junquera, C.; et al. Comparison of autologous bone marrow and adipose tissue derived mesenchymal stem cells, and platelet rich plasma, for treating surgically induced lesions of the equine superficial digital flexor tendon. Veterinary Journal 2017, 224, 76-84, doi:10.1016/j.tvjl.2017.04.005.

11. Bari, E.; Perteghella, S.; Di Silvestre, D.; Sorlini, M.; Catenacci, L.; Sorrenti, M.; Marrubini, G.; Rossi, R.; Tripodo, G.; Mauri, P.; et al. Pilot Production of Mesenchymal Stem/Stromal Freeze-

Dried Secretome for Cell-Free Regenerative Nanomedicine: A Validated GMP-Compliant Process. Cells 2018, 7, doi:10.3390/cells7110190.

12. Bari, E.; Perteghella, S.; Catenacci, L.; Sorlini, M.; Croce, S.; Mantelli, M.; Avanzini, M.A.; Sorrenti, M.; Torre, M.L. Freeze-dried and GMP-compliant pharmaceuticals containing exosomes for acellular mesenchymal stromal cell immunomodulant therapy. Nanomedicine 2019, 14, 753-765, doi:10.2217/nnm-2018-0240.

13. Meeson, R.L.; Todhunter, R.J.; Blunn, G.; Nuki, G.; Pitsillides, A.A. Spontaneous dog osteoarthritis - a One Medicine vision. Nature Reviews Rheumatology 2019, 15, 273-287, doi:10.1038/s41584-019-0202-1.

14. Bari, E.; Perteghella, S.; Di Silvestre, D.; Sorlini, M.; Catenacci, L.; Sorrenti, M.; Marrubini, G.; Rossi, R.; Tripodo, G.; Mauri, P.; et al. Pilot Production of Mesenchymal Stem/Stromal Freeze-Dried Secretome for Cell-Free Regenerative Nanomedicine: A Validated GMP-Compliant Process. Cells 2018, 7, doi:https://doi.org/10.3390/cells7110190.

15. Bari, E.; Perteghella, S.; Catenacci, L.; Sorlini, M.; Croce, S.; Mantelli, M.; Avanzini, M.A.; Sorrenti, M.; Torre, M.L. Freeze-dried and GMP-compliant pharmaceuticals containing exosomes for acellular mesenchymal stromal cell immunomodulant therapy. Nanomedicine 2019, doi:10.2217/nnm-2018-0240.

16. Bari, E.; Di Silvestre, D.; Mastracci, L.; Grillo, F.; Grisoli, P.; Marrubini, G.; Nardini, M.; Mastrogiacomo, M.; Sorlini, M.; Rossi, R.; et al. GMP-compliant sponge-like dressing containing MSC lyo-secretome: Proteomic network of healing in a murine wound model. European Journal of Pharmaceutics and Biopharmaceutics 2020, 155, 37-48, doi:10.1016/j.ejpb.2020.08.003.

17. Bari, E.; Ferrarotti, I.; Di Silvestre, D.; Grisoli, P.; Barzon, V.; Balderacchi, A.; Torre, M.L.; Rossi, R.; Mauri, P.; Corsico, A.G.;

et al. Adipose Mesenchymal Extracellular Vesicles as Alpha-1-Antitrypsin Physiological Delivery Systems for Lung Regeneration. Cells 2019, 8, doi:10.3390/cells8090965.

18. Dominici, M.; Le Blanc, K.; Mueller, I.; Slaper-Cortenbach, I.; Marini, F.C.; Krause, D.S.; Deans, R.J.; Keating, A.; Prockop, D.J.; Horwitz, E.M. Minimal criteria for defining multipotent mesenchymal stromal cells. The International Society for Cellular Therapy position statement. Cytotherapy 2006, 8, 315-317, doi:10.1080/14653240600855905.

19. Shah, K.; Drury, T.; Roic, I.; Hansen, P.; Malin, M.; Boyd, R.; Sumer, H.; Ferguson, R. Outcome of Allogeneic Adult Stem Cell Therapy in Dogs Suffering from Osteoarthritis and Other Joint Defects. Stem Cells International 2018, 2018, doi:10.1155/2018/7309201.

20. How, K.L. Clinical signs of elbow dysplasia and osteoarthritis. In Proceedings of the Proceedings of the 30th Annual Meeting IEWG 2016, Vienna, 2016; pp. 5-7.

21. Daems, R.; Van Hecke, L.; Schwarzkopf, I.; Depuydt, E.; Broeckx, S.Y.; David, M.; Beerts, C.; Vandekerckhove, P.; Spaas, J.H. A Feasibility Study on the Use of Equine Chondrogenic Induced Mesenchymal Stem Cells as a Treatment for Natural Occurring Osteoarthritis in Dogs. Stem Cells International 2019, 2019, doi:10.1155/2019/4587594.

22. Hielm-Bjorkman, A.K.; Rita, H.; Tulamo, R.-M. Psychometric testing of the Helsinki chronic pain index by completion of a questionnaire in Finnish by owners of dogs with chronic signs of pain caused by osteoarthritis. American Journal of Veterinary Research 2009, 70, 727-734, doi:10.2460/ajvr.70.6.727.

23. Hielm-Bjorkman, A.K.; Kuusela, E.; Liman, A.; Markkola, A.; Saarto, E.; Huttunen, P.; Leppaluoto, J.; Tulamo, R.M.; Raekallio, M. Evaluation of methods for assessment of pain associated with chronic osteoarthritis in dogs. Journal of the American Veterinary Medical Association 2003, 222, 1552-1558, doi:10.2460/javma.2003.222.1552.

24. Canapp, S.O., Jr.; Leasure, C.S.; Cox, C.; Ibrahim, V.; Carr, B.J. Partial Cranial Cruciate Ligament Tears Treated with Stem Cell and Platelet-Rich Plasma Combination Therapy in 36 Dogs: A Retrospective Study. Frontiers in Veterinary Science 2016, 3, doi:10.3389/fvets.2016.00112.

25. Mitchell, R.; Mellows, B.; Sheard, J.; Antonioli, M.; Kretz, O.; Chambers, D.; Zeuner, M.T.; Tomkins, J.E.; Denecke, B.; Musante, L.; et al. Secretome of adipose-derived mesenchymal stem cells promotes skeletal muscle regeneration through synergistic action of extracellular vesicle cargo and soluble proteins. Stem Cell Research & Therapy 2019, 10, doi:10.1186/s13287-019-1213-1.

26. Zhang, S.; Hu, B.W.; Liu, W.J.; Wang, P.; Lv, X.; Chen, S.F.; Liu, H.J.; Shao, Z.W. Articular cartilage regeneration: The role of endogenous mesenchymal stem/progenitor cell recruitment and migration. Seminars in Arthritis and Rheumatism 2020, 50, 198-208, doi:10.1016/j.semarthrit.2019.11.001.

27. Phinney, D.G.; Pittenger, M.F. Concise Review: MSC-Derived Exosomes for Cell-Free Therapy. Stem Cells 2017, 35, 851-858, doi:10.1002/stem.2575.

28. Elahi, F.M.; Farwell, D.G.; Nolta, J.A.; Anderson, J.D. Preclinical translation of exosomes derived from mesenchymal stem/stromal cells. Stem Cells 2020, 38, 15-21, doi:10.1002/stem.3061.

29. Gupta, R.C.; Lall, R.; Srivastava, A.; Sinha, A. Hyaluronic Acid: Molecular Mechanisms and Therapeutic Trajectory. Frontiers in Veterinary Science 2019, 6, doi:10.3389/fvets.2019.00192.

30. Lee, M.-I.; Kim, J.-H.; Kwak, H.-H.; Woo, H.-M.; Han, J.-H.; Yayon, A.; Jung, Y.-C.; Cho, J.-M.; Kang, B.-J. A placebo-controlled study comparing the efficacy of intra-articular injections of hyaluronic acid and a novel hyaluronic acid-platelet-rich plasma conjugate in a canine model of osteoarthritis. Journal of Orthopaedic Surgery and Research 2019, 14, doi:10.1186/s13018-019-1352-1.

31. Kriston-Pal, E.; Haracska, L.; Cooper, P.; Kiss-Toth, E.; Szukacsov, V.; Monostori, E. A Regenerative Approach to Canine Osteoarthritis Using Allogeneic, Adipose-Derived Mesenchymal Stem Cells. Safety Results of a Long-Term Follow-Up. Frontiers in Veterinary Science 2020, 7, doi:10.3389/fvets.2020.00510.

32. Silva Junior, J.I.S.; Rahal, S.C.; Santos, I.F.C.; Martins, D.J.C.; Michelon, F.; Mamprim, M.J.; Tomacheuski, R.M.; Correia, L.E.C.S. Use of Reticulated Hyaluronic Acid Alone or Associated With Ozone Gas in the Treatment of Osteoarthritis Due to Hip Dysplasia in Dogs. Frontiers in Veterinary Science 2020, 7, doi:10.3389/fvets.2020.00265.

CONCLUSIONS AND FUTURE PERSPECTIVES

In therapeutic practice, there are many limiting conditions to establish an efficient MSC therapy. Indeed, number of cells, therapeutic doses required, route of administration, cell survival and maintenance of MSC in pathological and pro-inflammatory microenvironment of affected organs, as well as rejection problems at the injury sites are relevant topics in therapeutic design. A strategy for the medicinal use of MSC in musculoskeletal disorders is isolating its secretome, which opens up novel therapeutic perspectives aimed at developing cell-free strategies. However, even secretome therapies showed limitation in their use, as the standardization of an isolation process, characterization of bioactive factors, dosing, optimizing the delivery mode, and uncovering of mechanisms of action of stem cell secretome.

This Ph.D. thesis aimed to proceed the research in this field: secretome derived from adipose MSC of canine and equine species has been investigated in terms of its features profile in vitro, and three-case report were provided. Thanks to an optimization of the manufacturing process, previously developed for human combining ultrafiltration and freeze-drying, secretome it now scalable and a ready-to-use product. Lyosecretome showed efficacy for in vitro equine model as well as in dogs and a safety profile towards osteoarthritis was also demostrated in canine, confirming its potential use in clinics.

Because MSC-based therapies are in their early stages, an increasing number of investigations focused on the potential of secretome to

facilitate tissue regeneration and recovery, is yet to be carried out. Such studies would support the importance of secretome as an alternative, promising approach in regenerative medicine. Concerns remain because of insights into mechanisms of action have not revealed enough information, and the technical discrepancies in methods for defining secretome characteristics prevents general interpretations of the results. Therefore, despite the improvements, more data regarding the biological effect(s) and therapeutic efficacy are needed, starting from our method for isolating and characterizing secretome. Reaching this goal, central to the therapeutic utility of secretome would be the setting up of clinical trials to have a continuos evaluation of both safety and efficacy. Within a large number of MSC-based clinical trials being approved by national agencies, obtaining regulatory approval for the application of cell-free therapy in clinics should be much easier. In this way, not only symptomatic therapies occur, but new opportunities for treating MSDs could be given.

APPENDIX

Alternative strategies have been also investigated for the treatment of musculoskeletal pathologies.

Silk is mainly composed by two proteins (fibroin and sericin) largely employed to produce drug delivery systems, as they demonstrate enviable features in terms of biocompatibility and biodegradability, in this regard fibroin exert also anti-inflammatory properties, being an interesting candidate for MSDs treatment. **Paper 5** reports an overview of silk-fibroin nano-drug delivery systems with particular attention to nanoparticles, nanocapsules and nanofibers and their production techniques. Interestingly, **Paper 6** aims at demonstrating that silk fibroin nanoparticles promote anti-inflammatory properties of celecoxib or curcumin, and thus, it could be applied for osteoarthritis treatment. At the same time, **Paper 7** as an important impact on the circular economy, demostrated how the silk sericin derived from industrial wastewater has many biological properties and over the years could be used as an eco-friendly product for pharmaceutical purposes.

Paper 5. Mocchi M and Bari E. Silk-fibroin Nano-drug Delivery Systems; Book Chapter. Royal Chemestry, 2020

Abstract. This chapter focuses on silk-fibroin nano-drug delivery systems, with particular attention to nanoparticles, nanocapsules and nanofibers. The currently employed methods for their production are described, including those based on solvent or microemulsion, those requiring specific instruments such as the milling technique, the electrospray and the supercritical fluid technology, and finally those considered as ''niche'' techniques, such as the microcapillary dot method. The employment of silk-fibroin nanosystems for the delivery of drugs, including protein/enzymes, genetic material and small molecules, is also described.

---

1. Introduction

According to the European Union directive 2011/696/EU, a nanomaterial should consist for 50% or more of particles having a size between 1 nm 100 nm. Nanomaterials, in the form of nanoparticles, nanocapsules and nanofibers, are often used as delivery agents by encapsulating drugs and delivering them to target tissues, eventually with a controlled release. Overall, the employment of nano-drug delivery systems allows improving the safety and effectiveness of drugs. Mainly, it is possible to protect the active ingredient from degradation, increase its biological stability, allow its absorption at a specific site, increase its bioavailability and cellular penetration, as well as reduce the risks of associated toxicity (for the drugs with low therapeutic index). Due to their small size, nano-drug delivery systems can be easily injected, without the risk of causing thrombi, thus achieving a complete distribution of the drug in all body compartments. Generally, the accumulation of the nanoparticulate system in the region of interest (e.g. in the tumour) occurs by non-

specific (passive) drug targeting which is dependent on the properties of the particle, as widely discussed in Chapter 1. Otherwise, better localization of the drug in specific tissues or organs, thus increasing its effectiveness and minimizing the systemic side effects, can be achieved by preparing nano-drug delivery systems with sensitivity to different stimuli (e.g. variations in temperature, pH, magnetic field, light, and salt concentrations) or by the use of a targeting agent (passive and active targeting, respectively) [1].

Natural polymers, and specifically those characterised by a protein structure, have been extensively investigated over the years for the production of nano-drug delivery systems, due to their excellent biocompatibility and biodegradability, self-organisation skills and easy of functionalisation (due to their aminoacidic groups). Among them, silk fibroin occupies a key position, due to its mechanical, physico-chemical and biological features (described in detail in Chapter 2).

This chapter highlights the development of nano-drug delivery systems based on silk fibroin and describes the production techniques employed, as well as the in vitro and in vivo investigations (Table 1). Of note, silk fibroin is produced by a wide variety of arthropods, including silkworms, scorpions, bees, and spiders [2]. Of these, the Bombyx mori silkworm fibroin is the most employed in the preparation of nano-drug delivery systems, while spider silk is not commonly employed due to the lack of commercially established supply chains (as occurs for sericulture) and due to the smaller yield and wilder nature of spiders compared to silkworms. Therefore, this chapter will focus mainly on nano-drug delivery systems based on Bombyx mory silk fibroin; where present, examples of drug delivery systems based on fibroin from other species will also be reported.

Table 1. Some examples of fibroin-based nano-drug delivery systems.

Drug delivery dosage form	Preparation technique	Size and morphology	Drug loaded	Intended administration route	Note	Reference
Nanoparticles	Desolvation	35-125 nm in size; round shape	-	-	Among other solvents, acetone was the most preferable to induce nanoparticle formation. In the final nanoparticles, fibroin was in the β-sheet configuration.	[7]
		About 100 nm in size; spherical shape	Curcumin/ curcumin + celecoxib	Intravenous/ intraarticular	Acetone was used as a desolvating agent. An intrinsic anti-inflammatory activity was	[8, 9]

					demonstrated for fibroin.	
		About 150-170 nm in size; spherical shape	Vascular Endothelial Growth Factor (VEGF)	-	Dimethyl sulfoxide was used as a desolvating agent.	[10]
		About 100 nm in size	Resveratrol	Oral	Methanol was used as a desolvating agent. A prolonged-release (up to 80 hours) of resveratrol was observed. Fibroin synergistically improved resveratrol properties.	[11]
		80-90 nm in size; spherical shape	Vancomycin	Implantation	Acetone was used as a desolvating agent. A prolonged-release	[13]

					(up to 14 days) of vancomycin was observed.	
		From 40–120 nm in size; spherical shape	Insulin	-	Acetone was used as a desolvating agent. Insulin was conjugated covalently by cross-linking with glutaraldehyde. Fibroin nanoparticles increased insulin half time more than 2.5 times.	[14]
		About 90 nm in size; spherical shape	Gentamicin	Implantation	Acetone was used as a desolvating agent. *Antheraea mylitta* fibroin was used. After an	[15]

					initial burst release, the drug was released until 24 hours.	
		About 200 nm in size; round shape	Doxorubicin	Intravenous	Acetone was used as a desolvating agent. Fibroin nanoparticles were coated with different cationic polymers (glycol chitosan, N,N,N-trimethyl chitosan, polyethylenimine or PEGylated polyethylenimine) that improved colloidal stability in biological media.	[16]

		About 50–120 nm in size; round shape	L-asparaginase	-	Acetone was used as a desolvating agent. Fibroin nanoparticles increased the stability of L-asparaginase.	[17]
		About 130 nm in size; spherical shape	Paclitaxel	Local injection	Ethanol was used as a desolvating agent. Silk I or random coil structure was the main conformation of fibroin in nanoparticles.	[18]
		About 170 nm in size; round shape	Quercetin	Oral	Methanol was used as a desolvating agent. A synergic antioxidant activity was	[19]

					found between fibroin and quercetin. After an initial burst, quercetin was slowly released.	
		From 100 to 500 nm in size; round shape	Doxorubicin	-	*Antheraea pernyi* fibroin was used. Instead of organic solvents, Na^{+}, Ca^{2+} and Ce^{3+} were employed to induce the change of fibroin conformation from Silk I to Silk II. Fibroin conformation changes from α-helical to a β-sheet as a function	[20]

					of the ionic strength and the hydrophobic and electrostatic interactions.	
	Salting-out	About 130 nm in size; spherical shape	Doxorubicin	Intravenous injection	Magnetic Fe_3O_4 nanoparticles were coated with fibroin. Nanoparticles can be delivered to the tumour under the guidance of a magnetic field. Doxorubicin was released from the nanosystem in a pH-dependent manner.	[21]
	Supercritical fluid	50 nm in size;	Indomethacin	-	Fibroin was turned	[43]

	technology	spherical shape			from random coil to β-sheet structure with ethanol treatment. Nanoparticles showed a sustained drug release over two days without a burst effect.	
		Lower than 100 nm in size; spherical shape	Curcumin	Oral	Nanoparticles showed time-dependent intracellular transportability and nuclei-targeting potential. The anticancer activity of curcumin was	[44]

					enhanced when encapsulated in nanoparticles.	
		About 75 nm in size; round shape	Methotrexate	Transdermal	Fibroin was precipitated on the surface of Fe_3O_4 nanoparticles. Nanoparticles effectively permeated across the skin under magnetic field.	[79]
	Electrospraying	From 59 to 75 nm; round shape	Cisplatin	-	The drug was slowly and sustainably released from nanoparticles for more than 15 days.	[45]
		About 80 nm in	-	-	Particle size was influence	[46]

		size; rounded shape			d by fibroin concentration and process parameters such as needle-collector distance and applied voltage. Fibroin in nanoparticles had a β-sheet conformation. No functional group change occurs after the conversion of fibroin into nanoparticles.	
	Milling technique	About 200 nm in size; irregular shape	-	-	The particle size was influenced by the degree of fibroin degumming, the size of	[49]

					milling media, water and lubricant on the particle refinement.	
		About 700 nm in size; irregular shape	-	-	Particle size, density and morphology can be manipulated through appropriate changes in the fibroin degumming process.	[50]
		About 200 nm in size; nearly spherical shape	-	-	The particle size was influenced by the pH of alkaline hydrolysis and milling time.	[51]
		About 200 nm in size;	-	-	Tween 80 was used as co-excipient	[52]

		nearly spherical shape			to prevent aggregation.	
	Emulsification-diffusion method	About 170 nm in size; round shape	Rhodamine B	-	Cyclohexane was used as the oil phase and Triton X-100 as a surfactant. Particle size was not affected by the loading of rhodamine B, which was more stable when encapsulated. The fibroin in nanoparticles showed a β-sheet conformation	[54]
		From 500 nm to about 2 mm in size;	Tetramethylrhodamine conjugated bovine serum albumin, tetramethylr	-	PVA was used as the external phase of the emulsion.	[55]

		porous internal structure	hodamine conjugated dextran and rhodamine B		Varying fibroin and PVA concentration or applying ultrasonication to the blend solution were able to control sphere size and distribution. The porous interior space facilitated the entrapment of drugs and make drug release controllable.	
	Gelification	From 10 nm to several μm in size; spherical shape	-	-	Fibroin self-assembled from random coil to metastable nanoparticles (about 10	[57]

					nm) that under an electric field aggregated to form nano- or microspheres with sizes of tens of nanometers	
		From 200 nm to 3 μm in size; round shape	Bovine serum albumin	-	Particle size was influenced by the pre-incubation time of fibroin (at 70 °C).	[58]
	Capillary-microdot techniqu e	Less than 100 nm in size; almost round shape	Curcumin	-	Chitosan was used as co-excipient. The addition of chitosan caused the generation of nanosystems with hydrophilic properties,	[59]

					reducing the curcumin entrapment.	
Nanocapsules	Mild sonochemical	From 438 to 888 nm in size; spherical shape	Rhodamine B, crystal violet, Evans blue, methotrexate	Intravenous	Albumin was used as co-excipient. PH-responsive drug delivery was observed, especially when the albumin/fibroin ratio was 1:1.	[67]
		About 450 nm in size; round shape	Glutathione	Topical	Albumin was used as co-excipient. PH-responsive drug delivery was observed.	[68]
Nanofibers	Electrospinning	About from 300 to 1300 nm in diameter; smooth	-	-	Fibroin fibres with desired properties can be prepared by controllin	[71]

		surface			g the sodium carbonate concentration in the degumming step (that affects fibroin molecular weight).	
		From 200 to 2300 nm in diameter;	-	-	Fibre morphology was affected by salt concentrations (in the starting fibroin solution) and applied voltage.	[72]
		From 440 to 1900 nm in diameter	-	-	Fibre morphology and diameter were influenced by the salt concentrations in the starting fibroin solution.	[73]

		About from 200 to 700 nm in diameter; smooth surface	-	-	A comparison between roller and needle electrospinning was performed. Fibre diameter was smaller when produced by needle electrospinning.	[74]
		From 312 to 542 nm in size; smooth surface	-	Implantation	Chitosan was used as co-excipient; it switched fibroin nanofibers morphology from flat strip to cylindrical. Also, chitosan reduced fibres thermal stability but	[76]

					improved cell adhesion.	
		From 300–760 and 400–1,000 nm in diameter; smooth surface	-	Implantation	*Gonometa postica* and *Gonometa rufobrunnae* fibroin were used. Among others, trifluoroacetic acid was selected as the best solvent. Fibroin in nanofibres exhibited predominantly random coil/α-helical structures.	[77]

2. Silk Fibroin Nanoparticles

For the preparation of fibroin nanoparticles, several methods, employing silk self-assembly behaviour or a vast spectrum of techniques, including those requiring specific types of equipment, can be used [1] These last are for example the milling technique, the electrospraying and the supercritical fluid technology; the ones based

on solvent or microemulsion formation, and finally others considered as ''niche'' techniques, such as the microcapillary dot method. The different varieties of preparation methods for fibroin-based nanoparticles are reported in Table 2, mentioning their benefit and drawbacks.

Table 2. Advantages and disadvantages of the different preparation methods

Preparation method	**Advantages**	**Disadvantages**
Desolvation	Simplicity of operation Mild conditions Small particle size	Easy to aggregate Low drug loading Residue of organic solvents
Salting out	Low cost and high yield Simple procedures Avoids the use of toxic solvents Maintains activity of protein	Particles with big size Salting out agents residue
Supercritical fluid technologies	Low or no organic solvent residues High drug load Controllable particle size	High cost Complicated operations Needs post-treatment to induce silk III conformation
Electrospraying	Particles with high purity Excellent monodispersity Controllable particle size Simplicity of operation	Needs post-treatment to induce silk II conformation
Mechanical comminution	Easy to operate	Requires high energy and long times

		Particles with big size, wide size distribution and different geometry Presence of impurities and grinding aids
Emulsification method	Controllable particle size	Residual surfactant and organic solvents
PVA blend film method	Mild operating conditions Easy to manipulate Time and energy efficient No use of organic solvents	Bigger particles Not easy to obtain a homogeneous size distribution PVA residues
Electric fields (e-gel)	Mild operating conditions No use of organic solvents	Particles with big size and size distribution
Capillary-microdot technique	Simplicity of operation	Organic solvent residue

Importantly, during the formulation of fibroin-based nanoparticles for drug delivery systems, the selection of an appropriate method turns to be essential. Unfortunately, not all the variables of the process are controllable. For instance, there are some intrinsic factors which can influence fibroin nanoparticles preparation, such as the high molecular weight and protein nature, which results to be challenging to manage and control. Plus, if fibroin is exposed to some factors such as heat, salt, pH change and high shear forces, it tends to self-assemble into fibres or gels, making it unsuitable for the next preparation steps.

The desolvation process, also called coacervation, is the most commonly exploited method to obtain fibroin nanoparticles due to relatively moderate conditions employed. The desolvation process consists of reducing fibroin chain solubility, thanks to the presence of organic solvents, such as ethanol, acetone, dimethyl sulfoxide and

methanol, leading to phase separation. Specifically, by adding a desolvation agent, the fibroin conformation changes from Silk I to Silk II, providing coacervation or precipitation of the protein (Figure 1) [3-5]. Unfortunately, the presence of organic solvents represents the main drawback of this method; indeed, in order to avoid any cytotoxicity events, solvents must be removed through many centrifugations or by intense dialysis cycles.

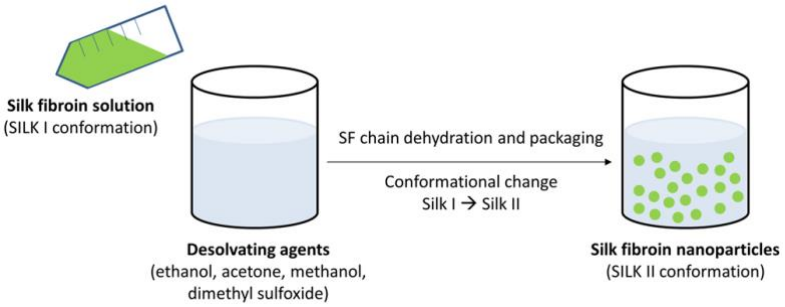

Figure 1. A representative diagram on how to produce SF nanoparticles applying the desolvation method. For the fibroin nanosystem formation, it is necessary to shift from Silk I to Silk II conformation; for this reason, through the use of organic solvent, SF dehydration is needed. Fibroin is at first dissolved in a solvent and then slowly physically removed into a non-solvent phase. Because of phase separation, two phases are formed: one with a coacervate/colloidal component, and the other one with solvent/non-solvent. Herein, the solvent must be mixable with the non-solvent. Stable particle size is achieved, and further desolvation only leads to an increased particle yield. Adapted from ref [1] with permission from The Royal Society of Chemistry.

Above all the process parameters, the pH of the protein solution is one of the major factors to take into account [6]. In fact, the pH influences the degree of ionisation of the protein functional groups, such as the amino group and the carboxyl group. Indeed, the desolvation process is more rapid and effective at zero net charge

conditions (when the pH of the solution is equal to the isoelectric point of the protein).

The formation of fibroin nanoparticles by mixing the aqueous fibroin solution with protonic organic solvents (such as methanol and ethanol) or polar aprotic organic solvents (such as acetone), has been proposed by many authors from the literature. Zhang and colleagues prepared fibroin nanoparticles by a desolvation method, preferring acetone to other solvents [7]. It is not clear why acetone was the most preferable to induce nanoparticle formation. The researchers hypothesized that this could be due to its moderate hydrophilicity, dipole distance or molecular structure. Here, fibroin nanoparticles were characterised by a β-sheet conformation and crystallinity close to native fibres and could reach a size range of 35~125 nm. The size of the nanoparticles is an important parameter, as it determines the surface area to volume ratio and governs the drug release profile. Many factors, such as the type and the amount of the desolvating agent used, can affect the particle size and the size distribution. For example, the pH before the desolvation step, as mentioned earlier, imparts a net positive or negative charge on fibroin and the final nanoparticles. A high surface charge leads to intermolecular repulsions and hence a stable suspension with limited aggregation, while a low surface charge may lead to more aggregation of the nanoparticles.

A research group from Italy [8] prepared fibroin nanoparticles by the desolvation with acetone, in which the hydrophobic drug, the curcumin, was dissolved. The nanoparticles showed a diameter of about 100 nm, a spherical geometry, and they were effectively internalised by mesenchymal stem cells, during in vitro experiments, showing a cytoplasmic localization. Of note, the encapsulation into nanoparticles avoided the cytotoxicity of curcumin. In a subsequent research [9], the authors prepared fibroin nanoparticles in the same manner but loaded with curcumin and celecoxib aiming for the treatment of osteoarticular diseases. Interestingly, by testing the

nanosystems in an in vitro model of osteoarthritis, the authors demonstrated an intrinsic anti-inflammatory therapeutic potential of fibroin.

Fibroin nanoparticles obtained by coacervation technique were also investigated by Kundu and co-workers using dimethyl sulfoxide as an organic solvent [10]. Even in this case, the nanoparticles resulted in being stable, negatively charged, but with a slightly increased diameter (around 150~170 nm). All the fibroin nanoparticles showed mainly Silk II structure and did not exhibit any apparent toxicity.

On this trail, a Spanish research [11] evaluated the intestinal anti-inflammatory properties of fibroin nanoparticles loaded with resveratrol by adsorption onto the surface, keeping a size range of approximately 100 nm. The biological evaluation was performed both in vitro, using mouse macrophages, which enhanced immunomodulatory properties, and in vivo, testing on a rat model of colitis. Specifically, when resveratrol-loaded nanoparticles were tested in vivo, the suitability of resveratrol in the treatment of colitis, due to its anti-inflammatory properties [12], was confirmed and an increased biological effect, probably due to a synergic action between fibroin and resveratrol, was observed.

Desolvation method using acetone was also applied for the preparation of silk fibroin nanoparticles loaded with antibiotic vancomycin [13]. In the present study, the aim was to evaluate the capability of fibroin nanoparticles to control the release kinetics of vancomycin pursuing a therapy against severe osteomyelitis infections. To this end, nanoparticles were also entrapped in silk-based scaffolds to form a well-supported drug delivery systems, which was subsequently evaluated upon implantation in a rat model with severe osteomyelitis. Regarding nanoparticle characterisation, Dynamic Light Scattering (DLS) was performed, revealing uniform size distribution around 80-90 nm and a polydispersity index of 0.1. Scanning Electron Microscopy (SEM) images confirmed sizes and showed spherical

shape with no apparent aggregation. The release kinetics of vancomycin from nanoparticles alone and when entrapped in silk scaffolds were determined, setting up two different pH values, 4.5 and 7.4. Authors demonstrated that acidic conditions impact the drug release from the nanoparticles, due to the repulsive forces between the positive charges of vancomycin and high protonation in acidic solution, while the releasing rate was closer to 100% for pH 7.4.

Similarly, many other examples of fibroin-based nanoparticles prepared by the desolvation method are reported, loading different types of drugs and intended for different administration routes [14-19].

An alternative to the commonly employed desolvation techniques is the ionic-induced self-assembly. Even with this method, a desolvation process is involved, and the fibroin chain solubility is reduced by the use of ions. As an example, Wang and colleagues prepared Antheraea pernyi fibroin nanoparticles using cations (Na+, Ca^{2+}, Ce^{3+}) as reagents under mild conditions (aqueous solutions and a temperature of 37 °C) [20]. Nanoparticles ranging in size from 100 to 500 nm and with a round shape were prepared; no differences were revealed among the different cations. Ions promote fibroin solution conformational changes from a random coil and α-helix to β-sheet structures. Then, due to hydrophobic and electrostatic interactions, fibroin molecules combine to form nanoparticles. Upon an increase in the ion concentration, nanoparticles were formed more quickly, as the more attractive force between the cation and fibroin molecules triggered faster fibroin conformational change. Doxorubicin was effectively loaded into the nanoparticles and was released in a pH-dependent manner.

Another valid and straightforward approach employed for the preparation of fibroin nanoparticles, even if it leads to particles with higher dimensions than the desolvation method (500–2000 nm), is the salting-out technique [1]. Generally, this process starts with the

preparation of a salting bath, composed of potassium phosphate salts, such as K_2HPO_4–KH_2PO_4. Then, the fibroin solution is added to the potassium phosphate salt, and the salting-out occurs (Figure 2). The major drawback of this method is related to the usage of high amounts of salts, which result challenging to remove with standard dialysis cycles only [21].

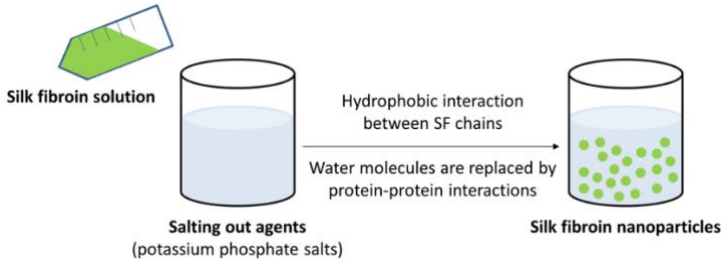

Figure 2. Schematic diagram on how to produce fibroin nanoparticles applying the salting-out method. Fibroin, like any protein, is composed of both hydrophobic and hydrophilic parts, this latter can interact with the surrounding water molecules forming hydrogen bonds. When the salt concentration increase, the salt ions draw water molecules, allowing the replacement of the water molecules-protein bond and increasing the protein-protein interactions. As a consequence, the protein molecules aggregate together forming fibroin nanosystems. Adapted from Adapted from ref [1] with permission from The Royal Society of Chemistry.

Small molecules used as model drugs, such as rhodamine B, were loaded into the fibroin particles prepared by this method only by absorption due to electrostatic interactions. The process yield, along with nanoparticle morphology, secondary structure, zeta potential and stability are influenced by several factors, such as the choice of salt, pH, ionic strength and the fibroin concentration. In detail, the pH value of the potassium phosphate affects the charge and secondary structure of fibroin nanoparticles, which in turn influence the drug release. In

general, alkaline pH is preferred over-acidic to avoid aggregates. Changing the fibroin concentration may have a consequence on the size of the nanoparticles. As an example, when pH 8 potassium phosphate is used, increasing the concentration of fibroin can lead to larger particles. Below pH 5, increasing fibroin concentration, the particles aggregated into non-dispersible aggregates [22, 23].

Tian and colleagues applied the salting-out method to coat hydrophilic magnetic Fe_3O_4 nanoparticles with fibroin, thus entrapping doxorubicin for targeted cancer therapy [21]. Briefly, the researchers dispersed the magnetic nanoparticles and doxorubicin into a potassium phosphate bath (1.25 M, pH 8) before adding the fibroin solution. During the formulation studies, the authors evidenced that insufficient amount of magnetic nanoparticles lead to macroscopic gelation while increasing the magnetic nanoparticle concentration, the agglomeration of fibroin disappears, and particles with uniform and spherical shape are obtained. Of note, doxorubicin was released from the nanosystem in a pH-dependent manner. At pH 5.0 (mimicking endosomes and lysosomes microenvironment), the drug release is significantly higher than those at pH 6.5 (mimicking the tumour tissue environment) and pH 7.4 (mimicking the blood plasma). The drug release is likely accelerated because of the weak electrostatic interactions between fibroin and doxorubicin at low pH values (Figure 3).

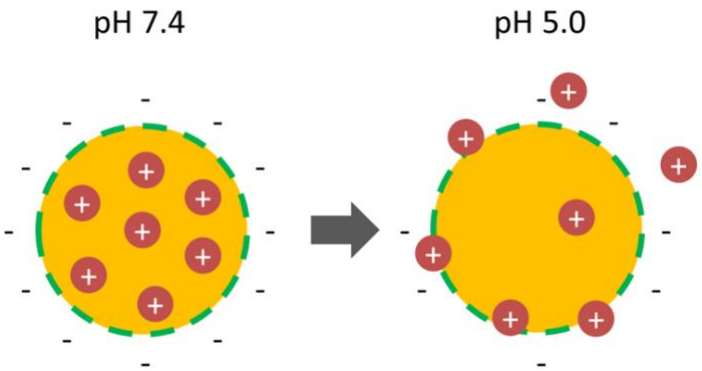

Figure 3. Schematic illustration of the pH-dependent release behaviour of DOX in silk fibroin magnetic nanoparticles. At high pH values, strong electrostatic interactions exist between fibroin (negatively charged) and doxorubicin (positively charged). Decreasing pH, fibroin is less negatively charged and, therefore, doxorubicin is more easily released due to the weak electrostatic interactions.

In vitro, the nanoparticles were effectively uptaked and internalised by cancer cells, and, when tested in vivo, they induced tumour targeting ability and effective chemotherapy of multidrug-resistant cancer. With their work, the authors demonstrate how providing magnetic targeting ability to fibroin nanoparticle is a promising strategy for multidrug-resistant cancer, thus expanding the clinical applications of fibroin-based nanomaterials.

Recently, a valid new supercritical fluid technology (SCF) in pharmaceutical manufacturing has been employed, representing a good alternative for the preparation of nanoparticles, minimising failures of conventional methods [24-26]. Furthermore, SCF is gaining attention as it involves the use of non-flammable and non-reactive reagents, and free of toxic organic solvents, thus reducing the environment matter [27, 28]. SCF was reported for the first time by James Ballantyne Hannay and colleagues in 1879. They discovered, studying the influence of pressure and temperature, that supercritical fluids dissolve solids [29]. The effective yield of this technology is based on choosing the most appropriate solvent and adjusting the temperature and the pressure, which are considered the critical parameters during the procedure [30]. Indeed, during the process, both temperature and pressure can affect physical properties such as density and viscosity [31,32]. Between all the different supercritical fluid technologies, the most commonly used is the supercritical CO_2 (sCO_2), which is capable in the micronisation of many substances, thanks to its favourable temperature and pressure conditions (T = 31.1

°C, P = 7.38 MPa) [6]. The particle formation can be obtained by different method categorised by the behaviour of supercritical fluid technology. Until now, the elective techniques through scCO2, include i) supercritical fluid technology as solvent (rapid expansion of supercritical solutions, RESS) [33]; ii) supercritical fluid technology as solute (particles from gas-saturated solutions, PGSS), and iii) supercritical fluid technology as gas or supercritical fluid antisolvent (GAS or SAS) [34, 35]. In all the previously mentioned methods, SCF plays a crucial role as the re-precipitation supports solute rapid and uniform nucleation for the particle formation. As discussed above, the success of this technology is highly due to proper solvent selection, and by tuning the critical parameters (temperature and pressure). Thus, an understanding of some of the various supercritical processes for particle formation will be briefly given. In the RESS process, SCF acts as a solvent, and the formation of small particles size is due to a solution expansion, after spraying through a nozzle, leading to a rapid drop of both the temperature and pressure [36]. When processing with this technique, the solubility of the substances (such as polymers, proteins and drugs) plays an essential role in the particle formation. In fact, most of them are polar in nature and thus small amounts of organic solvents can be added to improve the polar drug affinity [37]. Even if RESS is considered the most straightforward and most efficient method among SCF technology, its application is relatively limited, because of its poor solubility of polymers and high cost. In the PGSS technique, SCF acts as a solute [38]. After autoclave treatment, sc-CO_2 is compressed and dissolved in the melted polymer in which the solution increases and shift to cooled by the Joule-Thomson effect [39]. Adjusting the pressure parameter at a relatively low level, microparticles are formed. Among the other approaches, the advantage of this method is the low volumes of SCF implied. Nonetheless, the limitations of this process are due to particle aggregation and nozzle blockage [24], [40]. The SAS approach is

involved in processing poor soluble molecules in SCF. In this method, SCF behaves as a non-solvent to the solute. Usually, an organic solvent, like acetone or dimethyl sulfoxide, is used in the process to dissolve materials [32]. Over the process, low viscosity and high diffusivity of SCF demonstrate the high mass transfer ratio, which is responsible of the supersaturation mixture leading to rapid nucleation. The effect of this technique highly depends on the addition procedure and order of solvent, SCF and other substrates. Moreover, aspects like temperature, pressure, solute chemical composition (drug, polymer/protein), and organic solvent need to be optimized. Compared with RESS process, SAS results having a better drug loading for particles micronization [37]. GAS is a modified SAS and it is based on the recrystallization of SCF insoluble solute. This process has less limitations if compared to SAS process; indeed for example, to increase solubility, the choice of the organic solvent is flexible and it is a easy scale-up production [35] Solution-enhanced dispersion by supercritical fluids (SEDS) is another modified SAS important process, which has been particularly used for micro or nanoparticles formation, even based on fibroin (Figure 4).

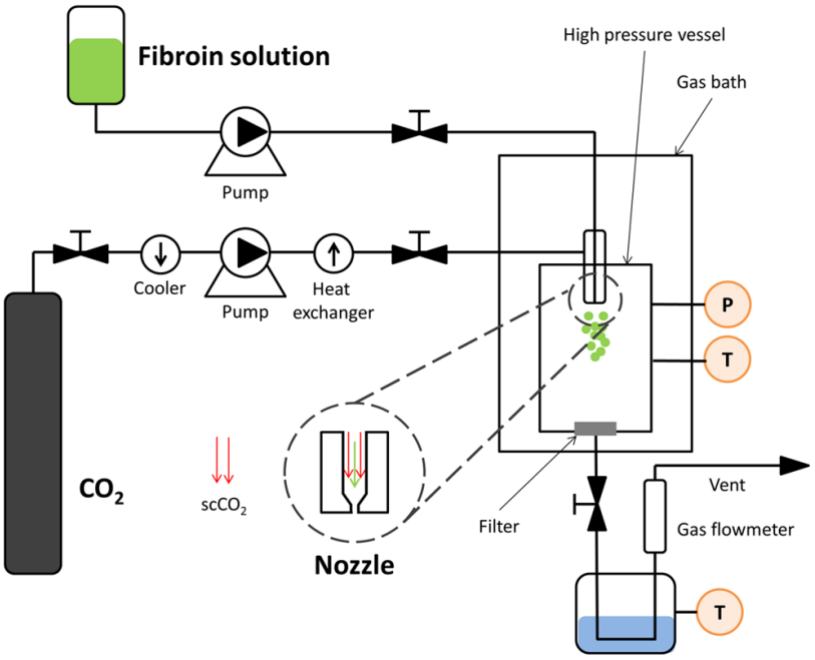

Figure 4. Schematic diagram of the SEDS process for preparing fibroin nanoparticles. Fibroin solution is mixed with supercritical CO_2 and flowed into a coaxial nozzle under controlled pressure and temperature. When fibroin solution makes contact with supercritical CO_2, the high speed breaks up fibroin solution into small droplets, leads to phase separation and saturation of protein solution, with consequent nucleation and precipitation of nanoparticles. Adapted from ref [78] with permission from American Chemical Society, Copyright 2013.

In the SEDS process, the solution containing solute and $scCO_2$ is sprayed through a particular designed coaxial nozzle so that the fluid is atomized [37]. Improving mixing turns into a rapid SFC mass transfer rates into the sprayed droplets, which determines smaller particle size with less agglomeration and allows faster nucleation [41] In detail, a nozzle with two coaxial channel grant $scCO_2$ and solution flow into the high-pressure vessel, maintaining pressure and temperature under control [42]. When the solution makes contact with

the $scCO_2$, the high speed of the $scCO_2$ breaks up the solution into small droplets and increases mass transfer, leading to phase separation and supersaturation of the polymer solution. This causes nucleation and precipitation of very small polymer particle. The particle size distribution and morphology of micro-nano particles are strongly influenced by SEDS process parameters, such as temperature and pressure of $scCO_2$, the flow rate of solution, and solute concentration.

Fibroin nanoparticles have been prepared by SEDS process for the first time successfully by Zhao and colleagues [43]. To do so, after reaching the desired pressure and temperature that keep the CO_2 in a supercritical state, fibroin dissolved in 1,1,1,3,3,3-hexafluoroisopropanol (0.5% w/v) was delivered into the high-pressure vessel via a coaxial nozzle simultaneously with the supercritical CO_2. Zhao and co-workers used the fibroin nanoparticles as drug carrier and loaded them with indomethacin, that was added to the fibroin solution during the preparation procedures. The researcher obtained nanoparticles of 50 nm in average diameter and with a narrow size distribution; moreover, the nanoparticles showed excellent biocompatibility and no burst effect in releasing the drug.

In a similar procedure, Xie and colleagues prepared fibroin nanoparticles loaded with curcumin [44]. Briefly, fibroin and curcumin were mixed and dissolved in hexafluoroisopropanol to the desired concentration (1% w/v). After dissolving completely, the blend solution was ready for the SEDS process. The nanoparticles had a mean diameter lower than 100 nm and significantly improved the solubility of the incorporated curcumin. When tested in vitro on colon cancer cells, the nanoparticles showed time-dependent intracellular transportability and nuclei-targeting potential and exhibited superior anticancer potential with respect to free curcumin.

Electrospraying (electrohydrodynamic spraying) is a rapid technique that provides liquid atomization of fibroin solution by using

electrical forces to obtain high throughput of nanoparticles production. Because of the absence of desolvating agents, fibroin nanoparticles obtained by electrospraying result to be extremely pure, although they have to be treated with organic solvents to shift from Silk I to the stable Silk II conformation.

Qu and colleagues formulated fibroin nanoparticles with a size range between 59 and 75 nm by using electrospraying method at high-voltage [45]. The nanoparticles were incorporated with cisplatin for antitumor therapy. The researchers demonstrated in vitro that the drug was slowly and sustainably released from nanoparticles for more than 15 days. Interestingly, the nanoparticles were easily internalised by A549 lung cancer cells, transferring cisplatin and then triggering their apoptosis, but not from L929 mouse fibroblast cells.

Similarly, a research group from Iran prepared fibroin nanoparticles with a constant rounded shape and particle size starting from 80 nm [46]. Of note, the researchers proved that increasing the concentration of fibroin solutions and increasing the distance between the needle and the collector, fibroin nanoparticles were of bigger particle size. Interestingly, it was proved that intensifying voltage till 20 kV, the particle size decreases, while at higher voltages (25 and 30 kV) the particle size increases. Additionally, the obtained fibroin nanoparticles resulted in unaltered in terms of structural and functional group conformation.

Even mechanical methods have been reported among the broad spectrum of techniques used to develop fibroin nanoparticles. In detail, comminution reduces solid materials from more significant to smaller particle sizes, by crushing, grinding, shotting, or milling. Despite the milling technique is a method easy to operate, it is generally not much employed in the production of fibroin nanoparticles. In fact, it implies dry or wet milling process at high energy, the need for specific milling apparatus and long times, ranging from several hours up to many days

[47, 48]. Additionally, this method is challenging to ensure that all the particles are milled maintaining the same geometry and shape, and often the particle size distribution is diversified.

Rajkhowa and colleagues prepared fibroin nanoparticles with an average particle size around 200 nm by rotary and ball milling [49]. After the degumming process, silk fibers were cut up into short fragments and then shattered by rotary and planetary ball milling. Interestingly, the researchers studied the effects of degree of degumming, size of milling media, water and lubricant on the particle refinement. Harsh degumming reduces fiber strength, thus cutting the milling time drastically; however, an excessive reduction in fiber strength is detrimental to obtain small particle size due to increased particle aggregation. Visual observations with scanning electron microscopy revealed the micro and nano fibrillar architecture of fibroin fibers due to milling. Additionally, rotary milled particles remained fibrous through the size reduction process while with ball milling particles with variable shapes were obtained.

In another work [50], the same authors formulated ultrafine silk powder with an average particle size of about 700 nm by attritor and jet milling. The procedure involves all the following procedures in sequence: silk degumming, chopping, wet attritor milling, spray drying and air-jet milling. Unlike the previous study [49], where a rotating container was set up in a planetary ball mill, in the attritor, balls are stirred inside a stationary container. The latter method allows more irregular movement and rotation, following in a higher shear force and more frequent and intense particle impact.

Fibroin nanoparticles made by a combination of attritor and bead milling techniques were later developed in 2013 by Kazemimostaghim and co-workers [51]. At first, silk fibers were degummed by alkaline hydrolysis, followed by attritor milling process reaching fibroin particle size of 7 μm in diameter. Subsequently, fibroin particle size was further reduced around at 200 nm due to the bead milling process.

Even with this technique, the particle size is strongly influenced by adjusting parameters, such as the pH of degumming and milling time. Nevertheless, certain high pH level during the degumming may cause chemical silk damage.

Interestingly, an alternative to overcome this alkali degradation issue was presented by Kazemimostaghim and colleagues in another work [52] In detail, the researchers formulated fibroin nanoparticles applying bead milling method associated with a biocompatible surfactant, Tween 80. The presence of Tween 80 during the milling process can prevent and elide aggregation, instead of using repulsing charges at high pH during particles size reduction. Silk particles were obtained initially around 7 μm by attritor milling, then shrank through the combined bead milled beads and Tween 80. Finally, fibroin nanoparticles around 200 nm and with a limited particle size distribution were achieved.

Also, the emulsification techniques have been employed for the preparation of nanoparticles. A microemulsion is a dispersion, thermodynamically stable, of two immiscible phases (water dispersed in oil w/o or oil dispersed in water o/w) with the presence of surfactant. The internal phase has a size between 1 nm and 1000 nm. The surfactant results essential for the stabilisation of small droplets of one liquid into the other one, forming a monolayer at the oil-water interface. Considering the w/o microemulsions, the aqueous phase forms droplets having a size range of nanometer, in a continuous hydrocarbon-based continuous phase, usually placed towards the oil highest part of a w/o/surfactant triangular phase diagram. In this region, the thermodynamic surfactant, due to its self-assembly, produces aggregates known as reverse or inverted micelles that can reduce the surface tension [53]. The extraction from the mixture of the precipitate is provided by the addition of an organic solvent, e.g. ethanol. The primary benefit of this method is the controllable particle

size by choosing and adjusting the type and amount of surfactant and co-surfactant, the oil phase or the reacting parameters.

Preparation of fibroin nanoparticles through a w/o microemulsion method was investigated by Myung and colleagues, as reported in Figure 5 [54].

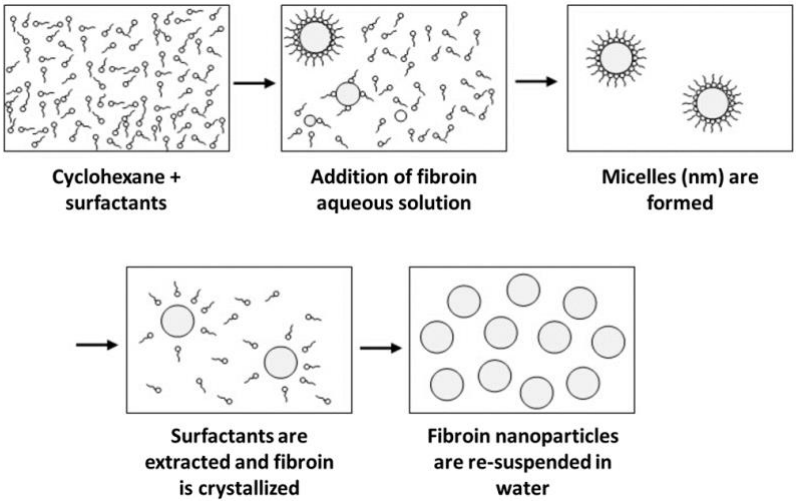

Figure 5. Schematic diagram of the microemulsion method for the preparation of fibroin nanoparticles. Fibroin solution (with or without the drug) is added to the cyclohexane solution containing surfactants. Once micelles (nm) are formed, the surfactant is extracted, and fibroin is crystallized in Silk II conformation by alcohol treatment. Finally, fibroin nanoparticles are re-suspended in water. Adapted from ref. [54] with permission from Springer Nature, Copyright 2008.

In this case, the elective surfactant considered was Triton X-100. The process started with the addition of fibroin aqueous solution into the blended Triton X-100 and cyclohexane under stirring. Extracting surfactant was then possible by adding a mixture of both methanol and ethanol; thus, the microemulsion breaks and particles are recovered. Moreover, by adding to the solution with fibroin a colour dye (rhodamine B), fluorescent dye-encapsulated fibroin nanoparticles

were achieved. The fibroin nanoparticles had a mean size around 167-169 nm which was not affected by the presence of rhodamine B. Of note, the authors demonstrated the stability of the fluorescent molecule incorporated in the fibroin nanoparticles, suggesting their potential in molecular imaging applications.

Sometimes, the external phase of the emulsion is made of polymers. In the literature, this method is often reported as fibroin blended micro/nanosphere production. It consists of combining fibroin with different polymers, such as Polyvinyl alcohol (PVA), to create an emulsified system formed by the natural phase separation that occurs when the protein and the polymer are mixed. In detail, PVA was successfully used for the preparation of fibroin blended micro/nanospheres (particles sizing between 500 nm and 2 mm) by Wang and colleagues [55]. The researches adopted a three-step process: i) blended fibroin-PVA solutions were prepared and dried to form films; ii) films were dispersed in water; iii) the obtained solution was centrifuged to eliminate PVA residues and obtain a suspension of fibroin nanoparticles (Figure 6). The complete drying of the blend emulsion into a film revealed to be an essential step for the formation of stable fibroin nano/microspheres.

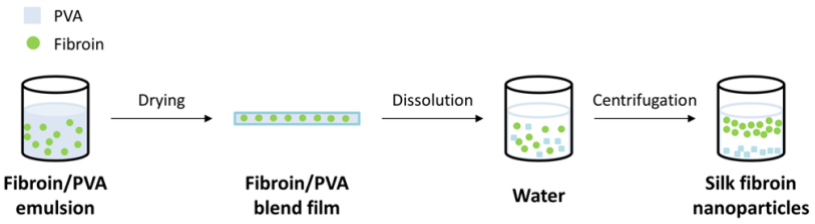

Figure 6. Schematic preparation of fibroin nanoparticles from fibroin/PVA blend films. Silk fibroin and PVA are mixed, forming an emulsion in which fibroin aqueous droplets (micro-nano sized) are finely dispersed into PVA. The emulsion is dried to form films, which are then dispersed in water and centrifuged (to eliminate PVA) obtaining a nanoparticle suspension.

Interestingly, the authors have been able to control sphere size and distribution by varying the concentration of fibroin and PVA or by applying ultrasonication to the blend solution. For example, decreasing the concentration of fibroin and PVA in the blend solution to 0.2% w/w, while keeping the weight ratio of silk and PVA constant at 1:4, nanospheres with a relatively homogeneous size distribution (100–500 nm) were obtained. The morphological investigation of fibroin nano/microparticles revealed a porous interior space that, together with the amphiphilic nature of fibroin, facilitated the entrapment of drugs with different molecular weights and hydrophobicities, making drug release controllable.

Another possible way to develop fibroin particles is the gel system (e-gel). E-gel is formed due to weak electric fields, and micro/nanoparticles can reach sizes of several nanometers [56]. Based on this previous study, Lu Q and colleagues discovered that the formation of fibroin nanoparticles of 10 nanometers could be a crucial step in the formation of e-gels [57]. Notably, in the presence of an electric field, the authors observed how fibroin self-assemble into nano- or microspheres with sizes starting from 10 nm to several microns on the positive electrode. This behaviour can be explained considering that in aqueous solutions with neutral pH, the self-assembly of fibroin is prevented by the negative surface charge due to the acidic charged groups of the protein. When an electric voltage is applied, a higher proton concentration is achieved in the proximity of the positive electrode, thus resulting in a decreased pH in the bulk of the solution, in a reduction of the acidic surface charged groups and allowing fibroin to assemble (Figure 7).

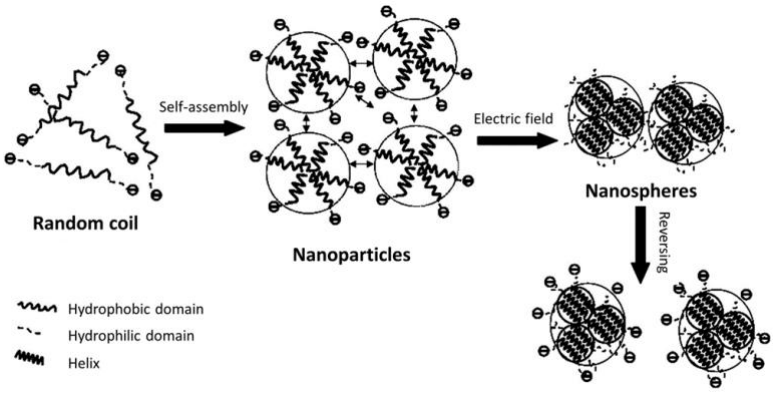

Figura 7. Electrogelation mechanisms of fibroin. Silk fibroin firstly assembles into nanoparticles with a size of 10 nanometers; then, in the presence of an electric field, the reduction of the acidic surface charged groups, a consequence of the local solution pH decrease, allows fibroin to assemble into microspheres of several microns. In reversing the process, the microspheres are dispersed into the solution rather than separated into nanoparticles. Reproduced from ref. [57] with permission from Elsevier, Copyright 2011.

As an example, under weak electric fields, Huang and colleagues prepared fibroin nano/microparticles with sizes ranging from around 200 nm to 3 μm [58]. Briefly, electrodes were dipped in fibroin aqueous solution (0.8% w/w), and a voltage of 25 V was applied. Few seconds after the application of the voltage, a visible gel was formed at the positive electrode. After several washes using purified water, fibroin gels were placed into liquid nitrogen. Eventually, using the freeze-drying process, fibroin nano-microspheres were formed. Interestingly, the authors pre-incubated fibroin solution at 70 °C for different times and evaluated the effect on the particle size. After 6 h of heat treatment, fibroin nanoparticles assumed 300 nm in diameter. After heat treatment for 6~24 h, some nanoparticles with a 500 nm in diameter were formed. When increasing heat treatment to 48~72 h, fibroin microspheres sizing around 2-3 μm were obtained. Thus, the size of the microspheres was regulated from about 200 nm up to 3 μm by only changing the incubation time (keeping 70 °C).

In 2009, for the first time, Gupta and colleagues prepared fibroin and chitosan nanoparticles loaded with curcumin applying the capillary-microdot technique [59] Briefly, curcumin powder was added into a fibroin solution to form drug suspension that was then placed on glass slides through a microcapillary system. After freezing, the drops were lyophilised and the derived dry dots, enclosing fibroin-encapsulated curcumin nanoparticles, were scrabbled from the slides and crystallised by processing with methanol (Figure 8).

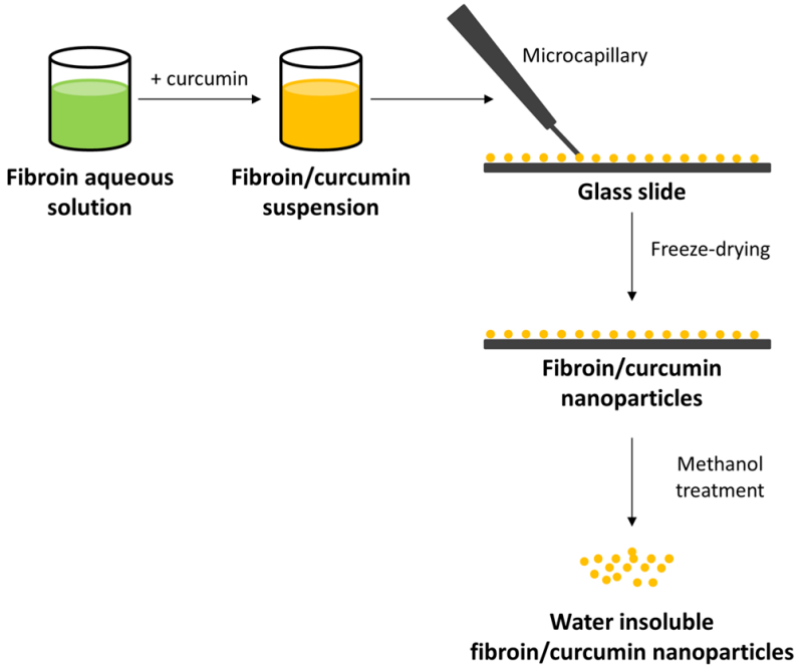

Figure 8. Schematic diagram of the capillary-microdot technique for preparing fibroin nanoparticles. Adapted from ref [6] https://doi.org/10.3390/ijms16034880, under the terms of the CC BY 4.0 licence, https://creativecommons.org/licenses/by/4.0/.

The formulated nanoparticles were less than 100 nm in size as investigated by using transmission electron microscopy. The addition of chitosan caused the generation of nanosystems with hydrophilic properties, causing the reduction of curcumin entrapment, which is an

active molecule with a highly hydrophobic profile, and lower drug release.

2.1 Functionalised Fibroin Nanoparticles

Nanofibers are gaining a global interest for multiple application fields, including tissue engineering, drug delivery, preparation of functional nanotubes, catalyst supports, thin fibres for filtration application, and so on. In biology, the term nanofibre more frequently refers to a fibre with diameter below 100 nm. Fibres are then categorised as continuous or discontinuous/short fibres depending on their lengths. A fibre, to be defined as continuous, must have an aspect ratio (length divided by diameter) above 200. The terms mat or mesh define a collection of nanofibers and depending on the orientation of fibres, they are termed as either woven (oriented in highly regular patterns) or non-woven (randomly orientated).

There are various approaches to produce nanofibers, and between those, electrospinning represents an excellent choice due to its low cost and easy way to produce nanomaterials in the fibre form. Electrospinning was patented by Anton Formhals in 1934 and consisted of a combination of two methods: the electrospray and spinning of fibres [69]. Specifically, this technique produces slight fibres by forcing a viscous polymer solution through a spinneret to which an electric field is applied. When the equilibrium between the electronic force of the charged surface and the surface tension is reached, droplets organise into a structure called Taylor cone. Higher applied voltage elongates the Taylor cone until when the threshold voltage is exceeded, and a jet is emanated. By tuning the solution viscosity and surface tension, a stable jet is formed, and its breakup is prevented (Figure 9).

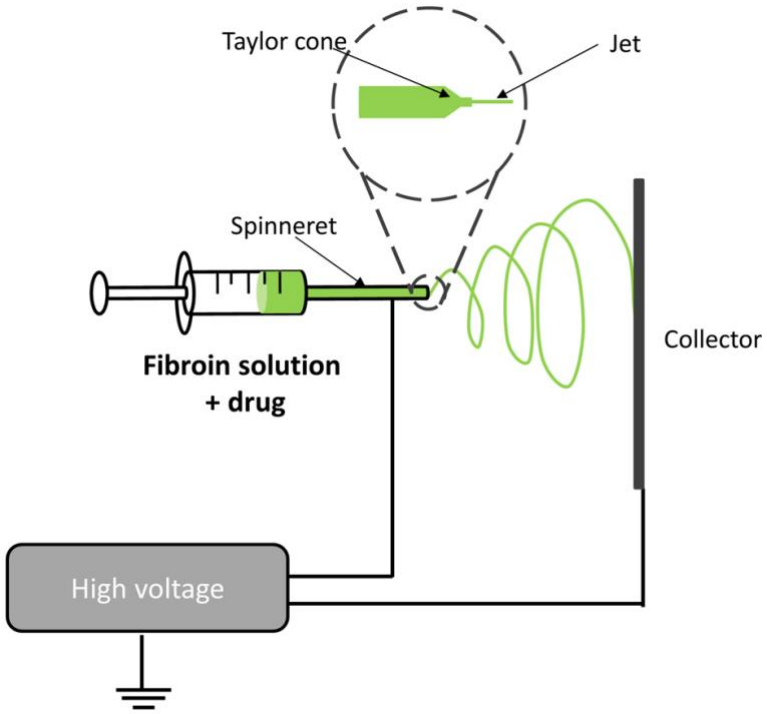

Figure 9. Preparation of electrospun fibroin nanofibers. Fibroin solution is forced by a syringe pump to pass through a spinneret to which a voltage is applied. Liquid droplets organize into an elongated Taylor cone structure, and a jet is emanated. Then, the solvent evaporates, and nanofibers are collected.

The primary step in the electrospinning process is the polymer/protein dissolution in a suitable solvent. Ideally, the solvents should possess good intrinsic properties, such as good volatility, and the capacity to maintain the consistency of the polymer/protein solution. Solvents that have been studied and are suitable for electrospun silk fibroin are, for example, formic acid (FA) at different concentration (ranging from 85 up to 98%), 1,1,1,3,3,3-hexafluoro-2-propanol (HFIP), H_2O, acetic acid, and LiBr [70].

In addition to the solvent chosen, other parameters can affect the electrospun fibre morphology at the nanoscale effect. Some of the most commonly considered are, for example, the molecular weight, the

viscosity and the solubility of the electrospinned polymer/protein [70]. As an example, fibroin molecular weight can be strongly influenced by the sodium carbonate concentration used during the silk degumming process. In this regard, literature data showed that the degumming process profoundly impacts the microstructure types and influence the electrospinning performance of regenerated silk fibroin.

Specifically, Dou and colleagues investigated the effect of sodium carbonate concentrations for silk degumming on the formation of electrospun silk fibroin nanofibers [71]. The researcher found that when increasing the sodium carbonate concentration, a transformation from nanofibrils to nanoparticles was observed in the electrospinning solutions, leading to changes in rheological properties. Indeed, when the nanofibrils structure is present, the solution owns remarkably higher viscosity with respect to nanoparticles, which shows very low viscosity. As a consequence, electrospun nanofibers formation is favoured by nanofibrils with ease, even at low concentration (2% w/v), while when nanoparticle structures are present, high spinning concentration (8% w/v) has to be used. Hence, sodium carbonate concentrations provide a controllable choice for the preparation of silk-based electrospun biomaterials with desired properties.

One study was conducted in order to obtain a nonwoven sheet from fibroin using needleless electrospinning method with an alternative way of solvent preparation [72]. The authors used a mixture of formic acid and calcium chloride as a solvent and investigated the effects of both salt concentrations (1-8% w/w) and voltage of electric field (20 kV-50 kV) on fibre morphology. Calcium chloride concentrations of 2-3% w/w were found to be optimal to solubilize fibroin in formic acid adequately and to obtain nanofibers with a low diameter. Instead, increasing the voltage, the size distribution becomes more uniform even if the average diameter was not affected.

In complementary research published in 2016 [73], preparation and characterization of electrospinning silk fibroin nanofibres using a

mixture solvent of formic acid and calcium chloride was investigated. According to the previous study, results exhibit how the concentration of calcium chloride can improve fibroin solubility in formic acid, and also enhanced how its presence influences other elements, such as silk electrospun fibre morphology and diameter. In this case, the obtained nanofibres diameter was ranging from 440 to 1900 nm.

Again, the same silk nanofibres preparation was applied by Sasithorn and Martinová, which further confirmed the outcomes mentioned above in both spinning systems (roller and needle) taken into account [74]. Differences between the two techniques were noticed in terms of electrospun fibres diameters, which was smaller in the one produced by needle electrospinning, and in terms of the high voltage applied to the spinning process, which improved the production rate in roller electrospinning and had a minor effect for the needle electrospinning.

Regarding the electrospinning method to produce nanofibrous scaffold, a key point investigated was the potential effect of using methanol bath as a collector [75]. Comparing wet-electrospun mats with the conventional ones, an increase of average fibre diameter, crystallinity and stiffness were found when soaking time is prolonged. Moreover, wet-electrospun mats were found to improve cellular viability of the osteoblast-like cells (MG63). Finally, it seems that wet electrospinning in soaking methanol is optimal for bone regeneration. In another work, silk fibroin/chitosan nanofibers were investigated [76]. It was noticed that by adding chitosan at 10% w/w, the electrospinnability of fibroin solution was much ameliorated, and the morphology of fibroin nanofibers switched from flat strip to cylindrical. Moreover, the average diameters of nanofiber decreased by approximately 200 nm (from 542 to 312 nm), also leading to an increase in fibre diameter uniformity. Nevertheless, when the chitosan load was higher than 15% w/w, the fibroin/chitosan nanofibers seem to be polarised due to the phase separation of the two polymers in

solution. Regarding the decomposition temperature of the above electrospun nanofibers, it was observed that by increasing chitosan content, the decomposition temperature decreased, probably due to the lower decomposition temperature of chitosan. Furthermore, in this study was also demonstrated that fibroin nanofibers improved cell adhesion with 10% w/w chitosan rather than electrospun pure fibroin nanofibers.

Finally, to our knowledge, Mhuka et all have been the first reporting on the production and characterisation of electrospun nanofibres derivated from Gonometa postica and Gonometa rufobrunnae silk fibroin [77]. Different silks have differences features in terms of chemical and structural change, also leading to different properties and efficiency of nanofibers. In detail, Gonometa species have many polar amino acids that provide reactive sites that could be functionalised; indeed in this study, the structural transformation was investigated depending on the type of solvent used and whether it is better to perform freeze-dried electrospun nanofibres or via rotary evaporation. Dissolution of Gonometa silk fibroin was conducted testing various concentration of several solvents, including LiBr, LiCl, $Ca(NO_3)_2$, and several solvent systems like LiBr:EtOH:H_2O (4:4:1); LiCl:EtOH:H_2O (4:4:1); $Ca(NO_3)_2$:H_2O:MeOH (1:4:2); $CaCl_2$:EtOH:H_2O (1:2:8). Regarding the electrospinning process, some studies have been carried out to optimise the affective parameters as the selection of electrospinning solvent. Indeed, the solvent influences the electrospinnability, and thus its selection, results in an important step to take into account; in this case, trifluoroacetic acid was found to be the best choice. The effect of freeze-dried and rotary evaporation techniques, and their impact on the nanofibres quality was checked. Results indicated that both drying methods successfully obtained nanofibers, but rotary evaporation led to smaller nanofibre diameters.

References

1. Crivelli, B.; Perteghella, S.; Bari, E.; Sorrenti, M.; Tripodo, G.; Chlapanidas, T.; Torre, M. L., Silk nanoparticles: from inert supports to bioactive natural carriers for drug delivery. Soft Matter 2018, 14 (4), 546-557.

2. Fu, C.; Shao, Z.; Fritz, V., Animal silks: their structures, properties and artificial production. Chemical Communications 2009, (43), 6515-6529.

3. Jahanshahi, M.; Babaei, Z., Protein nanoparticle: A unique system as drug delivery vehicles. African Journal of Biotechnology 2008, 7 (25), 4926-4934.

4. Lohcharoenkal, W.; Wang, L.; Chen, Y. C.; Rojanasakul, Y., Protein Nanoparticles as Drug Delivery Carriers for Cancer Therapy. Biomed Research International 2014.

5. Reis, C. P.; Neufeld, R. J.; Ribeiro, A. J.; Veiga, F., Nanoencapsulation I. Methods for preparation of drug-loaded polymeric nanoparticles. Nanomedicine-Nanotechnology Biology and Medicine 2006, 2 (1), 8-21.

6. Zhao, Z.; Li, Y.; Xie, M. B., Silk Fibroin-Based Nanoparticles for Drug Delivery. International Journal of Molecular Sciences 2015, 16 (3), 4880-4903.

7. Zhang, Y.-Q.; Shen, W.-D.; Xiang, R.-L.; Zhuge, L.-J.; Gao, W.-J.; Wang, W.-B., Formation of silk fibroin nanoparticles in water-miscible organic solvent and their characterization. Journal of Nanoparticle Research 2007, 9 (5), 885-900.

8. Perteghella, S.; Crivelli, B.; Catenacci, L.; Sorrenti, M.; Bruni, G.; Necchi, V.; Vigani, B.; Sorlini, M.; Torre, M. L.; Chlapanidas, T., Stem cell-extracellular vesicles as drug delivery systems: New frontiers for silk/curcumin nanoparticles. International Journal of Pharmaceutics 2017, 520 (1-2), 86-97.

9. Crivelli, B.; Bari, E.; Perteghella, S. Catenacci, L.; Sorrenti, M.; Mocchi, M.; Farago, S.; Tripodo, G.; Prina-Mello, A.; Torre, M. L., Silk fibroin nanoparticles for celecoxib and curcumin delivery: ROS-scavenging and anti-inflammatory activities in an in vitro model of osteoarthritis. European Journal of Pharmaceutics and Biopharmaceutics 2019, 137, 37-45.

10. Kundu, J.; Chung, Y.-I.; Kim, Y. H.; Taeb, G.; Kundu, S. C., Silk fibroin nanoparticles for cellular uptake and control release. International Journal of Pharmaceutics 2010, 388 (1-2), 242-250.

11. Lozano-Perez, A. A.; Rodriguez-Nogales, A.; Ortiz-Cullera, V.; Algieri, F.; Garrido-Mesa, J.; Zorrilla, P.; Rodriguez-Cabezas, M. E.; Garrido-Mesa, N.; Utrilla, M. P.; De Matteis, L.; de la Fuente, J. M.; Cenis, J. L.; Galvez, J., Silk fibroin nanoparticles constitute a vector for controlled release of resveratrol in an experimental model of inflammatory bowel disease in rats. International Journal of Nanomedicine 2014, 9, 4507-4520.

12. Martin, A. R.; Villegas, I.; Sanchez-Hidalgo, M.; Alarcon de la Lastra, C., The effects of resveratrol, a phytoalexin derived from red wines, on chronic inflammation induced in an experimentally induced colitis model. British Journal of Pharmacology 2006, 147 (8), 873-885.

13. Besheli, N. H.; Mottaghitalab, F.; Eslami, M.; Gholami, M.; Kundu, S. C.; Kaplan, D. L.; Farokhi, M., Sustainable Release of Vancomycin from Silk Fibroin Nanoparticles for Treating Severe Bone Infection in Rat Tibia Osteomyelitis Model. Acs Applied Materials & Interfaces 2017, 9 (6), 5128-5138.

14. Yan, H.-B.; Zhang, Y.-Q.; Ma, Y.-L.; Zhou, L.-X., Biosynthesis of insulin-silk fibroin nanoparticles conjugates and in vitro evaluation of a drug delivery system. Journal of Nanoparticle Research 2009, 11 (8), 1937-1946.

15. Sharma, S.; Bano, S.; Ghosh, A. S.; Mandal, M.; Kim, H.-W.; Dey, T.; Kundu, S. C., Silk fibroin nanoparticles support in vitro sustained antibiotic release and osteogenesis on titanium surface. Nanomedicine-Nanotechnology Biology and Medicine 2016, 12 (5), 1193-1204.

16. Wang, S.; Xu, T.; Yang, Y.; Shao, Z., Colloidal Stability of Silk Fibroin Nanoparticles Coated with Cationic Polymer for Effective Drug Delivery. Acs Applied Materials & Interfaces 2015, 7 (38), 21254-21262.

17. Zhang, Y.-Q.; Wang, Y.-J.; Wang, H.-Y.; Zhu, L.; Zhou, Z.-Z., Highly efficient processing of silk fibroin nanoparticle-L-asparaginase bioconjugates and their characterization as a drug delivery system. Soft Matter 2011, 7 (20), 9728-9736.

18. Wu, P. Y.; Liu, Q.; Li, R. T.; Wang, J.; Zhen, X.; Yue, G. F.; Wang, H. Y.; Cui, F. B.; Wu, F. L.; Yang, M.; Qian, X. P.; Yu, L. X.; Jiang, X. Q.; Liu, B. R., Facile Preparation of Paclitaxel Loaded Silk Fibroin Nanoparticles for Enhanced Antitumor Efficacy by Locoregional Drug Delivery. Acs Applied Materials & Interfaces 2013, 5 (23), 12638-12645.

19. Lozano-Perez, A. A.; Rivero, H. C.; Hernandez, M. D. P.; Pagan, A.; Montalban, M. G.; Villora, G.; Cenis, J. L., Silk fibroin nanoparticles: Efficient vehicles for the natural antioxidant quercetin. International Journal of Pharmaceutics 2017, 518 (1-2), 11-19.

20. Wang, J.; Zhang, S.; Xing, T.; Kundu, B.; Li, M.; Kundu, S. C.; Lu, S., Ion-induced fabrication of silk fibroin nanoparticles from Chinese oak tasar Antheraea pernyi. International Journal of Biological Macromolecules 2015, 79, 316-325.

21. Tian, Y.; Jiang, X.; Chen, X.; Shao, Z.; Yang, W., Doxorubicin-Loaded Magnetic Silk Fibroin Nanoparticles for Targeted Therapy of Multidrug-Resistant Cancer. Advanced Materials 2014, 26 (43), 7393-7398.

22. Qi, Y.; Wang, H.; Wei, K.; Yang, Y.; Zheng, R.-Y.; Kim, I. S.; Zhang, K.-Q., A Review of Structure Construction of Silk Fibroin Biomaterials from Single Structures to Multi-Level Structures. International Journal of Molecular Sciences 2017, 18 (3).

23. Lammel, A. S.; Hu, X.; Park, S.-H.; Kaplan, D. L.; Scheibel, T. R., Controlling silk fibroin particle features for drug delivery. Biomaterials 2010, 31 (16).

24. Kankala, R. K.; Zhang, Y. S.; Wang, S.-B.; Lee, C.-H.; Chen, A.-Z., Supercritical Fluid Technology: An Emphasis on Drug Delivery and Related Biomedical Applications. Advanced Healthcare Materials 2017, 6 (16).

25. Chen, A.-Z.; Li, L.; Wang, S.-B.; Zhao, C.; Liu, Y.-G.; Wang, G.-Y.; Zhao, Z., Nanonization of methotrexate by solution-enhanced dispersion by supercritical CO2. Journal of Supercritical Fluids 2012, 67, 7-13.

26. Byrappa, K.; Ohara, S.; Adschiri, T., Nanoparticles synthesis using supercritical fluid technology - towards biomedical applications. Advanced Drug Delivery Reviews 2008, 60 (3), 299-327.

27. Hayashi, H.; Hakuta, Y., Hydrothermal Synthesis of Metal Oxide Nanoparticles in Supercritical Water. Materials 2010, 3 (7), 3794-3817.

28. Davies, O. R.; Lewis, A. L.; Whitaker, M. J.; Tai, H.; Shakesheff, K. M.; Howdle, S. M., Applications of supercritical CO(2) in the fabrication of polymer systems for drug delivery and tissue engineering. Advanced Drug Delivery Reviews 2008, 60 (3), 373-387.

29. Wisniak, J., James Ballantyne Hannay. CENIC Ciencias. Químicas 2010.

30. Vemavarapu, C.; Mollan, M. J.; Lodaya, M.; Needham, T. E., Design and process aspects of laboratory scale SCF particle formation systems. International Journal of Pharmaceutics 2005, 292 (1-2), 1-16.

31. Pasquali, I.; Bettini, R., Are pharmaceutics really going supercritical? International Journal of Pharmaceutics 2008, 364 (2), 176-187.

32. Kalani, M.; Yunus, R., Application of supercritical antisolvent method in drug encapsulation: a review. International Journal of Nanomedicine 2011, 6, 1429-1442.

33. Gosselin, P. M.; Thibert, R.; Preda, M.; McMullen, J. N., Polymorphic properties of micronized carbamazepine produced by RESS. International Journal of Pharmaceutics 2003, 252 (1-2), 225-233.

34. Zhao, X.; Zu, Y.; Li, Q.; Wang, M.; Zu, B.; Zhang, X.; Jiang, R.; Zu, C., Preparation and characterization of camptothecin powder micronized by a supercritical antisolvent (SAS) process. Journal of Supercritical Fluids 2010, 51 (3), 412-419.

35. Yeo, S. D.; Lim, G. B.; Debenedetti, P. G.; Bernstein, H., FORMATION OF MICROPARTICULATE PROTEIN POWDERS USING A SUPERCRITICAL FLUID ANTISOLVENT. Biotechnology and Bioengineering 1993, 41 (3), 341-346.

36. Kayrak, D.; Akman, U.; Hortacsu, O., Micronization of ibuprofen by RESS. Journal of Supercritical Fluids 2003, 26 (1), 17-31.

37. Mishima, K., Biodegradable particle formation for drug and gene delivery using supercritical fluid and dense gas. Advanced Drug Delivery Reviews 2008, 60 (3), 411-432.

38. Kerc, J.; Srcic, S.; Knez, Z.; Sencar-Bozic, P., Micronization of drugs using supercritical carbon dioxide. International Journal of Pharmaceutics 1999, 182 (1), 33-39.

39. Hakuta, Y.; Hayashi, H.; Arai, K., Fine particle formation using supercritical fluids. Current Opinion in Solid State & Materials Science 2003, 7 (4-5), 341-351.

40. Pilcer, G.; Amighi, K., Formulation strategy and use of excipients in pulmonary drug delivery. International Journal of Pharmaceutics 2010, 392 (1-2), 1-19.

41. Shoyele, S. A.; Cawthome, S., Particle engineering techniques for inhaled biopharmaceuticals. Advanced Drug Delivery Reviews 2006, 58 (9-10), 1009-1029.

42. Omenetto, F. G.; Kaplan, D. L., New Opportunities for an Ancient Material. Science 2010, 329 (5991), 528-531.

43. Zhao, Z.; Chen, A.; Li, Y.; Hu, J.; Liu, X.; Li, J.; Zhang, Y.; Li, G.; Zheng, Z., Fabrication of silk fibroin nanoparticles for controlled drug delivery. Journal of Nanoparticle Research 2012, 14 (4).

44. Xie, M.; Fan, D.; Li, Y.; He, X.; Chen, X.; Chen, Y.; Zhu, J.; Xu, G.; Wu, X.; Lan, P., Supercritical carbon dioxide-developed silk fibroin nanoplatform for smart colon cancer therapy. International Journal of Nanomedicine 2017, 12, 7751-7761.

45. Qu, J.; Liu, Y.; Yu, Y.; Li, J.; Luo, J.; Li, M., Silk fibroin nanoparticles prepared by electrospray as controlled release carriers of cisplatin. Materials Science & Engineering C-Materials for Biological Applications 2014, 44, 166-174.

46. Gholami, A.; Tavanai, H.; Moradi, A. R., Production of fibroin nanopowder through electrospraying. Journal of Nanoparticle Research 2011, 13 (5), 2089-2098.

47. Zhang, D. L., Processing of advanced materials using high-energy mechanical milling. Progress in Materials Science 2004, 49 (3-4), 537-560.

48. Koch, C. C., TOP-DOWN SYNTHESIS OF NANOSTRUCTURED MATERIALS: MECHANICAL AND THERMAL PROCESSING METHODS. Reviews on Advanced Materials Science 2003, 5 (2), 91-99.

49. Rajkhowa, R.; Wang, L.; Wang, X., Ultra-fine silk powder preparation through rotary and ball milling. Powder Technology 2008, 185 (1), 87-95.

50. Rajkhowa, R.; Wang, L.; Kanwar, J.; Wang, X., Fabrication of ultrafine powder from eri silk through attritor and jet milling. Powder Technology 2009, 191 (1-2), 155-163.

51. Kazemimostaghim, M.; Rajkhowa, R.; Tsuzuki, T.; Wang, X., Production of submicron silk particles by milling. Powder Technology 2013, 241, 230-235.

52. Kazemimostaghim, M.; Rajkhowa, R.; Tsuzuki, T.; Wang, X., Ultrafine silk powder from biocompatible surfactant-assisted milling. Powder Technology 2013, 249, 253-257.

53. Eastoe, J.; Hollamby, M. J.; Hudson, L., Recent advances in nanoparticle synthesis with reversed micelles. Advances in Colloid and Interface Science 2006, 128, 5-15.

54. Myung, S. J.; Kim, H.-S.; Kim, Y.; Chen, P.; Jin, H.-J., Fluorescent Silk Fibroin Nanoparticles Prepared Using a Reverse Microemulsion. Macromolecular Research 2008, 16 (7), 604-608.

55. Wang, X.; Yucel, T.; Lu, Q.; Hu, X.; Kaplan, D. L., Silk nanospheres and microspheres from silk/pva blend films for drug delivery. Biomaterials 2010, 31 (6), 1025-1035.

56. Leisk, G. G.; Lo, T. J.; Yucel, T.; Lu, Q.; Kaplan, D. L., Electrogelation for Protein Adhesives. Advanced Materials 2010, 22 (6), 711-+.

57. Lu, Q.; Huang, Y.; Li, M.; Zuo, B.; Lu, S.; Wang, J.; Zhu, H.; Kaplan, D. L., Silk fibroin electrogelation mechanisms. Acta Biomaterialia 2011, 7 (6), 2394-2400.

58. Huang, Y. L.; Lu, Q.; Li, M. Z.; Zhang, B.; Zhu; H.S., Silk fibroin microsphere drug carriers prepared under electric fields. Chin. Sci. Bull. 2011.

59. Gupta, V.; Aseh, A.; Rios, C. N.; Aggarwal, B. B.; Mathur, A. B., Fabrication and characterization of silk fibroin-derived curcumin nanoparticles for cancer therapy. International Journal of Nanomedicine 2009, 4 (1), 115-122.

60. Totten, J. D.; Wongpinyochit, T.; Carrola, J.; Duarte, I. F.; Seib, F. P., PEGylation-Dependent Metabolic Rewiring of Macrophages with Silk Fibroin Nanoparticles. Acs Applied Materials & Interfaces 2019, 11 (16), 14515-14525.

61. Wongpinyochit, T.; Uhlmann, P.; Urquhart, A. J.; Seib, F. P., PEGylated Silk Nanoparticles for Anticancer Drug Delivery. Biomacromolecules 2015, 16 (11), 3712-3722.

62. Mao, B.; Liu, C.; Zheng, W.; Li, X.; Ge, R.; Shen, H.; Guo, X.; Lian, Q.; Shen, X.; Li, C., Cyclic cRGDfk peptide and Chlorin e6 functionalized silk fibroin nanoparticles for targeted drug delivery and photodynamic therapy. Biomaterials 2018, 161, 306-320.

63. Mottaghitalab, F.; Kiani, M.; Farokhi, M.; Kundu, S. C.; Reis, R. L.; Gholami, M.; Bardania, H.; Dinarvand, R.; Geramifar, P.; Beild, D.; Atyabi, F., Targeted Delivery System Based on Gemcitabine-Loaded Silk Fibroin Nanoparticles for Lung Cancer Therapy. Acs Applied Materials & Interfaces 2017, 9 (37), 31600-31611.

64. Gou, S.; Huang, Y.; Wan, Y.; Ma, Y.; Zhou, X.; Tong, X.; Huang, J.; Kang, Y.; Pan, G.; Dai, F.; Xiao, B., Multi-bioresponsive silk fibroin-based nanoparticles with on-demand cytoplasmic drug release capacity for CD44-targeted alleviation of ulcerative colitis. Biomaterials 2019, 212, 39-54.

65. Rodriguez-Nogales, A.; Algieri, F.; De Matteis, L.; Lozano-Perez, A. A.; Garrido-Mesa, J.; Vezza, T.; de la Fuente, J. M.; Cenis, J. L.; Galvez, J.; Rodriguez-Cabezas, M. E., Intestinal anti-inflammatory effects of RGD-functionalized silk fibroin nanoparticles in trinitrobenzenesulfonic acid-induced experimental colitis in rats. International Journal of Nanomedicine 2016, 11, 5945-5958.

66. Bian, X. Y.; Wu, P. Y.; Sha, H. Z.; Qian, H. Q.; Wang, Q.; Cheng, L.; Yang, Y.; Yang, M.; Liu, B. R., Anti-EGFR-iRGD recombinant protein conjugated silk fibroin nanoparticles for enhanced tumor targeting and antitumor efficiency. Oncotargets and Therapy 2016, 9, 3153-3162.

67. Tallian, C.; Herrero-Rollett, A.; Stadler, K.; Vielnascher, R.; Wieland, K.; Weihs, A. M.; Pellis, A.; Teuschl, A. H.; Lendl, B.; Amenitsch, H.; Guebitz, G. M., Structural insights into pH-responsive drug release of self-assembling human serum albumin-silk fibroin nanocapsules. European Journal of Pharmaceutics and Biopharmaceutics 2018, 133, 176-187.

68. Tallian, C.; Rumpler, V.; Skopek, L.; Russmayer, H.; Steiger, M. G.; Vielnascher, R.; Weinberger, S.; Pellis, A.; Vecchiato, S.; Guebitz, G. M., Glutathione from recovered glucose as ingredient in antioxidant

nanocapsules for triggered flavor delivery. Journal of Materials Chemistry B 2019, 7 (25), 3958-3969.

69. Schiffman, J. D.; Schauer, C. L., A review: Electrospinning of biopolymer nanofibers and their applications. Polymer Reviews 2008, 48 (2), 317-352.

70. Yukseloglu, S. M.; Sokmen, N.; Canoglu, S., Biomaterial applications of silk fibroin electrospun nanofibres. Microelectronic Engineering 2015, 146, 43-47.

71. Dou, H.; Zuo, B., Effect of Sodium Carbonate Concentrations on the Formation and Mechanism of Regenerated Silk Fibroin Nanofibers by Electrospinning. Journal of Nanomaterials 2014.

72. Sasithorn, N.; Martinová, L., EFFECT OF CALCIUM CHLORIDE ON ELECTROSPINNING OF SILK FIBROIN NANOFIBRES. In RMUTP International Conference: Textiles & Fashion 2012, Bangkok Thailand, 2012.

73. Sasithorn, N.; Rattanaphol, M.; Lenka, M., Preparation of Silk Fibroin Nanofibres by Needleless Electrospinning Using Formic Acid-Calcium Chloride as the Solvent. Applied Mechanics and Materials 2016, 848, 203-206.

74. Sasithorn, N.; Martinova, L., Fabrication of Silk Nanofibres with Needle and Roller Electrospinning Methods. Journal of Nanomaterials 2014.

75. Hadisi, Z.; Nourmohammadi, J.; Haghighipour, N.; Heidari, S., How direct electrospinning in methanol bath affects the physico-chemical and biological properties of silk fibroin nanofibrous scaffolds. Micro & Nano Letters 2016, 11 (9), 514-517.

76. He, J.; Cheng, Y.; Li, P.; Zhang, Y.; Zhang, H.; Cui, S., Preparation and characterization of biomimetic tussah silk fibroin/chitosan composite nanofibers. Iranian Polymer Journal 2013, 22 (7), 537-547.

77. Mhuka, V.; Dube, S.; Nindi, M. M.; Torto, N., Fabrication and structural characterization of electrospun nanofibres from Gonometa Postica and Gonometa Rufobrunnae regenerated silk fibroin. Macromolecular Research 2013, 21 (9), 995-1003.

78. Zhao, Z.; Li, Y.; Chen, A.-Z.; Zheng, Z.-J.; Hu, J.-Y.; Li, J.-S.; Li, G., Generation of Silk Fibroin Nanoparticles via Solution-Enhanced

Dispersion by Supercritical CO2. Industrial & Engineering Chemistry Research 2013, 52 (10), 3752-3761.

79. Chen, A.-Z.; Chen, L.-Q.; Wang, S.-B.; Wang, Y.-Q.; Zha, J.-Z., Study of magnetic silk fibroin nanoparticles for massage-like transdermal drug delivery. International Journal of Nanomedicine 2015, 10, 4639-4651.

Paper 6. Crivelli B, Bari E, Perteghella S, Catenacci L, Sorrenti M, Mocchi M, Faragò S, Tripodo G, Prina-Mello A, Torre ML (2019). Silk fibroin nanoparticles for celecoxib and curcumin delivery: ROS-scavenging and anti-inflammatory activities in an *in vitro* model of osteoarthritis. European Journal of Pharmaceutics and Biopharmaceutics 137, 37-45; doi: 10.1016/j.ejpb.2019.02.008.

Abstract. This paper aims at demonstrating silk fibroin nanoparticles (SFNs) promote anti-inflammatory properties of celecoxib (CXB) or curcumin (CUR) and could be exploited for osteoarthritis (OA) treatment. Nanoparticles were prepared by desolvation method and physico-chemically characterized (FT-IR, DSC, TGA, SEM, size distribution and drug release); empty and drug loaded nanoparticles were tested for their ROS-scavenging activity, hemolytic properties, cytotoxicity, and anti-inflammatory potency in an OA in vitro model. Results indicate that a controlled drug release has been achieved by varying the drug loading. Curcumin plus SFNs exhibited a synergistic antioxidant effect, while CXB was, in some manner, inhibitory. Both free drugs resulted highly cytotoxic while cell viability reached high values when encapsulated in SFNs. No appreciable differences in anti-inflammatory activity was evidenced between CUR loaded SFNs and CXB. In conclusion, SFNs is an optimal carrier to improve cyto- and hemo-compatibility of both CUR and CXB.

Keywords: osteoarthritis, nanoparticles, drug delivery systems, silk fibroin, curcumin, Celecoxib

---

1. Introduction

Osteoarthritis (OA) represents a pathological condition characterized by both inflammation and chronic degeneration of musculoskeletal compartment, which is triggered by an overproduction of interleukin- 1β (IL-1β) and tumour necrosis factor-α (TNF-α), leading to extra- cellular matrix degradation and cartilage tissue damage. Moreover, cytokine-activated chondrocytes, in inflammatory conditions, overexpressed several cytokines and chemokines including Regulated on Activation, Normal T cell Expressed and Secreted (RANTES) [1].

Currently, a standard regenerative therapy for treating OA does not exist: the available pharmacological strategies are several and aimed to reach and modify different biological targets, albeit the majority is targeted to pain relief. Among these, non-steroidal anti-inflammatory drugs (NSAIDs) and cyclooxigenase-2 (COX-2) selective inhibitors such as celecoxib (CXB), are employed for the treatment of symptomatic pain, inflammation and swelling. More recently, polymeric micelles loaded with CXB have been reported to have also anti-angiogenic activity [2].

Since the established pharmacological therapy covers the entire patient lifespan and is characterized by severe long-term side effects or expensiveness, natural herbal compounds have been recently introduced. Among these, curcumin (CUR), a natural hydrophobic polyphenol extracted from the Curcuma longa rhizome, has shown to retain remarkable anti-inflammatory and antioxidant properties exploitable in musculoskeletal pathologies [3,4].

OA is commonly treated with systemic therapies, based on free drugs, albeit they are still suffering from several drawbacks due to their limited solubility [5,6] and consequently poor in vivo bioavailability, fast metabolism, and bloodstream clearance; these problems could be easily overcome by encapsulating them in nanosystems [6–11]. It is therefore to be noted, nanoparticles have gained much attention in biomedical and biotechnological fields

thanks to their capability to efficiently control the drug release and targeting while protecting them from degradation activities and avoiding undesired side effects, when compared to con- ventional formulations [12,13].

Table 1. Nanoparticles Formulation and Composition details. The drug loading, the process yield and the encapsulation efficiency (as % w/w) are reported as mean values ± standard errors (ES).

Nanoparticle formulation	Process yield (%) (mean ± SE)	Drug concentrations in the acetone (mg/ml)	Drug loading (% w/w) (mean ± SE)	Encapsulation efficacy (%)
SFNs	88.46 ± 7.83	0.0	0.00	0.00
SFNs/CXB-5	82.58 ± 8.39	0.1	5.29 ± 0.31	11.14 ± 5.85
SFNs/CXB-11	71.62 ± 10.69	0.5	11.40 ± 0.76	5.14 ± 1.94
SFNs/CUR-1.5	71.24 ± 10.64	0.8	1.50 ± 0.11	48.86 ± 9.82

In this context, silk fibroin stand out for its biocompatibility, biodegradability, appropriate mechanical properties and therapeutic retention at the target site [14–18]. Recently, our research group developed a novel drug delivery system by combining silk fibroin nanoparticles (SFNs) loaded with curcumin (SFNs/CUR) and extracellular vesicles secreted by mesenchymal stem cells (MSCs).

SFNs/CUR were successfully taken up by MSCs, showing a cytoplasmic localization; notably, the application of a nanotechnological approach avoided CUR cytotoxic events.

Furthermore, MSCs were able to release extracellular vesicles entrapping SFNs/CUR, achieving a novel carrier- in-carrier system. [19,20].

The aim of the present study is to evaluate the antioxidant, anti-inflammatory and cytotoxicity profile of nano-encapsulated CXB and CUR in an OA in vitro model. First, SFNs, SFNs/CUR and SFNs/CXB were prepared and characterized in terms of physico-chemical properties, particle size and drug release profile; subsequently, they were in vitro tested, in comparison with free drugs, on human inflamed articular chondrocytes, evaluating the effect on cell viability and on secretion of inflammatory mediators, such as nitric oxide (NO), IL-6 and RANTES.

2. Materials and methods

2.1. Materials

Sodium carbonate, lithium bromide, acetone, CUR, CXB, ethanol, methanol, collagenase IA, 3-(4,5-dimethylthiazol-2-yl)-2,5-diphenyl-tetrazolium bromide (MTT) and DMSO were purchased from Sigma-Aldrich (Milan, Italy). Dialysis cellulose tubes were obtained from Visking, Medicell Membranes Ltd (London, UK). 70 μm nylon meshes were obtained from Greiner Bio-One GmbH (Kremsmunster, Austria). Griess Reagent kit was purchased from Biotium (Fremont, California, USA), human RANTES and human IL-6 enzyme-linked immunosorbent assays were obtained from PeproTech (Rocky Hill, USA). All reagents used for cell cultures were purchased from Euroclone (Milan, Italy).

2.2. Silk fibroin extraction

Bombyx mori cocoons were cut and degummed in Na_2CO_3 (0.02 M) aqueous solution for 30 min; degummed fibers were washed in distilled water and dried at room temperature. Silk fibroin (SF) fibers

were solubilized in LiBr solution (9.3 M) at 60 °C for 4 h [21,22]; obtained solution was dialyzed against distilled water using dialysis cellulose tubes (3–5 kDa MWCO) at room temperature for 72 h. The SF final concentration, calculated by freeze-drying (Modulyo® Edwards Freezedryer, Kingston, NY, USA) of known SF volumes, was about 8% w/v.

2.3. Nanoparticles preparation

SF aqueous solution was diluted (1.5% w/v) before carrying out the nanoparticles preparation by desolvation method, as previously reported [19,23]. SF solution was added dropwise to the acetone, leading to the nanoparticles (named SFNs) formation by solvent precipitation. After dialysis (12 kDa MWCO), SFNs suspension were freeze dried at $8*10^{-1}$ mbar and −50° C for long term preservation for further investigations. SFNs loaded with CXB (SFNs/CXB) or with CUR (SFNs/ CUR) were obtained dissolving each drug in the respective precipitation solvent (Table 1). Overall, we considered four nanoparticle formulations: SFNs, SFNs/CXB-5, SFNs/CXB-11 (loaded with 5 and 11% w/w of celecoxib, respectively), and SFNs/CUR-1.5 (loaded with 1.5% w/w of curcumin). All formulations were produced in triplicate.

2.4. Characterization of nanoparticles

2.4.1. Drug loading, production yield and encapsulation efficiency evaluation

SFNs drug loading was evaluated by spectrophotometric analysis (Uvikon 860, Kontron Instruments, Zurich, Switzerland) at 254 and 425 nm for CXB and CUR, respectively. Briefly, for each formulation, freeze-dried nanoparticles were dissolved in 96% v/v ethanol (0.1 mg/ml), maintaining mild magnetic stirring in the dark. The total drug content was evaluated from standard calibration curves ($r^2 > 0.9924$

and $r^2 > 0.9902$ for CXB and CUR, respectively), obtained analysing a concentration range of 2.00 – 20.00 μg/ml for CXB, and of 0.25 –10.00 μg/ml for CUR. Ethanol was considered as blank. Each experiment was performed in triplicate. The drug loading (% w/w) of each formulation was calculated from the ratio between the total drug content (extrapolated from calibration curve) and the concentration of analysed nanoparticles. For each batch, nanoparticle production yield (Y%) was calculated as follow:

$$Y(\%) = [\text{total weight nanoparticles} / (\text{weight of polymer} + \text{weight of drug})] \times 100$$

Encapsulation efficiency (EE%) was determined as percentage ratio between the actual entrapped drug and the drug dissolved in acetone solution during nanoparticle preparation.

2.4.2. Nanoparticles size distribution and evaluation of polydispersity index

The size distribution of nanoparticles was analysed by Nanoparticle Tracking Analysis using NanoSight NS500 equipment (Malvern Instruments, UK). All measurements were repeated for 6 cycles of 60 s each [24].

The polydispersity index (PDI) of each nanoparticle formulation was also determined by Dynamic Light Scattering (DLS Zetasizer Nano S particle analyser, Malvern Instruments). Ten measurements of 300 s each were processed. Samples (0.5 mg/ml aqueous suspension) were sonicated (37 kHz) and filtered (0.45 μm) before carrying out both analyses.

2.4.3. Morphological evaluation by scanning electron microscopy (SEM)

Nanoparticles were observed using SEM (MIRA3, Tescan, Brno, Czech Republic). Briefly, freeze-dried samples were gold-sputter coated

under argon prior to perform the morphological analysis measurements.

2.4.4. Fourier transform infrared (FT-IR) spectroscopy

FT-IR spectra of nanoparticles were obtained using a Spectrum One Perkin-Elmer spectrophotometer (Perkin Elmer, Wellesley, MA, USA) equipped with a MIRacle™ ATR device (Pike Technologies, Madison, WI, USA). The IR spectra in transmittance mode where recorded in the spectral region of 650 – 4000 cm^{-1} with a resolution of 4 cm^{-1} [25]. Each experiment was performed in triplicate.

2.4.5. Differential scanning calorimetry (DSC)

Temperature and enthalpy values were measured with a Mettler STARe system (Mettler Toledo, Columbus, OH, USA) equipped with DSC81e Module and an Intracooler device for sub-ambient temperature analysis (Jukabo FT 900) on about 3 mg of samples in 40 μl sealed aluminium pans with pierced lid (method: −10 – 400 °C temperature range; heating rate 10 K min^{-1}; nitrogen air atmosphere flux 50 ml min^{-1}). The instrument was previously calibrated with Indium, as standard reference. Each experiment was performed in triplicate [26].

2.4.6. Simultaneous thermogravimetric analysis (TGA/DSC 1)

Mass losses were recorded with a Mettler STARe system TGA on 3 – 4 mg samples in 70 μl alumina crucibles with lid (30 – 400 °C temperature range; heating rate 10 K min^{-1}; nitrogen air atmosphere flux 50 ml min^{-1}). The instrument was previously calibrated with Indium, as standard reference and experiments were performed in triplicate.

2.4.7. In vitro drug relese

The dialysis technique was applied to investigate the CXB and CUR in vitro cumulative release as previously reported, with some modifications [19,27–29]. Briefly, for each batch 15 mg of nanoparticles (SFNs/CXB-5, SFNs/CXB-11 and SFNs/CUR-1.5) were suspended in 4 ml of deionized water and put into dialysis membrane (3 – 5 kDa MWCO). Each dialysis tube was incubated in 10 ml of ethanol/water 50% v/v, maintained under mild magnetic stirring, at 37 °C. At each considered time point, all release medium was removed and replaced with fresh medium to ensure sink conditions. The amount of released drug was determined via spectroscopic method (by reading the release media at 254 and 425 nm for CXB and CUR, respectively). For each considered drug, a calibration curve was prepared (CXB 2.00- 20.00 μg/ml, r^2 = 0.990; CUR 0.25 – 10.00 μg/ml, r2 = 0.987). Results were expressed as mean ± standard deviation; for each formulation, three batches were analysed.

2.5. Determination of ROS-scavenging activity by DPPH assay

ROS-scavenging activity of each nanoparticle formulation was evaluated by DPPH assay, according to previous works [30,31]. Briefly, SFNs/CXB-5 and SFNs/CUR-1.5 were tested considering three different nanoparticle concentrations (200, 400 and 800 μg/ml) and their free drug equivalent concentrations calculated from drug loading data (11, 22 and 44 μg/ml for CXB; 3, 6 and 12 μg/ml for CUR) (Table 2).

Samples were resuspended in 70% v/v methanolic solution under magnetic stirring. 50 μl of each considered sample were miXed with 1950 μl of DPPH methanolic solution and incubated, at room temperature, for 60 min avoiding light exposure. Finally, samples were centrifuged (3000 g, 10 min) and the optical density (OD) of supernatants was analyzed at 515 nm. As negative control, a reaction

mixture without sample was considered. The percentage of ROS-scavenging activity was calculated according to the following formula:

$$\text{Antioxidantactivity (\%)} = [(\text{ODctr} - \text{ODsample}) / \text{ODctr}] \times 100$$

where ODctr is the absorbance of negative control and ODsample is that of samples.

Table 2. Concentration comparison table for in vitro studies (ROS-scavenging, cytoxicity, anti-inflammatory). Drug loading concentrations in SFNs nanoparticles (SFNs/CXB-5 and SFNs/CUR-1.5) compared to the absolute concentrations of free drug (CXB or CUR) calculated by the drug loading data.

	Absolute concentrations of loaded drug (μg/ml) (calculated by the drug loading data)	
Drug loading concentrations into SFNs (μg/ml)	CXB	CUR
200	11	3
400	22	6
800	44	12

2.6. Hemolytic assay

Hemolytic assay was performed on human red blood cells (RBCs), as reported by [32], with some modifications. Human blood samples, collected from three informed healthy donors, were centrifuged at 1500

g for 5 min, to separate RBCs from plasma serum. Obtained RBCs were washed twice with PBS without Ca^{2+} and Mg^{2+} (pH = 7.4). RBCs suspension (90 μl) was co-incubated with freeze-dried nanoparticle suspensions (10 μl) or with free drug (10 μl). For each considered formulation (SFNs/CXB-5 and SFNs/CUR-1.5), nanoparticles were suspended in PBS and sonicated (37 °C, 45 min, 37 kHz) in order to eliminate particle aggregates. For this study, we used three nanoparticle concentrations (200, 400 and 800 μg/ml) and their equivalent free drugs concentration, as reported in Table 2. Untreated RBCs drugs were considered as negative control, while RBCs treated with distilled water as positive control (considered as 100% of hemolysis). After incubation, samples were centrifuged at 3000 g for 10 min. The OD of recovered supernatants were analyzed at 540 nm (Synergy HT, Biotek, Winooski, VT, USA), which corresponds to the absorption maxima of hemoglobin. The overall hemolytic response was evaluated as percentage versus controls (Hemolysis%) with the following equation:

$$\text{Hemolysis (\%)} = [(OD_{sample} - OD_{negative\ CTR}) / OD_{positive\ CTR}] \times 100$$

2.7. In vitro biological assays

2.7.1. Human articular chondrocytes isolation and culture

Three knee cartilage samples, obtained during arthroplasty surgery, were cut into 1 – 2 mm^3 segments and washed three times with PBS before being digested with trypsin-EDTA 1X, for 30 min, 37 °C, 5% CO_2, followed by overnight incubation with 200 IU type IA collagenase. The resulting cell suspension was filtered using 70 μm nylon meshes to completely remove undigested tissue and cells were centrifuged at 300 g for 5 min. Obtained chondrocytes were seeded onto flasks (7000 cells/cm^2) with Dulbecco's Modified Eagle's Medium High Glucose (DMEM-HG) enriched in 10% fetal bovine serum (FBS),

penicillin (100 IU/ml), streptomycin (100 μg/ml), amphotericin B (2.5 μg/ml), Fibroblast Growth Factor-2 (FGF-2, 10 μg/ml) and Transforming Growth Factor beta-1 (TGF-β1, 10 μg/ml) at 37 °C, 5% CO_2. Each cell line was used up to three culture passages. The study was conducted in accordance with the Declaration of Helsinki, and the protocol was approved by the Ethics Committee of ASST Grande Ospedale Metropolitano Niguarda (Milan, Italy) (Ref. 12.11.2009).

2.7.2. Cell metabolic activity evaluation

Chondrocytes metabolic activity was examined using the MTT assay; cells were seeded in 96-well plate (12000 cells/cm^2) and incubated for 72 h with 100 μl of SFNs, SFNs/CXB-5 and SFNs/CUR-1.5 (at 200, 400 and 800 μg/ml concentrations, respectively), and with 100 μl of free drug, considering the equivalent amounts of CXB and CUR contained in the nanoparticles. After incubation time, all samples were removed and 100 μl of MTT solution (0.5 mg/ml) was added to each well for 3 h. After this time, MTT solution was removed, and formazan crystals were solubilized with 100 μl of DMSO. The OD was measured using a microplate reader (Synergy HT) at 570 nm and 670 nm (reference wavelength). Relative cell metabolic activity (%) was calculated as follows: 100 × (ODs/ODc), where ODs represents the mean value of the measured optical density of the tested sample and ODc is the mean value of the measured optical density of untreated cells (control).

2.7.3. Chondrocyte stimulation and treatment

Chondrocytes were seeded in 24-well plates (12000 cells/cm^2) and cultured for 24 h; then, cells were stimulated with IL-1β (10 ng/ml) in FBS deprived medium, as reported by [33,34], to reproduce the mechanisms involved in OA raise, and simultaneously treated with nanoparticle samples (and free drugs) for 72 h. Freeze-dried nanoparticle formulations (SFNs, SFNs/CXB-5 and SFNs/CUR-1.5)

were re-suspended in cell culture medium and sonicated at 37 kHz for 1 h before carrying out the incubation, while free drugs were solubilized in DMSO (2 mg/ml) and diluted in cell culture medium, achieving the same drug concentration loaded in each considered nanosystem formulation. For biological tests, SFNs, SFNs/CXB-5, SFNs/CUR-1.5 were considered at three different concentrations (200, 400 and 800 μg/ml). IL-1β stimulated chondrocytes, not treated with nanoparticles were considered as positive control, while untreated chondrocytes as negative control.

Supernatants were collected and stored at −80 °C for further quantification of IL-6 and RANTES, by enzyme-linked immunosorbent assay (ELISA); while nitric oxide (NO) was quantified by Griess method on fresh supernatants.

2.7.4. Determination of nitric oxide (NO), IL-6 and RANTES levels

NO released in cell culture supernatants was detected by using the Griess method, following the manufacturer's instructions. The secretion of IL-6 and RANTES was evaluated using a quantitative ELISA kits, according to manufacturer's instructions. IL-1β stimulated chondrocytes, not treated with nanoparticles were considered as positive control, while untreated chondrocytes as negative control.

2.8. Statistical analysis

Raw data of in vitro drug release, antioxidant activity, hemolytic assay, cellular viability and in vitro biological assays (NO, IL-6 and RANTES levels) were processed using STATGRAPHICS XVII (Statpoint Technologies, Inc., Warrenton, Virginia, U.S.) and a linear generalized Analysis of Variance model (ANOVA) was used to evaluate the data. The post-hoc LSD's test for multiple comparisons was employed to analyze the differences between groups. Unless

differently specified, data are expressed as mean ± standard deviation. Statistical significance was set at $p \leq 0.05$.

3. Results and Discussion

In this research paper, we compared the biological activity and physicochemical properties of two different drugs encapsulated in silk fibroin-based nanoparticles: CXB, a sulfonamide synthetic compound belonging to the COX-2 selective inhibitors class, which is actually employed as the "first choice" for OA treatment, and CUR, a natural polyphenol extracted from the rhizome of Curcuma Longa, characterized by anti-inflammatory and antioxidant activities. Albeit CXB is still considered as the best therapeutic option in treating OA pain, its long-term use in high-dosage could trigger severe cardiotoxicity and renal complications [35]. Conversely, CUR showed the ability to attenuate the inflammatory condition related to OA without significant side-effect [36,37]. Unfortunately, both drugs are characterized by low solubility, which determines a low bioavailability. To the best of our knowledge, nanoencapsulation of CXB in fibroin-based systems has not attempted yet. In literature nanocarrier or nanosystems other than SF were proposed such as liposomes [38], solid lipid nanoparticles [39] and micelles [2].

3.1. Nanoparticle characterization

SFNs, SFNs/CXB and SFNs/CUR formulations were obtained via desolvation method, exploiting the solubility of CXB and CUR in acetone (Table 1).

The process yield (%) in SFNs formation ranged from 71.24 ± 10.64 to 88.46 ± 7.83, for SFNs/CUR-1.5 and SFNs, respectively; while the EE (%) ranged from 5.14 ± 1.93 to 48.86 ± 9.82, for SFNs/CXB-11 and SFNs/CUR-1.5, respectively (Table 1). Our assumption is that all drug was completely internalized in the core of nanoparticles, considering the SFNs/CUR-1.5 particle. Conversely, considering the higher drug

loading of SFNs/CXB, we expected that, during the nanoparticle formation, the drug is partially absorbed on the surface of nanosystems. Thus, partial loss of absorbed drug is occurring during the dialysis purification, causing a reduction of EE values in SNFs/CXB-5 and SFNs/CXB-11.

All nanoparticle formulations showed a mean diameter of about 110 nm (Fig. 1), characterized by a defined distribution, confirming our previous results [19]. The PDI, measured with Zetasizer, was about 0.15 for all formulations, indicating a narrow size distribution of the nanoparticles. SEM morphological investigation showed a spherical shape and confirmed that the encapsulation of both CXB and CUR does not influence the homogeneous size distribution of nanoparticles (Fig. 1). The particle size distribution and morphology of the obtained nanoparticles (Fig. 1) were in agreement with those reported by other researchers [23,39,40].

Nanoparticle formulation	Size (nm)	Mode	d10	d50	d90
SFNs	118.1 ± 1.0	74.5 ± 2.3	64.2 ± 1.2	88.3 ± 0.6	200.2 ± 9.7
SFNs/CXB 5	112.8 ± 4.2	67.9 ± 2.8	53.1 ± 2.2	75.6 ± 3.9	211.7 ± 12.4
SFNs/CXB 11	114.4 ± 1.5	70.1 ± 2.9	62.7 ± 1.8	77.9 ± 2.8	206.4 ± 8.9
SFNs/CUR 1.5	113.2 ± 1.4	92.2 ± 3.8	71.3 ± 1.7	91.2 ± 0.5	177.3 ± 6.9

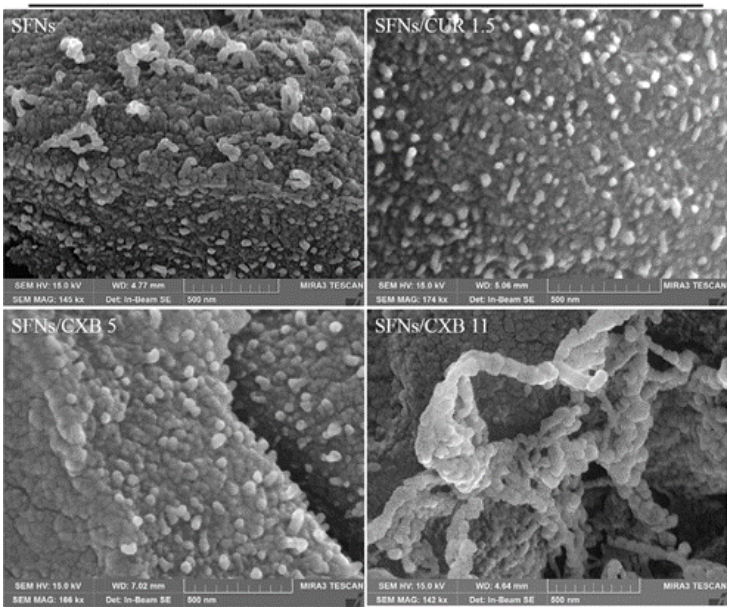

Fig. 1. SEM micrographical images: particle size and morphological investigation of SFNs, SFNs/CXB-5, SFNs/CXB-11 and SFNs/CUR-1.5. NTA results were reported as mean values ± standard deviation.

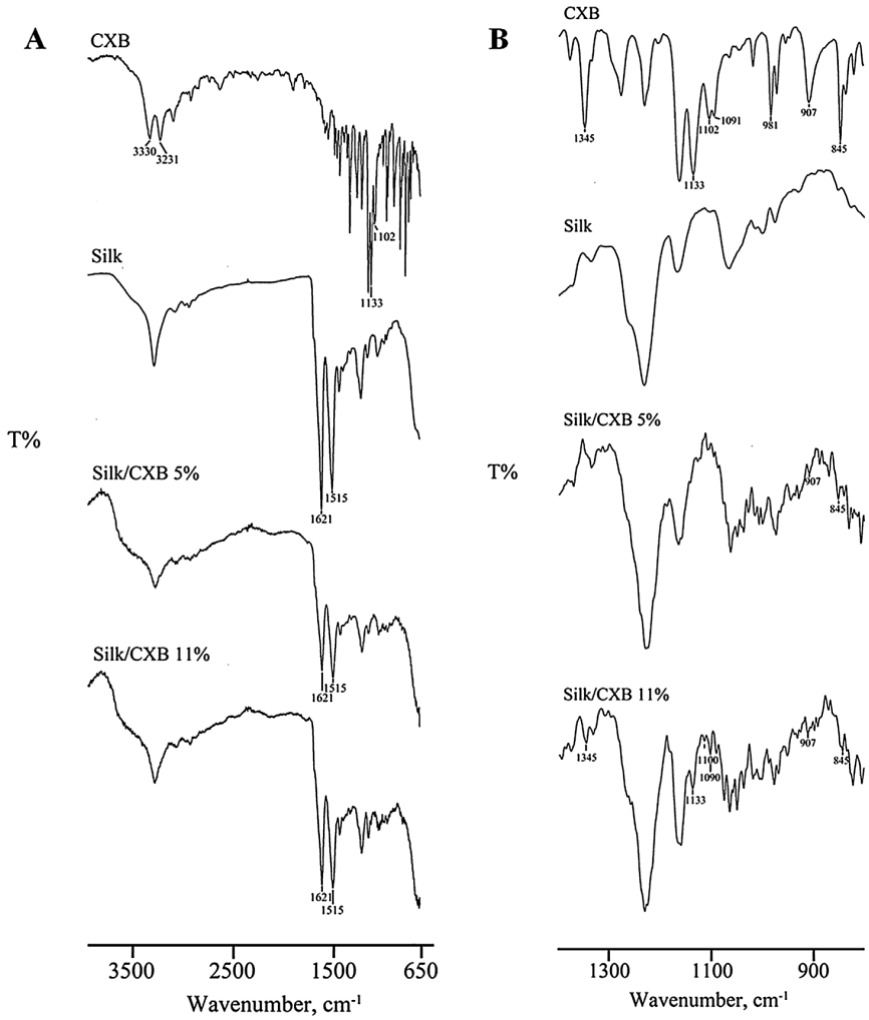

Fig. 2. Fourier transform infrared (FT-IR) spectra of "naked" celcecoxib (CXB), SFNs (silk), SFNs/CXB-5% and SFNs/CXB-11% in the spectral region of 4000 – 650 cm^{-1} (A) and in the region where typical CXB bands appeared (amplified between 1400 and 800 cm^{-1}) (B).

As seen in Table 1, the EE% could appear low in absolute values. These values are under-estimated, due to the absence of specific interactions between the material and the drug (e.g., ionic interactions). The FT-IR analysis was carried out to confirm the

effective nanoencapsulation of the considered active (CXB) into the nanocarrier and to assure the conformational change of SF. In the Fig. 2A are reported the FT-IR spectra of CXB, SFNs, and SFNs/CXB at two different drug concentrations, 5% and 11%, respectively. The IR spectrum of SF showed characteristic peaks that can be identified in the spectra region of amide I (at about 1620 cm^{-1}, C=O stretching), amide II (at about 1520 cm^{-1}, N-H bending) and amide III (at about 1230cm^{-1}, C-N and N-H functionalities), in all tested formulations (Fig. 2). The FT-IR spectrum of CXB showed the characteristic S=O symmetric and asymmetric stretching in the region 1130 and 1345 cm^{-1}, and the bands of N-H stretching vibration of SO_2NH_2 group at 3330 and 3231 cm^{-1}. The typical absorption bands of CXB are completely hidden for SFNs/CXB-5, while they can be visible in SFNs/CXB-11, related to its higher drug loading. To better compare the spectra of unloaded and loaded nanoparticles, the region between 1500 and 700 cm^{-1} was amplified (Fig. 2B). This has allowed to identify some typical bands of CXB (1345 and 1133 cm^{-1}) only in the spectrum of nanoparticles with higher active content. FT-IR data were supported by thermal analysis. From DSC analysis, CXB results as an anhydrous crystalline compound characterized by melting endothermic peak at 162.6 ± 0.4 °C (T_{onset},m = 161.1 ± 0.2 °C; ΔHm = 92.0 ± 1.0 J g^{-1}) with a mass loss recorded in TGA curve (not shown) starting at around 300 °C, due to drug decomposition. The unloaded SFNs showed a typical profile of an amorphous sample with an endothermic effect at around 270 °C, associated to a mass loss in TGA curve, related to sample decomposition. The presence of CXB was also observed in the thermal trace of nanoparticles at the higher drug content, as a small endothermic peak at 161.2 ± 0.6 °C, similarly to the FT-IR spectra. The broad endothermic effects between 30 and 100 °C in the DSC of SFNs/CXB were due to dehydration (mass loss in TGA analyses of about 5.7 ± 0.3%) (not shown).

For SFNs/CUR-1.5 a similar physicochemical characterization was performed and reported in our previous research paper [19]. The FT-IR spectra supported by thermal analysis confirmed also for this system the encapsulation of the drug in SFNs.

3.2. In vitro drug release studies

The drug release studies for CXB and CUR showed that both formulation and release-time were statistically significant ($p < 0.0001$) in influencing their performance. Up to three hours, SFNs/CXB-5 and SFNs/CXB-11 formulations showed a similar release profile while, after this time, a different release profile can be seen for the two formulations (Fig. 3).

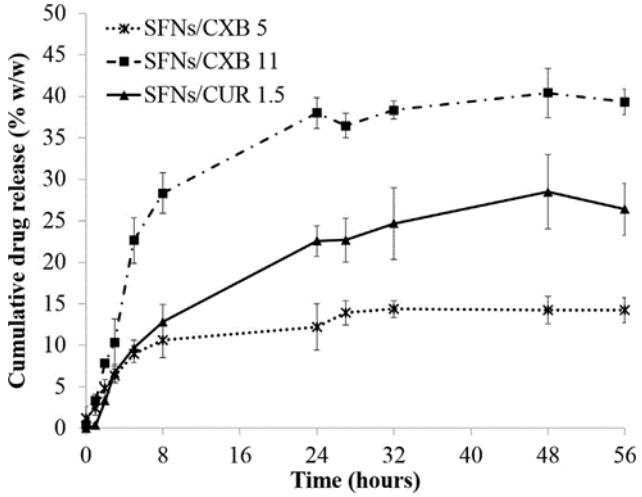

Fig. 3. In vitro drug release profiles of SFNs/CXB-5, SFNs/CXB-11 and SFNs/ CUR-1.5. Data are reported as cumulative drug release percentage (mean value ± standard deviations) of at least three independent experiments.

In particular, SFNs/CXB-11 released up to 40% of the whole drug after 24 h; while 14% of CXB was released by SFNs/CXB-5 at the same time. The encapsulation of CXB in fibroin-based nanoparticles improved the drug solubility. Considering the Noyes–Whitney

equation, an increase of dissolution rate can be observed when the particle size is reduced. These results were in agreement with other researchers that demonstrated the higher solubility and the increase of release after the encapsulation of CXB in solid-lipid nanoparticles and nanosuspensions [41,42]. The release profiles shown in Fig. 3, suggest that the drug found on the surface or external layer of the nanoparticles is released in a controlled manner up to 8 h for SFNs/CXB-5 and up to 24 h for SFNs/ CXB-11. This effect could be simply explained by a controlled dissolution/desorption of the drug from the outer layer of the nanocarrier (SFNs) which makes the nanosystems. This is a fundamental result because allows the preparation of nanosystems with a time-dependent release, controlled by the loaded drug amount.

Considering the release profile of SFNs/CUR-1.5, up to 8 h, a burst release of about 15% was observed (Fig. 3). Silk nanoparticles allowed the drug release of 30%, reaching the plateau after 24 h; these results were in according to our previous research [19] and to the release profile of poor soluble drug loaded in silk nanoparticles [43,44].

3.3 ROS-scavenging activity

Articular chondrocytes degradation is governed by a combination of several mechanisms including an increasing in ROS production, leading to a lack of equilibrium between oxidant and antioxidant systems. For this reason, employing therapeutic molecules with antioxidant properties could ameliorate the symptoms of OA or to prevent structural changes in damaged cartilage [45] with observable clinical benefits.

Thus, here were tested the ROS-scavenging activity of CXB-loaded and CUR-loaded nanoparticles at three concentrations (200, 400 and 800 μg/ml); in particular, for these experiments we selected three nanoparticle formulations (SFNs, SFNs/CXB-5 and SFNs/CUR-1.5) and the equivalent free drugs (CXB and CUR). DPPH assay results showed that formulations and concentrations were statistically significant

(ANOVA, $p < 0.0001$); in particular, a dose related response was appreciated for SFNs/CUR 1.5 and free CUR (Fig. 4).

Free CUR exhibits a significant and native antioxidant activity, which becomes higher when included into the SFNs, 80% vs 90% respectively. No statistical differences were observed between SFNs, SFNs/CXB-5 and CXB, since they all showed a ROS scavenging activity lower than 10%. According to other studies, CXB does not show any in vitro antioxidant activity [46], while could be slightly increased by SFNs encapsulation (Fig. 4). Based on this finding, we could speculate that the native antioxidant effects of SF and CUR are additive. SFNs resulted as an efficient vehicle for antioxidant compounds, as example curcumin, thanks to the free radical scavenging activity of silk fibroin itself, probably correlated to the aromatic residues present (about 4%) [43,47].

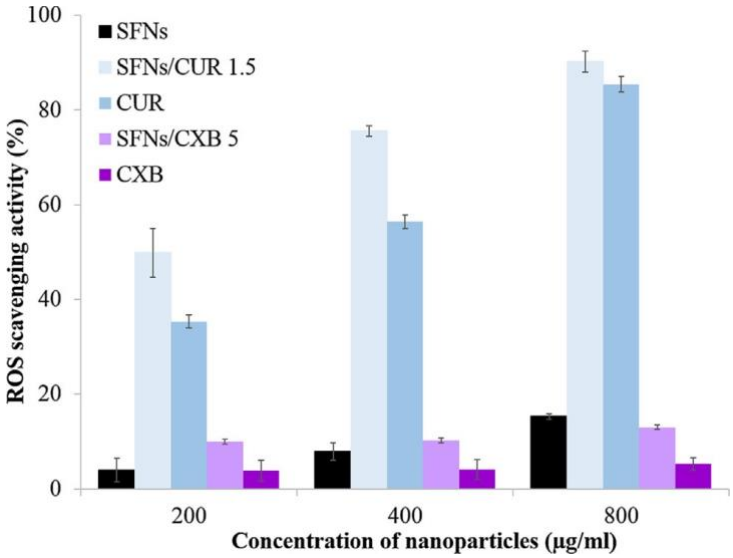

Fig. 4. ROS scavenging activity of SFNs, SFNs/CXB-5, SFNs/CUR-1.5, and equivalent amount of free drugs (CXB and CUR). Data are reported as mean values ± standard deviation of at least three independent experiments.

3.4. Hemocompatibility evaluation

Hemocompatibility studies were performed. Considering the hemolytic results (%), ISO/TR 7406 classified the hemolytic effect as: low for values lower than 5, slight for percentages comprised between 5 and 10, and high for values higher than 10. The SFNs were tested at 200 and 400 μg/ml showing a high hemocompatibility, while at 800 μg/ml, our unloaded nanoparticles presented a slight hemolytic effect (Fig. 5). We also tested the hemocompatibility of selected drugs (CXB and CUR), both free and encapsulated in SFNs: our results demonstrated that silk nanoparticles can be considered a good encapsulation method to significantly reduce the high hemolytic properties of free CXB and CUR. Free drugs induced a hemolysis percentage higher than 10 already at lower concentration (Fig. 5). Conversely, considering both SFNs/CUR-1.5 and SFNs/CXB-5, we observed a low hemolysis percentage at 200 and 400 μg/ml and a slight hemolysis at 800 μg/ml (Fig. 5).

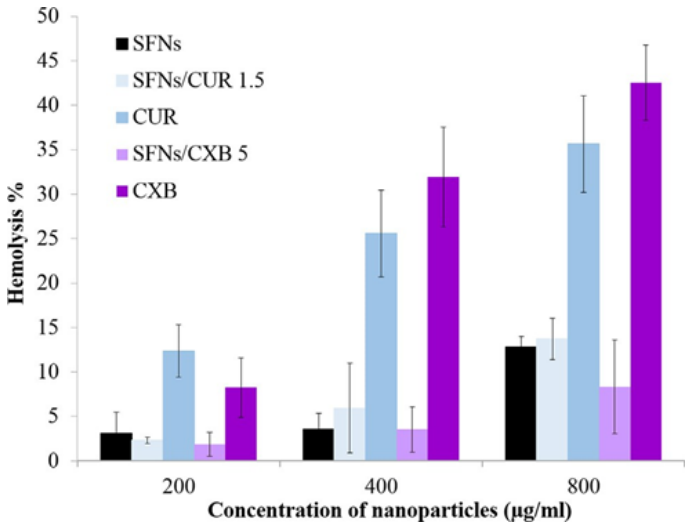

Fig. 5. Hemolysis (%) of Red Blood Cells (RBCs) after treatment with SFNs, SFNs/CUR 1.5, SFNs/CXB 5 (at three different concentrations 200, 400 and 800 μg/ml) and equivalent amount of free drugs (CUR and CXB). Data are

reported as mean values ± standard deviation of at least three independent experiments.

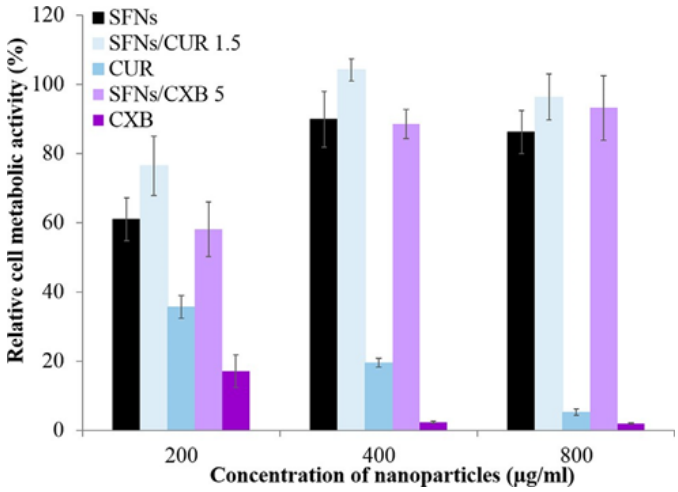

Fig. 6. Relative cell metabolic activity (%) of human articular chondrocytes after treatment (72 h) with SFNs, SFNs/CXB-5 and SFNs/CUR-1.5 (200, 400 and 800 µg/ml) and equivalent amount of free drugs (CXB and CUR). Data are reported as mean values, and relative standard deviations, of at least three independent experiments.

3.5. Osteoarthritis in vitro model: biological assays

3.5.1. Chondrocyte metabolic activity

To further test the biologic effectiveness of the nanosystems, we tested the effect of free and encapsulated drugs on human articular chondrocytes viability and functionality. Cell metabolic activity was measured by MTT on chondrocytes treated with nanoparticles or with their equivalent free drugs (Table 2) to evaluate their cytotoxicity effect. Both formulations and concentrations were statistically significant (ANOVA, $p < 0.0001$). Drug nanoencapsulation avoided cytotoxicity phenomena, showing viability higher than 70% for all nanoparticle formulations, independently from the employed concentration; on the contrary,

free drugs affected cellular viability in a dose dependent manner (Fig. 6).

The encapsulation of CXB and CUR in silk fibroin nanoparticles protected the cells by the cytotoxic effects of free drugs. Chondrocytes maintained a higher cell metabolic activity after treatment with both unloaded and loaded nanoparticles, while free celecoxib and curcumin induced a significant reduction of cell metabolic activity (lower than 40%). In treating OA, cytotoxic events must be avoided because an increase in IL-1β secretion leads to a higher apoptotic event [48]. Previously was reported that the incorporation of CUR into polymeric micelles avoided free drug cytotoxic phenomena, which were observed when employing "naked" CUR [9]. Furthermore, CXB also showed severe cytotoxic effects on several cellular lineages, reaching a viability of 50% at 100 μM concentration [49].

3.5.2. Anti-inflammatory activity of nanoparticles on IL-1β stimulated chondrocytes

We evaluated the cell functionality developing an in vitro inflammation model and treating the cells with pro-inflammatory cytokine IL-1β. After the stimulus, we evaluated the secretion of Interleukin- 6 (IL-6), a pro-inflammatory cytokine, Nitric Oxide (NO), a compound that promotes chondrocytes apoptosis, and of RANTES, a key mediator of inflammatory condition.

The efficacy of our experimental model was demonstrated by the increase of inflammation mediator release by the cells. The treatment of chondrocytes with IL-1β (CTR+), compared to untreated cells (CTR-), significant increased ($p < 0.001$) the production of NO (21.09 ± 2.56 and 0.92 ± 0.51 μM, respectively), IL-6 (30.79 ± 5.94 and 0.37 ± 0.13 ng/ml, respectively) and RANTES (3.24 ± 0.354 and 0.29 ± 0.06 ng/ml, respectively).

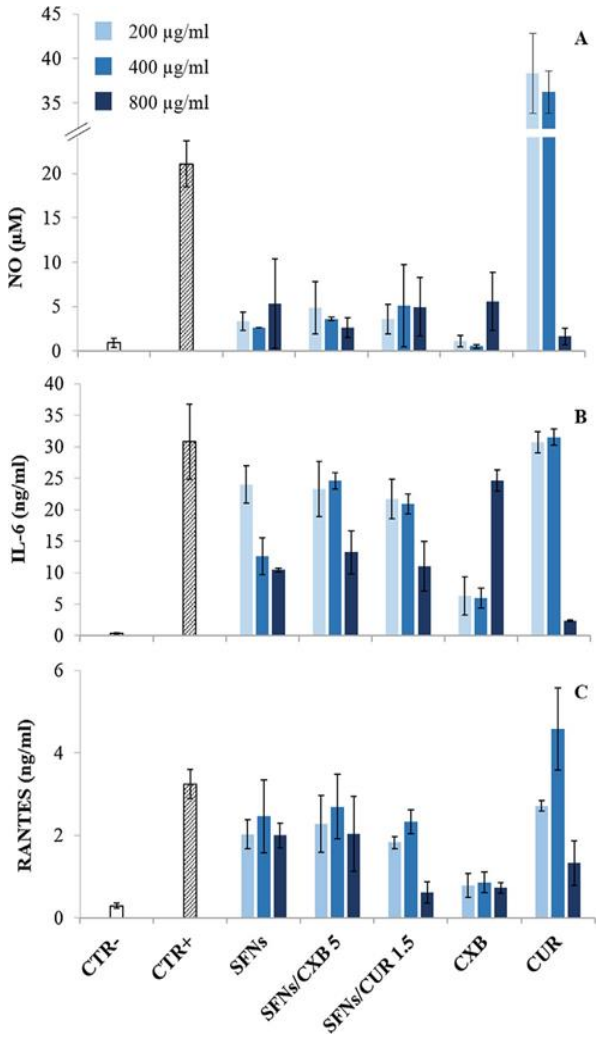

Fig. 7. Production of inflammation mediators NO (A), IL-6 (B) and RANTES (C) by human articular chondrocytes after treatment with pro-inflammatory cytokine IL-1β (10 ng/ml). Cells were stimulated and, at the same time, treated with SFNs, SFNs/CUR-1.5 and SFNs/CXB-5 (200, 400 and 800 µg/ml) and equivalent concentration of free drugs (CUR and CXB). Data are expressed as mean values ± standard deviations (n = 3). Positive control (CTR+) is represented by IL-1β stimulated cells (not treated with samples), while negative control (CTR-) is composed of unstimulated cells.

Considering NO secretion, all nanoparticle formulations, at all considered concentrations, significantly reduced the production of this mediator by the inflamed chondrocytes with respect to positive control (ANOVA, $p < 0.0001$) (Fig. 7A). The inhibition allowed by the nanoparticle treatment was not correlated with the concentration of our nanosystems. Comparing free drugs and positive control, we obtained a significant reduction of NO production ($p < 0.0001$) after the treatment with celecoxib at every investigated concentration. Conversely, the incubation with lower amounts of curcumin (equivalent to 200 and 400 μg/ml of SFNs/CUR 1.5) induced an increase of inflammation mediator ($p < 0.05$). The NO secretion reduction induced by free CXB could be related to its cytotoxic effect (Fig. 6) that dramatically decreased the cell viability. Here, we hypnotized a low percentage of live cells (low density also) thus not able to secrete a quantifiable amount of NO. Of interest, SFNs showed the same efficacy in decreasing NO levels with respect to loaded nanoparticles, thus showing an intrinsic anti-inflammatory activity (Fig. 7A).

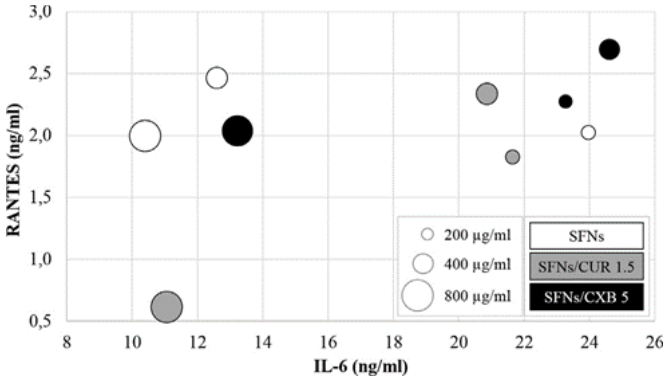

Fig. 8. Relationship between IL-6 and RANTES production by inflamed human chondrocytes after treatment with SFNs (white), SFNs/CUR 1.5 (grey) and SFNs/CXB 5 (black). The diameter of the circles in the plot is proportional to the nanoparticle concentrations: the larger circles correspond to 800 μg/ml, the intermediate circles are those of 400 μg/ml,

while smaller circles represent the mediator production after treatment with nanosystems at the concentration 200 μg/ml.

Concerning the production of IL-6 by stimulated chondrocytes the results show a dose-response for all nanoparticles, with a pronounced effect at higher concentration (800 μg/ml) (ANOVA, $p < 0.0001$) as reported in Fig. 7B. Similarly, to NO secretion, the amount of IL-6 significantly decreased when employing SFNs, highlighting its anti-inflammatory potential; in particular the inhibition of IL-6 production was comparably detected with SFNs at 400 μg/ml and the other nanosystems at the highest concentration (800 μg/ml) (Fig. 7B). As obtained for NO, free celecoxib reduced the cell viability and, consequently, the IL-6 secretion. Results obtained after incubation with lower concentrations of free curcumin were no different with respect to positive control, whereas from the higher amount of curcumin we could speculated its cytotoxic effect (Fig. 6) as responsible for the IL-6 level reduction.

Both formulation and concentration were statistically significant for RANTES secretion (ANOVA, $p < 0.0001$); RANTES levels were significantly reduced by all nanoparticle formulations. In particular, SFNs/ CUR-1.5, at 800 μg/ml, showed a marked reduction of RANTES (lower than 1 ng/ml) with respect to other considered groups (Fig. 7C). As previously observed, free celecoxib significantly reduced the mediator secretion but could be correlated to its cytotoxic effect. Curcumin resulted as cytotoxic at higher considered concentration while, at lower concentrations induced an increase of RANTES secretion (Fig. 7C).

IL-6 and RANTES dependencies and relationship are reported in Fig. 8. The presence of nanosystems, at the higher concentration (800 μg/ml), decreased both IL-6 and RANTES production. In particular, SFNs/CUR-1.5 showed the most promising results, while SFNs/ CXB-5 resulted less efficacious with respect to SFNs at 800 μg/ml. IL-6 and RANTES expression is regulated by the PKCδ/c-

Src/c-Jun and AP-1 signaling pathways, as demonstrated by Tang and colleagues in human synovial fibroblasts [50]. Moreover, CUR is able to reduce iNOS and NO radicals in lipopolysaccharide stimulated rats [51], in both formulations, as free or encapsulated in solid lipid nanoparticles [52].

SF showed an anti-inflammatory activity comparable to that of SFNs/CXB and SFNs/CUR in our in vitro model, highlighting its great potential in treating inflammatory diseases. This effect was reported in several biomedical fields: SF peptides, obtained during biodegradation, are the main effectors of anti-inflammatory property [53,54]. SF cannot be considered anymore as an inert polymer, but it must be listed as a "real" active principle ingredient able to effectively inhibit the expression of pro-inflammatory markers, with suitable therapeutic application in inflammatory diseases.

4. Conclusion

This work strongly addresses the use of SFNs as nanodrug delivery systems (DDS) for the treatment of osteoarticular diseases (OA). Advantageously, with a single DDS, we show evidence for a trimodal treatment approach for OA, where to: (i) treating the oxidative stress, (ii) treating the inflammatory pathway and (iii) controlling the drug released over the time.

We demonstrated that, by loading CUR into the SFNs, its intrinsic antioxidant effect is additive to the already one existing by the native SF. Concerning the anti-inflammatory effect, SFNs (unloaded as nanoparticle) and CXB or CUR loaded SFNs (as nanosystem or DDS) showed similar anti-inflammatory magnitude in an in vitro model of OA.

These results are fundamental and not trivial since allow to control the time of drug release while maintaining the dose within the expected delivery window. This support the explained biological

effects seen over the time and enable the drug release designing from the SFNs by controlling the amount of loaded drug. This is what we demonstrated in this work where at higher drug loadings, corresponds a longer time-release and not a higher dose-release. This opens opportunity for personalised medicine in Osteoarthritis where to fine tune the drug delivery within the effective therapeutic window.

References

1 N. Alaaeddine, T. Olee, S. Hashimoto, L. Creighton-Achermann, M. Lotz, Production of the chemokine RANTES by articular chondrocytes and role in cartilage degradation, Arthritis Rheum. 44 (2001) 1633–1643.

2 D. Mandracchia, G. Tripodo, A. Trapani, S. Ruggieri, T. Annese, T. Chlapanidas, G. Trapani, D. Ribatti, Inulin based micelles loaded with curcumin or celecoxib with effective anti-angiogenic activity, Eur. J. Pharm. Sci. 93 (2016) 141–146.

3 B.B. Aggarwal, K.B. Harikumar, Potential therapeutic effects of curcumin, the antiinflammatory agent, against neurodegenerative, cardiovascular, pulmonary, metabolic, autoimmune and neoplastic diseases, Int. J. Biochem. Cell Biol. 41 (2009)40–59.

4 O. Naksuriya, S. Okonogi, R.M. Schiffelers, W.E. Hennink, Curcumin nanoformulations: a review of pharmaceutical properties and preclinical studies and clinical data related to cancer treatment, Biomaterials 35 (2014) 3365–3383.

5 S.K. Paulson, M.B. Vaughn, S.M. Jessen, Y. Lawal, C.J. Gresk, B. Yan, T.J. Maziasz, C.S. Cook, A. Karim, Pharmacokinetics of celecoxib after oral administration in dogs and humans: effect of food and site of absorption, J. Pharmacol. Exp. Ther. 297 (2001) 638–645.

6 L. Catenacci, D. Mandracchia, M. Sorrenti, L. Colombo, M. Serra, G. Tripodo, Insolution structural considerations by H-1 NMR and solid-state thermal properties of inulin-D-alpha-tocopherol succinate (INVITE) micelles as drug delivery systems for hydrophobic drugs, Macromol. Chem. Phys. 215 (2014) 2084–2096.

7 S. Onoue, S. Yamada, H.-K. Chan, Nanodrugs: pharmacokinetics and safety, Int. J. Nanomed. 9 (2014) 1025–1037.

8 G. Tripodo, G. Pasut, A. Trapani, A. Mero, F.M. Lasorsa, T. Chlapanidas, G. Trapani, D. Mandracchia, Inulin-D-alpha-tocopherol succinate (INVITE) nanomicelles as a platform for effective intravenous administration of curcumin, Biomacromolecules 16 (2015) 550–557.

9 G. Tripodo, T. Chlapanidas, S. Perteghella, B. Vigani, D. Mandracchia, A. Trapani, M. Galuzzi, M.C. Tosca, B. Antonioli, P. Gaetani, M. Marazzi, M.L. Torre, Mesenchymal stromal cells loading curcumin-INVITE-micelles: A drug delivery system for neurodegenerative diseases, Coll. Surf. B-Biointerf. 125 (2015) 300–308.

10 D. Mandracchia, G. Tripodo, A. Latrofa, R. Dorati, Amphiphilic inulin-d-alpha-tocopherol succinate (INVITE) bioconjugates for biomedical applications, Carbohydr. Polym. 103 (2014) 46–54.

11 B. Crivelli, S. Perteghella, E. Bari, M. Sorrenti, G. Tripodo, T. Chlapanidas, M.L. Torre, Silk nanoparticles: from inert supports to bioactive natural carriers for drug delivery, Soft Matter 14 (2018) 546–557.

12 K. Roy, R.K. Kanwar, J.R. Kanwar, Molecular targets in arthritis and recent trends in nanotherapy, Int. J. Nanomed. 10 (2015) 5407–5420.

13 E. Nogueira, A. Gomes, A. Preto, A. Cavaco-Paulo, Update on therapeutic approaches for rheumatoid arthritis, Curr. Med. Chem. 23 (2016) 2190–2203.

14 D. Yao, H. Liu, Y. Fan, Silk scaffolds for musculoskeletal tissue engineering, Exp. Biol. Med. 241 (2016) 238–245.

15 S. Perteghella, B. Vigani, L. Mastracci, F. Grillo, B. Antonioli, M. Galuzzi, M.C. Tosca, B. Crivelli, S. Preda, G. Tripodo, M. Marazzi, T. Chlapanidas, M.L. Torre, Stromal vascular fraction loaded silk fibroin mats effectively support the survival of diabetic mice after pancreatic islet transplantation, Macromol. Biosci. 17 (2017) 1700131.

16 S. Farago, G. Lucconi, S. Perteghella, B. Vigani, G. Tripodo, M. Sorrenti, L. Catenacci, A. Boschi, M. Faustini, D. Vigo, T. Chlapanidas, M. Marazzi, M.L. Torre, A dry powder formulation from silk fibroin microspheres as a topical auto-gelling device, Pharm. Dev. Technol. 21 (2016) 453–462.

17 B. Kundu, R. Rajkhowa, S.C. Kundu, X. Wang, Silk fibroin biomaterials for tissue regenerations, Adv. Drug Deliv. Rev. 65 (2013) 457–470.

18 B. Vigani, L. Mastracci, F. Grillo, S. Perteghella, S. Preda, B. Crivelli, B. Antonioli, M. Galuzzi, M.C. Tosca, M. Marazzi, M.L. Torre, T. Chlapanidas, Local biological effects of adipose stromal vascular fraction

delivery systems after subcutaneous implantation in a murine model, J. Bioactive Compatible Polym 31 (2016) 600–612.

19 S. Perteghella, B. Crivelli, L. Catenacci, M. Sorrenti, G. Bruni, V. Necchi, B. Vigani, M. Sorlini, M.L. Torre, T. Chlapanidas, Stem cell-extracellular vesicles as drug de- livery systems: new frontiers for silk/curcumin nanoparticles, Int. J. Pharm. 520 (2017) 86–97.

20 B. Crivelli, T. Chlapanidas, S. Perteghella, E. Lucarelli, L. Pascucci, A.T. Brini, I. Ferrero, M. Marazzi, A. Pessina, M.L. Torre, Italian mesenchymal stem cell, me- senchymal stem/stromal cell extracellular vesicles: from active principle to next generation drug delivery system, J. Control. Release 262 (2017) 104–117.

21 D.N. Rockwood, R.C. Preda, T. Yucel, X. Wang, M.L. Lovett, D.L. Kaplan, Materials fabrication from Bombyx mori silk fibroin, Nat. Protoc. 6 (2011) 1612–1631.

22 D.M. Phillips, L.F. Drummy, D.G. Conrady, D.M. Fox, R.R. Naik, M.O. Stone, P.C. Trulove, H.C. De Long, R.A. Mantz, Dissolution and regeneration of bombyx mori silk fibroin using ionic liquids, J. Am. Chem. Soc. 126 (2004) 14350–14351.

23 F.P. Seib, G.T. Jones, J. Rnjak-Kovacina, Y. Lin, D.L. Kaplan, pH-Dependent antic- ancer drug release from silk nanoparticles, Adv. Healthcare Mater. 2 (2013) 1606–1611.

24 C.M. Maguire, K. Sillence, M. Roesslein, C. Hannell, G. Suarez, J.J. Sauvain, S. Capracotta, S. Contal, S. Cambier, N. El Yamani, M. Dusinska, A. Dybowska, A. Vennemann, L. Cooke, A. Haase, A. Luch, M. Wiemann, A. Gutleb, R. Korenstein, M. Riediker, P. Wick, P. Hole, A. Prina-Mello, Benchmark of nanoparticle tracking analysis on measuring nanoparticle sizing and concentration, J. Micro Nano-Manuf. 5 (2017).

25 P. Bhatt, R. Lalani, I. Vhora, S. Patil, J. Amrutiya, A. Misra, R. Mashru, Liposomes encapsulating native and cyclodextrin enclosed paclitaxel: Enhanced loading effi- ciency and its pharmacokinetic evaluation, Int. J. Pharm. 536 (2018) 95–107.

26 J. Patel, J. Amrutiya, P. Bhatt, A. Javia, M. Jain, A. Misra, Targeted delivery of monoclonal antibody conjugated docetaxel loaded PLGA nanoparticles into EGFR overexpressed lung tumour cells, J. Microencapsul. 35 (2018) 204–217.

27 J. Shaikh, D.D. Ankola, V. Beniwal, D. Singh, M.N.V.R. Kumar, Nanoparticle en- capsulation improves oral bioavailability of curcumin by at least 9-fold when compared to curcumin administered with piperine as absorption enhancer, Eur. J.Pharm. Sci. 37 (2009) 223–230.

28 D. Mandracchia, A. Trapani, S. Perteghella, M. Sorrenti, L. Catenacci, M.L. Torre, G. Trapani, G. Tripodo, pH-sensitive inulin-based nanomicelles for intestinal site-specific and controlled release of celecoxib, Carbohydr. Polym. 181 (2018) 570–578.

29 C. Yewale, D. Baradia, S. Patil, P. Bhatt, J. Amrutiya, R. Gandhi, G. Kore, A. Misra, Docetaxel loaded immunonanoparticles delivery in EGFR overexpressed breast carcinoma cells, J. Drug Delivery Sci. Technol. 45 (2018) 334–345.

30 E. Bari, C.R. Arciola, B. Vigani, B. Crivelli, P. Moro, G. Marrubini, M. Sorrenti L. Catenacci, G. Bruni, T. Chlapanidas, E. Lucarelli, S. Perteghella, M.L. Torre, In Vitro effectiveness of microspheres based on silk sericin and chlorella vulgaris or arthrospira platensis for wound healing applications, Materials 10 (2017).

31 T. Chlapanidas, S. Farago, G. Lucconi, S. Perteghella, M. Galuzzi, M. Mantelli, M.A. Avanzini, M.C. Tosca, M. Marazzi, D. Vigo, M.L. Torre, M. Faustini, Sericins exhibit ROS-scavenging, anti-tyrosinase, anti-elastase, and in vitro im- munomodulatory activities, Int. J. Biol. Macromol. 58 (2013) 47–56.

32 S. Maji, I.K. Yan, M. Parasramka, S. Mohankumar, A. Matsuda, T. Patel, In vitro toxicology studies of extracellular vesicles, J. Appl. Toxicol. 37 (2017) 310–318.

33 M. Galuzzi, S. Perteghella, B. Antonioli, M.C. Tosca, E. Bari, G. Tripodo, M. Sorrenti, L. Catenacci, L. Mastracci, F. Grillo, M. Marazzi, M.L. Torre, Human engineered cartilage and decellularized matrix as an alternative to animal osteoarthritis model, Polymers 10 (2018).

34 C. Cannava, S. Tommasini, R. Stancanelli, V. Cardile, F. Cilurzo, I. Giannone, G. Puglisi, C.A. Ventura, CelecoXib-loaded PLGA/cyclodextrin microspheres: char- acterization and evaluation of anti-inflammatory activity on human chondrocyte cultures, Coll. Surf. B-Biointerf. 111 (2013) 289–296.

35 L.J. Marnett, The COXIB Experience: a look in the rearview mirror, Annu. Rev.Pharmacol. ToXicol. 49 (2009) 265–290.

36 D.-O. Moon, M.-O. Kim, Y.H. Choi, Y.-M. Park, G.-Y. Kim, Curcumin attenuates inflammatory response in IL-1 beta-induced human synovial fibroblasts and col- lagen-induced arthritis in mouse model, Int. Immunopharmacol. 10 (2010) 605–610.

37 Z. Zhang, D.J. Leong, L. Xu, Z. He, A. Wang, M. Navati, S.J. Kim, D.M. Hirsh, J.A. Hardin, N.J. Cobelli, J.M. Friedman, H.B. Sun, Curcumin slows osteoarthritis progression and relieves osteoarthritis-associated pain symptoms in a post-trau- matic osteoarthritis mouse model, Arthritis Res. Therapy 18 (2016).

38 E. Moghimipour, S. Handali, Utilization of thin film method for preparation of celecoxib loaded liposomes, Adv. Pharm. Bull 2 (2012) 93–98.

39 S. Sharma, S. Bano, A.S. Ghosh, M. Mandal, H.-W. Kim, T. Dey, S.C. Kundu, Silk fibroin nanoparticles support in vitro sustained antibiotic release and osteogenesis on titanium surface, Nanomed.-Nanotechnol. Biol. Med. 12 (2016) 1193–1204.

40 Y.-Q. Zhang, W.-D. Shen, R.-L. Xiang, L.-J. Zhuge, W.-J. Gao, W.-B. Wang, Formation of silk fibroin nanoparticles in water-miscible organic solvent and their characterization, J. Nanopart. Res. 9 (2007) 885–900.

41 E.S. Ha, G.H. Choo, I.H. Baek, M.S. Kim, Formulation, characterization, and in vivo evaluation of celecoxib-PVP solid dispersion nanoparticles using supercritical antisolvent process, Molecules 19 (2014) 20325–20339.

42 S.B. Murdande, D.A. Shah, R.H. Dave, Impact of nanosizing on solubility and dissolution rate of poorly soluble pharmaceuticals, J. Pharm. Sci. 104 (2015) 2094–2102.

43 M.G. Montalban, J.M. Coburn, A.A. Lozano-Perez, J.L. Cenis, G. Villora, D.L. Kaplan, Production of curcumin-loaded silk fibroin nanoparticles for cancer therapy, Nanomaterials 8 (2018).

44 P.Y. Wu, Q. Liu, R.T. Li, J. Wang, X. Zhen, G.F. Yue, H.Y. Wang, F.B. Cui, F.L. Wu, M. Yang, X.P. Qian, L.X. Yu, X.Q. Jiang, B.R. Liu, Facile preparation of paclitaxel loaded silk fibroin nanoparticles for enhanced antitumor efficacy by locoregional drug delivery, ACS Appl. Mater. Interf. 5 (2013) 12638–12645.

45 S.B. Abramson, Nitric oxide in inflammation and pain associated with osteoarthritis, Arthritis Research & Therapy 10 (2008).

46 S. Sozer, G. Diniz, F. Lermioglu, Effects of celecoxib in young rats: histopathological changes in tissues and alterations of oxidative stress/antioxidant defense system, Arch. Pharmacal Res. 34 (2011) 253–259.

47 A.A. Lozano-Perez, H.C. Rivero, M.D.P. Hernandez, A. Pagan, M.G. Montalban, G. Villora, J.L. Cenis, Silk fibroin nanoparticles: efficient vehicles for the natural antioXidant quercetin, Int. J. Pharm. 518 (2017) 11–19.

48 F. Heraud, A. Heraud, M.F. Harmand, Apoptosis in normal and osteoarthritic human articular cartilage, Ann. Rheum. Dis. 59 (2000) 959–965.

49 M.A. Hashemipour, H. Mehrabizadeh Honarmand, F. Falsafi, M. Tahmasebi Arashlo, S. Rajabalian, S.A.H. Gandjalikhan Nassab, In vitro cytotoxic effects of celecoxib, mefenamic acid, aspirin and indometacin on several cells lines, J. Dentistry (Shiraz, Iran) 17 (2016) 219–225.

50 C.-H. Tang, C.-J. Hsu, Y.-C. Fong, The CCL5/CCR5 axis promotes interleukin-6 production in human synovial fibroblasts, Arthritis Rheum. 62 (2010) 3615–3624.

51 M. Onoda, H. Inano, Effect of curcumin on the production of nitric oXide by cul- tured rat mammary gland, Nitric OXide-Biol. Chem. 4 (2000) 505–515.

52 R. Arora, A. Kuhad, I.P. Kaur, K. Chopra, Curcumin loaded solid lipid nanoparticles ameliorate adjuvant-induced arthritis in rats, Eur. J. Pain 19 (2015) 940–952.

53 Rodriguez-Nogales, F. Algieri, L. De Matteis, A. Abel Lozano-Perez, J. Garrido- Mesa, T. Vezza, J.M. de la Fuente, J. Luis Cenis, J. Galvez, M. Elena, Rodriguez- Cabezas, Intestinal anti-inflammatory effects of RGD-functionalized silk fibroin nanoparticles in trinitrobenzenesulfonic acid-induced experimental colitis in rats, Int. J. Nanomed. 11 (2016) 5945–5958.

54 D.W. Kim, H.S. Hwang, D.-S. Kim, S.H. Sheen, D.H. Heo, G. Hwang, S.H. Kang, H. Kweon, Y.-Y. Jo, S.W. Kang, K.-G. Lee, K.W. Park, K.H. Han, J. Park, W.S. Eum, Y.-J. Cho, H.C. Choi, S.Y. Choi, Effect of silk fibroin peptide derived from silkworm Bombyx mori on the anti-inflammatory effect of Tat-SOD in a mice edema model, Bmb Reports 44 (2011) 787–792.

Paper 7. Orlandi G, Faragò S, Menato S, Sorlini M, Butti F, Mocchi M, Donelli I, Catenacci L, Sorrenti M, Croce S, Segale L, Torre ML and Perteghella S. (2020). Eco-sustainable silk sericin from by-product of textile industry can be employed for cosmetic, dermatology and drug deliver. Journal of Chemical Technology and Biotechnology, 95: 2549–2560; doi: 10.1002/jctb.6441.

Abstract. Background: In the last decade, many researchers demonstrated the biological activities of native Bombyx mori silk sericin (SS), and its use is widespread in the cosmetic and biomedical field. However, SS is a polluting material from the silk fibroin textile industry. This paper aims to demonstrate that the industrial wastewater-derived SS has many biological properties and can be used as an eco-friendly product for cosmetic/pharmaceutical purposes with an important impact on the circular economy. Results: We focused on the SS derived from an ad hoc extraction process or industrial degumming wastewater. Both products were preserved with three different methods: lyophilization, spray-drying and sterilization. All SS were characterized in terms of amino acid content, molecular weight, physical–chemical properties, morphology, and size distribution; then we evaluated the biological properties, the cytocompatibility/cytoprotective profile, and the immunomodulatory abilities of SS. Free radical scavenging, anti-tyrosinase, and anti-elastase activities of waste SS were confirmed. Waste and standard SS were cytocompatible on human fibroblasts; all SS samples inhibited the proliferation of stimulated peripheral blood mononuclear cells in a dose-dependent manner. Waste SS showed a significant effect on tumor necrosis factor α and interleukin 10 release.

Conclusions: These results pave the way for using textile wastewater-derived SS to obtain high-value-added products for cosmetic and/or pharmaceutical purposes.

Keywords: silk sericin; textile wastewater; immunomodulatory activity; anti-elastase activity; textile/biomedical circular economy; sericin cytocompatibility

1. Introduction

Silk produced by Bombyx mori silkworms is composed of two main proteins, namely fibroin and sericin. Silk fibroin (SF) is a fibrous protein widely used in textiles, industrial and medical fields, whereas silk sericin (SS) is a hydrophilic globular protein
proposed as a bioactive compound and/or as an excipient for cosmetic and pharmaceutical purposes [1–4] The numerous research studies carried out on SS have demonstrated that this protein possesses many intrinsic biological properties, such as photo-protective, antioxidant, moisturizing, antibacterial, proliferative and immunomodulant [5–9]. According to a 2015 Voluntary Cosmetic Registration Program–FDA survey, it was demonstrated that about 5000 tons of sericin were used only in the USA, and only for cosmetics, every year [10].

Before using SF and SS, it is necessary to separate the proteins by degumming processes (extraction in boiling water, alkaline extraction, and extraction in an autoclave) [11]. SS tested until now is derived by an ad hoc degumming process performed on Bombyx mori cocoons in research laboratories or industries producing sericin [9,12]. Despite the interesting biological properties of SS, this protein still represents a by-product of the textile industry; the discarded degumming wastewater leads to environmental contamination and requires high oxygen demand for microbe- mediated degradation. According to circular

economy fundamentals, it could be advantageous to recover and reuse this product in the cosmetics and/or pharmaceutical fields.

In the last decade, the circular economy had much resonance as a way to use resources more sustainably, reducing produced wastes and environmental pollution [13]. In the textile industry, the possibility to reuse SS as a bioactive excipient in pharmaceutical and cosmetic fields can be a concrete example of the adoption of the circular economy measures. The industrial degumming process exploits the addition of soap, alkalis, acids or organic amines to the water to remove SS more effectively, producing large amounts of SS in wastewater as pure waste. Properly treating SS-rich wastewater allows SS extraction, recovery and reuse, resulting in significant environmental, economic and social benefits. The textile company can experience reduced economic and environmental impacts: on one side, revenue can be generated by selling recovered SS; on the other, it reduces the processing costs of wastewater treatment. The filtration method can be used to extract SS, processing 50 L h^{-1} of SS-rich wastewater with half the energy consumption and an 80% reduction in production cost compared with the traditional lyophilization equipment adopted in the pharma industry [14]. To date, there are two reasons why those volumes are not recovered for cosmetics and pharmaceutical use: first, the quality of the SS fraction could be related to the degumming method, which leads to high sericin degradation, limiting its effectiveness in cosmetics applications [15]; second, the discharged SS-rich wastewater has to be treated in order to remove water from the solution. Several technologies can be used for this activity, including lyophilization, spray-drying and ultrafiltration. All of these require additional consumption of energy and the provision of equipment.

Despite the advantages related to the recycling of wastewater product, the use of SS obtained from the textile industry presents some limitations. In particular, the SS was in aqueous solution, and this physical form promotes microbial growth, reducing protein stability

over time. To overcome this problem, it is possible to dry or sterilize the product. This work aims to examine and demonstrate, for the first time, the feasibility of the pharmaceutical and cosmetic use of SS recovered from textile industry wastewater. This aim can be achieved with the physical–chemical characterization and determination of in vitro biological properties, hence demonstrating that the employment of waste sericin in a plethora of cosmetic, cosmeceutical, and pharmaceutical products will be possible, as an easily recoverable ingredient for cleverly sustainably closing the circular loop.

2. Materials and Methods

2.1. SS sample preparation

In this study, we combined two different sources of SS (an ad hoc degumming process developed in the laboratory or industrial wastewater containing SS and other compounds), and three different technological processes as preservation methods (lyophilization, spray-drying and sterilization) (Table 1). For all experiments, we used Bombyx mori polyhybrid cocoons (white monovoltine). Concerning the ad hoc degumming process, we used a simple method, previously reported in the literature [5,9,12,16], which allowed us to obtain a water-based SS solution and that was different from the degumming technique adopted in the textile industry (aimed at optimizing the characteristic of silk fibroin). Briefly, cocoons (supplied by Nembri Industrie Tessili s.r.l., Capriolo, BG, Italy) were cut and boiled in an autoclave (Systec V-65, Wurttemberg, Germany) at 120 °C for 30 min (20 mL water per gram of cocoons).

Table 1. Sericin samples considered for the study.

ID sample	Source	Treatmente
Deg-Lyo	Degumming	Lyophilization
Deg-Spray	Degumming	Spray-drying
Deg-Ster	Degumming	Sterilization

Waste-Lyo	Wastewater	Lyophilization
Waste-Spray	Wastewater	Spray-drying
Waste-Ster	Wastewater	Sterilization

Regarding the industrial degumming, the textile industry started from silk yarns (20/22 Den–22.444 Tex) purchased by a silk factory in Sichuan (China). Yarns are obtained by the immersion of Bombyx mori cocoons in hot water (40–50 °C), and by subsequent brushing and reeling procedures; all these steps are needed to stitch the seven single cocoon filaments need to obtain a silk yarn of 20/22 Den. For the wastewater-derived SS extraction, each silk yarn was subjected to an autoclave (100 °C, 30 min) degumming process using a commercial carbonate-based alkaline soap (GP SOLV PHT, GP TEXTRON s.r.l., CO, Italy; the chemical composition is not available because it is patented). At the end of the extraction, the obtained SS solution (containing alkaline soap) was concentrated and purified by the ultrafiltration technique (ceramic membranes, molecular cut off 15 kDa, a pump of 7.5 kW, pressure 2.5 bar). All obtained aqueous SS solutions (from both lab-scale and industrial process) were divided into three aliquots subjected to three different technological processes: lyophilization, spray-drying and sterilization. For the lyophilization, the samples were frozen at −80 °C and freeze-dried (Modulyo® Edwards freeze dryer, Kingston, New York, USA) at 8×10^{-1} mbar and − 50 °C for a week. The freeze-dried products were then stored at room temperature until use.

Spray-dried samples were obtained using a Büchi Mini Spray-Dryer (Flawil, Switzerland), equipped with a nozzle. In particular, both SS solutions (obtained by the ad hoc lab-scale process and by the industrial wastewater) were processed considering the same concentration range (0.8–1.4% w/w) and with the same process parameters: pump 6 mL min^{-1}; inlet temperature 120 °C; outlet temperature 80 °C; air pressure 3 bar; fluid flow 500–600 mL h^{-1}.

The sterilization process was performed using a cycle of the SS solutions in an autoclave (Systec V-65, Wurttemberg, Germany) at 121 °C for 15 min, as reported in Pharmacopoeia.

For each treatment group (Table 1), three batches were prepared and analyzed.

2.2. SS Characterization

The effect of SS source (lab-scale degumming water or wastewater) on amino acid composition was evaluated by analyzing the freeze-dried samples (Deg-Lyo and Waste-Lyo).

All SS samples (Table 1) were characterized in terms of molecular weight distribution by sodium dodecyl sulfate–polyacrylamide gel electrophoresis (SDS-PAGE), and physical–chemical properties by Fourier transform infrared spectroscopy (FTIR) and differential scanning calorimetry (DSC). Moreover, morphology and particle size distribution were evaluated by scanning electron microscopy (SEM) and dynamic light scattering (DLS), respectively.

2.2.1. Determination of the amino acid composition

The amino acid sequence of freeze-dried SS was evaluated through ion-exchange chromatography using an automatic amino analyzer (Biochrom 30+, Cambridge, UK), after acid hydrolysis of the protein. Freeze-dried samples were treated with HCl (6 mol L^{-1}) and phenol as a stabilizer, for 24 h at 110 °C. The samples were injected into a pre-column and then into a cation-exchange resin column at a checked temperature; as eluents, six buffer solutions, with different pH and ionic strength, were considered to separate the amino acids according to their affinity for the mobile and stationary phases. At the end of the chromatographic run, the eluent–sample mixtures were treated with ninhydrin, a highly selective indicator for the amino acids, which reacts with amino groups, leading to a purple-colored complex.

This so-called complex was analyzed with a spectrophotometer at 570 and 440 nm.

2.2.2. Electrophoresis

The molecular weight of the SS samples was evaluated using a vertical Mini-PROTEAN Tetra cell system (Bio-Rad, Milan, Italy). Two different running polyacrylamide gel concentrations were considered to evaluate low and high molecular weights (12% and 6%, respectively); stacking gels were used at 4%. SS samples were solubilized in bidistilled water at 70 °C to obtain solutions at a concentration of 10 mg mL^{-1}. The solutions were then dissolved in the reduced sample buffer (0.5 mol L^{-1} Tris–HCl, pH 6.8), containing bidistilled water, glycerol, SDS)10% w/v and Coomassie Brilliant Blue, in the presence of β-mercaptoethanol (ratio of sample to reduced sample buffer was 1:1) at 70 °C for 1 h. Two standards were used to identify high and low molecular weights. The high molecular weight markers were myosin, α_2- macroglobulin, β-galactosidase, transferrin, and glutamic dehydrogenase (Amersham HMW calibration kit 17-0615-01); the low molecular weight markers were phosphorylase B, albumin, ovalbumin, carbonic anhydrase, trypsin inhibitor and α-lactalbumin (Amersham LMW calibration kit 17-0446-01). When the electrophoretic run had finished, the gels were colored with Coomassie Brilliant Blue 0.1%, ethanol 40% and acetic acid 10% overnight, followed by two bleaching steps: the first (40% methanol, 7% acetic acid) for 1 h and the second (5% methanol, 7% acetic acid) for 1 h, until the marker bands appeared.

2.2.3. FTIR spectroscopy

FTIR spectra of the dried samples (Deg-Lyo, Waste-Lyo, Deg-Spray and Waste-Spray) were obtained using a spectrophotometer (Spectrum One, Perkin Elmer, Wellesley, MA, USA) equipped with a MIRacle™ ATR device (Pike Technologies, Madison, WI, USA). The IR

spectra in transmittance mode were obtained in the spectral region of 650–4000 cm^{-1} by the accumulation of 64 scans with a resolution of 4 cm^{-1}.

2.2.4. Differential scanning calorimetry

Temperature and enthalpy values were measured with a Mettler STARe system (Mettler Toledo, Italy) equipped with DSC81^{e} Module and an Intracooler device for sub-ambient temperature analysis (Jukabo FT 900) on 2–3 mg samples (Deg-Lyo, Waste-Lyo, Deg-Spray and Waste-Spray) in 40 μL sealed aluminum pans with pierced lid (method: 10–400 °C temperature range; heating rate β= 10 K min^{-1}; nitrogen air atmosphere flux 50 mL min^{-1}). The instrument was previously calibrated with indium as a standard reference, and measurement was carried out at least in triplicate.

2.2.5. Simultaneous thermogravimetric analysis (TGA/DSC 1)

Mass losses were recorded with a Mettler STARe system TGA on 3–4 mg samples in 70 μL alumina crucibles with lid (method: 30–400 °C temperature range; heating rate β= 10 K min−1; nitrogen air atmosphere flux 50 mL min−1). The instrument was previously calibrated with indium as a standard reference, and measurement was carried out at least in triplicate.

2.2.6. Morphological investigation

SS sample morphology was investigated using a scanning electron microscope with field emission gun (Mira 3, Tescan, Brno, Czech Republic), high vacuum mode, 15 kV and secondary electrons (SEs) detector. Samples were placed on aluminum stubs and coated with gold–palladium.

2.2.7 Dynamic light scattering

The particle size distribution of SS microparticles (Deg-Spray and Waste-Spray samples) was analyzed with a laser light scattering granulometer equipped with a small cell volume (120 mL, 5% obscuration) (Beckman Coulter LS230, Miami, FL, USA), setting the refractive index at 1.359 for ethanol. SS powders were dispersed in ethanol (99%, v/v) and sonicated for 10 min. The instrument performed five replicates of 90 s each.

2.3. SS in vitro biological properties

The biological properties of all SS samples were investigated in terms of free radical scavenging, anti-tyrosinase, and anti-elastase activity; cytotoxicity and cytoprotective effect against oxidative stress were determined on fibroblasts and immunomodulatory ability on peripheral blood mononuclear cells (PBMCs).

2.3.1.Free radical scavenging activity

The antioxidant activity of the SS samples was evaluated by 2,2-diphenyl-1-picrylhydrazyl (DPPH) colorimetric assay as reported by Fan et al. [17]. Briefly, DPPH solution (Sigma Aldrich; 0.0056% w/v in methanol) was added to aqueous SS solutions (2.5, 5, 8 and 10 mg mL^{-1}). The reaction mixture, composed of 120 μL sample and 1080 μL DPPH, was incubated in the dark at room temperature, and subsequently centrifuged at 3000 × g for 5 min in order to eliminate sericin-insoluble residues. The supernatant was subjected to spectrophotometric analysis (Synergy HT, BioTek, Swindon, UK) at 515 nm. For each sample, the absorbance data obtained were subtracted from the blank value (reaction mixture in the absence of DPPH). The reaction mixture in the absence of SS was considered as a negative control. The analyses were performed in triplicate. The free radical scavenging percentage activity was calculated using the following formula:

$$\text{Activity (\%)} = [(A_{CTR} - A_{samp})/A_{CTR}] \times 100$$

where A_{CTR} = negative control absorbance and A_{samp} = SS sample absorbance

2.3.2. Anti-tyrosinase activity

The anti-tyrosinase activity of SS was evaluated by spectrophotometric analysis of the kinetic reaction between the enzyme tyrosinase and L-tyrosine substrate (Sigma Aldrich, Milan, Italy) in accordance with Aramwit.18 SS samples were tested at concentrations of 2.5, 5, 8 and 10 mg mL^{-1}. A stock solution of silk sericin was prepared at a concentration of 10 mg mL^{-1}, corresponding to the maximum solubility of the protein in aqueous solution. Then, we diluted the stock solution appropriately to obtain the other selected dilutions. The same principle was adopted to prepare silk sericin samples to evaluate the antioxidant and anti-elastase activity. The enzyme tyrosinase was solubilized in phosphate buffer pH 6.8 to obtain a final concentration of 500 IU mL^{-1}. The tyrosinase solution was pre-incubated for 10 min with each SS sample and, consequently, the L-tyrosine substrate was added to the reaction mixture. The enzymatic reaction was spectrophotometrically analyzed (Synergy HT) at 480 nm for 30 min (measurements every minute). The reaction mixture in the absence of sample was used as a negative control, while arbutin (Sigma Aldrich) was considered as a positive control. Each absorbance value obtained during reaction kinetics was subtracted from the absorbance of the white mixture, composed of each SS sample in the absence of enzyme and substrate. All analyses were conducted in triplicate. The results were reported as a percentage anti-tyrosinase activity using the following formula:

$$\text{Activity (\%)} = [(A_{CTR} - A_{samp})/A_{CTR}] \times 100$$

where A_{CTR} = negative control absorbance and A_{samp} = SS sample absorbance

2.3.3. Anti-elastase activity

The inhibitory effect of each SS sample on the elastase enzyme was evaluated using the method previously described by Nam et al.,19 with some modifications. Pancreatic porcine elastase (Sigma Aldrich) was solubilized in phosphate buffer pH 6.8 (0.5 IU mL−1). The substrate N-succinyl-Ala-Ala-Ala-p-nitroanilide (Sigma Aldrich) was diluted in TRIS buffer to obtain a final concentration of 0.41 mmol L^{-1}. Each SS sample (2.5, 5, 8, 10 mg mL^{-1}) was incubated for 20 min with the enzyme and, subsequently, the substrate was added. The kinetic reaction was monitored by spectrophotometric analysis (Synergy HT) at 410 nm for 35 min (measurements every minute). The reaction mixture in the absence of sample was used as a negative control, while the epigallocatechin gallate (Sigma Aldrich) was considered as a positive control. Each absorbance value of the sample was subtracted from the absorbance of the white mixture (SS sample without enzyme and substrate). All analyses were performed in triplicate. The results were reported as a percentage anti-elastase activity using the following formula:

$$\text{Activity (\%)} = [(A_{CTR} - A_{samp})/A_{CTR}] \times 100$$

where A_{CTR} = negative control absorbance and A_{samp} = SS sample absorbance

2.3.4. Cytotoxicity evaluation by cell metabolic activity determination (MTT assay)

Human fibroblasts were cultured in vitro in Dulbecco's Modified Eagle's Medium (DMEM) High Glucose supplemented with 10% fetal bovine serum, penicillin 100 U mL^{-1}, streptomycin 100 μg mL^{-1}, amphotericin 0.25 μg mL^{-1}, glutamine 4 mmol L^{-1} and sodium pyruvate 1 mmol L^{-1}.

For MTT assay, cells were seeded into a 96-well plate (10 000 cells cm^{-2}) and treated for 24 and 48 h (37 °C, 5% CO_2) with SS samples (concentrations: 12, 120, 500, 1000 and 2500 μg mL^{-1}) [7,20]. Cells were then washed with phosphate- buffered saline (PBS), and 100 μL 3-(4,5-dimethylthiazol-2-yl)-2,5-diphenyltetrazolium bromide (MTT) solution (0.5 mg mL^{-1}) was added to each well. After 3 h incubation, the MTT solution was removed and 100 μL dimethyl sulfoxide (DMSO) was added. Untreated cells were considered as control (100% metabolic activity). Optical density was measured on Synergy HT at 570 and 670 nm (reference wavelength). Each condition was tested in triplicate.

Cell metabolic activity (%) was calculated as 100 × (ODsample/ODctr).

2.3.5. Cytoprotective effect against oxidative stress

Human fibroblasts were seeded in a 96-well plate (10 000 cells cm^{-2}) and treated with each SS sample (120, 500 and 1000 μg mL^{-1}). After 24 h incubation, cells were washed with PBS and treated with hydrogen peroxide (H_2O_2, 0.75 mmol L^{-1}) for 24 h. An MTT assay was then performed to evaluate the cell metabolic activity of cells using Synergy HT, as previously described. Untreated cells were considered as control (100% cell metabolic activity). Each condition was tested in triplicate [8].

2.3.6. Antiproliferative assay and release of tumor necrosis factor α (TNFα), interferon γ (IFN-γ) and interleukin 10 (IL-10)

Each SS sample was investigated for in vitro antiproliferative activity on activated PBMCs. In vitro TNF-α, IFN-γ and IL-10 secretion was also evaluated by enzyme-linked immunosorbent assay (ELISA; Tema Ricerca, Bologna, Italy). PBMCs were isolated from the heparinized venous blood of two healthy volunteers by gradient centrifugation (Lymphoprep, Axis-Shield) [21] and seeded (10 000 cells per well) into the 96-well plate using RPMI 1640 medium added with 10% fetal calf serum (FCS). To evaluated SS immunogenicity, PBMCs were treated with or without SS solutions at concentrations 12, 120 and 500 μg mL^{-1}. After 72 h of treatment, 3H-thymidine (3HTdR, 0.5 μCi per well; Amersham Pharmacia Biotech, Chalfont St Giles, UK) was added to each well, and the radioactivity was measured (TopCount, Packard Instruments, Waltham, MA, UA). Results were expressed as the stimulation index (SI = cpm of treated cultures/cpm of untreated cultures), where cpm of treated cultures were counted for a minute of cells treated with SS. To evaluate SS immunomodulatory activity, PBMCs were treated with or without SS at the above concentrations in the presence of phytohemagglutinin (PHA, 4 μg mL^{-1}), maintaining the same culture conditions. Results were expressed as residual proliferation (RP = SI treated/SI untreated * 100), where SI treated was calculated from PBMCs cultured in the presence of both SS and PHA, while SI untreated was obtained from PBMCs cultured in the presence of only PHA, without SS samples. The supernatants of PHA-activated PBMCs, cultured with or without SS samples, were also collected to quantify the cytokine release by ELISA according to the manufacturer's instructions. IL-10 was chosen as an example of the anti-inflammatory cytokine, with TNF-α and IFN-γ as models of pro-inflammatory cytokines. Absorbance was measured at 450 nm (Titertek Plus MS 212-ICN, Milan, Italy), and the cytokine concentration (expressed in pg mL^{-1}) was calculated with respect to the standard curve.

2.4. Statistical analysis

STATGRAPHICS XVII (Statpoint Technologies, Inc., Warrenton, VA, USA) was used to analyze the data by a linear generalized analysis of variance model (ANOVA). Fisher's least significant difference (LSD) procedure was applied to evaluate the differences between means.

The free radical scavenging data were elaborated considering the type of sample (source and treatment) and its concentration as fixed factors. To determine the IC50 value of the antioxidant activity – that is, the concentration of silk sericin that provokes a response equal to 50% – the data were elaborated by GraphPad Prism software, normalizing the response to run between 0% and 100%. The used model was $Y = 100/ (1 + 10^{(X\text{-Log IC50})})$. For anti-tyrosinase and anti-elastase results, we considered the time and type of sample and the sample concentration as fixed factors. The enzymatic kinetics of anti-tyrosinase and anti-elastase activity were elaborated with Michaelis–Menten model kinetics, $y = (Vmax \times x)/ (Km + x)$, where y is the absorbance at time x, Km is the moment at which the activity is equal to half the maximum and Vmax is the maximum speed of the enzyme [5]. Graph-Pad Prism software was used to calculate the curve parameters. For each curve, Vmax and Km were analyzed with an analysis of covariance (ANCOVA) model, considering the sample as a fixed factor and the sample concentration as a covariate. The differences between the groups were analyzed with the LSD test for multiple comparisons.

Cell metabolic activity data, obtained from MTT assay, was analyzed considering the SS concentration, type of sample, incubation time and hydrogen peroxide treatment as fixed factors. For all the analyses, the statistical significance was set at $P < 0.05$.

3. Results and Discussion

Many research studies have demonstrated that SS extracted from native silk cocoons is a bioactive compound. In our work, we aimed to prove that SS from textile wastewater maintains its biological properties and can be employed in an environmentally sustainable way, reducing produced wastes and environmental pollution. Three different conservation methods (freeze-drying, spray-drying and sterilization) have been employed to optimize SS shelf-life.

First, the effect of the SS source on the amino acid composition was evaluated by chromatographic analysis, after acid hydrolysis, on Waste-Lyo and Deg-Lyo samples (Table 2).

The obtained results did not evidence any substantial differences between the two SS sources; overall, our results confirmed that sericin is a hydrophilic protein with a high content of charged and polar amino acids. According to the findings reported by Siritientong and colleagues [22], we observed that the acids present in the highest percentage are serine, aspartic acid, glycine, threonine, tyrosine and glutamic acid for both Waste-Lyo and Deg- Lyo samples.

SDS-PAGE was performed to qualitatively evaluate the molecular mass distribution of the freeze-dried, spray-dried and sterilized SS (Fig. 1 and Table 3).

A unique and continuous band was observed for all samples, revealing a wide molecular mass distribution in the SS as a function of the source and the technological treatment considered. In particular, the SS discarded in the industrial wastewater showed a profile more populated by high molecular weights (from 20 to 220 kDa) than the SS degummed in the laboratory (from 20 to 170 kDa) [11]. Studies conducted at the industrial level have shown that using columns with different cut-off led to solutions of sericin with several ranges of molecular weights [23]. In fact, the process of tangential ultrafiltration conducted in the industry allows us to adopt a higher cut-off compatible with the required level of industrial productivity than laboratory processing [24].

Despite SDS-PAGE being a commonly used experimental method to analyze the molecular masses of protein or polypeptide subunits, for many researchers involved in electrophoresis experiments with silk sericin it seems that it is not easy to obtain a good SDS-PAGE profile with clear bands [25]. The main difficulty is not related to the SDS-PAGE method itself but it often due to the main experimental parameters such as processing, degumming, drying and dissolution steps, which cause physicochemical stress in the silk sericin, with a significant impact on polymerization grade and molecular weight distribution.

The samples were therefore characterized by FTIR spectroscopy, and the spectra of Deg-Lyo (a), Waste-Lyo (b), Deg-Spray (c) and Waste-Spray (d) samples are shown and compared in Fig. 2. All samples presented the sericin characteristic bands, principally correlated with the random coil conformation of SS. In particular, we observed three bands at about 1640, 1520 and 1250 cm^{-1} due to the presence of Amide I, Amide II and Amide III, respectively. The absorption of the C═O stretching was registered at about 1640 cm^{-1}, and therefore at a lower wavenumber than the traditional carbonyl, as a result of the resonance effect, and typical of the random coil conformation. Finally, all samples presented a band at 3330 cm^{-1} due to N─H stretching. This band is superimposed on ─OH group absorption of serine and threonine, amino acids which are abundant in silk protein, causing a broadening of the signal.

The absence of shifts in the characteristic bands of both Deg and Waste samples confirmed that there are no differences between the four dried samples.

In Fig. 3 are reported the DSC profiles of Deg-Lyo (curve a) and Waste-Lyo (curve b) samples and the TGA profiles of Deg-Spray (curve c) and Waste-Spray (curve d) samples as an example of thermal data. In all DSC traces a first large endothermic peak at about 90 °C due to water evaporation was evident. This peak was followed by a

glass transition effect (Tmidpoint = 200 ± 2 °C) related to the higher presence of random coil domains in the amorphous region in SS and other endo/exothermic effects attributable to the SS thermal decomposition.

The TGA profile of all samples confirmed water evaporation of about 8% in the temperature range 35–150 °C and the following thermal decomposition from about 220 °C, indicating no differences in thermal stability between the four products.

Solid-state characterization allowed us to conclude that both SS sources and dried treatments did not influence the physicochemical properties of obtained products.

SEM investigation of all SS samples demonstrated that the preservation method influenced protein morphology (Fig. 4).

In particular, the spray-drying technique allowed us to obtain collapsed microparticles, as reported by other authors [7,26]. Granulometric analysis showed a monomodal trend for both samples (data not presented); microparticles presented a volume-weighted mean diameter of 2.71 ± 1.310 μm and 1.86± 0.884 μm (mean ± standard deviation) for Deg-Spray and Waste-Spray, respectively. Minimal differences in the starting sample concentration could explain the differences in terms of mean diameter between the two treatment groups: however, we observed the same granulometric distribution profile and the same morphology and, for this reason, we demonstrated that the extraction technique does not influence the spray-drying process.

Table 2. The amino acid content (Waste-Lyo and Deg-Lyo) of the freeze-dried SS samples**.** For each amino acid are reported the retention time (minutes) and the weight percentage in two treatment groups.

Amino acid	Retention time	Waste-Lyo	Deg-Lyo
Aspartic acid	14.7	16.07	17.22
Threonine	20	7.97	8.12
Serine	21.8	26.26	28.05
Glutamic acid	27.2	4.47	4.95
Glycine	37.4	8.85	9.52
Alanine	38.6	3.13	3.36
Valine	44.5	2.52	2.72
Isoleucine	55.1	0.59	0.41
Leucine	56.5	1.85	1.29
Tyrosine	59.4	5.17	4.93
Phenylalanine	62.5	0.65	0.8
Lysine	80.6	2.68	2.94
Histidine	83.5	1.49	1.47
Arginine	94	4.18	4.28
Proline	35.2	0.78	<0.01
Total content		86.62	90.03

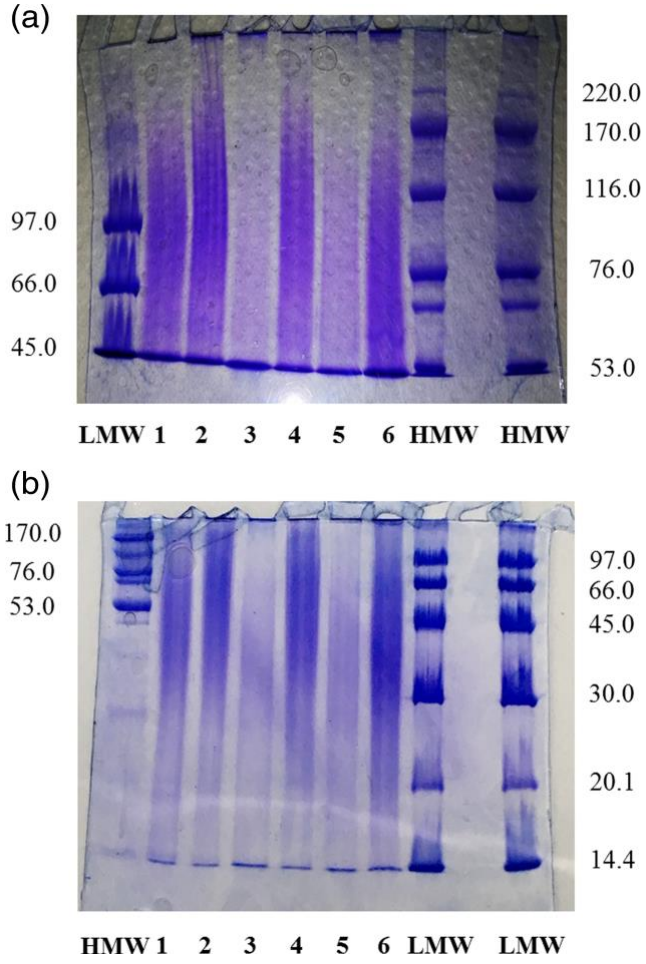

Figure 1. SDS-PAGE of sericin samples using stacking gel to 4% and running gel to 6% (a) and stacking gel to 4% and running gel to 12% (b).

Table 3. Sericin samples used for electrophoresis (SDS-page). For each treatment group, a code is reported according to the loading of the sample into the well. SDS-markers were used for molecular weight determination: standard 1 for low molecular weights (LMW) and standard 2 for high molecular weights (HMW).

Sample	Code
Deg-Lyo	1
Waste-Lyo	2
Deg-Spray	3
Waste-Spray	4
Deg-Ster	5
Waste-Ster	6
SDS-standard 1	LMW
SDS-standard 2	HMW

Spray-drying is a drying method useful to obtain sericincollapsed microspheres with controlled dimensions6; one of the principal advantages is the high drying speed to reduce thermal damage of the material. In fact, as long as the particles do not become completely dried, evaporation takes place without the product being subjected to overheating. Moreover, large amounts of product can be produced by spray-dryer; obtained powders are easily rehydrated and dispersed at the time of use. Freeze-dried samples (Deg-Lyo and Waste-Lyo) did not show any structural or morphological peculiarities; overall, both samples appeared as a rough and irregular surface. Freeze-drying is a valid drying method proposed in the literature to decrease the denaturation degree of a protein and to obtain a porous material with interconnecting pores [27]. Lyophilization ensures the permanent dispersion of a biomaterial, which can be dried, forming a porous solid [27], dissolving with great rapidity and effectiveness when necessary. Moreover, bacterial growth cannot take place in the frozen material, and a protein product is very resistant to such undesirable phenomena after being freeze-dried. High energy consumption, long process time and high costs represent the principal disadvantages of the

lyophilization and spray-drying techniques. In this contest, autoclave treatment could represent an alternative preservation approach for SS, in order to obtain sterilized biomaterial in a fast, cheap and ecofriendly way, routinely used in a laboratory to sterilize different reagents and equipment [17]. The morphological evaluation of two liquid sterilized samples (Deg-Ster and Waste-Ster) required solvent evaporation before SEM analysis; for this reason, sterilized SS were added to the stubs and dried to room temperature. SEM images showed that Deg-Ster and Waste-Ster samples presented an amorphous morphology. The in vitro biological properties of all SS samples were evaluated. Antioxidant, anti-tyrosinase and anti-elastase activities of SS were tested to define the anti-ageing and photoprotective profile of the protein after different treatments. Regarding the free radical scavenging potential, the data obtained from statistical analysis showed a significant effect of protein source and treatment ($P < 0.05$). Overall, degummed SS showed better antioxidant ability with respect to wastewaterderived protein. Degummed SS presented a concentrationdependen trend for all treatment groups (Fig. 5); freeze-dried SS (Deg-Lyo) allowed us to obtain the most promising results, reaching a free radical scavenging ability of 83.4 ± 13.51% (mean value ± standard deviation) at a concentration of 10 mg mL^{-1}.

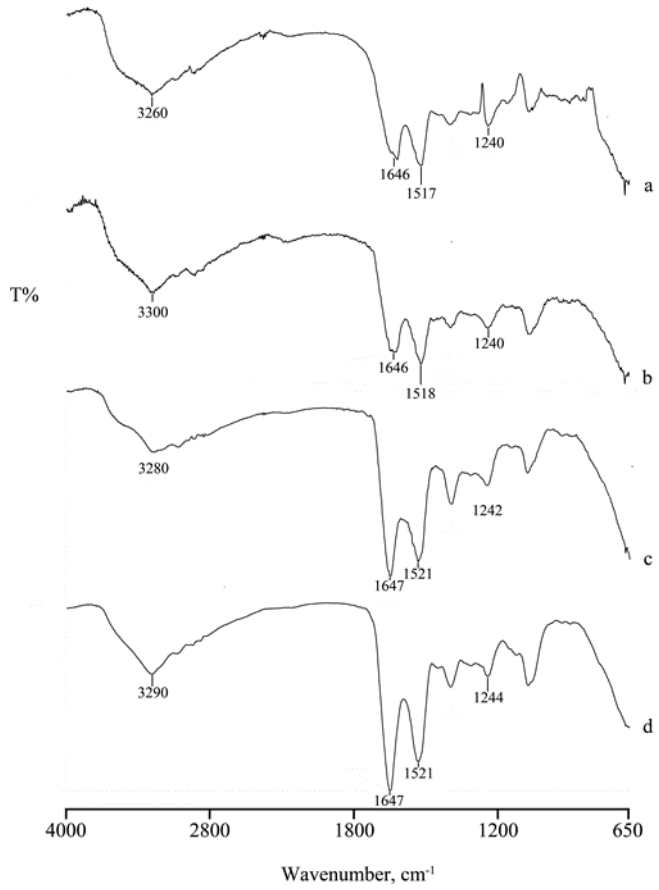

Figure 2. FTIR spectra of Deg-Lyo (a), Waste-Lyo (b), Deg-Spray (c) and Waste-Spray (d) samples

These data were in agreement with those reported by Fan and colleagues [17].

SS derived from the industrial process (Waste samples) had a lower antioxidant capacity than the native protein, at all tested concentrations. In detail, Waste-Lyo, Waste-Spray and Waste-Ster samples presented a mean antioxidant activity lower than 10%, without any differences between treatment groups and sample concentrations ($P > 0.05$, Fig. 5).

Data obtained by DPPH assay were also statistically analyzed to determine IC50 values. These results confirmed

that SS derived from textile wastewater had lower antioxidant properties (Table 4). On the other hand, Deg-Lyo SS resulted as the most promising sample, with an IC50 value of 4.43 mg mL^{-1}. No differences ($P < 0.05$) were revealed between Deg-Spray and Deg-Ster samples, which presented IC50 values of about 20 mg mL^{-1} (Table 4).

These data confirmed that the DPPH radical scavenging activity of the SS is strongly influenced by the technological procedure chosen to preserve silk protein, but also by the degumming process and other parameters, e.g. silkworm strain [5,28] and diet [29]. All these parameters influenced the chemical compositions of SS, and consequently the biological properties of silk protein. In addition, Manosroi et al. [30] demonstrated that freeze-dried SS, degummed by autoclave treatment, showed a higher free radical scavenging activity with respect to SS obtained by the soap-alkaline degumming process. Although the latter method is more effective for removing sericin from silk fibroin during industrial silk production, the recovered SS is often not of high quality, owing to its degradation and the purification steps needed to remove the chemical impurities into the SS aqueous solution [9].

In the work published by Wu et al. [31], the ethanol precipitation method was proposed to recover SS from silk industrial wastewater. This recovery method was effective in obtaining an SS-based dried product with a high degree of purity and an IC50 value of 31 mg mL^{-1}. SS can be used as a skin whitening agent, thanks to its tyrosinase inhibition activity. The statistical analysis demonstrated a significant effect of all considered variables (treatment group, time and sample concentration; $P < 0.0001$) on SS anti-tyrosinase activity. As observed from the DPPH assay, the degummed

samples presented a higher anti-tyrosinase ability. In particular, SS subjected to spray-drying technique (Deg-Spray) presented the highest inhibitory effect on tyrosinase enzyme already at a concentration of 5 mg mL^{-1}, as shown in Fig. 5 (60.45 ± 1.04%). Overall, Waste SSs had lower anti-tyrosinase capacity than the native protein extracted in our research laboratory. All waste-derived samples presented a mean activity lower than 20%, at all considered concentrations (Fig. 5). As additional reference material, see also Supporting Information Fig. S1. Tyrosinase is the main regulator of melanin production during the melanogenesis process, as a defense against UV rays [5,32]. Overexpression of tyrosinase is often responsible for hyperpigmentation disorders and ageing. In 2018, Aramwit et al. determined the anti-tyrosinase effect of urea-extracted SS on human Staphylococcus aureus peptidoglycan (PEG)-stimulated melanocytes and an artificial model of skin, using an in vitro model of hyperpigmentation. SS at all tested concentrations significantly caused a decrease in tyrosinase production on melanin pigments compared with non-treated melanocytes. Moreover, similar results were obtained after 10 days of SS treatment on the tyrosinase expression in artificial skin [33] Aramwith et al.'s results were in agreement with the data reported in this work.

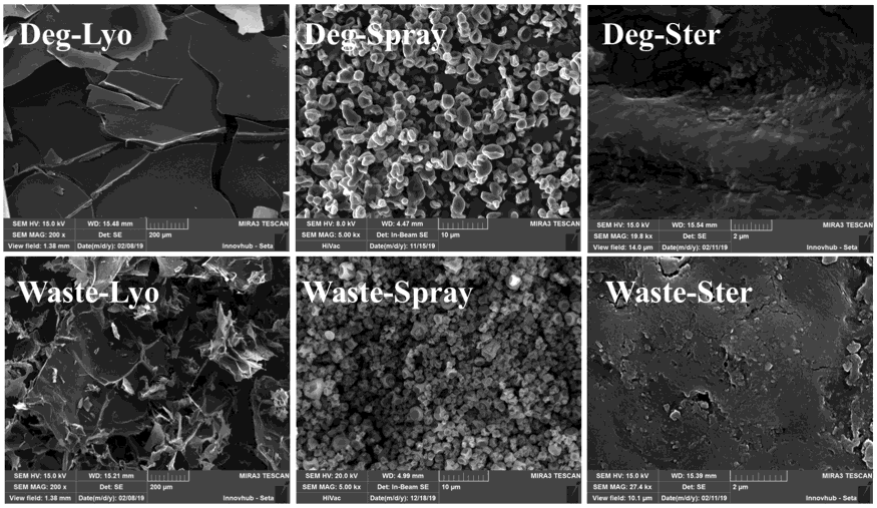

Figure 4 SEM. Images of the degummed (Deg) and wastewater (Waste) sericin, considering three treatments: lyophilization (Lyo, scale bar 200 μm), spray-drying (Spray, scale bar 10 μm) and sterilization (Ster, scale bar 2 μm). Different scale bars were considered in order to better observe each sample; the same scale bar was used for samples obtained by the same treatment (e.g. Waste-Spray and Deg-Spray).

SS amino acid composition influenced, in the same manner, both free radical scavenging and anti-tyrosinase activities of SS; in particular, a high content of hydroxyl groups, polyphenols and flavonoids positively improves the antioxidant and anti-tyrosinase profile of SS [5,34–36].

Raw data obtained from the spectrophotometric analyses of tyrosinase reaction kinetics were also processed to calculate Km and Vmax (Table 5). No differences ($P > 0.05$), in terms of Km and Vmax, were observed for Waste-Spray, Deg-Ster and Waster-Ster samples in comparison with negative control (substrate + enzyme, without sericin). On the other hand, Deg-Lyo, Waster-Lyo and Deg-Spray samples induced a significant modification of Km and/or Vmax values. According to the Michaelis–Menten kinetics, Deg-Spray acted as a mixed inhibitor of tyrosinase enzyme; in fact,

we observed that Km value was not significantly different with respect to negative control, while Vmax value was incremented ($P < 0.05$) (Table 5). Deg-Spray SS can bind both free enzyme and enzyme/substrate complex, causing a simultaneous change of Km and Vmax, compared to the negative control curve [37,38].

All SS samples were tested to evaluate their ability to inhibit elastase, a key enzyme in elastin fiber degradation. All considered variables (treatment group, time, and sample concentration) showed a significant effect on elastase inhibition ($P < 0.0001$).

The anti-elastase activity had a dose-dependent trend for all samples (Fig. 5). The Deg-Ster and Waste-Spray samples showed the highest anti-elastase properties. Deg-Ster activity was 53.07 ± 6.42% and 56.95 ± 7.16% (mean value ± standard deviation) at 8 and 10 mg mL^{-1}, respectively, while Waste-Spray activity was 46.60 ± 11.74% (mean value ± standard deviation) at 8 mg mL^{-1} and 41.07 ± 5.15% (mean value ± standard deviation) at 10 mg mL^{-1}. Overall, other samples did not exceed 35% of anti- elastase activity. As additional reference material, see also Supporting Information Fig. S1.

The Km and Vmax mean values of all SS samples and the negative control are reported in Table 6. According to Michaelis–Menten kinetics, sterilized SS, coming from industrial extraction (Waste-Ster), acted as a mixed inhibitor, causing a simultaneous change in Km and Vmax with respect to the negative control (CTR) (Table 6). Contrarily, Waste-Lyo, Deg-spray, and Waste-spray are examples of the non-competitive inhibitors of elastase. They bind the free enzyme or the enzyme/substrate complex in an allosteric site, causing a decrease in Vmax without Km value alterations [37].

The in vitro cytotoxicity of SS samples was evaluated in human fibroblasts. All SS samples resulted in cytocompatibility at all considered concentrations (Fig. 6). Statistical analysis

evidenced a significant effect of SS source (ad hoc degumming process-derived and industrial wastewater-derived SS) and sample concentration on cell viability ($P < 0.0001$). In particular, fibroblast metabolic activity was 97.08 ± 1.798% and 84.29 ± 1.798% (mean value ± LSD interval) for sericins derived from wastewater and degumming process, respectively.

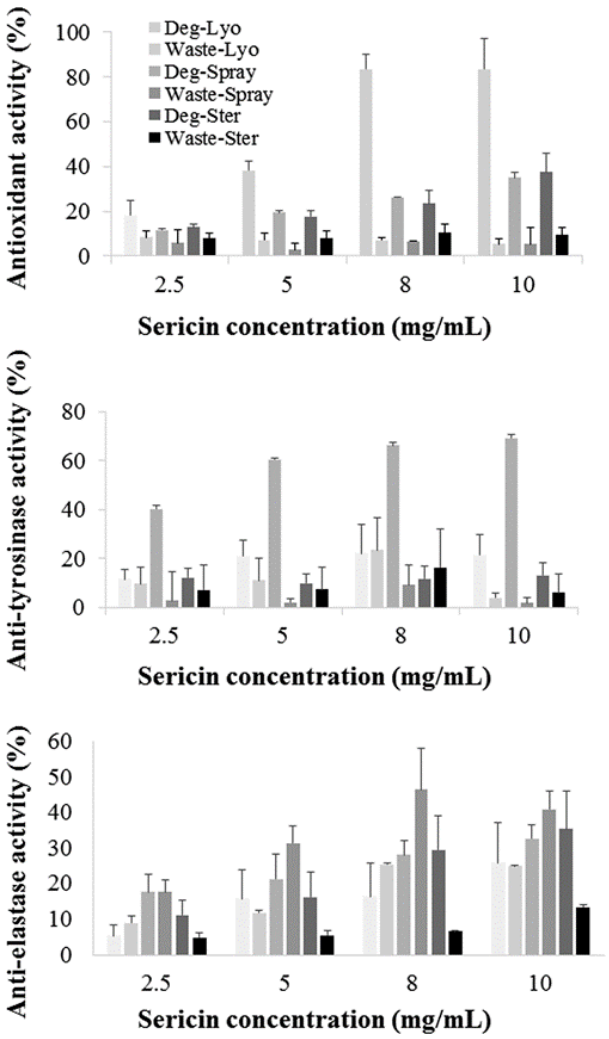

Figure 5. Free radical scavenging, anti-tyrosinase and anti-elastase activity percentage of SS samples. Data are reported as mean values and standard deviations (n = 3).

On the other hand, the treatment of SS samples (freeze-drying, spray-drying or sterilization) and time of incubation did not affect cell metabolic activity ($P = 0.2261$). A second statistical analysis was performed considering the type of SS source and the technological treatment as a unique fixed factor.

Table 4. Antioxidant activity of the silk sericin samples expressed in terms of IC50 values (mg mL^{-1}). Data are reported as mean values and 95% confidence intervals (n = 3). Different letters indicate significant differences ($P < 0.05$) between treatment groups.

ID Sample	IC_{50}	95%CI
Deg-Lyo	4.43d	3.40-5.72
Deg-Spray	20.28c	18.99-21.69
Deg-Ster	20.49c	18.87-22.32
Waste-Lyo	109.80a	85.19-152.00
Waste-Spray	135.10a	76.14-469.40
Waste-Ster	73.47b	59.29-95.19

As shown in Fig.6, there were significant differences between the analyzed groups. In detail, Waste-Spray showed the best cytocompatibility on human fibroblasts (102.18 ± 3.125%, (mean value ± LSD interval). Overall, our results confirmed the literature data, which demonstrated the cytocompatibility of SS on different cell lines [7,8,39,40].

We also tested the ability of SS to protect human fibroblasts from damage induced by hydrogen peroxide treatment (0.75 mmol L^{-1} H_2O_2); statistical analysis demonstrated that treatment group, sample and hydrogen peroxide concentrations significantly influenced the fibroblast viability ($P < 0.005$, n = 144; data not presented). In particular,

Deg-Ster and Waste-Spray SS showed a higher protective effect against oxidative damages at all considered concentrations. Treatment with these SS protects the cells and prevents the cell viability decrease, which was observed in the control group (no sericin treatment).

The in vitro antiproliferative activity of SS samples was evaluated on stimulated human PBMCs; moreover, we tested the effect of SS sample on the release of pro- and anti-inflammatory cytokines by PBMCs. PBMCs isolated from two healthy donors responded to the stimulation with PHA; all SS samples were able to inhibit the proliferation of stimulated cells in a dose-dependent manner and, in particular, the higher considered dose (0.5 mg mL^{-1}) allowed a greater reduction in the RP of PBMCs than did lower doses (0.12 and 0.012 mg mL^{-1}). Significant differences were observed between the considered treatment groups ($P < 0.0001$; Fig. 7); the most promising results were obtained with SS subjected to standardized degumming and then to autoclave sterilization (Deg-Ster sample). SS subjected to standardized degumming and then to autoclave sterilization (Deg-Ster sample).

Considering the cytokine release assay, the data showed statistical differences between treatment groups ($P < 0.0001$). PHA-stimulated cells treated with different SS samples released lower TNF-α amount with respect to control cells (Fig. 8). All samples had TNF-α levels lower than 4000 pg mL^{-1}. Moreover, the treatment group showed no significative effect on IFN-γ release ($P > 0.05$). All samples responded similarly to the untreated PBMCs (Fig. 8).

Finally, IL-10 release was evaluated on PHA-stimulated PBMCs (Fig. 8). Cells treated with SS showed lower IL-10 levels than the control (CTR).

Table 5. Km and Vmax of the anti-tyrosinase activity. Data are reported as mean values and standard error (n = 3). Different letters indicate significant differences (P < 0.05) between treatment groups.

ID Sample	Km		Vmax	
	Mean	Standard error	Mean	Standard error
CTR	47.66d	11.677	2.389c	0.257
Deg-Lyo	115.343a	12.037	4.161a	0.264
Waste-Lyo	77.754bc	8.533	3.099b	0.187
Deg-Spray	100.0734ab	10.431	1.158d	0.229
Waste-Spray	36.407d	8.533	1.961c	0.187
Deg-Ster	52.708d	8.698	2.362c	0.191
Waste-Ster	63.285cd	6.306	2.815bc	0.138

Table 6. Km and Vmax of the anti-elastase activity**.** Data are reported as mean values and standard error (n = 3). Different letters indicate significant differences (P < 0.05) between treatment groups.

ID Sample	Km		Vmax	
	Mean	Standard error	Mean	Standard error
CTR	11.694ab	2.131	1.013b	0.036
Deg-Lyo	13.108bc	2.349	1.263a	0.039
Waste-Lyo	20.818a	1.681	0.788c	0.028
Deg-Spray	14.345bc	2.349	0.856c	0.039
Waste-Spray	18.517ab	2.349	0.775c	0.039
Deg-Ster	15.685ab	1.859	1.252a	0.031
Waste-Ster	9.012c	1.681	0.863c	0.028

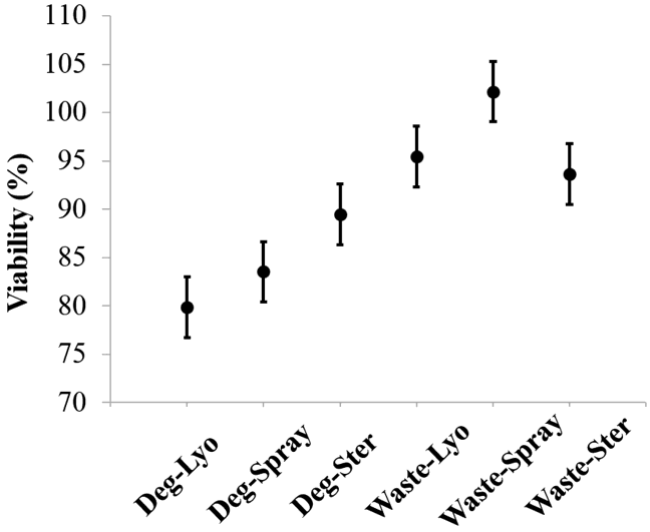

Figure 6. Cytocompatibility of SS samples on human fibroblasts. Data are expressed as mean values, of all tested concentrations, and LSD intervals of viability (n = 243). The overlap of two LSD intervals graphically indicates the absence of significant differences (P > 0.05).

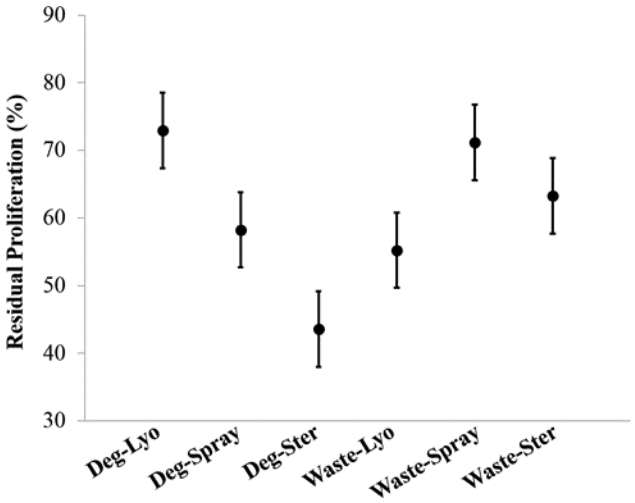

Figure 7. Antiproliferative effect of sericin samples on PHA-stimulated PBMCs. Data are expressed as mean values, of all tested concentrations, and LSD intervals of residual proliferation (n = 108).

The overlap of two LSD intervals graphically indicates the absence of significant differences ($P > 0.05$).

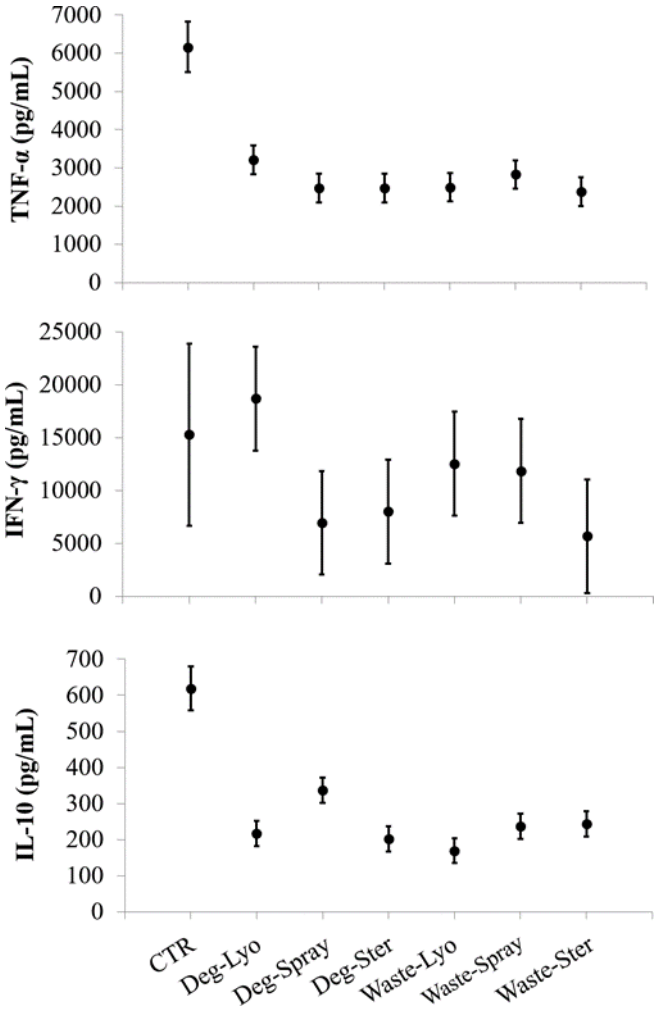

Figure 8. TNF-α, IFN-γ and IL-10 release (pg mL^{-1}) by PHA-stimulated PBMCs in the presence of sericin samples. Data are expressed as mean values and LSD intervals (n = 152). The overlap of two LSD intervals graphically indicates the absence of significant differences ($P > 0.05$).

4. Conclusions

Obtained results demonstrated that wastewater-derived SS is a biocompatible and non-immunogenic material. Moreover, we demonstrated many biological activities of the industrial SS, closely related to structural complexity, molecular weight distribution and stability, depending on the extraction and preservation methods.

Overall, wastewater-derived SS presented better anti-elastase properties and cytocompatibility with respect to the SS obtained in our research laboratory, while no differences were evidenced in terms of cytokine release. Regarding the stabilization technique, our results demonstrated that lyophilization and spray-drying are the most promising approaches, which allowed us to maintain both the protein stability and the biological properties of the final product.

Our research aims to be a starting point for the use of textile wastewater for the production of silk sericin usable in many biomedical and biotechnological fields. For this purpose, future research will be necessary to refine the industrial degumming process in order to optimize the extraction yield and to improve the stability and half-life of the protein.

Supporting Information

Supporting information may be found in the online version of this article (https://onlinelibrary.wiley.com/doi/full/10.1002/jctb.6441).

References

1 Crivelli B, Perteghella S, Bari E, Sorrenti M, Tripodo G, Chlapanidas T et al., Silk nanoparticles: from inert supports to bioactive natural carriers for drug delivery. Soft Matter 14:546-557 (2018).

2 Mandal BB and Kundu SC, Self-assembled silk sericin/poloxamer nanoparticles as nanocarriers of hydrophobic and hydrophilic drugs for targeted delivery. Nanotechnology 20 355101 (2009).

3 Kanoujia J, Singh M, Singh P and Saraf SA, Novel genipin crosslinked atorvastatin loaded sericin nanoparticles for their enhanced antihyperlipidemic activity. Mat Sci Eng C Mater 69:967-976 (2016).

4 Bari E, Perteghella S, Farago S and Torre ML, Association of silk sericin and platelet lysate: premises for the formulation of wound healing active medications. Int J Biol Macromol 119:37-47 (2018).

5 Chlapanidas T, Farago S, Lucconi G, Perteghella S, Galuzzi M, Mantelli M et al., Sericins exhibit ROS-scavenging, anti-tyrosinase, anti-elastase, and in vitro immunomodulatory activities. Int J Biol Macromol 58: 47-56 (2013).

6 Chlapanidas T, Perteghella S, Leoni F, Farago S, Marazzi M, Rossi D et al., TNF-alpha blocker effect of Naringenin-loaded Sericin microparticles that are potentially useful in the treatment of psoriasis. Int J Mol Sci 15:13624-13636 (2014).

7 Bari E, Arciola CR, Vigani B, Crivelli B, Moro P, Marrubini G et al., In vitro effectiveness of microspheres based on Silk Sericin and Chlorella vulgaris or Arthrospira platensis for wound healing applications. Materials 10:983-1000 (2017).

8 Bari E, Perteghella S, Marrubini G, Sorrenti M, Catenacci L, Tripodo G et al., In vitro efficacy of silk sericin microparticles and platelet lysate for intervertebral disk regeneration. Int J Biol Macromol 118:792-799 (2018).

9 Lamboni L, Gauthier M, Yang G and Wang Q, Silk sericin: a versatile material for tissue engineering and drug delivery. Biotechnol Adv 33:1855-1867 (2015).

10 Available: http://www.cir-safety.org/sites/default/?les/slkprt062015rep.pdf.

11 Chirila TV, Suzuki S and McKirdy NC, Further development of silk sericin as a biomaterial: comparative investigation of the procedures for its isolation from Bombyx mori silk cocoons. Progress Biomater 5: 135-145 (2016).

12 Aramwit P, Siritientong T and Srichana T, Potential applications of silk sericin, a natural protein from textile industry by-products. Waste Manag Res 30:217-224 (2012).

13 Assets FEI, Unlocking the circular economy potential (2016).

14 Procedimento e apparecchiatura per la preparazione di materiali proteici derivanti da fibroina, in particolare per uso medicale e cosmetico. Italy (2013).

15 Yang G, Xiao L and Lamboni L, Bioinspired Materials Science and Engineering. Wiley, Hoboken, NJ (2018).

16 Oh H, Lee JY, Kim MK, Um IC and Lee KH, Refining hot-water extracted silk sericin by ethanol-induced precipitation. Int J Biol Macromol 48: 32-37 (2011).

17 Fan JB, Wu LP, Chen LS, Mao XY and Ren FZ, Antioxidant activities of silk sericin from silkworm Bombyx mori. J Food Biochem 33:74-88 (2009).

18 Aramwit P, Damrongsakkul S, Kanokpanont S and Srichana T, Properties and antityrosinase activity of sericin from various extraction methods. Biotechnol Appl Biochem 55:91-98 (2010).

19 Nam KA, You SG and Kim SM, Molecular and physical characteristics of squid (Todarodes pacificus) skin collagens and biological properties of their enzymatic hydrolysates. J Food Sci 73:C249-C255 (2008).

20 Aramwit P, Kanokpanont S, Nakpheng T and Srichana T, The effect of Sericin from various extraction methods on cell viability and collagen production. Int J Mol Sci 11:2200-11 (2010).

21 Vijayalakshmi D, Dhandapani R, Jayaveni S, Jithendra PS, Rose C and Mandal AB, In vitro anti inflammatory activity of Aloe vera by down regulation of MMP-9 in peripheral blood mononuclear cells. J Ethnopharmacol 141:542-546 (2012).

22 Siritientong T, Bonani W, Motta A, Migliaresi C and Aramwit P, The effects of Bombyx mori silk strain and extraction time on the molecular and biological characteristics of sericin. Biosci Biotechnol Biochem 80:241–249 (2016).

23 Wu MH, Yue JX and Zhang YQ, Ultrafiltration recovery of sericin from the alkaline waste of silk floss processing and controlled enzymatic hydrolysis. J Clean Prod 76:154–160 (2014).

24 Gimenes ML, Silva VR, Vieira MGA, Meuris SGC and Scheer AP, High molecular sericin from Bombyx mori cocoons: extraction and recov- ering by ultrafiltration. Int J Chem Eng Appl 5:266–271 (2014).

25 Q. Zy, SDS-PAGE for Silk Fibroin Protein. Bio-101 Camberwell, VIC, Australia (2018).

26 Salunkhe NH, Jadhav NR, More HN and Jadhav AD, Screening of drug-sericin solid dispersions for improved solubility and dissolution. Int J Biol Macromol 107:1683–1691 (2018).

27 Tao W, Li MZ and Xie RJ, Preparation and structure of porous silk sericin materials. Macromol Mater Eng 290:188–194 (2005).

28 Butkhup L, Jeenphakdee M, Jorjong S, Samappito S, Samappito W and Butimal J, Phenolic composition and antioxidant activity of Thai and Eri silk sericins. Food Sci Biotechnol 21:389–398 (2012).

29 Takechi T, Wada R, Fukuda T, Harada K and Takamura H, Antioxidant activities of two sericin proteins extracted from cocoon of silkworm (Bombyx mori) measured by DPPH, chemiluminescence, ORAC and ESR methods. Biomed Rep 2:6 (2014).

30 Manosroi A, Boonpisuttinant K, Winitchai S, Manosroi W and Manosroi J, Free radical scavenging and tyrosinase inhibition activity of oils and sericin extracted from Thai native silkworms (Bombyx mori). Pharm Biol 48:855–860 (2010).

31 Wu J-H, Wang Z and Xu S-Y, Preparation and characterization of sericin powder extracted from silk industry wastewater. Food Chem 103: 1255–1262 (2007).

32 Schallreuter KU, Kothari S, Chavan B and Spencer JD, Regulation of melanogenesis - controversies and new concepts. Exp Dermatol 17:395–404 (2008).

33 Aramwit P, Luplertlop N, Kanjanapruthipong T and Ampawong S, Effect of urea-extracted sericin on melanogenesis: potential applications in post-inflammatory hyperpigmentation. Biol Res 51:54–67 (2018).

34 Chiocchio I, Mandrone M, Sanna C, Maxia A, Tacchini M and Poli F, Screening of a hundred plant extracts as tyrosinase and elastase inhibitors, two enzymatic targets of cosmetic interest. Indus Crops Product 122:498–505 (2018).

35 Kumar JP and Mandal BB, The inhibitory effect of silk sericin against ultraviolet-induced melanogenesis and its potential use in cosmeceutics as an anti-hyperpigmentation compound. Photochem Photo- biol Sci 18:2497–2508 (2019).

36 Jena K, Pandey JP, Kumari R, Sinha AK, Gupta VP and Singh GP, Free radical scavenging potential of sericin obtained from various ecoraces of

tasar cocoons and its cosmeceuticals implication. Int J Biol Macromol 120:255–262 (2018).

37 Nelson DL and Cox MM. Principi di Biochimica, Lehninger, Zanichelli, Bologna, Italy, fifth Italian edition, 2010, Chapter 6, pag. 203.

38 Zolghadri S, Bahrami A, Khan MTH, Munoz-Munoz J, Garcia-Molina F, Garcia-Canovas F et al., A comprehensive review on tyrosinase inhibitors. J Enzyme Inhib Med Chem 34:279–309 (2019).

39 Khatun H, Egashira J, Sakatani M, Takenouchi N, Tatemoto H, Wada Y et al., Sericin enhances the developmental competence of heat- stressed bovine embryos. Mol Reprod Dev 85:696–708 (2018).

40 Huang Y, Peng Q, Li HY, Jia ZD, Li Y and Gao Y, Novel sericin- based hepatocyte serum-free medium and sericin's effect on hepatocyte transcriptome. World J Gastroenterol 24:3398–3413 (2018).

ACKNOWLEDGMENTS

This Ph.D. thesis has been realized thanks to the multidisciplinary collaboration of different research groups and has been partially supported by Interreg V-A Italy-Switzerland 2014-2020 (ATEx—Advanced Therapies Experiences, Project ID 637541).

I want to thank Prof. Maria Luisa Torre, Dr. Giuseppe Tripodo, Dr. Milena Sorrenti, Dr. Laura Catenacci, Dr. Giorgio Marrubini, Dr. Sara Perteghella, and Dr. Elia Bari of the Cell Delivery System Lab, Department of Drug Sciences, University of Pavia, Pavia, Italy; Dr. Stefano Grolli of the Department of Veterinary Medicine, University of Parma, Parma, Italy, and Prof Maurizio Del Bue for clinical trial development; Dr. Silvia Dotti, Dr. Riccardo Villa, Dr. Sara Rota Nodari and Annalisa Ghizzardi of Istituto Zooprofilattico Sperimentale della Lombardia and Emilia Romagna, Brescia, Italy, for the production scale-up of clinical-grade batches, and for presenting the production protocol to the Italian Ministry of Health; Dr. Dario Di Silvestre and Dr. Pierluigi Mauri of Institute for Biomedical Technologies, CNR, Segrate, Milan, Italy, for proteomic investigation; Dr. Lorena Segale, Dr Lorella Giovannelli, and Dr. Andrea Foglio Bonda of the Department of Drug Sciences, University of Eastern Piedmont, Novara, Italy for the support during the freeze drying process set-up. Finally, I would like to thank Prof. Stefano Cinotti and Dott.ssa Maura

Ferrari who laid the foundations, supported the realization, and has believed in this project for years.